Stimuli-Responsive Polymers Derived from a Visible Light Photoswitchable Species

Matthew Andrew Lambie

A thesis submitted to the University of Kent in partial fulfilment of the requirements for the degree of Doctor of Philosophy.

University of Kent,

Canterbury,

Kent,

CT2 7NH

June 2020

Declaration

I declare that this thesis is my own work, and has been written in my own words. Appropriate care has been taken to accurately reference the works of others, where necessary.

Signed –

Matthew Andrew Lambie

25th June 2020

Acknowledgements

First and foremost, I would like to thank my supervisor Dr Simon Holder for his continued advice and providing me with the opportunity to follow an independent research pathway. What I truly appreciate is his balance of hands-on and -off supervision; allowing me access to a wealth of knowledge and experience when needed, but also allowing me to make, and learn from, my own mistakes. Although I haven't always been the easiest student to manage, Simon has displayed relentless patience. Without him, none of this would have been possible.

Secondly, I want to thank Dr Helena Shepherd who has always managed to ground me when I needed it and provided me with sage advice. I would also like to thank Dr Aniello Palma for his constant encouragement, advice and for always providing an engaging work environment. Next, I thank Dr Ewan Clark, Dr Jennifer Hiscock and Dr Stefano Biagini for their support regarding synthetic/NMR-based questions. I would like to further thank Ewan and Jen for their management of the NMR spectroscopic facilities. Thank you to Dr Emma McCabe for training me in the use of powder x-ray diffraction. It is important that I also thank Dr Maria Alfredsson, as her warm and engaging attitude during my open day encouraged me to join the University of Kent.

Further thanks go to Dr Alex Wright, Dr Yaroslav Kalinovskyy and Dr Aaron Hillier for bringing me into the fold of Lab 310, for teaching me the basic and advanced synthetic skills that I have learned over the years, and for providing general scientific advice. Thank you to Dr Jed Askew for, firstly, shouldering this journey alongside me, and secondly, being a constant standard that I should always work toward. I would also like to thank all of the friends I have made throughout my time at SPS, including: Anna, Athina, Giada, Toby, Matt, Josh, Sean, Saeed, Emma, Rachel, Charlie, JJ, Ian and Dr Andrew Morrell.

I would also like to thank my family, particularly Mum and Dad, for their constant, unconditional support and encouragement toward my life choices – and being there for me no matter what.

Finally, I want to thank my partner, Dr Nanami Yokota, who I met during this course through our mutual friends. She has always been there for me, supporting me when I didn't believe in myself and always encouraging me to strive toward self-betterment. I couldn't have written this thesis if it weren't for Nanami's support.

Abstract

The incorporation of photoswitches into polymeric materials is a favoured method for providing a degree of external control over certain macroscopic properties. Popularly used switches include: azobenzenes, spiropyrans and diarylethenes. However, species like these most often require damaging, high energy UV light for activation, as such visible light activated systems are highly sought after. Donor-Acceptor Stenhouse Adducts (DASAs) are a relatively new class of visible light photoswitches, that exhibit negative photochromism upon activation. These new switches are synthetically accessible and producible under mild conditions with relatively inexpensive reagents. Their large changes in polarity and the ability to almost completely decolourise when exposed to visible light, make them a highly desirable alternative to other more traditional photoswitches.

Herein, stimuli-responsive materials were produced through the doping of Sn-catalysed crosslinked polydimethylsiloxane (PDMS) networks with recently discovered visible light photoswitches, DASAs, and precursory species, known as Meldrum's activated furan (MAF). MAF reacts readily with secondary amines to produce a DASA, this synthetic route was exploited by the doping of a crosslinked PDMS network with the precursor molecule (PDMS-MAF). The amine-detection responses were evaluated through UV-Vis spectroscopy, an image analysis technique and changes in RFID sensing values. The applicability of the PDMS-MAF architecture as a colourimetric sensing device was demonstrated by simulation of a food packaging environment. The amine-sensing material was sealed in a container for 24 hours, along with a cod fillet cutting – the presence of decomposition product amines was indicated by a colour change in the material. The doping of a crosslinked PDMS network with a DASA culminated in a photo-responsive material (PDMS-DASA). Crystallisation of DASA at higher concentrations was apparent, encouraging the curing of PDMS-DASA networks in a sealed, solvent-rich environment. Powder X-ray diffraction provided evidence to suggest that the sealed atmosphere curing (SAC) reduced the concentration of crystallisation. The photoswitching kinetics of PDMS-DASA samples were examined using UV-Vis spectroscopy, with a focus on the effect of variation

in DASA concentration. Furthermore, initial investigations into photoswitching fatigue, the effect of solvent swelling of photoswitching kinetics and RFID-sensing applicability were conducted. Additionally, other investigations into the covalent incorporation of DASAs for stimuli-responsive polymers are detailed. These further investigations included various polymeric systems, such as polyethyleneimine, poly(methylhydrosiloxane-*co*-dimethylsiloxane) and building from a polyurea-based scaffold.

Abbreviations

abs. – absorbance

asym – asymmetric

BAF – barbituric activated furan

CD_3OD – deuterated methanol

CIE – International Commission on Illumination

CMC – critical micelle concentration

D_2O – deuterated water

DASA – donor-acceptor Stenhouse adduct

DCM – dichloromethane/methylene chloride

def – deformation

DI – deionised

EDG – electron donating group

EWG – electron withdrawing group

FTIR – Fourier transform infra-red (spectroscopy)

g – grams

HTPB - hydroxyl-terminated polybutadiene

LCST – lower critical solution temperature

MAF – Meldrum's activated furan

NIR – near-infrared

NMR – nuclear magnetic resonance (spectroscopy)

PANI – polyaniline

PDA – polydopamine

PDMS – polydimethylsiloxane

PEG – poly(ethylene glycol)

PEI – polyethyleneimine

PFPA – pentafluorophenyl acrylate

PFPMA – pentafluorophenyl methacrylate

PMMA – polymethylmethacrylate

Poly(MHS-DMS) – poly(methylhydrosiloxane-*co*-dimethylsiloxane)

ppm – parts per million

PS – polystyrene

PSS – photostationary state

PXRD – powder x-ray diffraction

Q_m – mass swelling ratio

Q_v – volume swelling ratio

RAFT – reversible addition-fragmentation chain-transfer

RFID – radio frequency identification

rock – rocking

ROMP – ring-opening metathesis

RT – room temperature

SA – sealed atmosphere

SM – silica microsphere

SP – silica micro/nanoparticles

str – stretching

sym – symmetric

TEOS – tetraethylorthosilicate

T_g – glass transition temperature

THF – tetrahydrofuran

UHF – ultra high frequency

UV-Vis – ultraviolet-visible (spectroscopy)

wt% - weight percentage

Contents

xiii

Chapter 1:

Introduction

1.1 Photoswitches

Photoswitches are molecules that, when exposed to light, will exhibit a reversible transformation from one isomer to another.[1] The two isomers are generally referred to as 'A' and 'B' forms.[2] Traditionally, the 'A' form is colourless or pale yellow, and the 'B' form is a highly coloured, conjugated system. The first reported example of a photoswitch was in 1867, when it was found that an orange-coloured solution of tetracene would decolourise when exposed to light and reform its colouration in the dark. This process was later named "photochromism" by Hirshberg, in 1950.[2] The nature of a photoswitch is dependent on the photoswitching mechanism of the species and the magnitude of the energetic barrier of transformation. Subsequently, they are classified into two groups: bi-stable species, whereby the forward and backward reactions can be induced through irradiation of different wavelengths of light; or a thermally reversible species, in that the 'B' form is thermally unstable and relaxes back to the original form over time. Those which exhibit bi-stability are known as P-type photoswitches, i.e. photo-type, and those which are thermally unstable are defined as T-type switches, i.e. thermal-type. The two most common mechanisms of operation for photoswitches are: a *trans-cis* double-bond photoisomerisation, or a light-activated cyclisation/ring-opening reaction. When a photoswitch undergoes one of these processes, material properties such as polarity, size, geometry and light absorption can change drastically. Furthermore, the application of light is a non-toxic, non-invasive, orthogonal method which provides high spatiotemporal control over those changes, at finely regulated wavelengths.[3] The main desirable characteristic of photoswitches is their reversibility and reusability – the inherent ability to be switched back and forth with very little decomposition. Consequently, photoswitches as control elements have been applied to a wide range of applications, such as materials sciences,[4–6] supramolecular chemistry,[7–9] and biological systems.[10–13] There is no ideal photoswitch that can be used for any application; each varying in their excitation wavelength(s), synthetic accessibility and stability, and so it is down to the user to decide what best fits the situation at hand.[14] To do this, a number of evaluative parameters have been established, such as: the quantum yield (QY), molar

absorptivity (ε), photostationary state (PSS), absorption profile, reliability and thermal half-life (t[1/2]).[15,16] The quantum yield is a ratio of the number of productive reactions taking place during absorption against the quantity of photons absorbed. Molar absorptivity denotes how strongly a species shall absorb light of a given wavelength. The photostationary state is the degree of attainable isomerisation for either switching pathway, i.e. the percentage conversion of isomer A to B. The absorption profile is important as the correct wavelength of light needs to be selected to provide stimulation, and a lack of overlap for the absorption of both isomers can lead to more wavelength-selective control. The reliability is also known as fatigue resistance; the resistance of a molecule to undergo undesirable side-reactions during photoisomerisation. Finally, thermal half-life is a measure of the thermal stability of the 'B' form, i.e. the time it takes for half the molecules to undergo a back-isomerisation to state 'A'. An additional factor to take into consideration when selecting a photoswitching species is the direction of photochromism that is required. Photochromism is divided into two sub-types: the more traditional positive photochromism, where by colourless 'A' isomerises to coloured 'B'; and the less-common negative photochromism which is the antithesis of that process.[17] When utilising high concentrations of a positive photoswitch that exhibits a high molar absorptivity, only the surface of the sample will react upon light exposure. Whereas in the case of negative photochromes the formation of the colourless, metastable species promotes further isomerisation deeper into the material, as there is no longer an absorption barrier situated at the interface. Perhaps the three most ubiquitous photoswitches are the azobenzenes, spiropyrans and the diarylethenes. The following sections will provide brief descriptions of each of those three families.

1.1.1 Azobenzene

The azobenzenes are possibly the most studied and utilised organic photoswitch family.[18] They are readily accessible and boast a fast photoisomerisation, with a high PSS, QY and low rate of reverse photobleaching.[19] Upon exposure to UV light, azobenzenes will isomerise around the nitrogen-nitrogen double-bond (Figure 1-1), transforming from the colourless/weakly coloured,

planar *trans* configuration to the highly coloured, less stable *cis*-azobenzene form, through a 55 ° tilt. This process is reversible with application of visible light or through thermal conversion.[20] Along with this transformation, comes a change in dipole moment of approximately 2.6 D and a decrease of end-to-end distance of 3.5 Å.[21,22] Changes in these properties have led to azobenzenes finding extensive use for applications such as the construction of a micellar drug delivery system, the production of a light-induced actuating polymer film, and the development of ion channel blockers.[23–25]

trans-azobenzene   *cis*-azobenzene
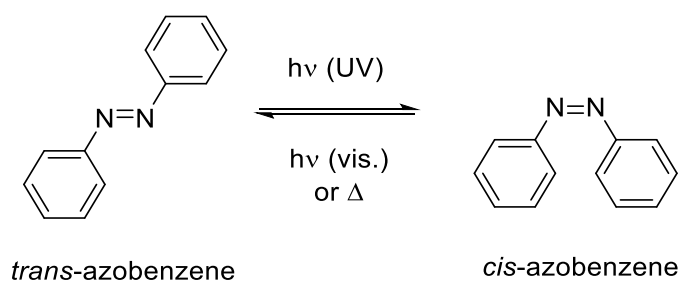
Figure 1-1 – The photoisomerisation of an unmodified azobenzene.

However, this class of photoswitches comes with a disadvantage; the absorbance bands of *trans* and *cis*-isomers overlap, leading to a 80% *trans-cis* conversion at best.[26] Attempts to eliminate this overlap have been made, by red-shifting the *trans* absorption band, but usually produce an unwanted side-effect such as the need for a more intense light source[27] - which could potentially damage living tissue - or lowering the stability of the photoswitch under reductive conditions.[28] Furthermore, it would seem that using longer irradiation wavelengths can produce less stable *cis*-isomers by lowering the thermal isomerisation energy barrier.[29] Past investigations into azobenzene modifications have yielded promising results, in that it has been shown that substitution along the benzene rings can lead to more stable *cis*-isomers under slightly raised temperatures or aqueous conditions.[30,31]

1.1.2 Spiropyran

Spiropyrans (SP) are the most well-known example of photoswitches that exhibit photo-induced ring opening.[2] Rather than undergo a *trans-cis* isomerisation around a double-bond, spiropyrans

transform through a heterolytic cleavage of the C-O bond (Figure 1-2) under UV light exposure. Resulting in the colourless/weakly coloured SP converting to a planar, highly coloured, highly conjugated zwitterion, called a merocyanine (MC). As such, the isomerisation is accompanied by a large increase in the dipole moment, of approximately 15 D.[32] Such a large change in polarity has led to spiropyrans driving the reversible disruption of polymeric micelles.[33]
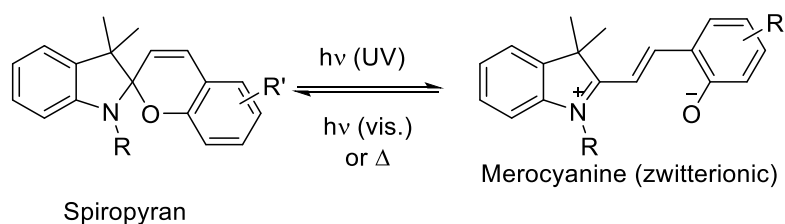
Figure 1-2 – Photoinduced ring-opening reaction of a spiropyran (SP) to a merocyanine (MC)

As with azobenzenes, this photoisomerisation process is reversible through visible light exposure or the application of heat; the rate of the latter is entirely solvent dependent.[20,34] Their overall photochemical behaviour is highly dependent on their environment, such that polar media can stabilise the zwitterionic MC form. Furthermore, substitution of a polar functional group, such as a nitro or sulphonate, on the phenyl ring (R') can further promote this stability.[35] Interestingly, a combination of these two effects will encourage thermodynamic favourability of the MC form, causing the species to exhibit negative photochromism, which highlights the versatility of this species.[36] Additionally, unlike azobenzenes, there is no overlap between the absorbance of SP and MC, and so a near-quantitative conversion of photoisomerisation can take place. On the other hand, spiropyrans are known for their lack of fatigue resistance, as they show a propensity to undergo undesirable, degradation-causing side-reactions when in solution. Therefore, it has been noted that they are best utilised when covalently-attached to a solid support.[37,38]

1.1.3 Diarylethene

Diarlyethenes were first established as a photoswitching family in 1988, where it was reported that UV irradiation of a 1,2-diarylethene holding methyl-substituted heterocyclic rings would

produce a colouration, with the application of visible light reversing this process.[39] Contrastingly to spiropyrans, this species would undergo a photocyclisation reaction, transforming from the flexible, open form to a more rigid, conjugated system (Figure 1-3). Additionally, it was found that both isomers of this new species were thermally stable; attributable to the low aromatic stabilisation energies provided by the terminal heterocyclic acryl groups.[40] This established diarylethenes as P-type photoswitches, in contrast to the more well-known azobenzenes and spiropyrans as T-type.
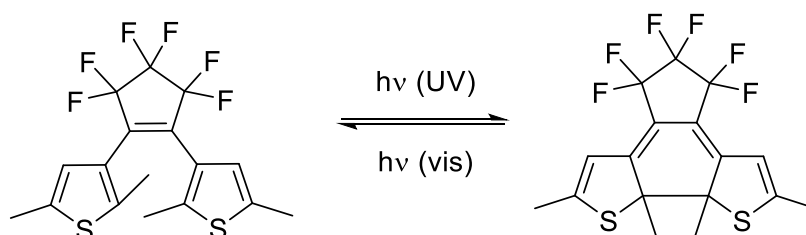
Figure 1-3 – The photoinduced cyclisation of a diarylethene.

On top of being thermally stable, this family of switches exhibits an impressive fatigue resistance of 10,000 cycles, a high QY thanks to minimal absorbance overlap, and extremely rapid forward and backward reactions.[41] A small disadvantage came with the realisation that these switches weren't particularly soluble in water, which limited their biological applications. Although, this was soon remedied by the inclusion of amphiphilic characteristics, leading to successful employment for LCST applications.[42] However, the increasing requirement for visible light activation, as opposed to UV, proved difficult for the diarylethene family. It was found that red-shifted absorbance profiles could be developed through such means as π-conjugation extension, but usually required complex and high-cost synthetic methods that would lead to a great reduction in QY. [43]

1.1.4 Visible and near-infrared photoswitches

Traditional photoswitches are reliant on high-energy UV light to enable photochemical reactions. This dependence on UV light as a switching stimulus is not ideal, as it is readily

absorbed and scattered by skin tissue, leading to cell damage and a reduction in effective penetration.[44] Whereas visible to near-infrared (NIR) light wavelengths are harmless, readily available and provide a greater range for photoswitch tunability. Consequently, the design of photoswitches which can operate under longer wavelengths, has garnered great interest over the years.[29] The two most commonly used methods for modification of existing switches include an extension to π-conjugation, or an addition of terminal electron donating/withdrawing groups (EDG/EWG) to produce a "push-pull", or "push-push" system (Figure 1-4).[43] Modifications such as these however, bring further complications such as a far shorter Z-isomer thermal half-life for azobenzenes,[45] or a greatly reduced QY for diarylethenes with the potential to lose reversibility altogether.[46] The separation of absorption bands must also be considered, as usually these processes entail the photoisomerisation of one coloured form to another. Hence, rigorous control over the irradiation wavelength is required. Summarily, attempts to red-shift the absorption profile of UV light active switches tends to require a sacrifice in other properties. As such, there has always been a need for visible light photoswitches that can be produced and tailored through facile means.

a) λ_{max} (E/Z) = 410 / >500 nm
$t_{1/2}$ = 15 hr (MeCN)

b) λ_{max} (E) = 400 nm
$t_{1/2}$ = 8 min (H$_2$O)

c) λ_{max} (E) = 500 nm
$t_{1/2}$ = 1 s (THF)
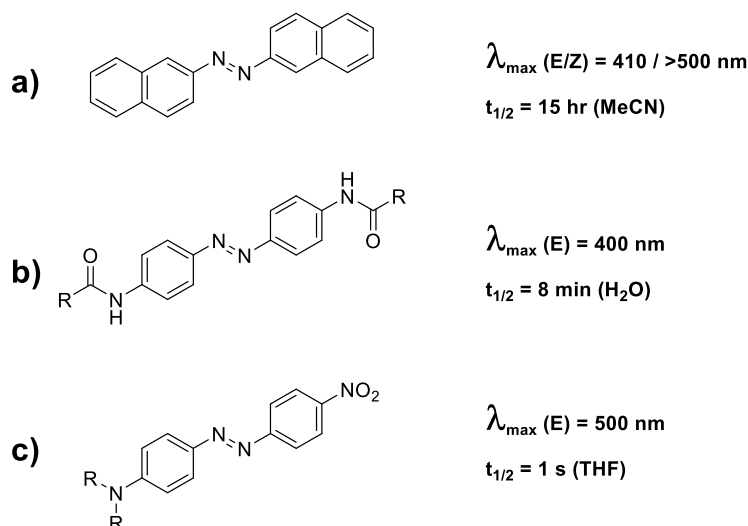
Figure 1-4 – Examples of: a) π-conjugation extension, b) "push-push" and c) "push-pull".

1.2 Donor-acceptor Stenhouse adducts (DASAs)

Recently, a new class of negatively photochromic, visible light-activated photoswitches was introduced by Read de Alaniz and co-workers, called donor-acceptor Stenhouse adducts (DASAs).[47] The stable chemical structure of a DASA is a push-pull, π-conjugated system which consists of a secondary amine (donor) and a carbon acid moiety (acceptor) linked through a triene-enol bridge. The visible light-triggered transformation of DASAs starts from the strongly coloured form and progresses to a colourless, cyclopentenone state; colloquially defined as "open" and "closed", respectively (Figure 1-5). This process is reversible through the application of heat and/or cessation of light irradiation, establishing these as T-type photoswitches. Hence, the open structure is generally more stable than the closed, although that can be highly dependent toward the nature of the surrounding environment – similarly to spiropyrans. Since the introduction of DASAs, improvements upon their chemical structure have culminated in the formation of second- and third-generation switches.[48,49]
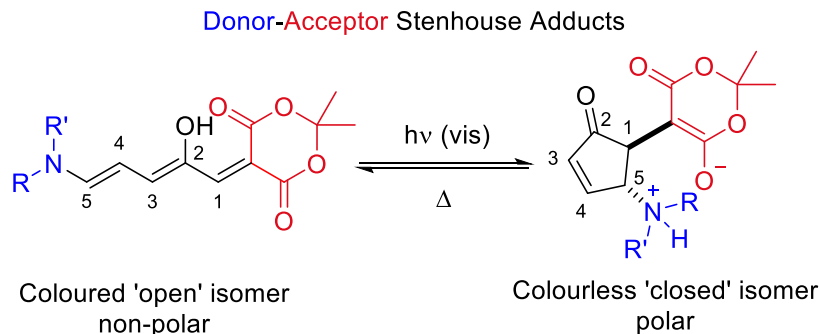
Figure 1-5 – The photoisomerisation of a first-generation DASA.

1.2.1 Synthesis

The progenitor molecule to DASAs is the Stenhouse salt, a five-carbon cyanine first discovered in 1870, by John Stenhouse (Figure 1-6). Stenhouse discovered that a reaction of aniline with furfural in the presence of acid would yield a brightly coloured dye.[50] It wasn't until the 1980's that it was found by Honda and co-workers, that the Stenhouse salts in fact exhibited photochromic properties.[51]
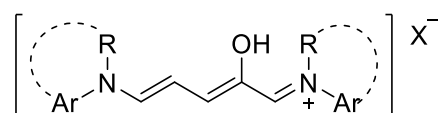
Figure 1-6 – Typical Stenhouse salt, structurally similar to the more recently discovered DASAs. Where X⁻ is acid-dependent.

Almost 20 years later and the first DASA molecule was synthesised, by Šafář et al.[52] It was reported that a Knoevenagel condensation of furfural and Meldrum's acid would result in a product that reacted rapidly with secondary amines to form a highly conjugated species. However, it wasn't until 2014 that the photochemical behaviour of this new structure would be studied and reported, by Read de Alaniz and co-workers.[47] Herein, the synthetic design for DASAs shall be described, with an initial focus on the first generation. A generalised synthetic scheme for first-generation DASAs is included as Figure 1-7.
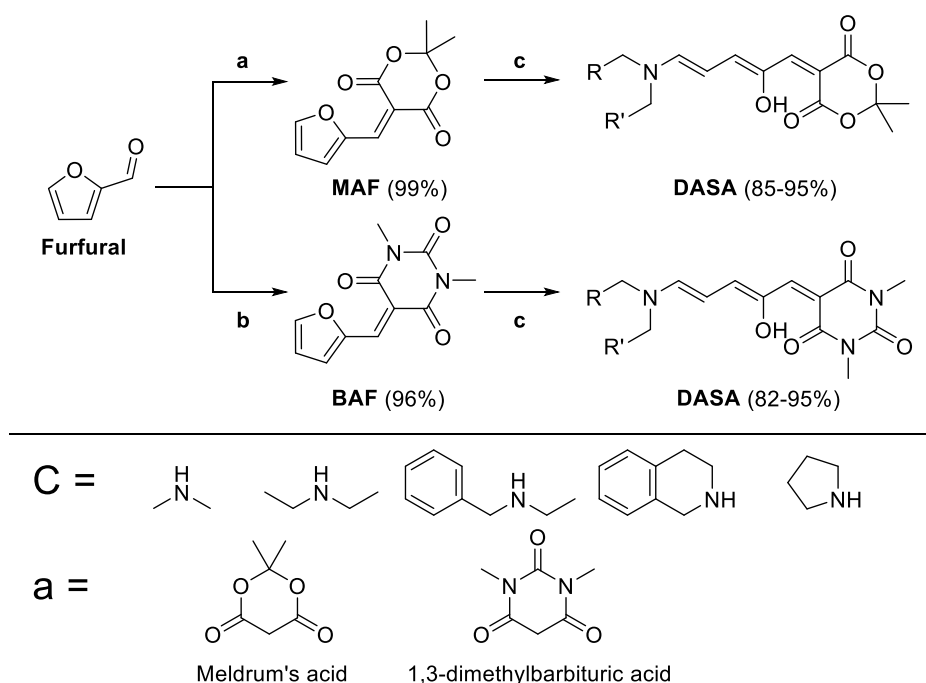
Figure 1-7 – Synthetic route for first-generation DASAs; a) Meldrum's acid, H_2O, 75 °C; b) 1,3-dimethylbarbituric acid, H_2O, RT; c) secondary amine (1-1.5 equiv), THF, RT. Adapted from literature.[47]

The syntheses of products **MAF** (Meldrum's activated furan) and **BAF** (Barbituric activated furan) were adapted from the Knoevenagel condensation of Meldrum's acid and aldehydes reported by Sartori.[53] Subsequently, the new precursor was then exposed to a secondary amine under ambient conditions in THF, which led to the opening of the furfural ring through nucleophilic attack from the nitrogen and producing a positively-charged species. Attempts in a handful of other solvents lead to longer reaction times, a mixture of open and closed isomers, or required heat.[47] The structure then unfolded and rearranged to stabilise the charge through electronic resonance, similarly to the previously-reported (aza-)Piancatelli rearrangements and (iso-)Nazarov cyclisation.[47,54,55] The end result was a conjugated, push-pull system consisting of a donor amine linked through a triene-enol bridge to a carbon acid acceptor. Reportedly, the MAF precursor displayed quicker amine-reactivity than the BAF counterpart, which led to an investigation into using the aforementioned as a platform for selective amine detection.[56,57] It has been noted that reactions with primary amines produce products with limited stability, though a mechanistic explanation has not been given.[47] Eventually, the synthetic scope of DASAs was expanded into three generations; the first and second share the same acceptor units, either the 1,3-dimethyl barbituric acid or Meldrum's acid, but what distinguishes them is the nature of the amine donor. First-generation DASAs employ dialkylamine donors, whereas the second generation utilises *N*-alkyl anilines.[48] The newest, third generation which was reported midway through 2018, separated itself by incorporation of six new carbon acid acceptor units (Figure 1-8).[49]
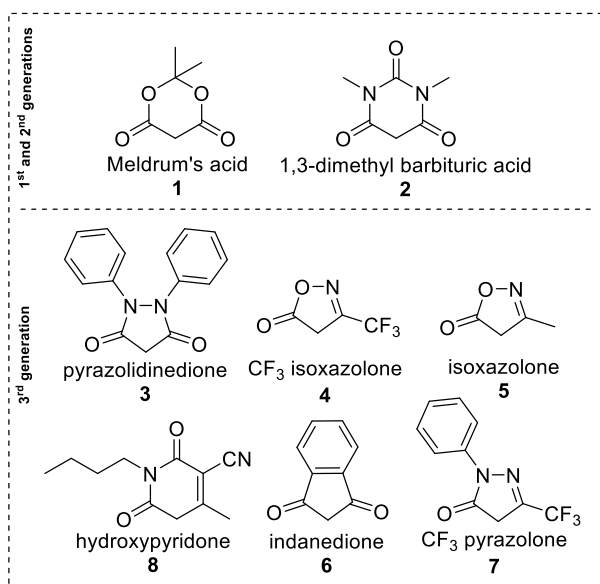
Figure 1-8 – Acceptor unit chemical structures for the three DASA generations.

The synthetic route toward second- and third-generation DASAs is largely the same; opening of the activated furan core with a basic secondary amine. However, the rate of ring opening with the less-basic aniline derivatives is much slower than that of dialkylamine counterparts, owing to the stabilising delocalisation of nitrogen electrons. As such, for the aniline-derived DASAs it is common to introduce heat, an excess of amine, or additional base to the reaction.[48] Despite this, it has been reported that an excess of reactive amine can lead to degradation of the product by way of nucleophilic addition to the triene bridge, but there does not seem to be an expansive explanation for this.[58] Concerning the third-generation switches, the six new carbon acid acceptors can be synthesised with minor variations to the originally reported procedures, and the reaction between amine and activated furan proceeds as expected.[49] Notably, the majority of new acceptor units removed the necessity for an excess of aniline-derived donors.

1.2.2 Photoswitching of DASAs

The photoswitching behaviour of DASAs encompasses two isomerisation procedures; upon irradiation with visible light the *Z-E* photoisomerisation of bond C_2-C_3 (Figure 1-5) begins a spatial rearrangement of the conjugated triene bridge, which eventually culminates in a thermally-allowed electrocyclization to form a metastable cyclopentenone. This process results in the

11

disruption of the "push-pull" conjugation that flows along the triene bridge, thereby inducing colour loss, making DASAs negatively photochromic. The stability of various intermediary species and the nature of the final product are dependent on the structure of the initial, open isomer. The electronic properties of DASAs also rely heavily on the selected donor and acceptor moieties, translating to their absorption profiles, immobilised behaviour and solvent interaction. Understanding the isomerisation mechanism and the effect that structural modification can have on the behaviour of these photoswitches is paramount to their selection for specific applications. As such, this section will describe and discuss those effects on absorption, interaction with environments and the photoswitching mechanism.

1.2.2.1 Absorption profile

The current absorption profile of DASAs is located in the visible region of the electromagnetic spectrum, between at least 500 and 735 nm. Advantageously, this band doesn't cover the intersection of visible and UV light, presenting the possibility of multi-photochromic species with well-separated absorption bands; such as the appendance of an aurone – a yellow-coloured plant flavonoid - for the purposes of information storage,[59] or azobenzenes for wavelength-selective uncaging and logic gate applications.[60,61] The colourless, cyclic form of DASAs absorbs in the UV region of the spectrum, however this reportedly is not utilised as excitation leads to photodegradation.[58] DASAs exhibit solvatochromism, such that a hypsochromic shift occurs with increasing solvent polarity.[58,62] Other changes in the visible absorption profile have been reported through modification of the acceptor and donor units, and the absence of a hydroxyl moiety on the bridging triene structure. On balance, the first-generation DASAs are extremely desirable photoswitches, as they exhibit visible light activation, impressive fatigue resistance, a large change in polarity and are synthetically accessible. However, they display the complete inability to reversibly switch in all but aromatic solvents. Furthermore, these switches display relatively poor spectral tunability, as the absorption window is approximately 540-570 nm. The change in absorption profile is largely a result of a 15 nm difference between Meldrum's and barbituric acid acceptors; dialkylamines don't provide significant absorbance shifts.[63] Initially,

the implementation of other acceptor units was attempted, however they either did not produce the desired triene, or those that did proved unable to photoswitch, such as the indanedione-derivative, featured in Figure 1-9. The lack of chromatic tunability can be seen as an advantage, however, as it has been realised that the switching kinetics of first generation DASAs can be altered without significantly affecting the absorption profile.[64]
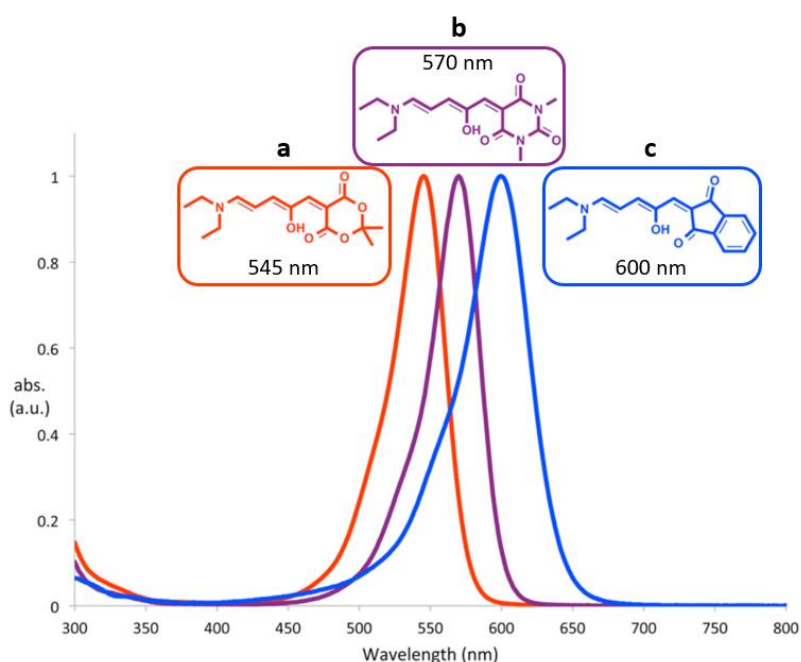
Figure 1-9 – UV-vis absorption spectra of first-generation DASAs with various acceptor groups: a) Meldrum's acid, b) 1,3-dimethyl barbituric acid, c) 1,3-indanedione. Image adapted from a previous report.[63]

Eventually, an investigation into donor modification was undertaken, leading to the advent of the second generation of DASA photoswitches.[48] This entailed using aromatic, secondary aniline-derivatives as the donor species, which displayed a much larger absorption band of 500-670 nm, consequential of the extended π-conjugation that the aromaticity had afforded. Concomitantly, absorption wavelengths could be fine-tuned by selective substitution at the *para-* and *ortho-*positions of the aromatic ring; electron-withdrawing groups (EWGs) such as fluoro- would produce a blue-shift, whereas electron-donating groups (EDGs) such as *p*-methoxy- provided a red-shift.[65] Further improvement of this characteristic was displayed by aryl-aniline based

donors such as indoline, due to the planarity that they shared with the "push-pull" system. Examples of the second-generation donors and their absorption maxima are included as Figure 1-10. This new generation of switches had brought the attractive advantage of colour tunability, with a new maximum absorption of 669 nm, in product '**e'.** However, '**e**' was far less susceptible to cyclisation in anything but a mixture of toluene and hexane, thereby limiting the effective switching wavelength to 629 nm. Additionally, there is a practical limit to the amount of red-shifting that can be generated by simply extending the π-conjugation of the donor. An extension in conjugation provides a greater amount of electron withdrawal from the nitrogen atom, as such this decreases the nucleophilicity of said species. A less-nucleophilic species is less likely to open the activated furan core, thereby preventing the formation of a DASA altogether.
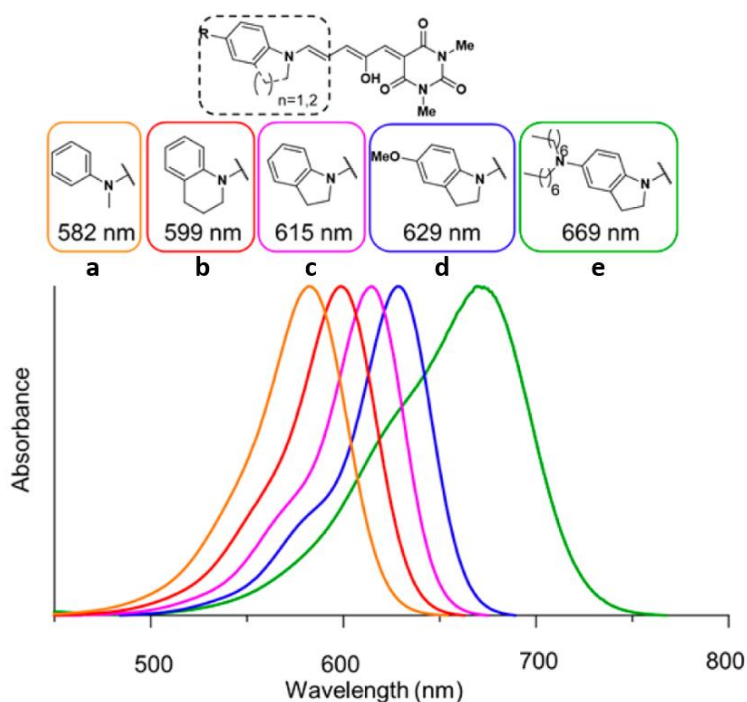
Figure 1-10 – Examples of aniline-derivative donors and their respective absorption wavelengths. Image adapted from a previous report.[48]

Realisations such as this, coupled with structural considerations regarding second-generation DASAs that shall be discussed in the next section (1.2.2.3), reinvigorated the need for carbon acid acceptor group modification. With this, the latest third generation was developed, focusing on substituting the older Meldrum's and barbituric acid-based units for more synthetically-

diverse species (Figure 1-8).[49] Through trial and tribulation, it was found that the ideal candidates for new acceptors needed cyclic, heteroatomic structures with similar pKa values to the already-established species. The electron withdrawing nature of these new acceptor groups was a natural fit for the "push-pull" mechanism of the conjugated triene system, and in combination with previously-inaccessible aniline-derivatives, provided absorption wavelengths of up to 735 nm. In other words, the third-generation DASAs provided synthetic access to far red light switching, something that is not commonly found in photoswitches.[66] The bathochromic shift, provided by combinatory donor- and acceptor-substitution, is highlighted in Figure 1-11, where it can be seen that an almost 100 nm increase is possible.
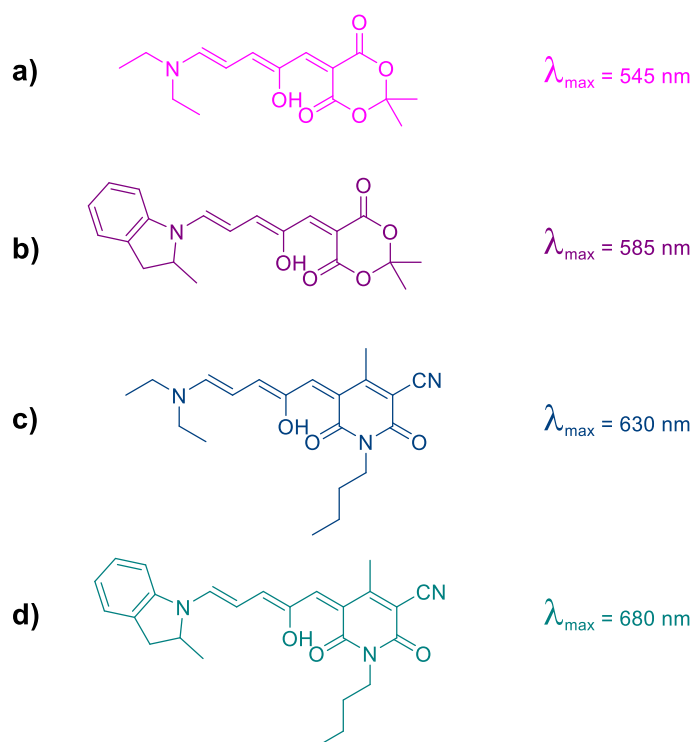
Figure 1-11 – All three generations of DASAs; a) first, b) second, c + d) third. Absorption maxima taken from literature.[49]

Thus far, DASA photoswitches have demonstrated an impressive degree of modular wavelength tunability, through substitution of donor and acceptor moieties. As shown by a previous report, if there is a need to alter switching kinetics without significantly affecting chromatic nature, then first generation DASAs appear to be the best choice. The final route to inducing bathochromic

shift to the system is through manipulation of the conjugated triene; an extension by a single CH group could potentially produce a red-shift of 100 nm.[58,67] Although, successful modification of the triene bridge is yet to be reported, and with the importance of the hydroxyl group having been established, any such route will require conscientious effort.[68]

1.2.2.2 Photoswitching mechanism

Evaluation and discussion of what factors can affect the photoswitching behaviour of DASAs requires insight into how they conduct such a process. Therefore, this section shall provide context to their behaviour by presenting a mechanistic discussion of how DASAs photoswitch. The overall mechanism can largely be described as a photo-induced *Z-E* isomerisation, followed by a thermally dependent 4π-electrocyclisation with a concomitant proton transfer, analogous to the (aza)Piancatelli rearrangement and (iso-)Nazarov cyclisation.[54,55] The process is far more complex than relatively simpler switching mechanisms of other photoswitches, and so has necessitated a great deal of study to fully elucidate. The nature of DASAs has been probed over the years, in the solution state and gas phase, using such methods as UV-vis spectroscopy, ultrafast time-resolved visible and IR pump-probe spectroscopies, tandem ion mobility mass spectrometry and density functional theory calculations.[62,68–75] These have provided a general consensus on the photoswitching mechanism, illustrated in Figure 1-12.
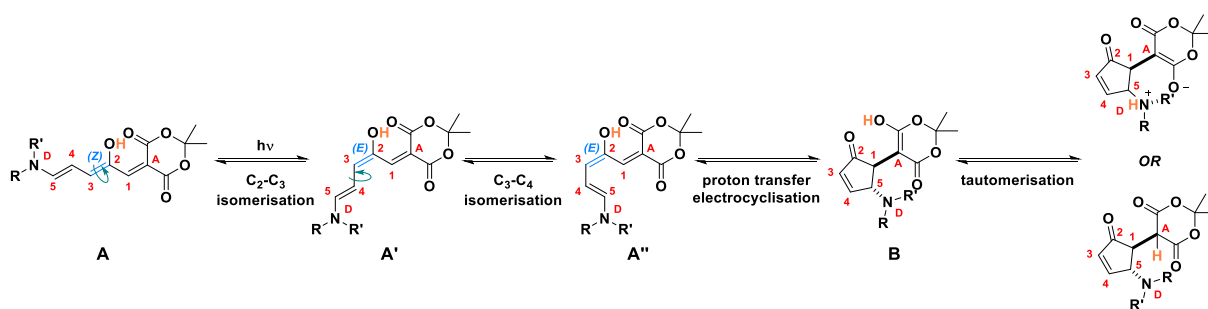
Figure 1-12 – Mechanistic proposal for the photoswitching of a DASA, adapted from a previous report.[71]

Photoswitching begins upon the absorption of visible light, stimulating a π-π* electronic transition. This is the only photochemical step of the process, whereby isomerisation is induced

around the C_2-C_3 enolic bond, transforming from a *Z*- to *E*-conformation, to produce isomer **A'**. From this time forward, the switching process is entirely thermally dependent, unless taking place in the gas phase.[73] Before cyclisation can occur, the triene chain needs to adopt a conformation such that it is energetically favourable and possible to do so. As such, a single-bond rotation takes places about C_3-C_4, transforming isomer **A'** to **A''**. The molecule is now spatially arranged, such that it can begin the cyclisation process; consisting of a thermally-allowed electrocyclisation, associated with a proton transfer. The proton transfer is vital for cyclisation and somewhat the initial isomerisation too. The synthesis of a DASA lacking a hydroxyl group on the triene bridge was performed[68] and Feringa and co-workers discovered that this species would exhibit photoisomerisation up to, but not including, electrocyclisation. A combination of ultrafast visible/IR pump probe spectroscopies and TD-DFT calculations elucidated that the hydroxyl group acts as a pre-selecting species for the photoisomerisation of the C_2-C_3 bond. In other words, without the hydroxyl functional group, the first photoisomerisation is not bond-specific and can instead occur at C_3-C_4. Additionally, and perhaps even more importantly, they discovered that the hydroxyl group is the source of the proton transfer; it drives the electronic rearrangement, culminating in the colourless, cyclised product. During the electrocyclisation process, a proton is transferred from the triene-enol to the acceptor unit, producing an enolic form, designated **B**. From here, the molecule needs to reach the most energetically stable form, existing as **B'''** or **C**, through tautomerisation; Figure 1-13 depicts the routes that can be taken for this process. The stability of forms **B'''** and **C** are structure-dependent and likely solvent-dependent. In general, it has been found that the first-generation DASAs opt for the enolate form (**B'''**), but structural differences can lead to the dione-like species (**C**) and even a mixture of both.[64] The second generation has largely been observed as the dione-like isomer, **C**.[71] Concerning the third generation, findings are mixed, such that only two examples have been investigated thoroughly, of which both adopt different conformations.[62] The route of **B** to **B'''** is most energetically favoured in this order: a nitrogen-inversion to **B'**, a single-bond rotation around C_1-C_A to **B''** and a rotation of the C_5-N_D single-

bond, associated with a proton transfer, placing nitrogen in a pyramidal conformation. Regarding formation of the dione-like structure (**C**), the process is somewhat different in that it can occur directly from **B**, **B'**, or **B''**. The former two involve a proton transfer mediated by the oxygen of the cyclopentenone ring, and the latter is also through a proton transfer, but this time made possible by the amino-functional group. With that, the photoswitching process is complete, however, a number of unproductive isomers can form over the course of this reaction.[71]
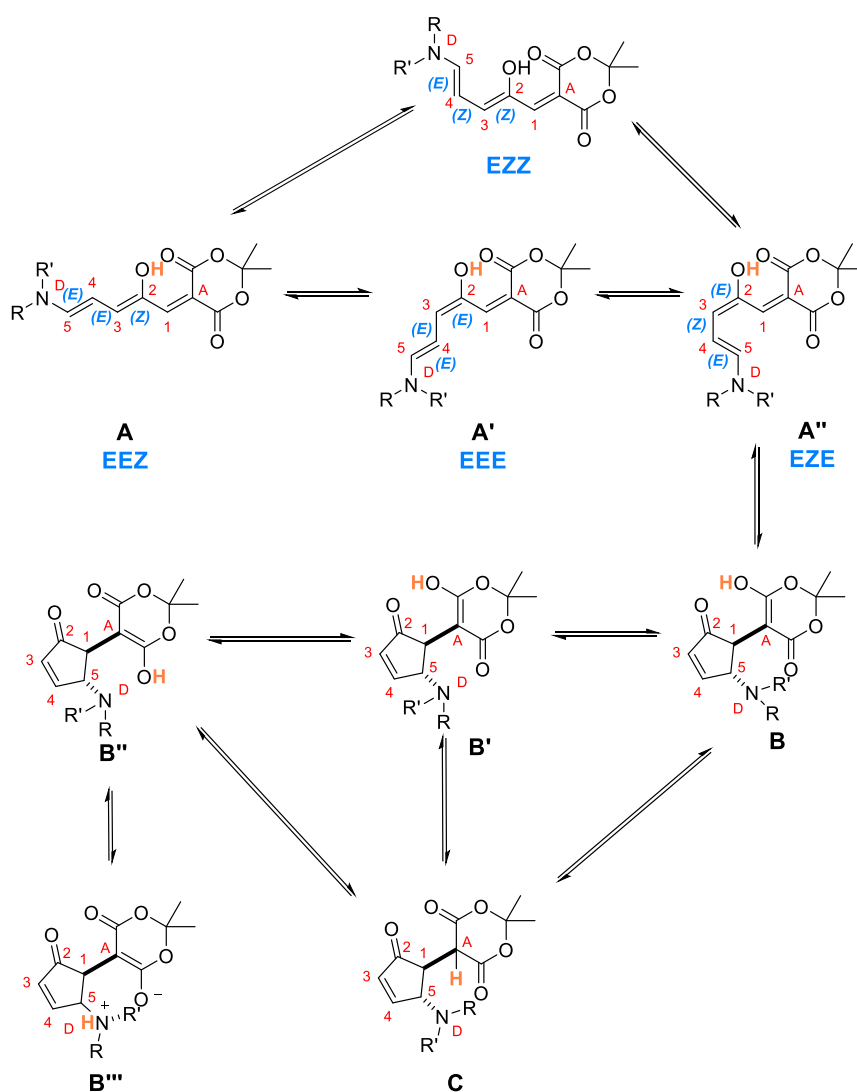
Figure 1-13 – The productive pathway of DASA photoswitching, including one of the unproductive products, EZZ. Scheme adapted from literature.[71]

One such isomer, designated **EZZ** (Figure 1-13) exists in equilibrium with first and second-generation DASAs, at the solution state, under dark conditions. In the case of first-generation DASAs, the **EZZ** isomer is produced along an unproductive, thermal isomerisation pathway from **A''** to **A.** This isomer is defined as unproductive because it has the propensity to revert back to form **A**, thereby requiring a traversal through species **A'** again. The formation of this isomer is significant, as any unproductive photoswitching pathway is essentially a reduction in the overall rate of the process. The reaction is solvent-dependent; **EZZ** does not appear to form in toluene, as high energy barriers prevent the back-transition. This partially explains why toluene encourages faster switching kinetics. Concerning the second generation, the **EZZ** isomer appears to form concomitantly with **A'**, from photoexcitation of **A** and is entirely solvent independent. It is believed that this is a product of the weakening of double-bonds, due to donor aromaticity. Additionally, formation of the other four open-form isomers is possible, albeit less common and understood; there has been less of a focus on these particular species.[71] These findings indicate that thermal interconversions play a large part in the determination of switching rates for DASAs. To increase switching efficacy, structural tailoring requires a minimalisation of these reactions, specifically the thermal back-transition from **A''** and photoinduction of **EZZ**. To conclude, the photoswitching mechanism of DASAs is far more complex than what was originally thought; recent investigations have completely mapped the switching process, only to find that energy barriers are structure and solvent sensitive, and that far more thermal interconversions are present. Granted, some more than others, however each effect plays its part in the ever-increasingly convoluted process. The following section shall discuss the photoswitching behaviour of DASAs, and how they can be affected by environments and structural modification.

1.2.2.3 Photoswitching behaviour

Successful application of DASAs is only possible with an understanding of how they behave in certain environments. Additionally, photoswitching kinetics and the thermodynamics of DASAs are greatly affected by manipulation of the donor, acceptor and triene modules. Subsequently, explanations behind their behaviours are generalised to three generations, however, it is

difficult to define a DASA's switching characteristics by its 'generation', alone. Therefore, this section shall discuss the inter-generational differences that have been discovered, how DASAs can be tailored to induce desirable switching properties, and how they are affected by their environment.

1.2.2.3.1 Inter-generational differences

The generations of DASAs are distinguished by the donor and acceptor species that they incorporate: the first consists of dialkylamine donors, with acceptors derived from Meldrum's acid or barbituric acid; the second shares the same acceptor species but utilises secondary aniline-derivatives instead; finally, the third generation enlists both dialkylamine and aniline-based donors, but with more structurally varied acceptor units. Initial studies detailed the photoswitching behaviour of first-generation DASAs in a small variety of representative solvents, i.e. various polar and non-polar examples.[47,48,63,65] Originally, it was believed that they would exhibit irreversible forward switching in polar-protic solvents, backward switching in halogenated solvents, and fully reversible switching in non-polar media.[76] Further investigations concluded that the first generation did in fact photoisomerise in halogenated solvents, but neglected to cyclise, thereby failing to photoswitch to the full extent.[69,70,72] It was eventually found that a certain division of first-generation DASAs, with less sterically-hindered donors groups, were in fact able to switch in halogenated solvents.[64] The reasoning behind this was confirmed not long after, in further investigations, through the use of ^{1}H NMR spectroscopy, rapid-scan FT-IR and DFT calculations.[64,71] The conformation of the donor nitrogen atom changes from trigonal planar to pyramidal after cyclisation and steric strain can build up between 'bulky' amino-substituents. This creates an unfavoured forward switching pathway. Subsequently, it was concluded that any alkyl chain that was longer than two units, i.e. propyl or larger, would present a large enough steric bulk, such that a pair of these substituents would significantly hinder the switching process. Hence, some first-generation DASAs are able to switch in polar, halogenated solvents and others are not. This characteristic applies, at least, to the third-generation DASAs bearing a diethylamine-donor, too.[49]

20

The second generation of DASAs have the added advantage of being able to reversibly switch in a variety of solvents.[48] When compared to first-generation switches, they exhibit quicker attainment of the PSS, suggesting faster switching kinetics.[64] Spectroscopic analyses and TD-DFT calculations elucidated this phenomenon through energy level determination, showing that the energy barrier between A' and A'' is smaller for the second-generation switches, hence a faster forward switching pathway is demonstrated.[70] However, the aniline-derived switches do exist as a ratio of linear to cyclic (from 2% to 70% linear) in dark equilibria, whereas the first-generation were seen to be almost exclusively (> 95%) in the linear form, within the same conditions.[49] In order to take full advantage of the photoswitchability, the structural property changes have to be maximised and therefore isomerisation from linear to open under dark conditions is not ideal. Consequently, the third generation of DASAs was developed.[49] As previously discussed, the new carbon acid acceptors were tailored to provide far red light switching, with the added control over dark equilibria that was lacking within the second generation (Figure 1-14).
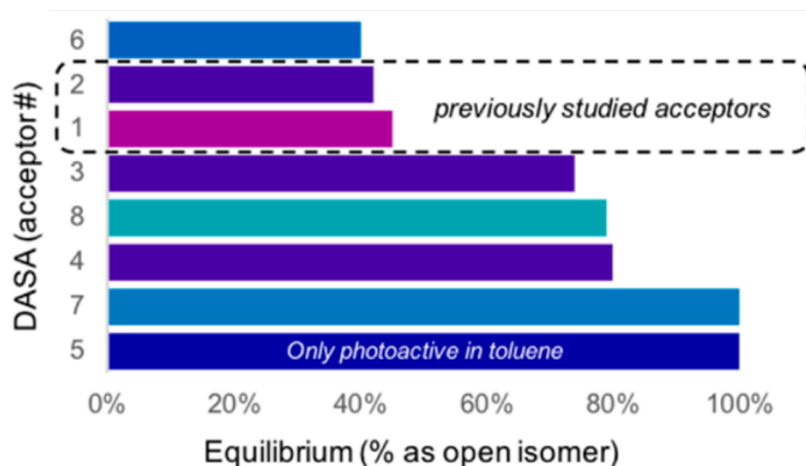
Figure 1-14 – Equilibrium positions of second and third generation DASAs, bearing a 2-methylindoline donor unit. Acceptor groups correspond to those shown in Figure 1-8. Adapted from a previous report.[49]

The third generation is far more synthetically diverse, in that it encompasses both aniline- and alkyl-derived donors, leading to a class whose properties vary greatly. Consequentially, the

reversibility in a range of solvents isn't standardised across the generation. For a particular third-generation DASA, the forward switching time was found to be relatively similar to the second-generation moieties bearing the same donor species, however it displayed a much faster thermal reversion timescale: 60 seconds compared to a number of hours (Figure 1-15). This rapid reversion time can be attributed to the relatively small energy barrier that exists between A'' and B for this particular DASA, allowing fast, bi-directional switching.[62] One example of the third-generation switches exhibited switching under red light, proceeding to demonstrate a thermal reversion up to 16-times faster than second-generation 2-methylindoline analogues. Although, it is important to note that this was only possible with a 3:1 mixture of toluene to octane, as pure toluene led to a 70% loss of recoverable absorbance, per cycle.
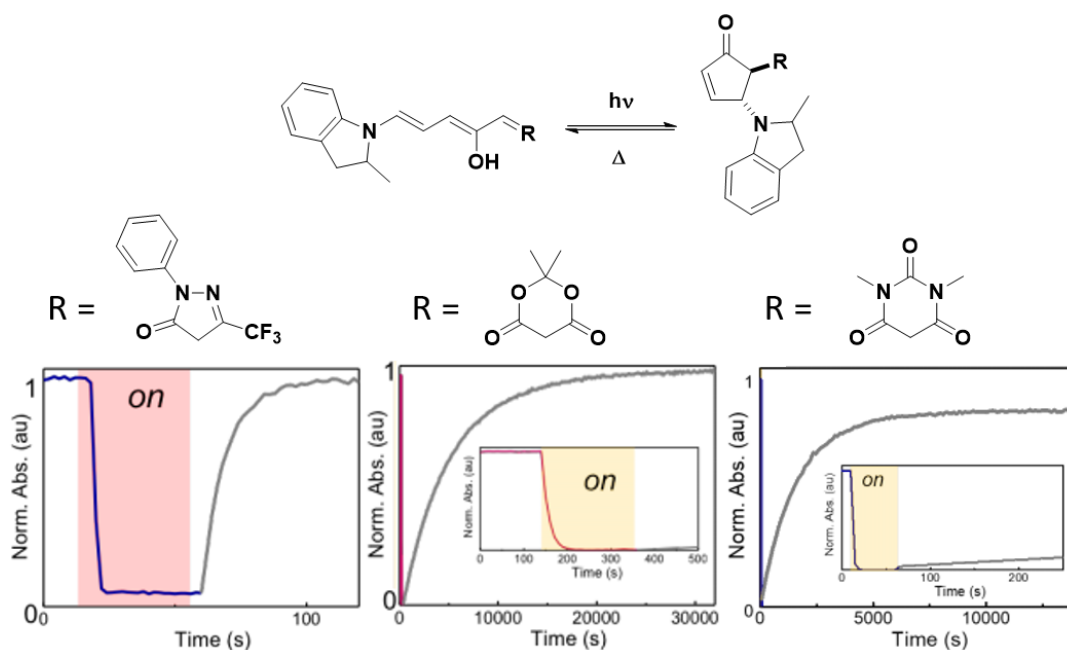
Figure 1-15 – The peak absorption over time for a third-generation (left) and two second-generation DASAs (middle, right), measured using pump-probe absorption spectroscopy. Data taken from a previous report.[49]

To summarise, each DASA generation presents its own advantages and disadvantages: the first is synthetically accessible under mild conditions, without a need for excess reagents or a catalytic species, but is limited to switching in a small range of media; the second provides a

much greater range of tunability and switching versatility, at the cost of potentially less-efficacious structural changes; and the third is open to a great deal of structural variety and even further chromatic tuning, with the slight disadvantage of being less synthetically accessible – requiring multiple steps, or greater monetary cost. Despite these seemingly clear-cut inter-generational differences, modularity of DASAs introduces multiple avenues for thermodynamic and kinetic variations. The next section shall detail and discuss some general solvent effects, reported concentration factors and examples of the intra-generational differences that DASAs display, through structural modification.

1.2.2.3.2 Solvent effects

DASAs are significantly solvent-dependent, with the first two generations effectively being defined by the way in which they interact with such media. Where the first only exhibits reversible switching in toluene, the second expands upon this, with the inclusion of acetonitrile, chloroform, DCM, THF and more.[48] Third-generation switches vary in their reversible behaviour; depending on what amine donor they bear. What is found for all generations, is a marked improvement in overall kinetics in non-polar solvents, such as an increased fatigue resistance and greater bleaching at the PSS.[64] The reasons for this, at least in the case of toluene, were elucidated through TD-DFT calculations, revealing that the energy barriers of transitions for the C_3-C_4 single-bond rotation and subsequent cyclisation were relatively low. This explains why reversible switching is accessible for many switches in this solvent.[70] Originally, it was believed that the actinic step of switching was largely insensitive to solvent polarity. However, solvent polarity is actually a very important factor to consider across the entire process, as can be seen in the energy profile of the forward and backward isomerisation processes of a first-generation DASA (Figure 1-16). The lack of reversible switching attributed to this species, in polar protic solvents, is consequential of the increased stability provided to the zwitterionic product and the large energy barrier incumbent to the B-A'' back-transition.[70,71] Furthermore, it has been elucidated that the A'-A'' and A''-B transition barriers increase, and the A-A' barrier decreases, in more polar solvents.[71] This produces a net hindering effect on the forward switching pathway.
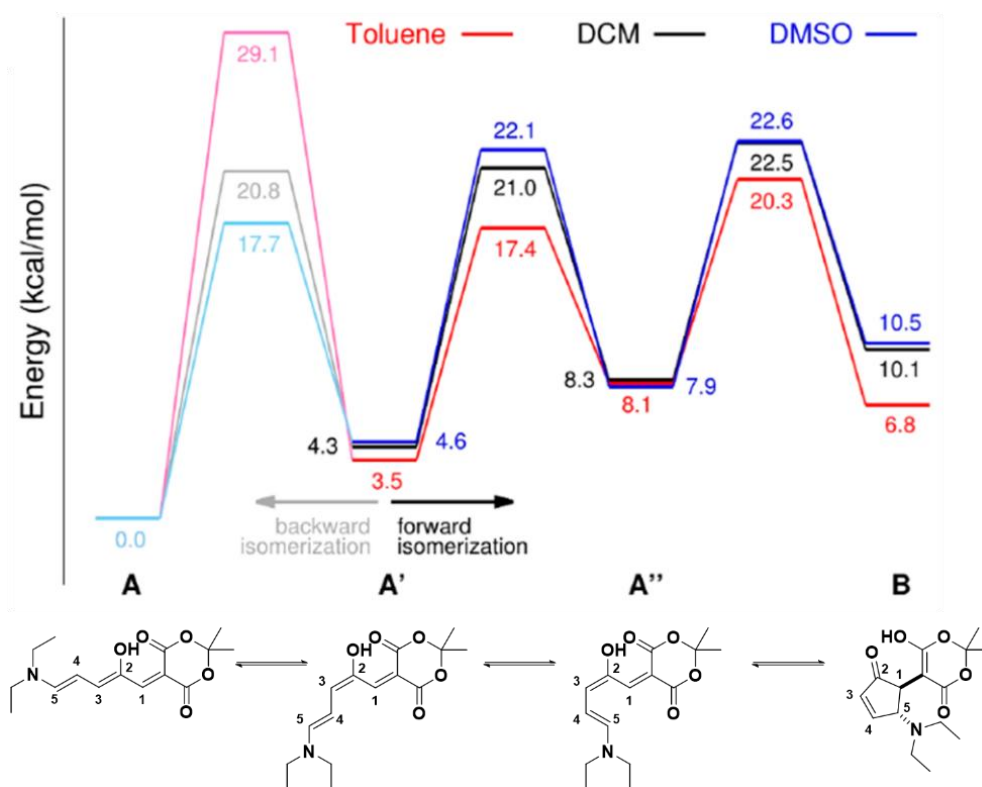
Figure 1-16 – Energy profile of the backward (light) and forward (dark) isomerisation reaction for A', the *E*-isomer of a first-generation DASA, highlighting the role of solvent variation. Adapted from literature.[71]

Another solvent was studied from a third generation DASA bearing a 2-methyindoline donor and the acceptor unit '**7**' (Figure 1-8). It was found that in acetonitrile cyclisation does not occur, as the energy barrier for thermal reversion is reduced by such a degree that the backward reaction effectively competes with forward photoswitching.[62] As such, the stabilities of linear and cyclic forms heavily rely on solvent interaction.

1.2.2.3.3 Concentration effects

A more elusive kinetics-affecting factor is that of DASA concentration; DASAs switch efficiently at low concentrations, in solution and solid-state matrices, albeit slightly perturbed for the latter. However, upon reaching higher concentrations, such as 10^{-3} M, photoswitching can be prevented entirely. This phenomenon is yet to be fully understood, as very few studies have

been dedicated to investigating its origin. Presently, only one such study exists, detailing the behaviour of a third generation DASA in the solution- and solid-states, finding very different performances for each.[77] The DASA was subjected to visible light irradiation in solutions, and polymer blends, of various concentrations, specifically in toluene and poly(methyl methacrylate) (PMMA). The *cis-trans* isomerisation was analysed using femtosecond transient absorption spectroscopy. No evidence was found to implicate the actinic step of the reaction, as such it was concluded that the slowing of photoswitching occurs around the thermally-allowed electrocyclization and/or proton transfer process. The focus of the investigation was a comparison of the thermal reversion rates (k_{back}) and the quantum yields of the forward photoswitching reaction (QY). Data drawn from the investigation has been tabulated in Table 1.1.

Table 1.1 - Tabulated thermal recovery rates and quantum yield values, at various concentrations, in toluene and PMMA. Data taken from a previous report.[77]

Toluene			PMMA		
Concentration (M)	k_{back} (s^{-1})	QY (%)	Concentration (M)	k_{back} (s^{-1}) (x 10^{-4})	QY (%) (x 10^{-3})
1×10^{-3}	0.303 ± 0.008	3.3 ± 1.2	1×10^{-1}	4.4 ± 0.3	7.9 ± 0.9
6×10^{-4}	0.356 ± 0.0011	5.4 ± 1.7	1×10^{-2}	7.6 ± 0.4	15.6 ± 1.4
1×10^{-4}	0.228 ± 0.0015	6.7 ± 2.4	8×10^{-3}	12.5 ± 0.8	39.6 ± 3.5
3×10^{-5}	0.139 ± 0.006	9.5 ± 1.3	9×10^{-4}	13.5 ± 1.0	209 ± 17
3×10^{-6}	0.046 ± 0.003	21 ± 1.7			

A general trend was found for solution studies, whereby an increase in concentration was concomitant with an increase in thermal reversion rate and a reduction in the achievable quantum yield. This same trend has been reported in a more recent investigation, too.[78] Interestingly, the opposite effect was found for polymer blends, concerning the thermally-reliant back isomerisation process; reversion rate and quantum yield would both experience a

net decrease at greater concentrations. Both sets of concentration effects were successful in hindering the forward photoswitching reaction. It was determined that the cause(s) of this was unlikely to be from steric interference of neighbouring DASAs or molecular aggregation, as the solution-state would provide adequate diffusivity and the absorption spectral shapes did not indicate excitonic coupling. Although the findings remained inconclusive, in that the exact cause could not be identified, there remained two theories that had not been disproved. Through TD-DFT calculations, it is believed that DASAs can exhibit long-range electrostatic interactions which possibly perturb the proton transfer process.[74] Secondly, a previous report had revealed that DASAs can favour the zwitterionic, enolate form at higher concentrations, associated with the possibility of hydrogen-bonding pairs.[64] This process would very likely prevent thermal reversion, but how it could hamper the forward reaction is not certain.

1.2.2.3.4 Structural effects

Earlier, it was outlined that DASAs holding a dialkylamine donor, other than dimethylamine, are unable to undergo complete forward photoswitching, i.e. cyclisation, in halogenated solvents. This is consequential of the steric strain that is introduced to a pyramidal conformation of nitrogen during cyclisation, but can be avoided by utilising asymmetry about the amino-substituents.[64] This is a prime example of how structural modification of DASAs can affect their photoswitching behaviour. Relating to this structural effect, it appears that some second-generation and first-generation DASAs display slower rates of thermal reversion, in comparison to the latter's sterically-hindered analogues, at least in chloroform.[64] Further supporting the notion that a select division of first-generation DASAs are ideal for applications that require fast thermal reversion. Regarding chloroform-switching, one such example pertains to the second generation, whereby it was found that DASAs bearing 2-methylaniline-derived donors by and large were able to reversibly switch in the solvent. However, it was found that another construct would exhibit very little switching, altering from a 83 : 17 (linear : cyclic) ratio, to 80 : 20 at the PSS. It was thought that the linear isomer was significantly stabilised by the *p*-dimethylamino aniline-substituent.[65] This finding led to the conclusion that increasingly basic donors would

influence the equilibrium of linear to cyclic, to favour the former. Continuing with basicity, it has been shown that a second-generation DASA utilising 2-methylindoline was unable to reversibly switch in toluene,[49] whereas it was possible with an electron-donating *p*-methoxyindoline species.[70] Overall, these findings not only suggest a degree of control over the dark equilibrium afforded by basicity, but also appear to enable switching in non-polar environments. Contrastingly, the inclusion of EWGs shifts the equilibrial position toward the cyclic isomer, this effect is highlighted by the difference in ratio displayed by fluoro- and *p*-methoxy-substituents.[65] Electron withdrawing also seems to benefit forward photoswitching; during isomerisation electron density flows towards the nitrogen centre, and as such the effect is amplified.[64] These few examples demonstrate the importance of donor selection and the differences that distinguish them.

One of the main attractions of the third-generation is its inherent structural diversity, afforded by modification on either ends of the molecule, in such a way that the photochemical properties can be tuned to exact requirements. This diversity entailed the variation of acceptor units, providing another level of control over the dark equilibrium states (Figure 1-14). Dark equilibrium isomers measured through ^{1}H NMR revealed that the DASAs which exhibited a greater percentage of the linear form, were constructed with more electron-deficient acceptor units.[49] The reasoning behind this was admittedly not fully understood, it was believed to be an effect dependent on acidity and orbital energy levels. Further acceptor variation effects were demonstrated through an investigation of the switching kinetics of second and third-generation DASAs, displayed as Figure 1-17a. For example, the compound **A2** exhibited a slower rate of *Z-E* photoisomerisation in comparison to **A1** and **A3**, believed to be consequential of a greater energy barrier between the two isomers, at least in chloroform and acetonitrile.[62] Furthermore, it was found that **A2** neglected to undergo thermal reversion in chloroform and toluene.[49] This acceptor unit was originally utilised for first-generation DASAs, where it was found that photoswitching was not possible.[63] Although the exact cause does not seem to have been addressed as of yet, it is likely that this heterocycle is not electron-deficient enough to facilitate

the photoswitching process, without the aid of a less-basic donor species, i.e. an indoline derivative. Regarding the same group of compounds, it was also found that a transition state between the *E*-isomer and initial cyclic derivative of **A3** was of particularly low energy, in comparison to **A1** and **A2**. This provided a favoured forward switching pathway and as such a faster photoswitching process, it was believed to be consequential of the strong acceptor ability inherent to the substituted pyrazolone.[62] Whereas **A1** and **A2** solely adopt the dione-like form as a final product, the **A3** species appears to exist in an equilibrium of the aforementioned and an intra-molecular, hydrogen-bonded zwitterionic-rotated state, due to their similar energies (Figure 1-17b). The 'regular' zwitterionic form is unstable for all three DASAs. To summarise, all of the factors discussed in this section demonstrate the difference in photochemical behaviour that can be attained, not only between generations, but also within them. This highlights the importance to be placed upon careful selection of structural combinations.
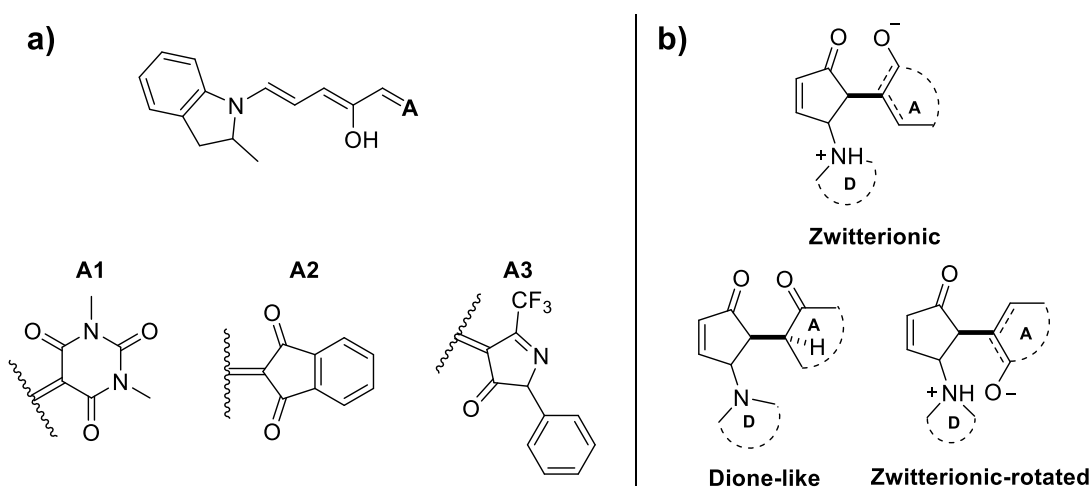
Figure 1-17 – a) Examples of second (A1) and third-generation DASAs (A2, A3), b) The possible conformations of the cyclised products of A1, A2 and A3. Diagram adapted from a previous report.[62]

1.2.2.3.5 Behaviour in polymeric media

DASAs tend to show a decrease in forward and backward isomerisation rates when incorporated into polymeric architecture. This is attributed to the steric interference of polymer chains hindering those physical rearrangements, as opposed to the freedom they are afforded when

dissolved in solution. Their behaviour appears to largely mimic that of the solution-state; the zwitterionic form of first-generation DASAs can be stabilised by more polar polymer environments. Whereas second- and third-generation based systems have less of a problem, owing to their more neutral cyclised state. There have been multiple academic reports that describe the irreversibility of covalently-bound first-generation DASAs, as a consequence of environmental polarity.[79–81] This is corroborated by an instance where reversibility was possible in the doping of a non-polar polymer matrix.[76] Irreversible switching behaviour does not solely depend on polarity, however, as it has been demonstrated in the past that first-generation DASAs are unable to revert to their linear isomer when bound to a non-polar polystyrene-based polymer.[82] Similarly, a third-generation DASA exhibited the same problem, but instead as a non-covalent dopant.[83] It is believed that both examples were consequential of the rigidity of the polystyrene chains; limiting physical rearrangement of the DASA pendants. Polymer rigidity also affects the second-generation switches, shown by the incorporation of aniline-derivatives in acrylate and methacrylate polymers, whereby reversible switching could only be attained above the polymer T_gs.[84] Furthermore, a recent example of covalent first-generation incorporation into acrylate, and methacrylate, polymers revealed that the degree of polymerisation (DP) can also affect switching kinetics.[78] In essence, when incorporating a first-generation DASA into a polymer, it is important to consider how the polarity of said polymer will affect its behaviour. Additionally, for integration of any DASA into polymeric media, the steric bulk and rigidity of those chains needs to be accounted for.

1.3 Applications of DASAs

Since the advent of DASAs, their ability to undergo large, photoinduced changes in polarity, geometry and colour has been utilised in a wide range of applications: the carrying and release of specific molecules, demonstrations of orthogonal photo-control, incorporation within functional materials, and chemo- and thermo-sensing platforms. A number of examples shall be described, herein.

1.3.1 Targeted molecular delivery

The large polarity change that comes with the photoswitching process of DASAs, makes them ideal subjects for incorporation into cargo delivery systems. Wang et al. reported a drug delivery device, capable of carrying, and releasing, hydrophilic and hydrophobic species.[85] The design consisted of conjugated poly(p-phenylene vinylene) nanoparticles functionalised with DASAs - through a PEG-chain Click-method - and folic acid units. These photo-responsive cargo carriers demonstrated not only utility in drug delivery and release, but also imaging technology. Another group demonstrated the utility of DASAs in a non-polymeric delivery system.[86] Silica microspheres (SM) were functionalised with an organosilane species bearing a terminal secondary amine group, which were further modified to yield DASA-appended SMs. The hydrophobic nature of the linear-DASA chains led to the formation of Pickering emulsions, when the SMs were suspended in a toluene/water biphasic solution. Visible light irradiation caused an inversion of the SMs, such that a transformation from water-in-oil to oil-in-water was observed. This was demonstrated visually by release of a sodium fluorescein salt cargo into the water layer. One of the first examples of DASA cargo delivery devices was described by Read de Alaniz and co-workers.[79] They reported the successful delivery of a chemotherapeutic agent, paclitaxel, to human breast cancer cells upon visible light irradiation of their self-assembled amphiphilic micelle. The design incorporated a DASA bearing a hydrophobic acceptor derived from 1,3-dimethyl barbituric acid and a hydrophilic tail consisting of an alkylamine donor conjugated to a poly(ethylene glycol) (PEG) chain through Click chemistry. The micellar structure would

destabilise when irradiated with visible light. This process was found to be irreversible, as the aqueous environment would stabilise the hydrophilic DASA isomer. They subsequently improved upon this work by developing a reversible system that incorporated second and third-generation DASAs.[87] These new polymersomes bio-catalysed reactions through enzyme exposure by light-driven membrane permeability changes. The polymersomes were formed by self-assembly of amphiphilic block copolymers, synthesised by reversible addition-fragmentation chain-transfer (RAFT) polymerisation of hydrophilic PEG-chains and hydrophobic poly(pentafluorophenyl methacrylate) units. Post-modification with activated furan cores derived from either Meldrum's acid or a pyrazolone-based species led to the formation of second- (MELD) and third- (PYRA) generation DASAs, respectively (Figure 1-18a/b). It was demonstrated that two separate species of polymersomes in the same environment could provide wavelength-selective control of activity; the MELD-polymersomes exhibited an excitation wavelength of 550 nm and contrastingly, the PYRA-based species would absorb at 595 nm. The functionality was demonstrated by a bio-catalysed cascade reaction, whereby the production of D-glucono-1,5-lactone and purpurogallin – a yellow-coloured moiety - were controlled by red (630 nm) and green (525 nm) light. This process was executed through the loading of glucose oxidase (GOx) and horseradish peroxidase (HRP) into the PYRA and MELD polymersomes, respectively. GOx would catalyse the reaction of $β$-D-glucose with oxygen to form D-glucono-1,5-lactone and hydrogen peroxide as a by-product. The hydrogen peroxide would proceed to be used for the oxidation of pyrogallol, catalysed by HRP, to produce purpurogallin and water (Figure 1-18c/d). The multi-wavelength functionality of the polymersome nanoreactors links to the next section; discussing further examples of the wavelength-selective control of systems that has been demonstrated via the incorporation of DASAs.
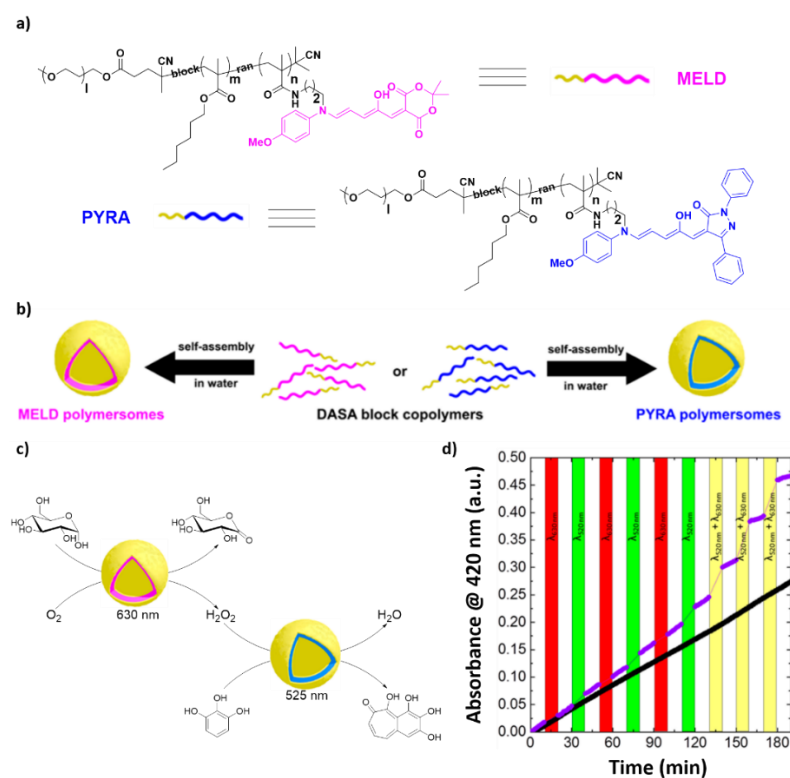
Figure 1-18 – a) DASA-functionalised methacrylate-PEG block copolymers, b) self-assembly of the DASA-polymers in aqueous media, c) biocatalytic cascade reaction utilising the polymersome nanoreactors, d) uv-vis spectroscopic monitoring of the cascade reaction, black line represents a blank reaction without nanoreactors. Data and diagrams reproduced from a previous report.[87]

1.3.2 Orthogonal photo-control

DASAs generally exhibit no significant absorption within the range of 300-450 nm, this provides an opportunity for inclusion of other photoswitching species that show activity within this area; an opportunity for wavelength-selective functionality. Feringa and co-workers exploited this through simultaneous activity of first-generation DASAs and azobenzenes, in toluene; whereby isomerisation of either moiety could take place, separately.[60] Following this, the photoswitches were linked through an alkyl chain, constructed from the nucleophilic substitution of a di-bromo alkane by the phenolic-half of an azobenzene. This was then further substituted to produce barbituric acid-derived DASAs. Irradiation of the newly-linked species at 370 nm led to the

expected *trans-cis* isomerisation of the azobenzene, and at 590 nm, initiated transformation of the DASA. Liu and Deng also reported a similar DASA-azo hybrid, again demonstrating the potential for orthogonal photo-control through relatively facile means.[61] This dyad was constructed through a three-step synthesis of bromination, nucleophilic substitution and finally nucleophilic opening of an activated furan core. The hybrid demonstrated the aptitude for selective switching and thermal reversion, revealing four distinct switchable states. It was then suspended in a polystyrene-based film, for the purposes of photopatterning, and demonstrating reversible light- and thermal-responsivity. Another example of a wavelength-selective dyad was the DASA-aurone introduced by Qu et al.; they found that four isomeric states could be realised, through three distinct irradiation wavelengths (365, 430 and 585 nm) and thermal relaxation.[59] Synthesised in a similar manner to the previously mentioned DASA-azo species, in which bromination and eventual nucleophilic substitution were required. As precursory work to their nanoreactor polymersomes (Figure 1-18), Read de Alaniz and co-workers demonstrated wavelength-selectivity using two second-generation DASAs.[48,84] The pair consisted of a Meldrum's acid-based *N*-methylaniline switch and a barbituric acid-derived 5-methoxyindoline species, providing excitation wavelengths of 514 and 650 nm, respectively. The following year, they proceeded to covalently attach other second-generation DASAs to acrylate and methacrylate polymers (Figure 1-19a). It was found that the glass transition (T_g) state of the polymer could have a profound effect on both forward and backward switching processes; isomerisation was hampered by more glassy matrices, as rigidity of the polymer chains prevented physical rearrangement of the DASA molecules. To demonstrate wavelength-selectivity, two copolymers were blended together; visible light exposure produced a photopatterned surface, which was fully reversible with the application of heat and cessation of irradiation (Figure 1-19b). This was one of many cases of DASA incorporation into functional materials, be it for photopatterning applications, the influence on surface wettability, or even temperature-sensing devices. Such examples shall be discussed in the next section.
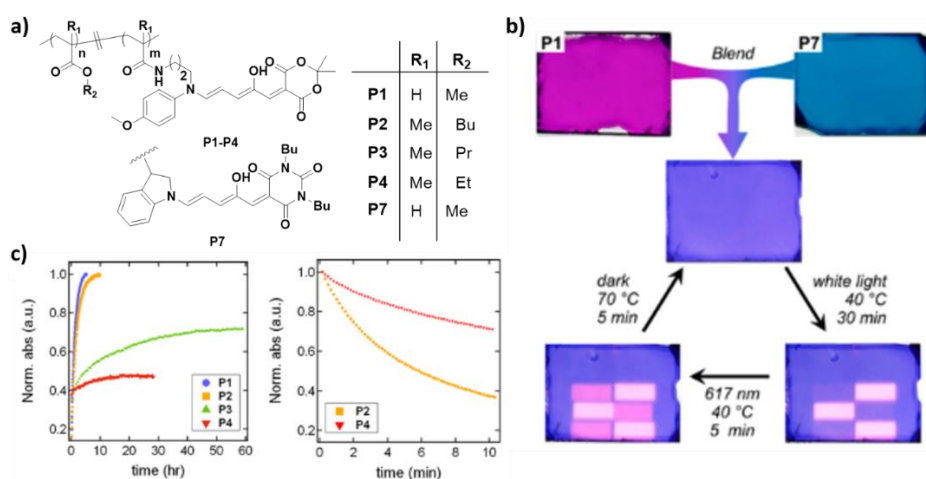
Figure 1-19 – a) DASA-functionalised acrylate and methacrylate polymers, b) physical blending of P1 and P7 with demonstrated photopatterning, c) thermal equilibrium of thin-film products P1-4 at 40 °C (left) and photoswitching of thin-films P2 and P4 (right) at 40 °C, under visible light - P1+2 above and P3+4 below their respective T$_g$s. Data and diagram reproduced from a previous report.[84]

1.3.3 Functional materials

The ability to convert between a vibrantly-coloured form and an isomer completely devoid of colour upon visible light irradiation is an attractive characteristic of DASAs, perfectly suited for photopatterning applications. Furthermore, their large polarity change enables influencing of surface wettability. The Singh group reported such an example, which included the covalent attachment of said photoswitches to a polycarbonate surface, afforded through appendation of branched polyethyleneimine (PEI).[80] Visible light irradiation of the PEI-DASA surfaces adorned with photomasks produced a striated pink and close-to-colourless appearance, with a line width of approximately 60 μm. Even more impressively, they demonstrated the ability for sub-micron precision by using a 3 μm test mask. A side-by-side comparison of uv-vis spectra and water contact angle (WCA) measurements indicated that a transformation of linear to cyclic isomer led to a reduction in the contact angle. This process was irreversible, likely due to the polarity of the surface stabilising the zwitterionic cyclic form. He et al. also produced a photopatterning device; they covalently-bound a first-generation DASA to a polystyrene-based copolymer.[82] The

DASA polarity change in this polystyrene-based system encouraged a 20.8 ° reduction in the WCA. They too found this process to be irreversible, surmising that the rigidity of polystyrene chains prevented a large physical rearrangement of the cyclic DASA pendants into the more sterically bulky linear forms. Biesalski, Seelinger and Nau applied hydroxypropyl cellulose (HPC)-ester polymers as nanoparticle coatings that produced superhydrophobic surfaces with WCAs of at least 150 ° and altered that angle through the inclusion of one of three different 1,3-dimethyl barbituric acid-derived DASAs – each varying in their N-alkyl chain length.[88] They had managed to encourage a complete reduction in the WCA, to 0 °, with one of the three DASAs, of which utilised didodecylamine as the donor unit. It was hypothesised that the alkyl chains of this DASA were experiencing intermolecular association with the nanoparticle surface's own alkyl chains, such that isomerisation encouraged switching of the surface polarity. Shorter alkyl chains led to solubility changes and longer chains potentially cause micelle formation, both effectively preventing interaction with the nanoparticle surface. Heating the sample to above 40 °C would cause the nanoparticle film to melt and combine to form a hydrophobic coating, making this a physically reversible process. Despite this, the colouration of the DASA could not redevelop in the solid state, as the HPC ester matrix stabilised the cyclic DASA isomer.

Not all examples of surface applications have been irreversible however, as shown by Zheng et al.[89] Polydopamine-coated (PDA) silica micro/nanoparticles (SP) were functionalised with first-generation DASAs. The modified SPs were immobilised onto glass substrates, via adhesive tape or cross-linked polydimethylsiloxane (PDMS). The inclusion of PDMS was to facilitate the successful reversion of the DASA-coatings, as adhesive tape demonstrated poor stability under 100 °C conditions. The authors had demonstrated reversible switching of the DASA-PDA coatings when bound to the SPs and directly to the glass substrate itself, although no explanation was given as to why this was possible. It is believed that the lack of long, free-flowing polymer chains in the PDA was a large factor that allowed the reversible, physical rearrangement of DASAs. The authors found that a small SP diameter would positively correlate with the wettability of the surface; a diameter of 0.2 μm encouraged a larger reduction in WCA than those of 85 μm, when

irradiated with green-light. The substantial polarity change of DASAs can also be used for deadhesion applications, as shown by Bardeen and Read de Alaniz.[83] They reported the light-dependent delamination of a polystyrene film from a glass substrate, through photoisomerisation of a third-generation DASA dopant physically pulling it away. Pull-off and shear adhesion measurements showed a direct proportionality between open-form DASA concentration and the force required to interrupt adhesion. It was found that DASA cyclisation could reduce the time taken to delaminate in aqueous conditions by 90%, at the highest loading employed (8 wt%). The practicality of this characteristic was demonstrated by a target molecule delivery experiment. A microscope well plate containing a red dye was adhered to another glass slide, using the aforementioned composite. The device had disassembled within 5 h of visible light irradiation, releasing the dye into the surrounding environment. Importantly, the reversion to a coloured state could not be achieved, unless the film was re-dissolved in DCM; most likely a consequence of the rigidity of polystyrene when below its T_g. The T-type photoswitchable nature of DASAs provides the opportunity for the facile construction of temperature-sensitive devices; demonstrated by Hooper and Read de Alaniz.[76] The device consisted of a dioctylamine-Meldrum's acid (donor-acceptor) species, dissolved into a polyurethane-based elastomer at 0.05 wt% (Figure 1-20a). The elastomer had shown an affinity for the cyclisation kinetics such that it would only revert upon heating; they had essentially created an elastomeric thermophore. The composite could be heated to 120 °C to reconstitute the DASA's coloured, open form, following this it could be safely stored for extended periods of time without the worry of decolourisation. This provided an avenue for a temperature-mapping device, demonstrated by perforation of the composite with ballistic projectiles. The localised temperature history could be examined, based on the vibrancy of the recovered DASA colouration (Figure 1-20b). The composite could then be recycled by long periods of visible light irradiation; however, it was noted that a degree of photodecomposition was seen (red reheat line) (Figure 1-20c). This study was one of the first to reveal the benefits of blending a DASA with polymers rather than covalently-binding them, as at the time, the latter had shown only irreversible photoswitching.[47,80,82]
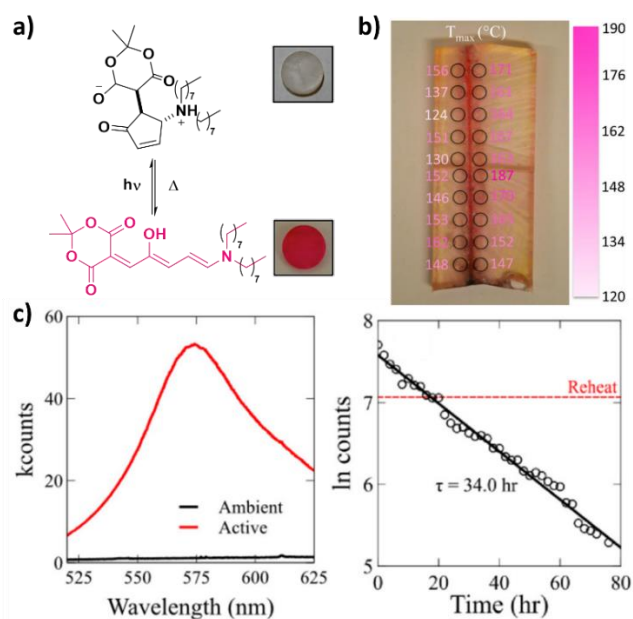
Figure 1-20 – a) Dioctyl-DASA, inset: polyurethane composite in both states; b) calculated localised temperatures, post-perforation with a 30 calibre rifle round; c) emission spectra of the colourless (ambient) and coloured (active) states (left) and the decay of fluorescence during visible light irradiation (right). Data and diagram reproduced from a previous report.[76]

The utility of DASAs in functional materials is constantly evolving; it was originally believed that first-generation DASAs would switch irreversibly when covalently-bound to polymers and surfaces,[90] however recent research has shown that this not true for all systems and can rely heavily on steric bulk.[78] The extent to which DASAs have been used for sensing applications shall be discussed in the next section.

1.3.4 Chemosensing

As demonstrated, DASAs exhibit thermo-sensing potential, consequential of their T-type nature. Another exploitable characteristic is their photoresponsivity, however they are not limited to just these two stimuli. They have also been employed to detect amines, nerve agent mimics, heavy metals and Lewis acids. A number of examples shall be discussed herein. The Wang group published a report that introduced dual-responsive polymer dots, through a facile grafting of MAF onto PEI, conducted in ethanol.[81] The nanoparticles were capable of light and pH

responsivity, and metal ion detection. They found that the DASA-PEI polymer dots would decolourise upon basification, or light irradiation, and recover their pink colouration upon acidification. The metal ion detection was afforded through the fluorescence of the polymer dots; found to be quenched by Fe^{3+} and Cu^{2+} ions in aqueous media. This fluorescence emission was not a product of PEI, DASA or the MAF moieties, but down to a combination of surface excited states. A second metal-detecting example was published by Qu and co-workers; describing the detection of Cu^{2+} ions, again through fluorescence quenching.[91] They used a dyad consisting of a second-generation DASA covalently-attached to 1,8-naphthalimide (NDI), a commonly used fluorophore. Fluorescence intensity of the species would increase when photoswitched to the cyclised-DASA isomer, as the linear form would quench the photoluminescence. They discovered a degree of acid and copper ion detection, too; upon dosing separate DASA-NDI chloroform solutions with trifluoroacetic acid and cupric acetate, fluorescence activity would decrease. It was reported that the quenching of fluorescence through acidic media was not reversible with the application of visible light, but was with the cupric acetate solution. DASAs have also seen use in the detection of nerve agent mimics, as reported by Lee and Balamurugan, featuring the diethyl cyanophosphate (DCNP).[92] They revealed first-generation DASAs covalently-bound to a RAFT-polymer. The polymer exhibited only forward photoswitching in a 1,4-dioxane solution, however reversion could be achieved through dark conditions and mild temperatures (40 °C) in chloroform. Following assessment of the photochromic properties of this new polymer, the detection of nerve agent mimics was investigated, such as DCNP, diethyl chlorophosphate (DCP), triethylphosphate and tributlyphosphate in a dioxane solution. It was found that addition of DCNP led to a marked decrease in visible light absorption, DCP less so and the other phosphates did not appear to produce a marked effect, therefore displaying a level of nerve agent selectivity. This was caused by the formation of a morpholino cation which disrupted the conjugation of the open DASA and eliminated the vibrant pink colouration (Figure 1-21). This process was only possible with the

open triene form of DASA, as the mechanism of action could not occur with an already pyramidal

nitrogen cation present, i.e. the cyclised species.
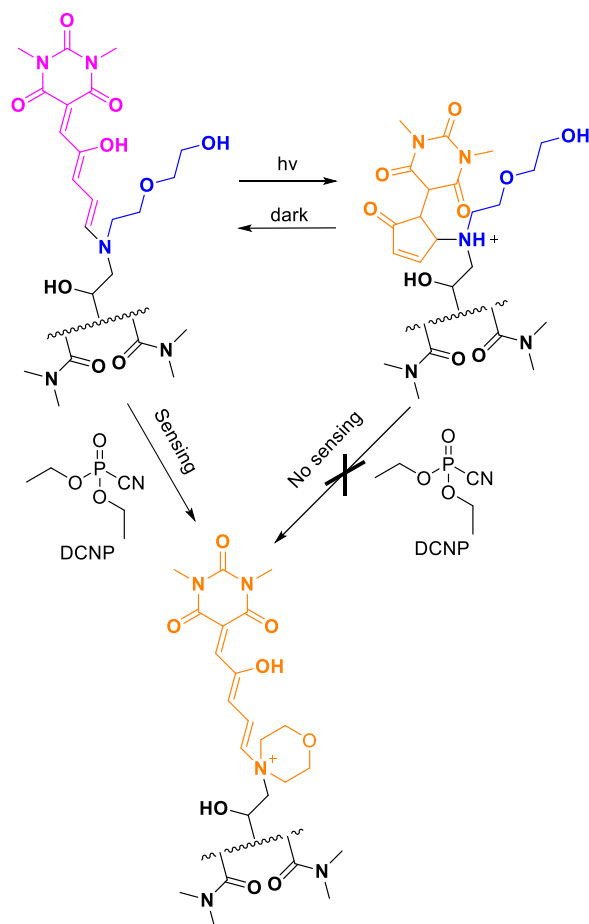
Figure 1-21 – Chemical structures of the three forms adopted by the nerve agent-detecting

DASA-polymer, showing that detection was only possible by exposure of the coloured form to

DCNP. Reproduced from a previous report.[92]

The synthetic route to DASAs is a convenient and accessible colourimetric amine-detection

platform. Reaction of an activated furan core, such as MAF, with a secondary amine yields a

vibrant purple to red-coloured species; a rapid and easily recognisable indicator for the presence

of amine. Naturally, this avenue was exploited by Read de Alaniz and co-workers to develop an

amine-detection device with sub-ppm sensitivity.[56] Their investigation elucidated that the amine

selectivity was possible; diethylamine (secondary) was found to react 11-times faster than

butylamine (primary) and 33-times faster than ammonia. Furthermore, they demonstrated that

MAF would react with diethylamine competitively in the presence of tertiary amines, thiols,

alcohols, phosphines and water. With this in hand, they utilised a great advantage of the second-generation DASAs, by demonstrating that different aromatic amines could be distinguished by colour analysis when spotted on a TLC plate – thanks to the visible light tunability that the aniline-based second-generation DASAs provide. They continued by demonstrating a practical example; the detection of volatile amines produced during food spoilage. They attempted the detection of fish decay, whereby nylon filter membranes soaked in a MAF-THF solution were placed in a sealed jar with either fresh cod or tilapia samples for 48 h. The findings were conclusive, in that the MAF-soaked filters underwent a drastic colour change, denoting DASA formation. Eventually, the same group had expanded the utility of the MAF amine-sensing platform.[57] In evaluating their initial investigation, they had determined that MAF immobilised onto a substrate such as filter paper and used for the detection of amines in solution, would inevitably leach into the surrounding environment. As such, this would severely limit its ability to detect amines in aqueous environments. Therefore, they developed a new Meldrum's acid-derived oxanorbornene acceptor moiety, and co-polymerised it through ring-opening metathesis (ROMP) (Figure 1-22).
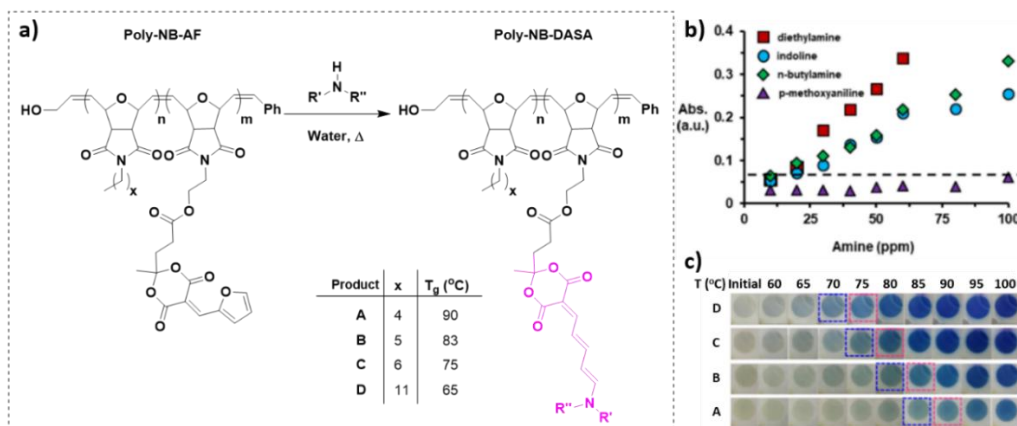
Figure 1-22 – a) Amination scheme of the Poly-NB-AF, b) the exposure of polymer film D to various aqueous amine solutions (10-100 ppm, 75 °C, 3 min), c) heating of bleached products A-D indicating the effect of T_g and potential temperature-mapping utility. Data and diagram reproduced from a previous report.[57]

The new polymer demonstrated amine responsivity and displayed remarkable stability in aqueous media. The alkyl chain lengths of the oxanorbornene monomers were varied in order to tune the T_g of the product polymer. The authors found that at a constant temperature, polymers with high T_gs would exhibit slower amine-reactivity, as the physical rearrangement of ring-opening would be subject to chain flexibility. Therefore, T_g played an important role in the responsivity of amine-detection and could be exploited as a thermal-sensing conduit, post-cyclisation. As such, ROMP polymers of varying T_gs were subjected to indoline-exposure to produce blue, second-generation DASA pendants, which were subsequently bleached with visible light. These polymers exhibited reversible switching and recoverable colouration upon heating, therefore they were subjected to heating at a steady rate. As the environmental temperature would reach the T_g of a specific polymer, the blue intensity of the indoline-based DASA would increase, in essence developing a visual map of temperature (Figure 1-22c) – similarly to their past investigation into first-generation doped polyurethane elastomers.[76]

Concerning sensing applications, DASAs constitute a versatile platform not only because of their photo- and thermo-responsivity, but also thanks to their chemo-selective behaviour. The aptitude for selective, rapid detection of amines has been shown; it has been proven that they can act as an indicating species for basic or acidic conditions; and demonstrated that they can yield responsivity toward certain heavy metals.

1.4 Polysiloxanes

Arguably the most popular inorganic polymers, polysiloxanes consist of a chain of alternating silicon and oxygen bonds, with the basic repeat unit of [-SiRR'-O-]$_n$. Their popularity is consequential of their unique and reliable properties; such as high thermal stability, flexibility and gas permeability, and their low T_gs, surface energy and chemical reactivity. The length of a Si-O bond is approximately 1.64 Å, with an average angle of 143 ° across a Si-O-Si bridge, contrastingly the average tetrahedral bond angle is 110 ° and a simple C-C bond has a length of 1.53 Å. Further yet, the Si-O bonds require very little energy to deform; the combination of these characteristics leads to a much greater flexibility in polysiloxanes, when compared to hydrocarbon-based organic polymers. Afforded by this great flexibility, is their low T_g, centred around -125 °C. Additionally, their side groups are able to rotate to the contact interface providing them with a low surface energy, hence making cross-linked polysiloxanes perfect for hydrophobic applications. Their thermal stability is afforded by the strength of their Si-O and Si-C bonds. Characteristics such as thermal stability and flexibility can be altered, however, simply by modifying the R-groups of the backbone. For example, introducing fluorine or phenyl side-groups can lead to an enhanced thermal stability, and implementing precursor silanes with functional vinyl groups can act as a platform for future cross-linking, improving their bulk rigidity.[93] As such, polysiloxanes are employed in a wide range of industrial and commercial devices; including sealants, coatings, adhesives for such areas as automation and construction, to the area of common kitchen utensils and even medical devices. The most commonly employed and synthetically simple polysiloxane is PDMS, greatly favoured for its low toxicity, low T_g, high flexibility and, most importantly for this body of work, its optical transparency.[94,95]

The synthetic precursors to polysiloxanes are functional organosilanes, such as dimethyldichlorosilane, with molecular formulae of $R_{4-n}SiX_n$ (X = Cl, OR_2, NR_2 or other hydrolysable substituents). These organosilanes are most commonly produced by what is known as the Direct Process; consisting of passing chloromethane vapour over a bed of silicon and copper metals, at elevated temperatures of 250-300 °C (Figure 1-23).[96]

$$\text{H}_3\text{C−Cl} \quad + \quad \text{Si} \quad \xrightarrow[\text{250-300 °C}]{\text{Cu}} \quad \underset{\underset{\text{Cl}}{|}}{\overset{\overset{\text{Cl}}{|}}{\text{H}_3\text{C−Si−Cl}}} \quad + \quad \underset{\underset{\text{Cl}}{|}}{\overset{\overset{\text{CH}_3}{|}}{\text{H}_3\text{C−Si−Cl}}} \quad + \quad \underset{\underset{\text{Cl}}{|}}{\overset{\overset{\text{CH}_3}{|}}{\text{H}_3\text{C−Si−Cl}}}$$
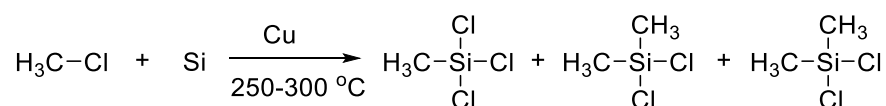
Figure 1-23 – Synthetic scheme for the Direct Process formation of a mixture of organosilanes from chloromethane vapour.

This process is modular in that the methyl groups can be substituted for species such as ethyl, phenyl or vinyl, thereby tailoring the structural properties of the desired organosilanes. The most industrially important product of this procedure is dimethyldichlorosilane, which is further hydrolysed to produce a mixture of oligomeric cyclic and silanol-terminated linear siloxanes, shown in Figure 1-24a. The ratio of cyclic to linear siloxanes, and the chain length of the latter, can be controlled by modification of the conditions; such as the ratio of chlorosilane to H_2O, the temperature and the solvents used. Additionally, a second one-step procedure exists whereby methanol is used instead of water; methanolysis. This eliminates the need to remove residual acid by washing (Figure 1-24b).

a)

b)
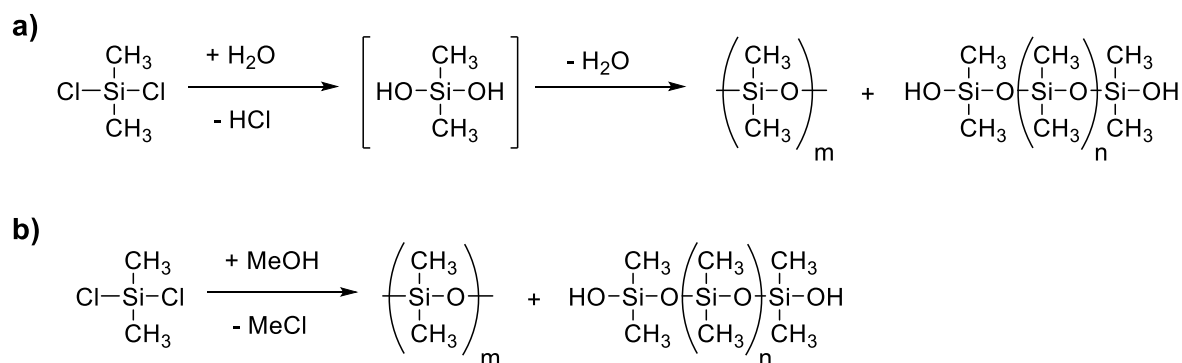
Figure 1-24 – Synthetic scheme for the a) hydrolysis of dimethyldichlorosilane and b) methanolysis of dimethyldichlorosilane, to produce a mixture of cyclic and silanol-terminated linear oligomeric siloxanes.

The linear products are generally employed for low to moderate molecular weight liquid and soft solid polysiloxanes, and the cyclic for more high molecular weight species for elastomer production. Linear siloxanes are polymerised by polycondensation reactions and cyclic siloxanes by cationic or anionic initiated ring-opening polymerisations. The polycondensation reaction has

been largely replaced by the ring-opening polymerisations, with regards to industrial settings.[97]

Both ring-opening polymerisations are generally performed with the cyclic trimer or tetramer siloxanes. Cationic ring-opening polymerisation is initiated with a strong protonic acid, such as sulphuric acid, that encourages the cyclic siloxane to ring-open. This process is then followed by concurrent polycondensation and chain polymerisation mechanisms. The anionic ring-opening route commonly employs basic metal hydroxides; initiation begins with the attack of an Si-O cyclic bond by the metal hydroxide anion. Both chains are then converted to silanolates and take part in the propagation, as such the reaction can instead be initiated by a pre-prepared silanolate species. This process is far less complex as only one mechanism is employed to produce the desired product; hence a large degree of conversion control is available. Termination of both ring-opening polymerisations can occur upon neutralisation of the initiating species, inclusion of an end-capping reagent such as trimethylchlorosilane, or the back-biting process – whereby a silanolate anion shall react with a δ-positive silicon atom from the same chain.

1.4.1 Polysiloxane cross-linking methods

The cross-linking of polysiloxanes allows for an expansion of the already versatile physical properties of these polymers. Three of the most popular methods for cross-linking PDMS shall briefly be described herein, they are: peroxide-curing, addition-curing and condensation-curing. Peroxide-curing relies on the formation of free radicals to encourage cross-linking, through the thermal decomposition of a peroxide species; whose nature can be acyl, arylalkyl or dialkyl-derived. The cross-linking reaction is initiated by the homolytic thermal cleavage of the peroxide into radical species, which then induce hydrogen abstraction from nearby siloxane methyl groups. The cross-link, a silethylene bridge, is then formed by dimerisation of the resultant methylene radicals, shown by Figure 1-25. The main disadvantage with this process is the entrapment of peroxide by-products.[98]
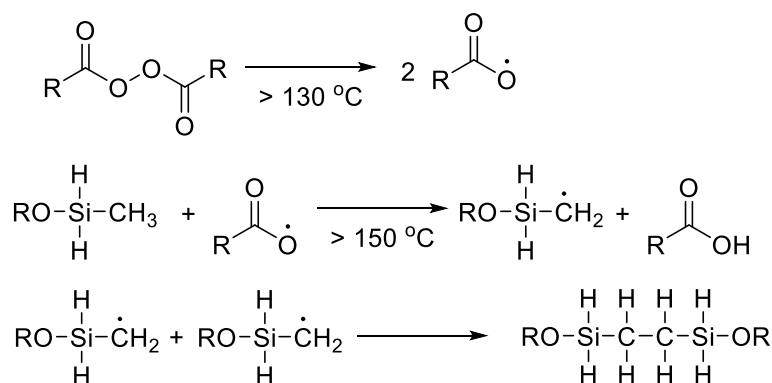
Figure 1-25 – Peroxide free radical cross-linking process of two siloxane chains.

The addition-cure system is a Pt-, or Rh-catalysed, cross-linking that occurs through hydrosilylation between vinyl-terminated PDMS chains and a cross-linking species functionalised with silicon hydrides across the backbone. An example reaction between such polymer chains is included as Figure 1.1-26, included beside the scheme is the structure of a common catalytic complex used for this process - Karstedt's catalyst. The cross-linking process can occur at room temperatures; hence this is known as a room-temperature vulcanisation (RTV), however it can be accelerated upon the application of heat. The process leaves no by-products other than trapped Pt residue, as such this curing method is widely used for silicone rubbers and coatings.[99]
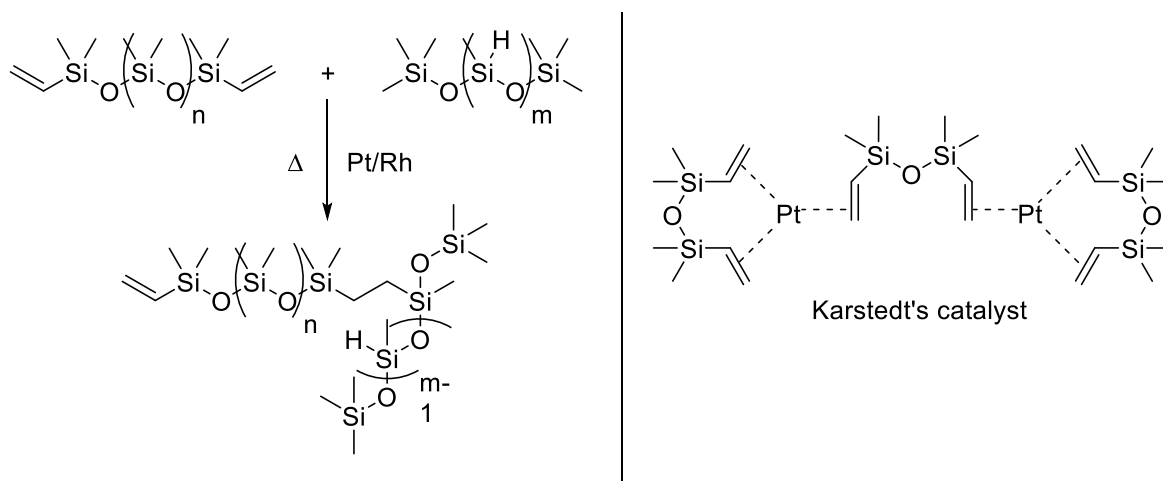
Figure 1.1-26 – Addition-cure cross-link reaction between two functional siloxanes.

The final method to be described here is the condensation-cure system, which has been utilised for the work described in this thesis. There are two sub-categories of condensation cross-linking

45

systems, known as RTV-1 and RTV-2; one-part and two-part RTV systems. The former is moisture-dependent, such that it relies on the in-diffusion of atmospheric moisture to drive the cross-linking process. The RTV-2 system does not rely on this stimulus, but can be accelerated by it, and usually employs an alkyoxysilane cross-linking species. Silanol-terminated linear polysiloxanes are generally the focus for this process, which undergo a hydrolytic condensation reaction with the alkyoxysilane species. The cross-linking reaction is commonly catalysed by an organotin or organotitanium complex, resulting in alcohol-based by-products and incorporation of the metal into the complex; therefore, these organometallic complexes aren't traditional catalysts. An example of the condensation cross-linking system used throughout this thesis is included as Figure 1-27. This process provides an inert, optically transparent, flexible network that is fitting for the entrapment of stimuli-responsive molecules.
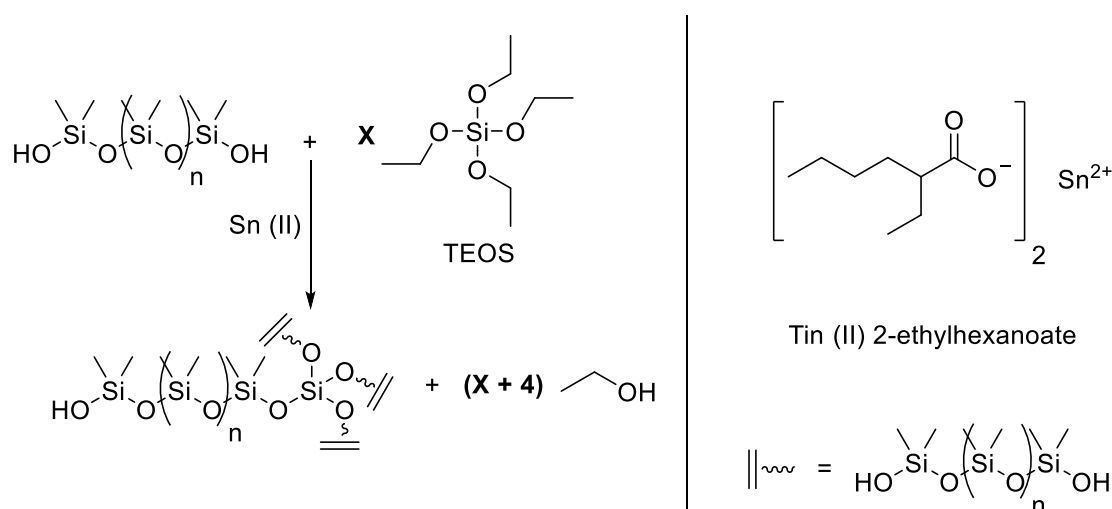
Figure 1-27 – The condensation-cure system used throughout this thesis, with the catalytic complex tin (II) 2-ethylhexanoate and cross-linking agent tetraethyl orthosilicate (TEOS).

1.5 Colourimetric detection of amines

Amine-sensing devices/materials have been utilised in industries such as explosives and drug detection,[100–102] to the monitoring of synthetic processes,[103] environmental pollution and working environment safety.[104–107] However, a much larger focus has been placed on the detection of medical conditions and,[108–112] more relevant to this thesis, the identification of food item spoilage.[109,112–118] The monitoring of meat/fish freshness generally relies on detection of the release of ammonia and certain biogenic amines, such as putrescine.[114,119,120] Techniques that rely on chemiresistivity[114] and fluorescence[117] measurements are able to provide close to sub-ppm detection limits, but usually require the use of an expensive setup and analytical equipment, and don't always allow for immediate *in-situ* examination. As such, cheaper, more readily-accessible alternatives can be found in the field of colourimetric sensing.[121] When exposed to stimuli such as pH,[122] heat,[76] light or force,[123,124] colourimetric sensors exhibit a colour change as a response. This enables convenient, rapid identification of analytes with the naked eye. Common stimuli-responsive materials that have been implemented into colourimetric sensing devices include: highly coloured metalloporphyrin complexes,[125,126] pH indicating dyes,[109,115] fluorescent moieties[110,127] and azobenzene-derivatives.[128,129] Some colourimetric methods are destructive in that spoilage is determined immediately through direct sensor contact with the product,[118] or through scanning of a dye-doped substrate that too requires contact with the product,[109,115,126] as such both techniques would break the seal of packaging in practical applications. Consequently, these methods could be seen as lacking in cost-efficiency, as the potential exists for fresh products to be wasted. Additionally, the requirement of specialised equipment is still present. Many non-destructive techniques have been demonstrated in the past, such as the In (III) octaethyl porphyrin complex detection system reported by Meyerhoff et al.[125] Their investigation exploited a dimer-monomer equilibrium that certain metallic porphyrins exhibit within polymeric media;[130] scission of the dimer-linking hydroxyl species was an indication of reactivity with gaseous amines. The process could be monitored through a decrease and increase in the absorption bands attributed to the dimer and

monomeric species, respectively. It should be noted however, that the expense of indium reduces the accessibility of this design. The Severin research group reported a novel sensing substrate consisting of a glass slide-bound PMMA film doped with 5 mol% of a coumarin-derivative.[131] Detection was denoted by a discolouration of the polymer film. The substrate reportedly detected the presence of gaseous putrescine and *n*-butylamine, but was not receptive to diethylamine or ammonia, limiting its general applicability. A further example of non-destructive food spoilage detection was published in 2012, by Ahmad and co-workers, they exploited the deprotonation susceptibility of polyaniline (PANI) in a composite film with polystyrene.[132] The PANI-polystyrene film was used as an internal label for sealed fish spoilage exposure trials, indication of the presence of ammonia was accompanied by a colour change of green to blue. The colour change was caused by deprotonation of the emeraldine salt (green) to form the emeraldine base (blue). This method had a slight disadvantage in that the PANI film production was a convoluted process, requiring multiple steps and extreme conditions. The non-destructive techniques discussed here all have a commonality; immobilising the stimuli-responsive species within or upon a surface that could exist as part of the packaging itself. This type of architecture allows for an immediate indication as to the freshness of the product, without the need for seal interference, hence eliminating the potential of wasted produce. Subsequently, they were of influence to chapter 2 of this thesis, introduced in the next section.

1.6 Amine-responsive cross-linked PDMS network

In 2017, it was shown by Read de Alaniz et al. that the synthetic route to DASAs could be exploited as an amine-sensing platform.[56] As already discussed in section 1.3.4, MAF presents itself as an ideal indicator for the presence of amines, as it reacts to form a brightly coloured chromophore. They continued this research by producing a new Meldrum's acid-derived acceptor based on oxanorbornene and co-polymerised it with other oxanorbornene derivatives.[57] This research, and the non-destructive food-spoilage detection techniques described in the previous section (1.5), were the inspiration for chapter 2 of this thesis. Presented in chapter 2, is the doping of a cross-linked PDMS network with MAF, to produce a colourimetric amine sensor that could be incorporated into the packaging of fresh meat and fish, for the non-destructive confirmation of spoilage. MAF was dissolved into DCM and mixed with silanol-terminated PDMS, cross-linking agent TEOS and a tin (II) catalyst complex solution (Figure 1-27). The loading of MAF was varied, in terms of weight percentage (wt%), relative to the mass of PDMS used, producing elastomeric networks that ranged from almost colourless to vibrant yellow. The mechanism of doping a receptive molecule into the network, rather than direct covalent attachment, can lead to leaching of said species into the environment.[57] However, this approach is facile and readily accessible, not requiring multiple-step procedures over long time-periods, as has been demonstrated previously.[133–135] The elastomers were subjected to multiple amine-exposure experiments, such as immersion in aqueous-amine solutions; exposure to amine vapours in a sealed container; and encased within an identical container that housed small cuttings of cod fillets, over the course of 24 hours. Amine detection was denoted by a colour change of the elastomers, from colourless (or yellow) to red. Colour changes were examined using image analysis in MATLAB and through uv-vis spectroscopy absorbance changes. A short follow-up study was undertaken, to investigate the possibility of amine-responsivity being detected through RFID tag impedance measurements.

1.7 Photoswitchable polymers

Photoswitchable polymers are a very interesting class of stimuli-responsive materials. The incorporation of photoswitches into polymers allows for the fabrication of materials with macroscopic properties that can be controlled through the external application of light. Photoswitches used in advanced materials commonly include spiropyran, spirooxazine, azobenzene, diarylethenes and, as discussed earlier (section 1.3.3), DASAs. Controllable properties are dependent on the chosen species. As previously mentioned (sections 1.1.1 and 1.1.2), azobenzenes are a perfect fit for actuating mechanisms as they experience a large degree of molecular volume change upon photoswitching, and spiropyrans exhibit great polarity change upon isomerisation – making them a natural choice for drug delivery systems. As such, a plethora of photoswitchable polymeric architectures have been demonstrated in the past, including photogelators,[136–138] molecular delivery devices,[139–141] photoactuators[142–144] and "smart" surfaces.[145–147]. These smart materials can be prepared by the incorporation of photoswitches into polymer matrices by several different methods: grafting onto the backbone,[148] incorporation into the main chain itself,[149] using structurally-modified switches as cross-linking species,[150] and physical blending/doping.[151] The first three methods all include a form of covalent-binding to the polymer, providing stability, a well-defined photoswitch concentration and preventing molecular aggregation. Although, these kinds of methods don't come without their disadvantages, such as the sometimes lengthy and convolute synthetic routes required and, at least in the case of DASAs, an inhibition of reversible switching below the host T_g. The doping of photoswitches into polymer networks is the most synthetically convenient method, as it only requires dissolution of the photoswitch into the polymer itself, allowing for convenient concentration tuning and easy variation on the photoswitch/polymer combination. Admittedly, this method is limited in that photoswitch leaching can occur and in some cases photoswitch crystallisation is possible.[152] Despite this, photoswitch-doping has remained a popular method through which the solid-state behaviour of light-responsive species can be examined.[77,153–156]

1.8 Photo-responsive cross-linked PDMS network

Cross-linked PDMS is a cost effective, flexible, processable, largely unreactive and optically transparent matrix that is conveniently producible (Figure 1-27, section 1.4.1), making it a perfect choice for the entrapment of photoswitchable species. Photoswitches such as spiropyrans, spirooxazines, diarylethenes and azobenzenes have been incorporated into PDMS networks through doping in the past.[157–161] Contrastingly, at present there are no reports on the inclusion of DASAs into PDMS-based systems; the closest example being that of immobilisation of silica nanoparticles modified with a DASA-functionalised polydopamine coating, onto a glass substrate, using cross-linked PDMS.[89] As such, the third chapter of this thesis focusses on the dissolution of a DASA species into PDMS, with subsequent cross-linking, using TEOS and a tin (II) catalyst complex solution. The DASA was incorporated at various loadings, of weight percentage (wt%), with respect to the mass of silanol-terminated PDMS employed. Teflon tile moulds were used to produce elastomer pads, these pads were subjected to infrared (IR) spectroscopic analysis and powder x-ray diffraction (PXRD); the latter, to ascertain the presence of DASA crystallisation. The chapter presents a kinetic study of the photoswitching and thermal reversion processes of the PDMS-DASA networks, using uv-vis spectroscopy, with a focus on the consequences of increased DASA concentration. Also included are: short studies investigating multiple photoswitching cycles of the lowest-loading composite; solvent swelling and the effect it has on photoswitching a PDMS-DASA network; and a preliminary examination into the viability of using a PDMS-DASA thin film as a substrate for light sensing in the field of RFID technology.

1.9 Aims and objectives

This thesis describes the production of stimuli-responsive cross-linked PDMS networks, through facile, accessible means. The investigations centre around the new class of visible light photoswitches, DASAs, either through the amine-sensitivity of their synthetic pathway or the light-responsivity that they inherently provide.

Chapter one has been an introduction to DASAs; their visible light absorption profile, behaviour in a variety of media, how structural modification can influence their behaviour, a mechanistic insight into their switching pathway and how they have presently been employed in academic research. A brief introduction to other, more traditional photoswitches has also been given. The versatile, processable polymer PDMS was introduced, with an insight into the most common cross-linking methods.

Chapter two of this thesis presents the development of an amine-sensing device composed of a DASA-precursor immobilised in a cross-linked PDMS network. Facile production without the need for extreme conditions and a simple but rapid detection mechanism, are described. Utility of the device is provided through qualitative and quantitative confirmation of amine detection in a simulated packaging environment. Performance of the platform in aqueous solution is also examined, by image analysis and uv-vis spectroscopy. Finally, a thin-film derivative is applied to an RFID tag and exposed to a similar packaging scenario, whereby the tag sensor value output is measured before and after.

Chapter three concerns the doping of cross-linked PDMS networks with DASAs, to produce a photo-responsive device. Again, a facile and accessible procedure to a stimuli-responsive platform is described. Two versions of the synthetic procedure are presented; air-curing of the elastomers and curing in a sealed container – to provide a solvent-rich atmosphere. The elastomers are subjected to PXRD analysis, to quantify the crystallisation of DASAs and how it is affected by the production pathway variation. Forward and backward photoswitching kinetics of the immobilised DASA are analysed using uv-vis spectroscopy and an exponential decay

model. The effects of photoswitch concentration on the aforementioned processes are investigated. Further studies include the effects of solvent swelling on photoswitching kinetics and a preliminary investigation into the utility of this platform for RFID sensing technology.

Chapter four reports multiple attempts at covalent modification of polymeric backbones, to produce DASA-polymer conjugates. This included PEI modification; synthesis of a barbituric acid-derived polymer, from a polyurea; and platinum-catalysed hydrosilylation of a siloxane chain, to transform it into an active site for DASA-appendation. Although not all were successful, the aim of this chapter was to report what was found and inform future investigations.

Chapter five is a closing conclusion of this work, describing and justifying what has been found.

1.10 References

1   V. I. Minkin, *Molecular Switches*, Wiley-VCH, Weinheim, Second edition, 2011.

2   H. Bouas-Laurent and H. Dürr, *Pure Appl. Chem*, 2001, **73**, 639–665.

3   G. Mayer and A. Hechel, *Angew. Chemie - Int. Ed.*, 2006, **45**, 4900–4921.

4   S. Iamsaard, S. J. Aßhoff, B. Matt, T. Kudernac, J. J. L. M. Cornelissen, S. P. Fletcher and N. Katsonis, *Nat. Chem.*, 2014, **6**, 229–235.

5   M. Baroncini, S. D'Agostino, G. Bergamini, P. Ceroni, A. Comotti, P. Sozzani, I. Bassanetti, F. Grepioni, T. M. Hernandez, S. Silvi, M. Venturi and A. Credi, *Nat. Chem.*, 2015, **7**, 634–640.

6   B. Lebeau and P. Innocenzi, *Chem. Soc. Rev.*, 2011, 40, 886–906.

7   R. S. Stoll and S. Hecht, *Angew. Chemie - Int. Ed.*, 2010, **49**, 5054–5075.

8   V. Blanco, D. A. Leigh and V. Marcos, *Chem. Soc. Rev.*, 2015, **44**, 5341–5370.

9   D.-H. Qu, Q.-C. Wang, Q.-W. Zhang, X. Ma and H. Tian, *Chem. Rev.*, 2015, **115**, 7543–7588.

10   W. Szymański, J. M. Beierle, H. A. V. Kistemaker, W. A. Velema and B. L. Feringa, *Chem. Rev.*, 2013, **113**, 6114–6178.

11   W. A. Velema, W. Szymanski and B. L. Feringa, *J. Am. Chem. Soc.*, 2014, **136**, 2178–2191.

12   J. Broichhagen, J. A. Frank and D. Trauner, *Acc. Chem. Res.*, 2015, **48**, 1947–1960.

13   A. A. Beharry and G. A. Woolley, *Chem. Soc. Rev.*, 2011, **40**, 4422–4437.

14   K. Stranius and K. Börjesson, *Scientific Reports,* 2017, **7**, 1-9.

15   B. Mravec, J. Filo, K. Csicsai, V. Garaj, M. Kemka, A. Marini, M. Mantero, A. Bianco and M. Cigáň, *Phys. Chem. Chem. Phys.*, 2019, **21**, 24749–24757.

16   D. J. Van Dijken, P. Kovaříček, S. P. Ihrig and S. Hecht, *J. Am. Chem. Soc.*, 2015, **137**, 14982–

14991.

17   V. A. Barachevsky, *Rev. J. Chem.*, 2017, **7**, 334–371.

18   F. Hamon, F. Djedaini-Pilard, F. Barbot and C. Len, *Tetrahedron*, 2009, **65**, 10105–10123.

19   C. Renner and L. Moroder, *ChemBioChem*, 2006, **7**, 868–878.

20   C. Brieke, F. Rohrbach, A. Gottschalk, G. Mayer and A. Heckel, *Angew. Chemie - Int. Ed.*, 2012, **51**, 8446–8476.

21   E. Pantuso, G. De Filpo and F. P. Nicoletta, *Adv. Opt. Mater.*, 2019, **7**, 1–35.

22   D. J. W. Bullock, C. W. N. Cumper and A. I. Vogel, *J. Chem. Soc.*, 1965, 5316–5323.

23   C. Alvarez-Lorenzo, L. Bromberg and A. Concheiro, *Photochem. Photobiol.*, 2009, **85**, 848–860.

24   Y. Yu, M. Nakano and T. Ikeda, *Nature*, 2003, **425**, 145.

25   A. Mourot, M. A. Kienzler, M. R. Banghart, T. Fehrentz, F. M. E. Huber, M. Stein, R. H. Kramer and D. Trauner, *ACS Chem. Neurosci.*, 2011, **2**, 536–543.

26   D. A. James, D. C. Burns and G. A. Woolley, *Protein Eng.*, 2001, **14**, 983–991.

27   A. A. Beharry, O. Sadovski and G. A. Woolley, *Org. Biomol. Chem.*, 2008, **6**, 4323–4332.

28   A. A. Beharry, O. Sadovski and G. A. Woolley, *J. Am. Chem. Soc.*, 2011, **133**, 19684–19687.

29   M. Dong, A. Babalhavaeji, S. Samanta, A. A. Beharry and G. A. Woolley, *Acc. Chem. Res.*, 2015, **48**, 2662–2670.

30   H. Nishioka, X. Liang, H. Kashida and H. Asanuma, *Chem. Commun.*, 2007, 4354–4356.

31   K. Rück-Braun, S. Kempa, B. Priewisch, A. Richter, S. Seedorff and L. Wallach, *Synthesis (Stuttg).*, 2009, 4256–4267.

32   M. Bletz, U. Pfeifer-Fukumura, U. Kolb and W. Baumann, *J. Phys. Chem. A*, 2002, **106**,

2232–2236.

33   H. Il Lee, W. Wu, J. K. Oh, L. Mueller, G. Sherwood, L. Peteanu, T. Kowalewski and K. Matyjaszewski, *Angew. Chemie - Int. Ed.*, 2007, **46**, 2453–2457.

34   B. S. Lukyanov and M. B. Lukyanova, *Chem. Heterocycl. Compd.*, 2005, **41**, 281–311.

35   A. K. Chibisov and H. Gorner, *J. Phys. Chem. A*, 1997, **101**, 4305–4312.

36   Y. Shiraishi, M. Itoh and T. Hirai, *Phys. Chem. Chem. Phys.*, 2010, **12**, 13737–13745.

37   R. Klajn, *Chem. Soc. Rev.*, 2014, **43**, 148–184.

38   A. Radu, R. Byrne, N. Alhashimy, M. Fusaro, S. Scarmagnani and D. Diamond, *J. Photochem. Photobiol. A Chem.*, 2009, **206**, 109–115.

39   K. Uchida, T. Ishikawa, M. Takeshita and M. Irie, *Tetrahedron*, 1998, **54**, 6627–6638.

40   S. Nakamura and M. Irie, *J. Org. Chem.*, 1988, **53**, 6136–6138.

41   M. Irie, T. Fukaminato, K. Matsuda and S. Kobatake, *Chem. Rev.*, 2014, **114**, 12174–12277.

42   T. Hirose, M. Irie and K. Matsuda, *Adv. Mater.*, 2008, **20**, 2137–2141.

43   D. Bléger and S. Hecht, *Angew. Chemie - Int. Ed.*, 2015, **54**, 11338–11349.

44   M. Wegener, M. J. Hansen, A. J. M. Driessen, W. Szymanski and B. L. Feringa, *J. Am. Chem. Soc.*, 2017, **139**, 17979–17986.

45   J. Garcia-Amorós, A. Bučinskas, M. Reig, S. Nonell and D. Velasco, *J. Mater. Chem. C*, 2014, **2**, 474–480.

46   A. Thomas Bens, D. Frewert, K. Kodatis, C. Kryschi, H.-D. Martin and H. P. Trommsdorff, *European J. Org. Chem.*, 1998, **1998**, 2333–2338.

47   S. Helmy, F. A. Leibfarth, S. Oh, J. E. Poelma, C. J. Hawker and J. R. De Alaniz, *J. Am. Chem.*

Soc., 2014, **136**, 8169–8172.

48 J. R. Hemmer, S. O. Poelma, N. Treat, Z. A. Page, N. D. Dolinski, Y. J. Diaz, W. Tomlinson, K. D. Clark, J. P. Hooper, C. Hawker and J. Read De Alaniz, *J. Am. Chem. Soc.*, 2016, **138**, 13960–13966.

49 J. R. Hemmer, Z. A. Page, K. D. Clark, F. Stricker, N. D. Dolinski, C. J. Hawker and J. Read De Alaniz, *J. Am. Chem. Soc*, 2018, **140**, 18.

50 J. Stenhouse, *Justus Liebigs Ann. Chem.*, 1870, **156**, 197.

51 K. Honda, H. Komizu and M. Kawasaki, *J. Chem. Soc. - Series Chem. Commun.*, 1982, 253–254.

52 P. Šafář, F. Považanec, N. Prónayová, P. Baran, G. Kickelbick, J. Kožíšek and M. Breza, *Collect. Czechoslov. Chem. Commun.*, 2000, **65**, 1911–1938.

53 F. Bigi, S. Carloni, L. Ferrari, R. Maggi, A. Mazzacani and G. Sartori, *Tetrahedron Lett.*, 2001, **42**, 5203–5205.

54 C. Piutti and F. Quartieri, *Molecules*, 2013, **18**, 12290–12312.

55 M. J. Riveira, L. A. Marsili and M. P. Mischne, *Org. Biomol. Chem.*, 2017, 15, 9255–9274.

56 Y. J. Diaz, Z. A. Page, A. S. Knight, N. J. Treat, J. R. Hemmer, C. J. Hawker and J. Read de Alaniz, *Chem. - A Eur. J.*, 2017, **23**, 3562–3566.

57 Q. Chen, Y. J. Diaz, M. C. Hawker, M. R. Martinez, Z. A. Page, S. Xiao-An Zhang, C. J. Hawker and J. Read De Alaniz, *Macromolecules*, 2019, **52**, 4370–4375.

58 M. M. Lerch, W. Szymański and B. L. Feringa, *Chem. Soc. Rev.*, 2018, 47, 1910–1937.

59 M. Li, S. Yang, W. Liang, X. Zhang and D. Qu, *Dye. Pigment.*, 2019, **166**, 239–244.

60 M. M. Lerch, M. J. Hansen, W. A. Velema, W. Szymanski and B. L. Feringa, *Nat. Commun.*, 2016, **7**, 1–10.

61   F. Y. Tang, J. N. Hou, K. X. Liang, Y. N. Y. Liu, L. Deng and Y. N. Y. Liu, *New J. Chem.*, 2017, **41**, 6071–6075.

62   C. García-Iriepa, M. Marazzi and D. Sampedro, *ChemPhotoChem*, 2019, **3**, 866–873.

63   S. Helmy, S. Oh, F. A. Leibfarth, C. J. Hawker and J. Read De Alaniz, *J. Org. Chem.*, 2014, **79**, 11316–11329.

64   N. Mallo, E. D. Foley, H. Iranmanesh, A. D. W. Kennedy, E. T. Luis, J. Ho, J. B. Harper and J. E. Beves, *Chem. Sci.*, 2018, **9**, 8242–8252.

65   N. Mallo, P. T. Brown, H. Iranmanesh, T. S. C. MacDonald, M. J. Teusner, J. B. Harper, G. E. Ball and J. E. Beves, *Chem. Commun.*, 2016, **52**, 13576–13579.

66   Y. Yang, R. P. Hughes and I. Aprahamian, *J. Am. Chem. Soc.*, 2014, **136**, 13190–13193.

67   W. König, *J. für Prakt. Chemie*, 1926, **112**, 1–36.

68   M. M. Lerch, M. Medved, A. Lapini, A. D. Laurent, A. Iagatti, L. Bussotti, W. Szymański, W. J. Buma, P. Foggi, M. Di Donato and B. L. Feringa, *J. Phys. Chem. A*, 2018, **122**, 955–964.

69   M. M. Lerch, S. J. Wezenberg, W. Szymanski and B. L. Feringa, *J. Am. Chem. Soc.*, 2016, **138**, 6344–6347.

70   M. M. Lerch, M. Di Donato, A. D. Laurent, M. Medved, A. Iagatti, L. Bussotti, A. Lapini, W. J. Buma, P. Foggi, W. Szymański and B. L. Feringa, *Angew. Chemie Int. Ed.*, 2018, **58**, 8063–8068.

71   H. Zulfikri, M. A. J. Koenis, M. M. Lerch, M. Di Donato, W. Szymański, C. Filippi, B. L. Feringa and W. J. Buma, *J. Am. Chem. Soc.*, 2019, **141**, 7376–7384.

72   M. Di Donato, M. M. Lerch, A. Lapini, A. D. Laurent, A. Iagatti, L. Bussotti, S. P. Ihrig, M. Medved, D. Jacquemin, W. Szymański, W. J. Buma, P. Foggi and B. L. Feringa, *J. Am. Chem. Soc.*, 2017, **139**, 15596–15599.

73   J. N. Bull, E. Carrascosa, N. Mallo, M. S. Scholz, G. Da Silva, J. E. Beves and E. J. Bieske, *J. Phys. Chem. Lett.*, 2018, **9**, 665–671.

74   A. D. Laurent, M. Medve and D. Jacquemin, *ChemPhysChem*, 2016, 1846–1851.

75   A. Belhboub, F. Boucher and D. Jacquemin, *J. Mater. Chem. C*, 2017, **5**, 1624–1631.

76   B. P. Mason, M. Whittaker, J. Hemmer, S. Arora, A. Harper, S. Alnemrat, A. McEachen, S. Helmy, J. Read de Alaniz and J. P. Hooper, *Appl. Phys. Lett.*, 2016, **108**, 041906-1–4.

77   B. F. Lui, N. T. Tierce, F. Tong, M. M. Sroda, H. Lu, J. Read De Alaniz and C. J. Bardeen, *Photochem. Photobiol. Sci.*, 2019, **18**, 1587–1595.

78   J. E. Yap, N. Mallo, D. S. Thomas, J. E. Beves and M. H. Stenzel, *Polym. Chem.*, 2019, **10**, 6515–6522.

79   S. O. Poelma, S. S. Oh, S. Helmy, A. S. Knight, G. L. Burnett, H. T. Soh, C. J. Hawker and J. Read De Alaniz, *Chem. Commun.*, 2016, **52**, 10525–10528.

80   S. Singh, K. Friedel, M. Himmerlich, Y. Lei, G. Schlingloff and A. Schober, *ACS Macro Lett.*, 2015, **4**, 1273–1277.

81   D. Zhong, Z. Cao, B. Wu, Q. Zhang and G. Wang, *Sensors Actuators, B Chem.*, 2018, **254**, 385–392.

82   G. Sinawang, B. Wu, J. Wang, S. Li and Y. He, *Macromol. Chem. Phys.*, 2016, **217**, 2409–2414.

83   S. H. Mostafavi, W. Li, K. D. Clark, F. Stricker, J. R. De Alaniz and C. J. Bardeen, *Macromolecules*, 2019, **52**, 6311–6317.

84   S. Ulrich, J. R. Hemmer, Z. A. Page, N. D. Dolinski, O. Rifaie-Graham, N. Bruns, C. J. Hawker, L. F. Boesel and J. Read De Alaniz, *ACS Macro Lett.*, 2017, **6**, 738–742.

85   T. Senthilkumar, L. Zhou, Q. Gu, L. Liu, F. Lv and S. Wang, *Angew. Chemie - Int. Ed.*, 2018,

57, 13114–13119.

86   Y. Chen, Z. Li, H. Wang, Y. Pei, Y. Shi and J. Wang, *Langmuir*, 2018, **34**, 2784–2790.

87   O. Rifaie-Graham, S. Ulrich, N. F. B. Galensowske, S. Balog, M. Chami, D. Rentsch, J. R. Hemmer, J. Read De Alaniz, L. F. Boesel and N. Bruns, *J. Am. Chem. Soc.*, 2018, **140**, 8027–8036.

88   M. Nau, D. Seelinger and M. Biesalski, *Adv. Mater. Interfaces*, 2019, **6**, 1–5.

89   H. Zhao, D. Wang, Y. Fan, M. Ren, S. Dong and Y. Zheng, *Langmuir*, 2018, **34**, 15537–15543.

90   J. F. Gohy and Y. Zhao, *Chem. Soc. Rev.*, 2013, **42**, 7117–7129.

91   S. Yang, J. Liu, Z. Cao, M. Li, Q. Luo and D. Qu, *Dye. Pigment.*, 2018, **148**, 341–347.

92   A. Balamurugan and H. Il Lee, *Macromolecules*, 2016, **49**, 2568–2574.

93   R. J. Young and P. A. Lovell, *Introduction to Polymers*, CRC Press, Boca Raton, Third Edit., 2011.

94   J. C. Lötters, W. Olthuis, P. H. Veltink and P. Bergveld, *J. Micromechanics Microengineering*, 1997, **7**, 145–147.

95   J. N. Lee, C. Park and G. M. Whitesides, *Anal. Chem.*, 2003, **75**, 6544–6554.

96   H. F. Mark, *Encyclopedia of Polymer Science and Technology*, Joh, Hoboken, Third Edit., 2004.

97   J. E. Mark, H. R. Allcock and R. West, *Inorganic Polymers*, Oxford University Press, New York, Second Edi., 2005, vol. 5.

98   S. B. Lin, L. D. Durfee, A. A. Knott and G. K. Schalau, *Technology of pressure-sensitive adhesives and products*, CRC Press, Boca Raton, 2008.

99   D. Ahn and A. Dhinojwala, *Silicone Surface Science*, Springer, New York, 2012, vol. 4.

100   T. Fan, W. Xu, J. Yao, Z. Jiao, Y. Fu, D. Zhu, Q. He, H. Cao and J. Cheng, *ACS Sensors*, 2016, **1**, 312–317.

101   S. W. Thomas, G. D. Joly and T. M. Swager, *Chem. Rev.*, 2007, 107, 1339–1386.

102   X. Sun, Y. Wang and Y. Lei, *Chem. Soc. Rev.*, 2015, **44**, 8019–8061.

103   F. Gaggini, A. Porcheddu, G. Reginato, M. Rodriquez and M. Taddei, *J. Comb. Chem.*, 2004, **6**, 805–810.

104   M. Comes, M. D. Marcos, R. Martínez-Máñez, F. Sancenón, L. A. Villaescusa, A. Graefe and G. J. Mohr, *J. Mater. Chem.*, 2008, **18**, 5815–5823.

105   L. Sutarlie and K. L. Yang, *Sensors Actuators, B Chem.*, 2008, **134**, 1000–1004.

106   H. N. Kim, Z. Guo, W. Zhu, J. Yoon and H. Tian, *Chem. Soc. Rev.*, 2011, 40, 79–93.

107   N. A. Rakow and K. S. Suslick, *Nature*, 2000, **406**, 710–713.

108   K. E. Secor and T. E. Glass, *Org. Lett.*, 2004, **6**, 3727–3730.

109   N. A. Rakow, A. Sen, M. C. Janzen, J. B. Ponder and K. S. Suslick, *Angew. Chemie - Int. Ed.*, 2005, **44**, 4528–4532.

110   A. Satrijo and T. M. Swager, *J. Am. Chem. Soc.*, 2007, **129**, 16020–16028.

111   P. A. Peixoto, A. Boulangé, M. Ball, B. Naudin, T. Alle, P. Cosette, P. Karuso and X. Franck, *J. Am. Chem. Soc.*, 2014, **136**, 15248–15256.

112   M. Gao, S. Li, Y. Lin, Y. Geng, X. Ling, L. Wang, A. Qin and B. Z. Tang, *ACS Sensors*, 2016, **1**, 179–184.

113   A. Pacquit, K. T. Lau, H. McLaughlin, J. Frisby, B. Quilty and D. Diamond, *Talanta*, 2006, **69**, 515–520.

114   S. F. Liu, A. R. Petty, G. T. Sazama and T. M. Swager, *Angew. Chemie - Int. Ed.*, 2015, **54**, 6554–6557.

115   U. Khulal, J. Zhao, W. Hu and Q. Chen, *RSC Adv.*, 2016, **6**, 4663–4672.

116   S. Bhadra, C. Narvaez, D. J. Thomson and G. E. Bridges, *Talanta*, 2015, **134**, 718–723.

117   Y. Hu, X. Ma, Y. Zhang, Y. Che and J. Zhao, *ACS Sensors*, 2016, **1**, 22–25.

118   Z. Li and K. S. Suslick, *ACS Sensors*, 2016, **1**, 1330–1335.

119   J. Karovičová and Z. Kohajdová, *Chem. Pap.*, 2005, **59**, 70–79.

120   A. Naila, S. Flint, G. Fletcher, P. Bremer and G. Meerdink, *J. Food Sci.*, 2010, **75**, 139–150.

121   K. L. Bicker, S. L. Wiskur and J. J. Lavigne, *Chemosensors: Principles, Strategies and Applications*, John Wiley & Sons, Inc., Hoboken, 2011.

122   J. Courbat, D. Briand, J. Damon-Lacoste, J. Wöllenstein and N. F. de Rooij, *Sensors Actuators, B Chem.*, 2009, **143**, 62–70.

123   Y. Chen, Q. Fu, D. Li, J. Xie, D. Ke, Q. Song, Y. Tang and H. Wang, *Anal. Bioanal. Chem.*, 2017, **409**, 6567–6574.

124   D. A. Davis, A. Hamilton, J. Yang, L. D. Cremar, D. Van Gough, S. L. Potisek, M. T. Ong, P. V. Braun, T. J. Martínez, S. R. White, J. S. Moore and N. R. Sottos, *Nature*, 2009, **459**, 68–72.

125   W. Qin, P. Parzuchowski, W. Zhang and M. E. Meyerhoff, *Anal. Chem.*, 2003, **75**, 332–340.

126   H. Xiao-Wei, L. Zhi-Hua, Z. Xiao-Bo, S. Ji-Yong, M. Han-Ping, Z. Jie-Wen, H. Li-Min and M. Holmes, *Food Chem.*, 2016, **197**, 930–936.

127   A. R. Longstreet, M. Jo, R. R. Chandler, K. Hanson, N. Zhan, J. J. Hrudka, H. Mattoussi, M. Shatruk and D. T. McQuade, *J. Am. Chem. Soc.*, 2014, **136**, 15493–15496.

128   G. J. Mohr, C. Demuth and U. E. Spichiger-Keller, *Anal. Chem.*, 1998, **70**, 3868–3873.

129   E. Mertz and S. C. Zimmerman, *J. Am. Chem. Soc.*, 2003, **125**, 3424–3425.

130   E. D. Steinle, S. Amemiya, P. Buhlmann and M. E. Meyerhoff, *Anal. Chem.*, 2000, **72**, 5766–5773.

131   K. Crowley, A. Pacquit, J. Hayes, K. T. Lau and D. Diamond, *Proc. IEEE Sensors*, 2005, **2005**, 754–757.

132   B. Kuswandi, Jayus, A. Restyana, A. Abdullah, L. Y. Heng and M. Ahmad, *Food Control*, 2012, **25**, 184–189.

133   Y. S. Nam, I. Yoo, O. Yarimaga, I. S. Park, D. H. Park, S. Song, J. M. Kim and C. W. Lee, *Chem. Commun.*, 2014, **50**, 4251–4254.

134   M. E. Genovese, A. Athanassiou and D. Fragouli, *J. Mater. Chem. A*, 2015, **3**, 22441–22447.

135   Z. Zhao and J. Tian, *J. Appl. Polym. Sci.*, 2017, **134**, 1–9.

136   C. C. Phys ; Dry, S. R. . J. Struct ; White, J. M. Kelly, C. B. Mcardle, M. J. F. Maunder, V. Ramamurthy and K. Venkatesan, *Chem. Mater.*, 2004, **16**, 3982–3984.

137   K. M. Gattás-Asfura, E. Weisman, F. M. Andreopoulos, M. Micic, B. Muller, S. Sirpal, S. M. Pham and R. M. Leblanc, *Biomacromolecules*, 2005, **6**, 1503–1509.

138   S. J. Wezenberg, C. M. Croisetu, M. C. A. Stuart and B. L. Feringa, *Chem. Sci.*, 2016, **7**, 4341–4346.

139   Y. Wang, P. Han, H. Xu, Z. Wang, X. Zhang and A. V Kabanov, *Langmuir*, 2010, **26**, 709–715.

140   S. Son, E. Shin and B. S. Kim, *Biomacromolecules*, 2014, **15**, 628–634.

141   G. Petriashvili, L. Devadze, T. Zurabishvili, N. Sepashvili and K. Chubinidze, *Biomed. Opt. Express*, 2016, **7**, 442.

142   A. Koçer, M. Walko, W. Meijberg and B. L. Feringa, *Science (80-.).*, 2005, **309**, 755–758.

143 M. Yamada, M. Kondo, J. I. Mamiya, Y. Yu, M. Kinoshita, C. J. Barrett and T. Ikeda, *Angew. Chemie - Int. Ed.*, 2008, **47**, 4986–4988.

144 H. Zeng, O. M. Wani, P. Wasylczyk, R. Kaczmarek and A. Priimagi, *Adv. Mater.*, 2017, **29**, 1–7.

145 X. Pei, A. Fernandes, B. Mathy, X. Laloyaux, B. Nysten, O. Riant and A. M. Jonas, *Langmuir*, 2011, **27**, 9403–9412.

146 L. Li, S. Pan, X. Pang, H. Chen, D. Hu, L. Ke, Y. Xiong and W. Xu, *Soft Matter*, 2012, **8**, 7357–7360.

147 Y.-N. Zhou, J.-J. Li, Q. Zhang and Z.-H. Luo, *Langmuir*, 2014, **30**, 12236–12242.

148 X. Wang, J. I. Chen, S. Marturunkakul, L. Li, J. Kumar and S. K. Tripathy, *Chem. Mater.*, 1997, **9**, 45–50.

149 M. Sommer and H. Komber, *Macromol. Rapid Commun.*, 2013, **34**, 57–62.

150 S. Shinkai, H. Kinda and O. Manabe, *J. Am. Chem. Soc.*, 1982, **104**, 2933–2934.

151 T. Akitsu, C. Ishioka and T. Itoh, *Cent. Eur. J. Chem.*, 2009, **7**, 690–696.

152 A. M. Cox, R. D. Blackburn, D. P. West, T. A. King, F. A. Wade and D. A. Leigh, *Appl. Phys. Lett.*, 1996, **68**, 2801–2803.

153 N. Tamaoki, E. Van Keuren, H. Matsuda, K. Hasegawa and T. Yamaoka, *Appl. Phys. Lett.*, 1996, **69**, 1188–1190.

154 C. Barrett, A. Natansohn and P. Rochon, *Chem. Mater.*, 1995, **7**, 899–903.

155 F. Lagugné Labarthet, T. Buffeteau and C. Sourisscau, *J. Phys. Chem. B*, 1998, **102**, 2654–2662.

156 K. Janus, I. A. Koshets, J. Sworakowski and S. Nešpůrek, *J. Mater. Chem.*, 2002, **12**, 1657–1663.

157 S. D. George, V. S. Namboodiri and S. Hardt, in *Linear and Nonlinear Optics of Organic Materials X*, 2010, vol. 7774.

158 P. Tannouri, K. M. Arafeh, J. M. Krahn, S. L. Beaupré, C. Menon and N. R. Branda, *Chem. Mater.*, 2014, **26**, 4330–4333.

159 M. Saito, T. Nishimura, K. Sakiyama and M. Nakagawa, *Nanophotonic Mater. IX*, 2012, **8456**, 84560M.

160 L. Li, C. Peng, Q. Xu, S. Chen, Y. He, W. Xu and J. Jiang, *Mater. Lett.*, 2018, **214**, 150–153.

161 T. A. Kim, M. J. Robb, J. S. Moore, S. R. White and N. R. Sottos, *Macromolecules*, 2018, **51**, 9177–9183.

Chapter 2:

Developing an amine-responsive

cross-linked polysiloxane

2.1 Introduction

The ability to detect amines has been shown to be invaluable for a multitude of applications, such as the monitoring of food stuffs,[1–7] synthetic processes[8] and toxic industrial by-products,[9] to the identification of illicit drugs,[10,11] explosive devices[12,13] and heavy metals,[14–16] even including medical diagnoses.[17,18] The current state-of-the-art techniques provide an impressive sub-ppm sensitivity, attainable through chemiresistive[19–21] and fluorescence-based devices.[22–27] The prerequisites for systems like these are somewhat demanding, consisting of convoluted synthetic procedures and requiring the use of uncommon, expensive equipment. As such, sought-after alternatives involve the use of colourimetric sensors. Colourimetric sensors evoke a visible change in colour when exposed to certain stimuli, such as pH, heat or light.[8] Their efficient response times, coupled with the ease of output reading, are what make these a highly desirable architecture when it comes to the rapid detection of change in a system.[8,15,28–31] Colourimetric sensors have been improved to such a state that they are now able to provide desirable sensitivities.[32,33] However, some of these methods still require the use of bespoke equipment,[1,3,5] involve lengthy synthetic procedures,[4,6,7] or require interference with product packaging and are thereby destructive.[1,4,33,34] As such, a synthetically-accessible, easily-interpreted, non-destructive amine-sensing system is highly desirable.

Recently, research has been conducted into the synthesis of reversible, negatively photochromic, visible light photoswitches, named donor-acceptor Stenhouse adducts (DASAs).[35,36] It was found that a furan ring activated by a carbon acid acceptor group was readily reactive with secondary amine donors. This new class of photoswitch was easily producible from readily available starting materials and opened new avenues for tuneable light and heat responsivity.[37,38] Following the advent of DASAs, their versatility and selectivity was taken advantage of in the form of colourimetric sensors for the detection of nerve agents[37] and heat,[38] more recent advances utilised them as fluorescent chemosensors, too.[39] In 2017, the rapid opening of the carbon acid-activated furfural moiety, was utilised to exhibit the innate ability

67

that DASA-precursors had for amine-sensing.[40] It was found that the precursor known as Meldrum's activated furan (MAF), would display selectivity between primary and secondary amines, with a sub-ppm detection limit. Furthermore, this reaction was visually denoted by a distinctive colour change of yellow to red-purple. As these moieties were conveniently synthesised, it provided a new route for simpler alternatives to currently established amine detection systems. Read de Alaniz *et al* were inspired by the enhanced stability and versatility that covalent attachment to a polymeric backbone could bring to colourimetric amine sensors[15,31,41] and so this approach eventually lead to a MAF-based polymer backbone.[42]

The goal of the work described in this chapter was to produce a MAF-incorporated PDMS network that could be used as an amine-detection platform, ideally being non-destructive and easy to produce. This would consist of physically blending MAF and PDMS with a curing agent and catalyst complex, allowing suspension of the amine-sensitive moiety within an elastomeric network. Previous polymer architectures to incorporate MAF have had the disadvantage of being less responsive at room temperatures, due to the high T_g values of the polymer components.[42] Thus, PDMS was selected as it is known for its high flexibility, low T_g[43], facile processability and has been shown to exhibit high absorption of many organic vapours including amines.[44] The presence of amines such as ammonia is indicative of decay in meat/fish products[45,46] and so the ability to detect these toxins *in situ*, with rapid read-out, is key to following food product safety and quality guidelines.[47] Therefore, an envisioned application would be inclusion into food packaging, whereby product spoilage could be immediately identified by a simple colour change (Figure 2-1). The following chapter details experimental procedures in the attempt to provide qualitative and quantitative confirmation of amine detection in a simulated packaging environment, through visual observation, image analysis and the utilisation of UHF-RFID sensing. Also, an attempt was undertaken to determine whether this new composite could be utilised as an *in-situ* sensor for aqueous solutions, with monitoring through UV-Vis spectroscopy.
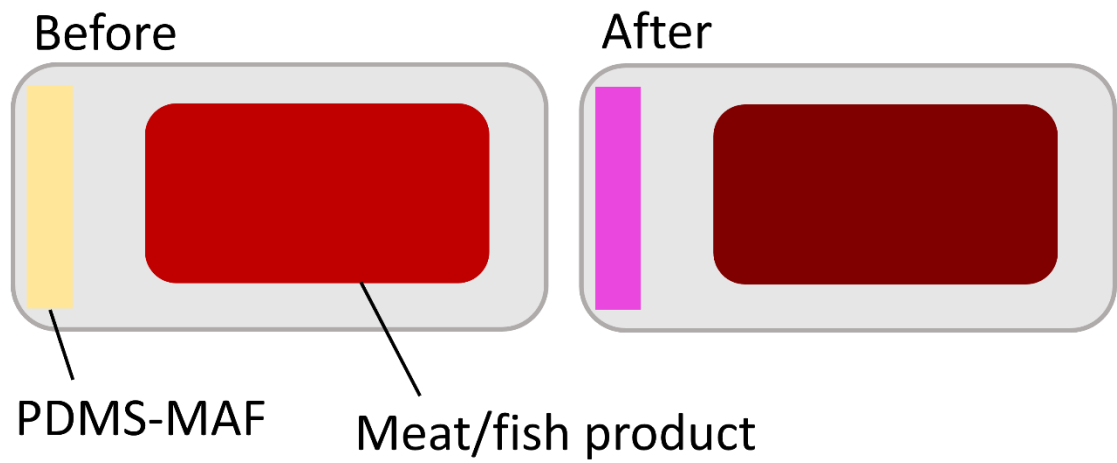
Figure 2-1 – A diagram representing the envisioned application of the PDMS-MAF composite, before and after exposure to the amines given off by decaying food products.

2.2 Experimental

2.2.1 Materials and apparatus

Silanol terminated polydimethylsiloxane (DMS-S31) (M_w 26,000, Gelest), tin (II) 2-ethylhexanoate (95%, Sigma-Aldrich), tetraethyl orthosilicate (99%, Sigma-Aldrich), dichloromethane (99%, Fisher Scientific), isopropylidene malonate (Meldrum's acid) (98%, Alfa Aesar), 2-furaldehyde (99%, Sigma-Aldrich), diethylamine (99+%, Acros Organics) and ammonia solution (35% w/w) (Fisher Scientific) were used as received. Fresh cod was obtained from a local Canterbury Fishmonger, sourced from Broadstairs, and frozen within 1 hour of purchase. RFMicron RFM3200-AFR temperature sensing tags were used as bought. The equal dispersion of reagents for the development of PDMS elastomers was made possible through use of a SpeedMixer™ DAC 150.1 FVZ-K bought from Synergy Devices Limited. Application of PDMS films to tags was performed using an automatic precision film applicator CX4 from mtv messtechnik, with a height-adjustable doctor blade.

2.2.2 Synthesis of 5-(furan-2-ylmethylene)-2,2-dimethyl-1,3-dioxane-4,6-dione (MAF)

The synthesis of **MAF** was carried out by following a modification of a previously-reported literature procedure.[35] Meldrum's acid (2.60 g, 25 mmol) and 2-furaldehyde (1.92 g, 20 mmol) were added sequentially to deionised water (20 ml) and stirred at 75 °C for 2 hours. The reaction mixture was then left to cool to room temperature, followed by isolation of the precipitate via vacuum filtration. The precipitate was recrystallised from (60 °C) hexane (100 ml), yielding bright yellow crystals (MAF) (3.63 g, 81.8 %). The final product was analysed using 1H and 13C NMR, and FT-IR spectroscopy, data match that of known literature.[35]

^{1}H NMR (400 MHz, CDCl$_3$, room temperature) found ppm δ: = *1.76* [**s, 6H (CH$_3$)$_2$C(OOC)$_2$C=C(C=CHCH=CHO)**], *6.74* [**dd,** *J* **=** 3.9, 0.9 Hz**, 1H** (CH$_3$)$_2$C(OOC)$_2$C=C(C=CH**CH**=CHO)], *7.84* [**d,** *J* = 1.8 Hz **1H** (CH$_3$)$_2$C(OOC)$_2$**C=C**(C=CHCH=CHO)], *8.35*

[s, 1H (CH$_3$)$_2$C(OOC)$_2$C=C(C=CHCH=**CH**O)], *8.46* [d, *J* = 3.9 Hz, 1H (CH$_3$)$_2$C(OOC)$_2$C=C(C=**CH**CH=CHO)].

^{13}C NMR (CDCl$_3$, room temperature) found ppm δ: = 27.62, 104.52, 107.60, 115.30, 128.10, 141.23, 150.25, 150.41, 160.22, 163.25.

FT-IR (cm^{-1}) MAF: 3173 (HC=CH, CH str.); 3129 (HC=CH, CH str.); 3112 (HC=CH, CH str.); 3005 (HC=CH, CH str.); 1703 (C=O str.); 1582 (C=O str.); 1277 (C-O str); 1202 (C-O str); 782 (C=C bend).

2.2.3 Sn catalysed cross-linking of silanol terminated PDMS

The following is a previously-reported procedure that has been modified.[48] Silanol terminated PDMS (2.00 g, 76.9 µmol, DMS-S31, M_w 26,000) and the cross-linking agent tetraethyl orthosilicate (0.04 g, 1.92*10^{-4} mol) (molar ratio of SiOH groups in PDMS to SiOR groups in TEOS, 1:4) were added to a plastic beaker and speed-mixed at 3,500 rpm for 60 seconds. Next, tin (II) 2-ethyl hexanoate (60 µl, 0.6 M solution in toluene) was added and the mixture was speed-mixed for a further 60 seconds. Lastly, DCM (0. 5 ml) was added and the mixture was speed-mixed, for a final 60 seconds. The mixture was poured into square PTFE moulds (width = 2 cm, length = 2 cm, height = 0.2 cm) and allowed to cure under ambient conditions overnight. Finally, each sample was then rinsed with deionised water, to remove any external, residual reagents. Networks were analysed using FT-IR spectroscopy, with values matching that of known literature.[48]

FT-IR (cm^{-1}) PDMS: 2966 (CH$_3$, CH str); 1438 (Si – CH$_3$, CH$_3$ asym def); 1261 (Si – CH$_3$, CH$_3$ sym def); 1103, 1020 (Si – O – Si str); 786 (Si – C str and CH$_3$ rock).

FT-IR (cm^{-1}) TEOS: 2981 (CH$_3$, C – H asym str); 2929 (CH$_2$, C – H asym str), 2890 (C – H asym str); 1443 (CH$_3$, C – H asym bend); 1391 (CH$_3$, C – H sym bend); 1294 (C – H twist/wag); 1164, 995 (CH$_3$, C – H rock); 1072 (C – O asym str); 779 (SiO$_4$ asym); 525 (O – C – C def).

2.2.4 Sn catalysed cross-linking of silanol terminated PDMS-MAF physical blends

Silanol terminated PDMS (2.00 g, 76.9 µmol, DMS-S31, M_w 26,000) and the cross-linking agent tetraethyl orthosilicate (0.04 g, $1.92*10^{-4}$ mol) (molar ratio of SiOH groups in PDMS to SiOR groups in TEOS, 1:4) were added to a plastic beaker and speed-mixed for 60 seconds. Next, tin (II) 2-ethyl hexanoate (60 µl, 0.6 M solution in toluene) was added and the mixture was speed-mixed for another 60 seconds. Lastly, **MAF** (for amounts, see Table 2.1) in a minimum of DCM was added and the mixture was speed-mixed for a final 60 seconds. The mixture was poured into square PTFE moulds (width = 2 cm, length = 2 cm, height = 0.2 cm) and allowed to cure under ambient conditions overnight. Finally, each sample was then rinsed with deionised water, to remove any external, residual reagents. Following this, they were analysed using FT-IR spectroscopy.

FT-IR (cm^{-1}) PDMS-MAF: 2964 (CH_3, CH str); 1406 ($Si - CH_3$, CH_3 asym def); 1258 ($Si - CH_3$, CH_3 sym def); 1084, 1011 ($Si - O - Si$ str); 785 ($Si - C$ str and CH_3 rock). Data obtained for each sample were practically identical, additional peaks are included in Table 2.1.

Table 2.1 - A table depicting the amount of MAF used for each iteration of PDMS-MAF composites.

Elastomer	MAF conc.[a] (wt%)	Mass of MAF used (mg)	MAF moles (mmol)	Additional peaks (cm^{-1})
MAF-0.05	0.05	1	$4.5*10^{-3}$	N/A
MAF-0.1	0.1	2	$9.0*10^{-3}$	N/A
MAF-0.5	0.5	10	0.045	1703, 1585
MAF-1	1	20	0.090	1741, 1578
MAF-5	5	100	0.45	N/A

[a] **with respect to mass of PDMS used.**

2.2.5 Film-casting of PDMS-MAF physical blends onto RFID tags

Drawing from the procedure established in section 2.2.4: following the speed-mixing process, curing mixtures were poured atop an RFMicron RFM3200-AFR temperature sensing tag using a tape-well and doctor-blading method,[49] upon an automatic precision film applicator CX4 from

mtv messtechnik (Figure) to achieve the desired thickness of 500 µm. Measurement of film thickness was conducted using Duratool digital Vernier calipers, film thickness was calculated by subtracting the thickness of an RFID tag (average thickness of 50 µm) pre-application from post-application.
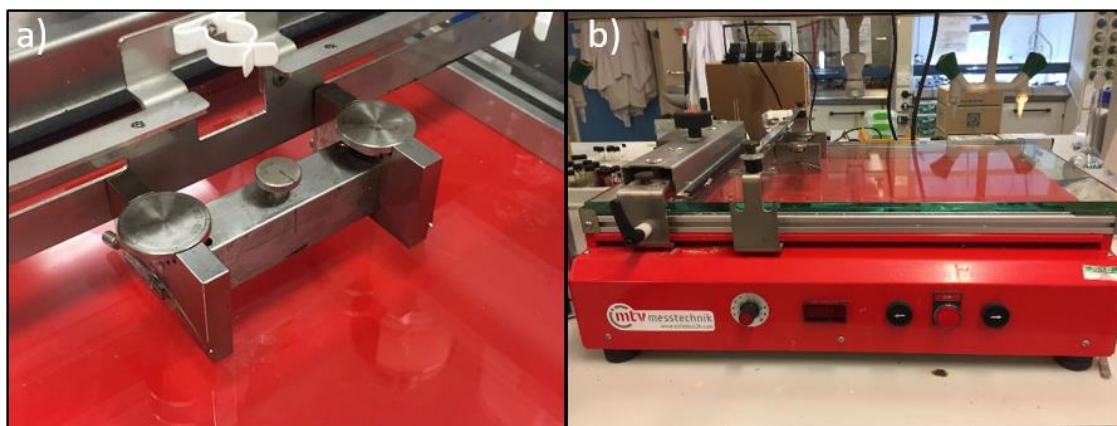
Figure 2-2 – An automatic precision film applicator CX4 from mtv messtechnik, used for the application of elastomeric films.

2.2.6 Suspension of PDMS-MAF squares in aqueous-amine solutions for detection limit determination

Ten concentrations (100 to 1000 ppm, 100 ppm increments) of diethylamine in water (5 ml) were produced through serial dilution of a 1000 ppm stock solution. A PDMS-MAF composite of dimensions 20 x 5 x 2 mm was immersed in each solution and the absorbance of each elastomer measured every 10 minutes up to 1 hour, each hour up to 3 and then finally a 24th hour. For each scan, the sample was removed from the solution-containing glass vial and placed into a standard quartz cuvette, in which it was immersed in fresh DI H_2O. Following this, the sample was dabbed dry with white tissue paper and re-immersed in its respective amine solution, and cuvette water was refreshed, ready for the next elastomer. A second iteration of the experiment was conducted whereby image analysis was instead used to determine the amine sensitivity across the concentration range. A single PDMS-MAF square (approx. 5 x 5 x 2 mm) was immersed into each aqueous amine solution within a 7 ml glass vial, which was sealed with a plastic screwcap.

This was performed for each loading iteration of MAF, therefore in total there were 50 samples. Images were taken at various time intervals: 0 minutes, 10 minutes, 1 hour and 24 hours, using the built-in camera of an Apple Inc. iPhone 6 smartphone (flash off, HDR off), with a 30 cm overhead perspective. The images were analysed using the computer software MATLAB, to acquire magnitudes of RGB colours which were then converted to CIELAB (L*a*b*) colour space values. The CIELAB data was used to produce a quantitative measure of colour difference, ΔE*. Sample illumination was made possible by a 25 W 6,500 K LED lamp placed at an angle of approximately 50 ° from the subject.

2.2.7 Preliminary amine exposure experiment

The 0.5 wt% PDMS-MAF sample was exposed to diethylamine and a concentrated ammonia solution. Each set-up consisted of a Sistema® food container, inside were two plastic 3 ml cuvettes containing a 20 x 5 x 2 mm slice of either the PDMS-MAF composite or a standard cross-linked PDMS elastomer. Approximately 20 µl of either ammonia or diethylamine was deposited into the middle of the container, an example setup is included as Figure 2-3. Photographs were taken under conditions presented in section 2.2.6, but at far shorter time stamps: before deposition of amine, immediately after, 1 minute later and 10 minutes later. They were also subjected to image analysis as described in section 2.2.6.
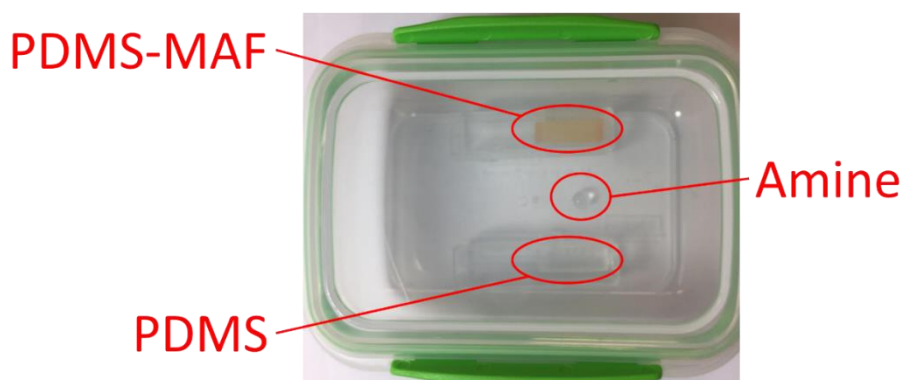
Figure 2-3 – Example setup for the preliminary amine exposure experiment.

2.2.8 Cod decomposition experiment

2.2.8.1 Image analysis setup

Small cuttings of each PDMS-MAF composite (Table 2.1) were taken (approximately 5 x 5 x 2 mm) and placed into separate petri dishes lined with filter paper, each were given a label of 1 – 5 denoting their loading of MAF, 0.05 wt% labelled as 1 and 5 wt% designated as 5. The dish was placed into a Sistema® food container along with a defrosted cutting of cod fillet (approximately 50 x 25 x 25 mm). The setup was left on a bench top under ambient conditions for 24 hours, with images being taken at 0 hr and 24 hr.

2.2.8.2 RFID tag setup

An RFMicron RFM3200-AFR temperature sensing tag was covered with a 500 µm film of PDMS-MAF, with 0.5 wt% loading of MAF. The film was applied to the backside of the tag, the opposite side to where the antenna is located, and the device was applied to the lid of a Sistema® food container through the use of its own adhesive film. A cutting of cod was then patted dry with tissue paper and taped to the base of the same food container, with Scotch magic tape. RFID measurements were performed on the tag at 0 and 24 hours, both including the presence of the container and fish sample.

2.3 Measurements and Instruments

2.3.1 FT-IR spectroscopic measurements

FTIR spectroscopic analysis was performed on a Shimadzu IRAffinity-1 spectrometer with a Specac Golden Gate™ ATR sampling accessory, under ambient conditions, with 64 scans at a resolution of 4 cm^{-1}. Good optical contact between the sample and the diamond was obtained by clamping of samples via the Golden Gate™, each elastomer was bisected with a clean scalpel, in order to obtain cross-sectional and surface scans.

2.3.2 UHF-RFID measurements

RFID measurements were performed by Dr Aaron Hillier and Joshua Savage, using Voyantic TagformancePro UHF RFID characterisation apparatus. All tags were scanned in triplicate, each placed at a distance of 30 cm from the apparatus antenna, within a range of 800 to 1,000 MHz.

2.3.3 UV-Vis spectroscopic measurements

UV-Vis analysis was performed with a Shimadzu UV-1800 spectrophotometer. Samples were prepared by dividing a 20 x 20 x 2 mm (*l* x *w* x *h*) piece into four 5 x 20 x 2 mm slices. These slices were placed into aqueous solutions of differing concentrations of diethylamine (100 to 1000 ppm) and were scanned at various time periods in quartz cuvettes filled with DI H_2O. Each sample was placed in the same position within the cuvette, relative to the incident light beam. After scanning, the cuvette was refilled with fresh DI H_2O, ready for the next sample. A baseline was established by scanning a "blank" standard cross-linked PDMS sample suspended in DI H_2O, this would ensure that any light absorption could then be characterised to the presence of MAF and/or DASA moieties. Samples were scanned within the range of 200 to 800 nm.

2.3.4 NMR spectroscopic measurements

^{1}H and ^{13}C NMR data were acquired using a Bruker AVANCE-400 spectrometer, spectra were obtained at 19 °C in chloroform-d (d-99.8 atom %, CIL) solution, unless stated otherwise.

2.3.5 Imaging and conversion measurements

Photographs were acquired using the built-in camera of an Apple Inc. iPhone 6 smartphone (flash off, HDR off). Lighting consisted of a 25 W 6,500 K LED lamp placed at an angle of approximately 50 ° from the subject, images were taken with an overhead perspective. The photographs were analysed using the computer software MATLAB, to acquire magnitudes of RGB colours which were then converted to L*a*b* values. The colour difference, ΔE*, was calculated using the L*a*b* values.

2.4 Results and discussion

2.4.1 Synthesis and characterisation of Meldrum's activated furan (MAF)

The MAF precursor was chosen as it is regarded as being the favourable activated furan for amine-sensing applications, owing to its optical properties and rapid reactivity.[40,42,50] The product was synthesised successfully, yielding bright yellow crystals.[35,36] ^{1}H NMR, ^{13}C NMR and FT-IR spectroscopic analysis of the product confirmed the successful formation of MAF (Figure 2-4), in agreement with literature values.[35,51]
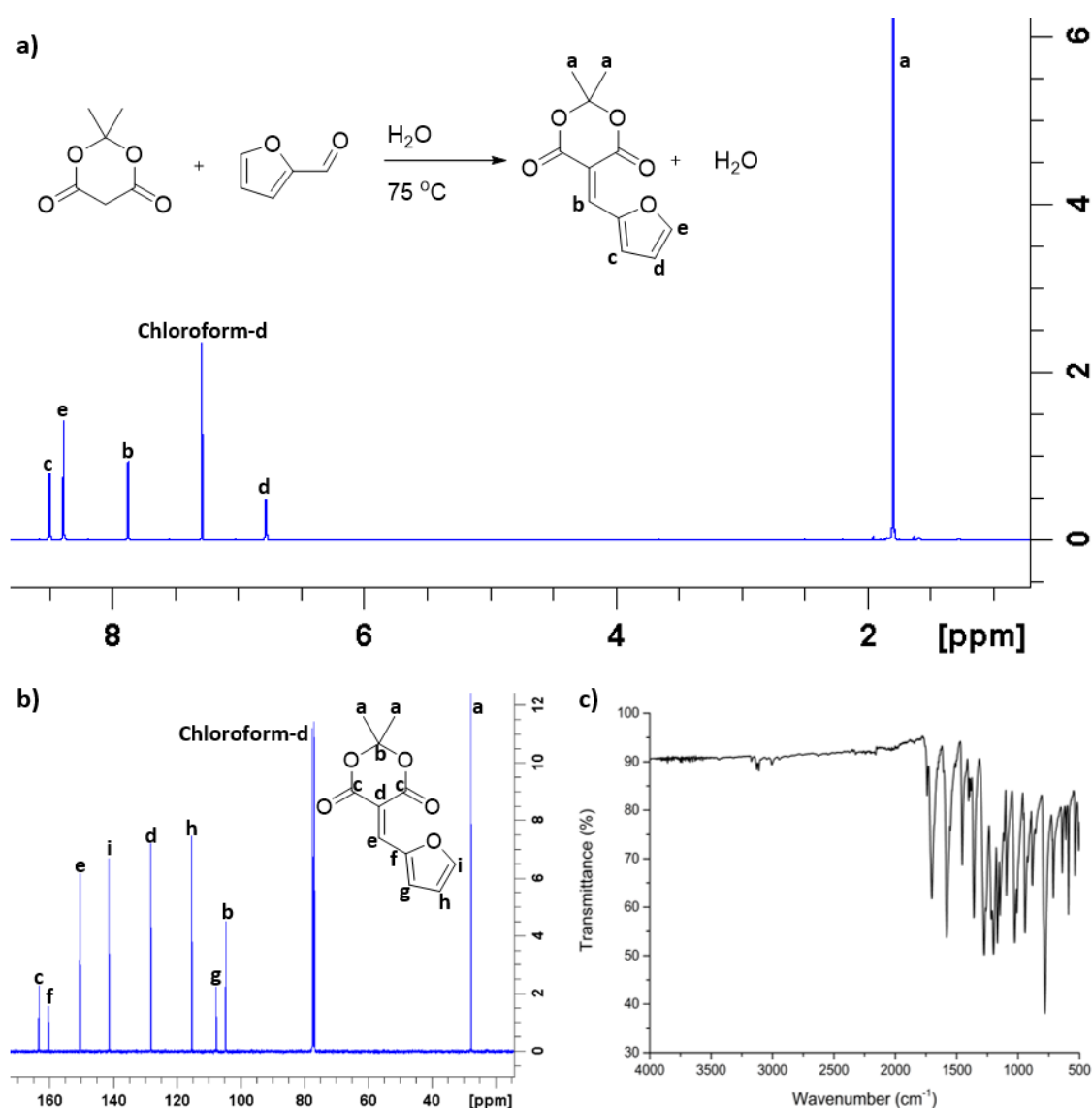
Figure 2-4 - Full characterisation of MAF, including: a) ^{1}H NMR with the reaction scheme inset, b) ^{13}C NMR, and c) FT-IR spectrum.

2.4.2 Characterisation of cross-linked PDMS elastomers and PDMS-MAF elastomers

2.4.2.1 Cross-linked PDMS elastomers

The product was synthesised according to a modified version of a previously-reported procedure,[48] whereby silanol-terminated PDMS (DMS-S31 Gelest, M_w 26,000) was mixed with an organotin catalyst solution, DCM and a cross-linking agent (TEOS), and allowed to cured under ambient conditions overnight. These were produced as a reference/blank for the characterisation and analysis of PDMS-MAF samples. The elastomers were rubber-like in texture and had a transparent appearance (Figure 2-5).
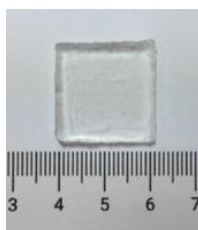
Figure 2-5 - Photograph of a cross-linked silanol terminated PDMS square, scale bar in cm.

Usually, a solvent would not need to be employed for this procedure, however it would be required for solvation and dispersion of the MAF species, and so it was deemed necessary to include this for the production of blank samples as well. It was thought that rapid evaporation of solvent would form bubbles within the matrix before curing could finish, so throughout the study, the decision was taken to not use an oven for the curing process of PDMS and PDMS-MAF as a preventative measure. As air has a very low permittivity, air-bubbles within films would likely have affected any RFID sensing values acquired and so it would not have been possible to solely attribute any changes in data to the formation of DASA moieties. A cross-section of this blank PDMS sample was subjected to FT-IR analysis, data is included as Figure 2-6a. The band attributed to asymmetrical C-H stretching of TEOS at 2889 cm^{-1} had largely disappeared, indicating a loss of this species, and a successful cross-linking process.[52,53] Overall, the spectra of the product and the pre-treated PDMS were very much identical, as indicated by Figure 2-6b.
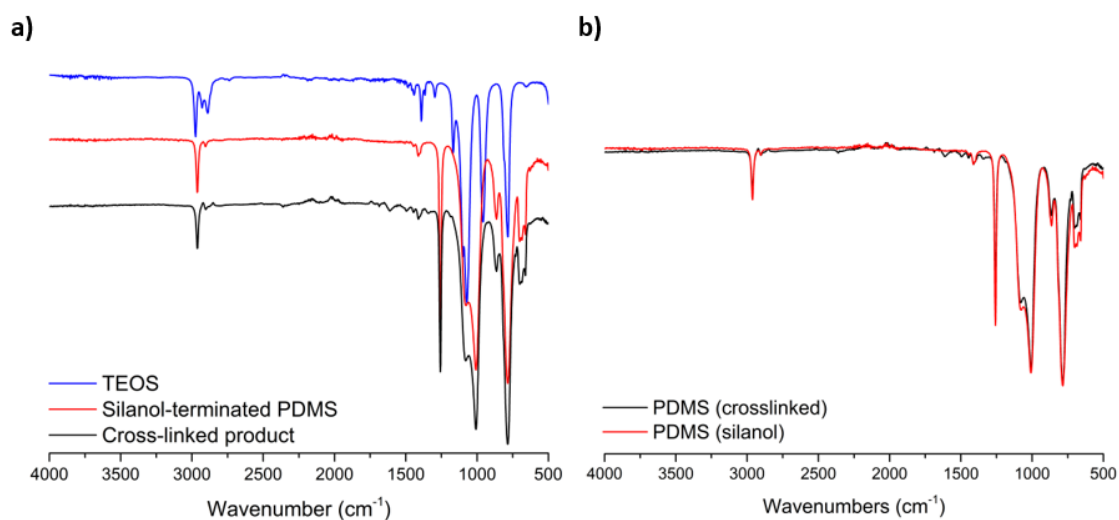
Figure 2-6 - FT-IR spectral overlay of a) TEOS, silanol-terminated PDMS and the cross-linked product, and b) silanol-terminated PDMS and the cross-linked PDMS product.

2.4.2.2 PDMS-MAF composites

The purpose of blending MAF into PDMS was to develop an easily reproducible, polymeric system that was capable of amine-detection, for such purposes as food spoilage monitoring. The PDMS-MAF composites were synthesised in an identical manner to that of regular crosslinked PDMS samples (section 2.4.2.1), with the exception of the addition of MAF, dissolved in DCM. The samples were designated as **MAF-X,** whereby **X** denoted the loading of MAF as a weight percentage, with respect to the mass of silanol-terminated PDMS used, i.e. MAF-0.05 would incorporate 1 mg of MAF for 2 g of PDMS. Batches of various MAF loadings were produced: 0.05, 0.1, 0.5, 1 and 5 wt%. The synthetic procedure consisted of mixing PDMS with a cross-linking agent (TEOS), an organotin catalyst and a MAF-DCM solution, and allowing the mixture to cure overnight. Although the use of a SpeedMixer™ was employed, this was not necessary to carry out the procedure, simply used to ensure equal dispersion of reagents. The reaction scheme is presented as Figure 2-7. The elastomers had a rubbery texture and their appearance ranged from colourless to vibrant yellow. Figure 2-8 has been included to provide context to the elastomer; the top image is a photograph of MAF-5 situated against a centimetre scale bar and

the bottom is an approximation that attempts to provide context as to the relationship between MAF and the polymer chains.
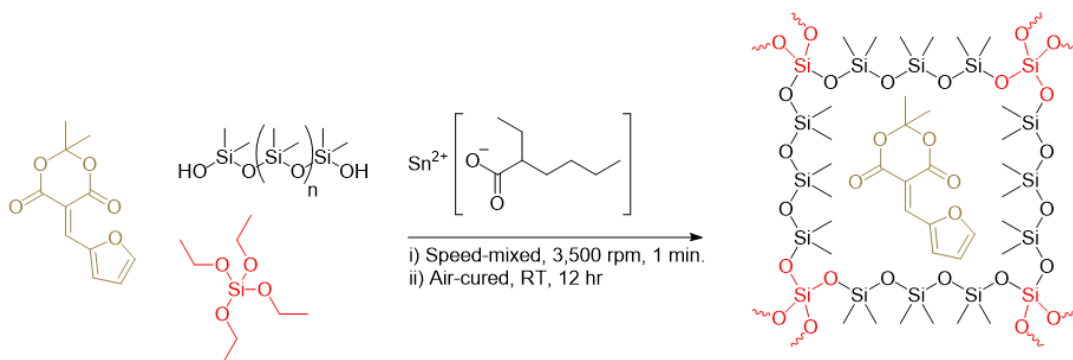
Figure 2-7 - A schematic representation of the production of the PDMS-MAF elastomers.
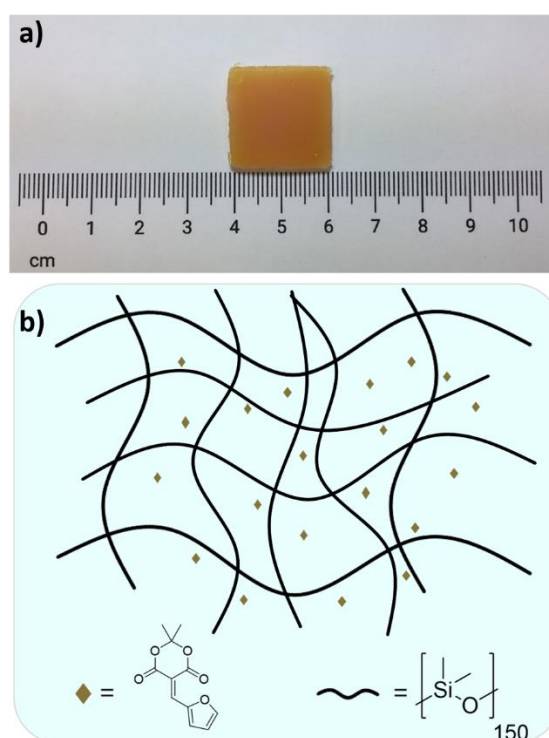
Figure 2-8 – a) Photograph of a sample from batch MAF-5, scale bar in cm, b) diagram depicting an approximate representation of the molar relationship between PDMS and MAF, for that sample, not to scale.

FT-IR data was obtained for each iteration, to see if an increase of MAF concentration would produce a marked difference in the spectra. The spectra of each product, overlaid with the those of TEOS, silanol-terminated PDMS and MAF, are shown in Figure 2-9. The data is reminiscent of

that obtained for ordinary cross-linked PDMS networks, with very little difference. The final

spectrum, Figure 2-9f, features an expanded overlay of the spectra for each product, between

2200 and 1200 cm^{-1}. Additional peaks were detected for MAF-0.5 and MAF-1, situated at 1703

and 1585 cm^{-1}, and 1741 and 1578 cm^{1}, respectively. It is thought that these signals are

characteristic of the carbonyl groups belonging to Meldrum's acid, though why they do not

appear so prominently in a higher concentration iteration such as MAF-5, is unknown.
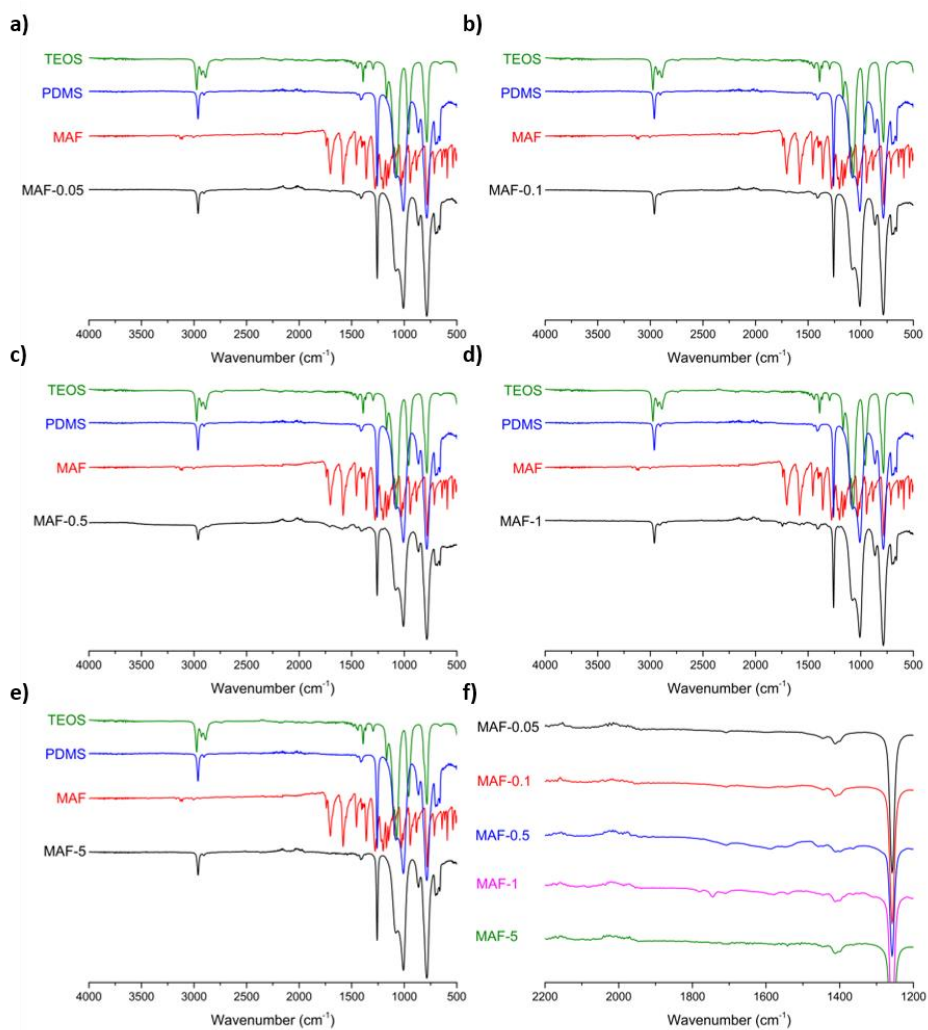
Figure 2-9 - Plots of FT-IR data acquired for each PDMS-MAF sample; a) MAF-0.05, b) MAF-0.1, c) MAF-0.5, d) MAF-1, e) MAF-5, f) overlay of each iteration displaying the additional peaks.

2.4.3 Quantification of diethylamine detection through UV-Vis spectroscopy

After characterisation of the PDMS-MAF composites, the propensity for amine-sensitivity had to be investigated. The nucleophilic attack of an amine on the activated furan cored of MAF yields a distinctive colour change of pale yellow to vibrant pink, as shown by Figure 2-10a; an ideal colourimetric indicator for appropriately-reactive amines. It was believed that UV-Vis spectroscopy would prove more sensitive to amine-reactivity than any other technique available, therefore this was the first course of action when determining and quantifying the amine-detection of PDMS-MAF composites. The method behind this investigation has been described in section 2.2.6. PDMS-MAF composites of dimensions 20 x 5 x 2 mm were exposed to aqueous-diethylamine solutions and subsequently scanned whilst immersed in DI H_2O, within 3 ml quartz cuvettes, as depicted by Figure 2-10b. This step was taken in order to simulate a situation in which this composite could be used to detect the presence of amines in a body of water; to establish whether this product could be analysed *in situ*, rather than needing to remove it from the subject environment for each analytical step.
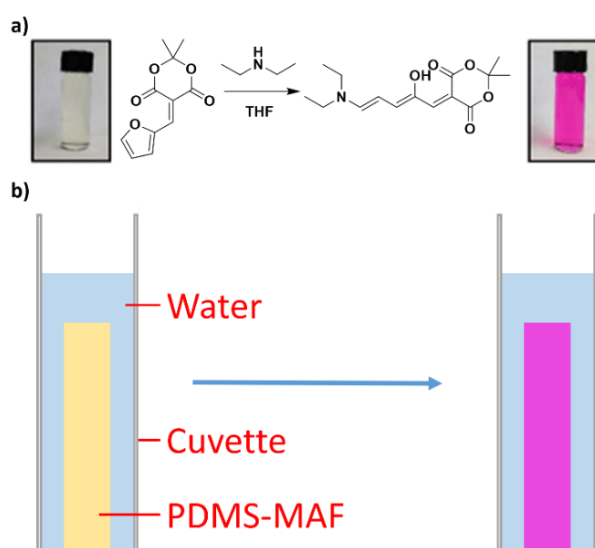
Figure 2-10 – a) Synthesis of diethylDASA and its colour change, b) diagram depicting an unreacted (left) and reacted (right) PDMS-MAF sample in a water-filled quartz cuvette, for UV-Vis spectral analysis. Photographs of vials taken from a previous report.[40]

The aim was to quantifiably prove detection of an amine through the typical DASA-synthesis colour change; in this case diethylDASA, as featured in Figure 2-10a. In order to prove that any colour change would be a result of amine-reactivity, and no other extraneous variables, a slice of MAF-0.5 composite was immersed in DI H_2O and used as a reference sample, shown as Figure 2-11a. It was clear that the elastomers were absorbing a large magnitude of visible light in the range of 400 nm and below, indicative of the yellow colouration that was characteristic of MAF.[35,36] Additionally, it has been demonstrated in the past that the absorbance of MAF in THF centres around 350 nm; although not the same solvent system, this provides an indication of what to expect from the water-insoluble species.[40] The absorbance of the elastomer within the < 400 nm region was too high to measure accurately, likely a combinatory result of light scattering, MAF microcrystals and the sample thickness. To ensure that the absorption profile was primarily a product of the MAF itself, a blank PDMS network was also scanned, featured as Figure 2-11b.
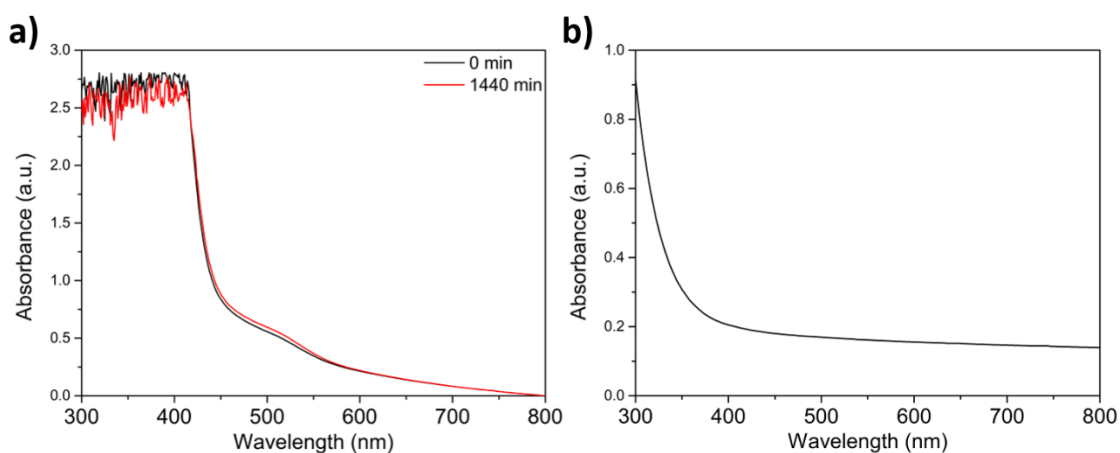
Figure 2-11 – UV-Vis time-lapse of a) MAF-0.5 and b) a blank PDMS pad, submerged in DI H2O.

The colour change of the MAF-to-DASA reaction progresses from yellow to pink-red, as such, the absorbance at approximately 400 nm was expected to decrease. This would lead to the appearance of a single peak situated around 480 nm, based on previously demonstrated absorption of the first-generation diethylDASA in water.[54] This dramatic colour change would be the indication of amine detection. Throughout the study, it was found that the baseline

absorbance of each spectrum would fluctuate between time periods, it was believed that Rayleigh scattering was taking place, likely explainable by microcrystals situated within the elastomer and thickness of the sample itself. As such, the data required correcting in order to draw any meaningful conclusions. These corrections entailed setting the absorbance value to 0 a.u. at 800 nm for each spectrum, thereby creating a point of reference from which all can originate and allowing for a more convenient comparison. An example of this is featured as Figure 2-12, for the composite exposed to a 1000 ppm diethylamine solution. The absorption centred around 400 nm had partially decreased within 24 hours, indicating a loss of yellow colouration as expected. This was preceded by the gradual appearance of a signal centred at 497 nm (30 min onward) and another at 463 nm (120 min onward), both believed to be indicative of the formation of diethylDASA. By the passage of 24 hours, these appeared to be combining into a single peak, centred at 480 nm. Visual observation of the samples agreed with these findings; the pale-yellow elastomer had begun to develop a pale-red colouring across the exterior, which over time had darkened significantly. Logically, a longer exposure time led to a larger reduction in the MAF-characteristic absorption and a greater increase in that which was characteristic of DASA formation. The absorbance below 350 nm did not appear to diminish, further supporting the Rayleigh scattering supposition.
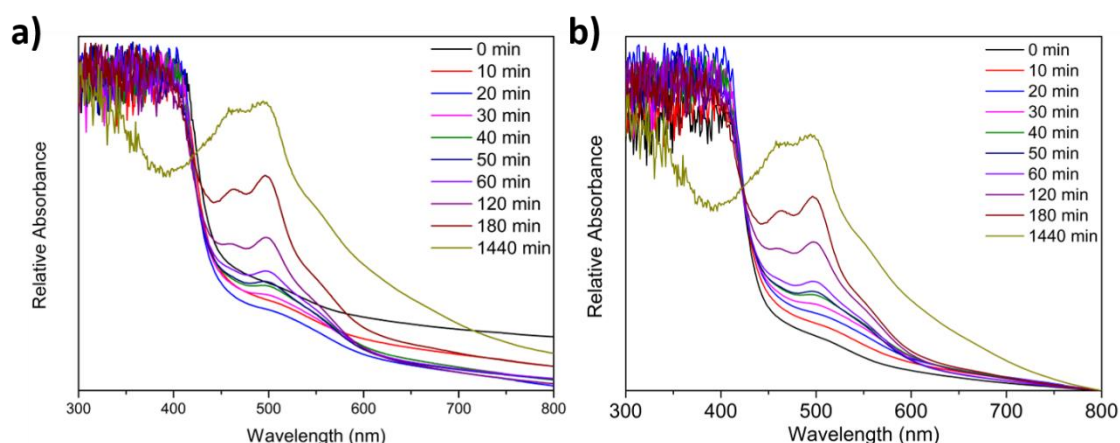
Figure 2-12 – UV-Vis spectroscopic time-lapse of a PDMS-MAF elastomer immersed in the 1000 ppm diethylamine solution, a) before and b) after correction of the data.

After determination of the effect that a longer exposure time had, the next course of action was to compare the effect of amine concentration variation. The UV-Vis spectroscopic data for 0, 30, 60 and 1,440 minutes were plotted as wavelength vs. relative absorbance, with each spectral line corresponding to a different amine concentration. The plots are displayed as Figure 2-13a-d, respectively. Spectra corresponding to other time periods are included in section 2.7 – appendix 2A. The first indication of amine-reactivity was within 30 minutes, corresponding to the 1000-ppm solution (Figure 2-13b). By the passing of 1 hour, solutions of 700 ppm and greater had produced a colourimetric response (Figure 2-13c). Within 24 hours, all concentrations except 100 and 200 ppm had produced an observable response (Figure 2-13d). The data elucidated a general trend, whereby solutions with greater amine concentrations would elicit larger changes in absorbance.
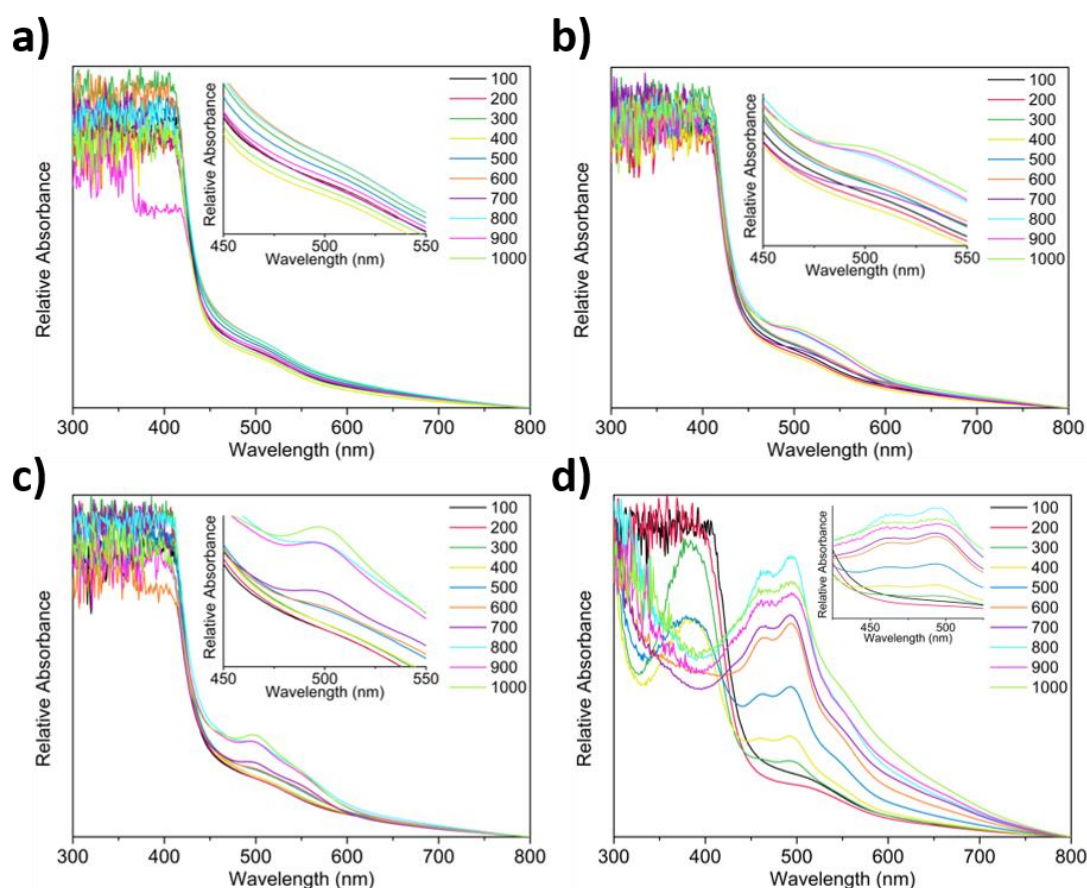
Figure 2-13 – UV-Vis spectra of MAF-0.5 immersed in aqueous diethylamine solutions, at concentrations of 100 to 1000 pm, at a) 0 min, b) 30 min, c) 60 min and d) 1,440 min (24 hr).

A clearer perspective of the concentration effect is provided by Figure 2-14, where the absorption values at 463 and 497 nm for each amine-concentration were plotted as a function of time. The two exceptions to this correlation were the absorption profiles of the 200- and 800-ppm solutions, however these were believed to be consequential of baseline distortion from light scattering. The inset images for Figure 2-14a/b highlight the degree of baseline fluctuation experienced by each profile. Following elucidation of the time and concentration trends, the detection limits for each time interval had to be considered. The detection limit at a certain time period was classified as being the earliest observable appearance of a significant signal; centred around 497 nm as this was the first peak to appear after amine exposure. The limits were determined from examination of the absorption profiles (Figure 2-13); those values have been tabulated and are displayed in Table 2.2.
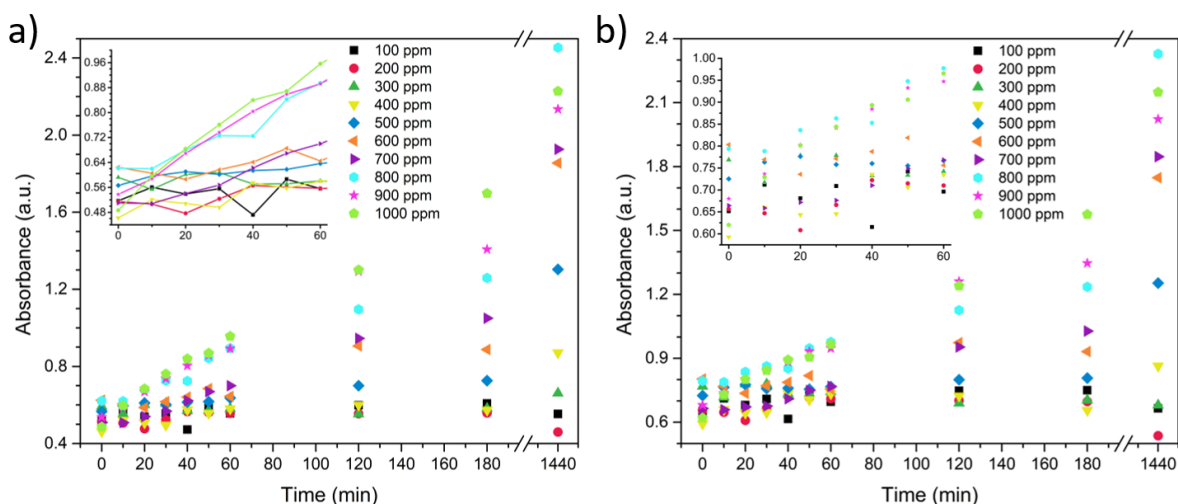
Figure 2-14 - Plots of the absorbance maxima of MAF-0.5 in aqueous-amine solutions of various concentrations at a) 497 nm and b) 463 nm, over the 24-hour period. Inset; absorbance magnitude over the exposure range of 60 minutes.

Immediately, it was clear that a general trend was exhibited in which a longer exposure time led to a lower detection limit. This was expected as a longer solution-immersion time period provides a larger window for reactivity with diethylamine. This data provided the supposition

that the detection limit of MAF-0.5 within practical time constraints, such as 1 hour, was 700

ppm. However, the composite was in fact witnessed to react at lower concentrations than this.

Table 2.2 - The determined diethylamine detection limits of MAF-0.5, at different time periods of exposure.

Time (min)	Observable limit (ppm)
0	N/A
10	>1000
20	>1000
30	1000
40	900
50	700
60	700
120	500
180	400
1,440	300

To conclude, the ability of PDMS-MAF to detect an amine was quantitatively demonstrated by

UV-Vis spectroscopy. It was found that more dilute amine solutions required a longer exposure

time to be detected, the earliest sensing indication was 30 minutes and the lowest detectable

concentration within 1 hour was 700 ppm. Although inclusion of all sample sets was originally

desired it was deemed unnecessary after analysis of MAF-0.5, as visual observation had

elucidated amine detection before it could be recorded with UV-Vis spectroscopy. It is believed

that the baseline distortion caused by scattering may have prevented observation of initial

characteristic DASA peaks. As such, the decision was taken to investigate the amine-sensing

ability of PDMS-MAF composites visually, through image analysis, as described in the next

section.

2.4.4 Quantification of diethylamine detection through image analysis

Thus far, it had been quantitatively established that the PDMS-MAF composites were reactive

with diethylamine, through UV-Vis spectroscopy. However, it appeared that visual observation

of the colour change was a better indicator than UV-Vis measurements, most likely because of

the interference that Rayleigh scattering was having on the baseline. Furthermore, as the primary utility of this architecture was as a colourimetric sensor, the visual indication of detection had to be assessed. Therefore, this section details the image analysis of photographs of PDMS-MAF composites immersed in aqueous-diethylamine solutions. The experiment consisted of immersing PDMS-MAF composites (5 x 5 x 2 mm squares) in aqueous solutions of various diethylamine concentrations within 7 ml glass vials, with each loading of MAF being investigated. Photographs were taken directly overhead of the vials at a 30 cm height, as it provided the best perspective of the samples, and the lighting angle was set to approximately 50 $^{\circ}$ to avoid unwanted reflections. Visual examination and photography of the composites were performed at time intervals of 0 minutes, 10 minutes, 1 hour and 24 hours. The images were analysed using MATLAB, collated and segregated by time periods (Figure 2-15). Loading of MAF incorporated into a network is situated on the y-axis of the matrices and the x-axis corresponds to the concentration of diethylamine in DI H_2O, in ppm. Alternative arrangements are displayed in section 2.8 – appendix 2B. The images in Figure 2-15a highlight the difference that MAF-loading has on colour vibrancy. As time progressed, the samples would transform from colourless/yellow, to a red colouration. Within 24-hours, this red colouration would darken to a browner tone, it is unknown exactly why this occurs. It is speculated that this is a case of further amine-reaction, such that the colour intensity increases so much that it appears brown to the naked eye. The data was further processed into a 3D colourmap with time, concentration and ΔE^* as x-, y- and z-values, respectively (Figure 2-16). The colourmap relates directly to ΔE^* values and the symbol size, to loading of MAF; size increases with loading, starting from 0.05 wt% and ending with 5 wt%. The plot provides a more distinct picture of the relationships between time, concentration and colour change. Again, a general trend was found whereby amine-reactivity increased with time; the majority of plot symbols reached higher ΔE^* values as time progressed. This trend was not all-encompassing, however, as it can be seen that the ΔE^* values for 0.05 and 0.1 wt% MAF (smaller spheres) showed a tendency to fluctuate rather than solely increase.

Diethylamine conc. (ppm)

MAF loading (wt. %)

a)

MAF loading	100	200	300	400	500	600	700	800	900	1000
0.05										
0.10										
0.50										
1.00										
5.00										

b)

MAF loading	100	200	300	400	500	600	700	800	900	1000
0.05	4.66	21.60	2.29	11.51	7.55	2.82	7.11	1.69	7.55	9.09
0.10	2.46	11.03	0.00	8.68	0.56	2.39	3.09	26.29	19.84	8.73
0.50	6.04	3.03	18.78	8.67	4.92	5.97	4.36	8.14	14.95	16.86
1.00	0.38	11.84	3.92	6.56	4.67	9.31	11.30	3.29	14.05	24.75
5.00	2.07	1.40	1.63	1.60	3.63	3.95	11.70	5.60	3.47	29.39

c)

MAF loading	100	200	300	400	500	600	700	800	900	1000
0.05	2.48	4.56	2.98	3.24	2.23	12.72	12.47	3.65	17.93	11.72
0.10	1.59	15.03	3.60	7.30	3.66	12.87	15.20	24.78	14.17	13.52
0.50	7.03	6.05	13.72	7.47	23.41	25.77	41.52	46.06	52.95	56.59
1.00	6.45	12.65	14.14	9.70	24.08	32.04	41.96	39.47	49.34	55.48
5.00	4.04	5.19	10.01	22.72	26.69	21.29	49.34	41.17	40.58	50.57

d)

MAF loading	100	200	300	400	500	600	700	800	900	1000
0.05	13.46	11.00	2.29	7.66	5.55	13.37	9.02	4.42	9.21	8.04
0.10	11.04	3.56	11.39	15.82	16.20	27.98	25.92	10.17	13.13	24.95
0.50	18.72	17.06	21.85	36.14	47.37	51.79	58.16	51.31	56.73	45.79
1.00	25.28	29.50	48.23	54.91	62.09	67.27	68.87	61.11	66.09	65.82
5.00	19.30	32.02	51.04	62.98	64.69	54.94	65.40	66.44	63.73	68.90

**Figure 2-15 – Photograph matrices of the PDMS-MAF composites, across the diethylamine concentration range, at various time periods: a) initial immersion, b) 10 minutes, c) 1 hour and d) 24 hours. The ΔE* values are shown on each individual sample.**
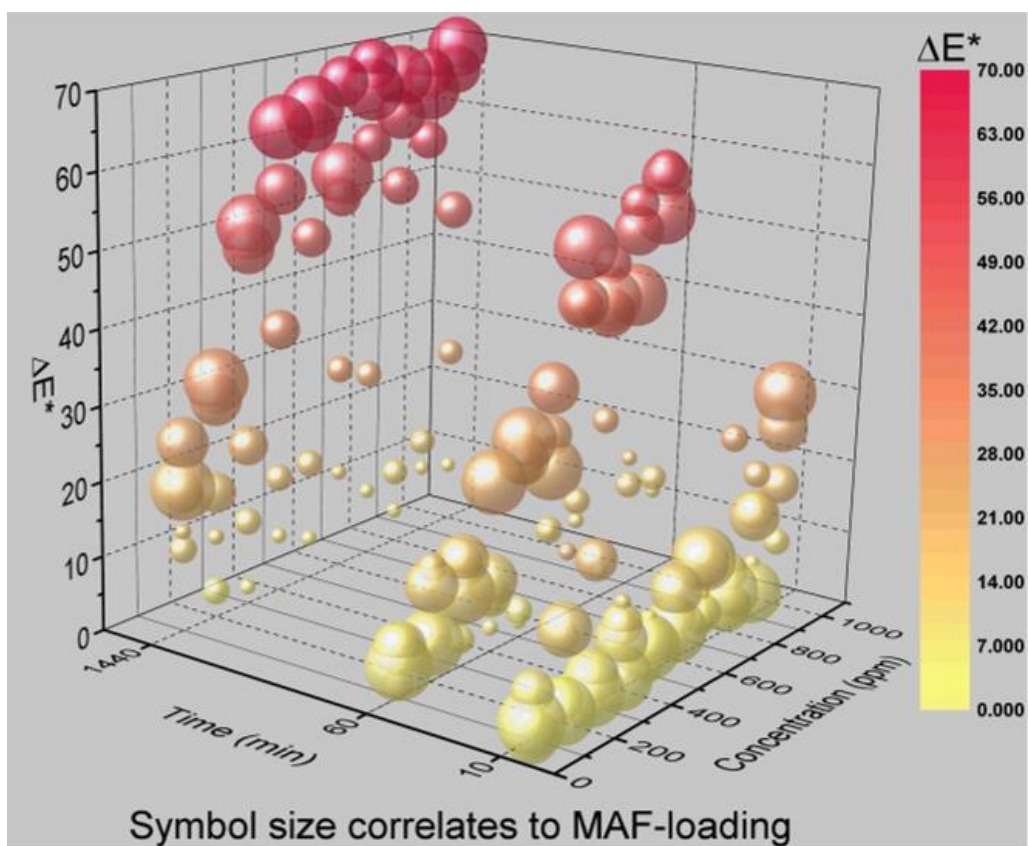
Figure 2-16 – A 3D colour map of the data displayed in Figure 2-15; timescale is logarithmic.

Largest symbols correspond to 5 wt% MAF, smallest to 0.05 wt%.

An example of this fluctuation can be seen with MAF-0.05 wt%, at 200 ppm of diethylamine; the ΔE^* values were 21.60, 4.56 and 11.00, for 10, 60 and 1,440 minutes, respectively. From this, it was clear that an unreliability in lighting conditions had a significant effect on the magnitude of ΔE^*, for the majority of the 0.05 wt% sample set and fewer of the 0.1 wt% batch. It is because of the almost-colourless nature of these elastomers that a small difference in lighting had such a profound effect. Therefore, it was decided that colour change values for MAF-0.05 and some members of MAF-0.1 were unreliable, because they could no longer be determined as objective measures of amine-detection. A clear trend was apparent between amine-concentration and ΔE^* values; for all loadings but 0.05 wt%, greater colour change occurred as the amine concentration increased from 100 to 1000 ppm. It was apparent that lower concentrations such as 100-300 ppm would not provide significantly large colour changes until at least 24-hours into the study. Following quantification of the colour change of the PDMS-MAF elastomers, the next step was to determine their apparent detection limits and compare them to what was determined by UV-Vis spectroscopy. The detection limits were determined by quantitative and qualitative examination of the colour change. As $\Delta E^* > 5$ is accepted as being a visually apparent change in colour,[40,55,56] this was a prerequisite for defining a detection limit. However, relying solely on this would provide false-positives, an example includes MAF-0.5, 100 ppm, at 10 minutes (Figure 2-15) where it is clear that a red colouration had yet to develop. Therefore, the detection limits were identified as the concentration at which $\Delta E^* > 5$ was concomitant with the development of a red colouration. Due to the almost colourless nature of the MAF-0.05 elastomers, and therefore visual ambiguity, limits could not be reliably identified. However, the rest were determined for each time period and are displayed in Figure 2-17. Made immediately apparent by the scatterplot; the detection limit logically decreased over time, for all composites. Similarly, the limit would also decrease as MAF-loading was increased; although there is an anomalous discrepancy between MAF-1 and MAF-5 with this trend, as it seemed that the former would generally exhibit greater sensitivity. From the data, it was apparent that the lowest detection limit within a practical time period, i.e. 1 hour, was 300 ppm, using MAF-1.

Sample	Time (min)	Detection limit (ppm)
MAF-0.1	10	1000
	60	600
	1,440	400
MAF-0.5	10	800
	60	500
	1,440	100
MAF-1	10	600
	60	300
	1,440	100
MAF-5	10	700
	60	400
	1,440	100
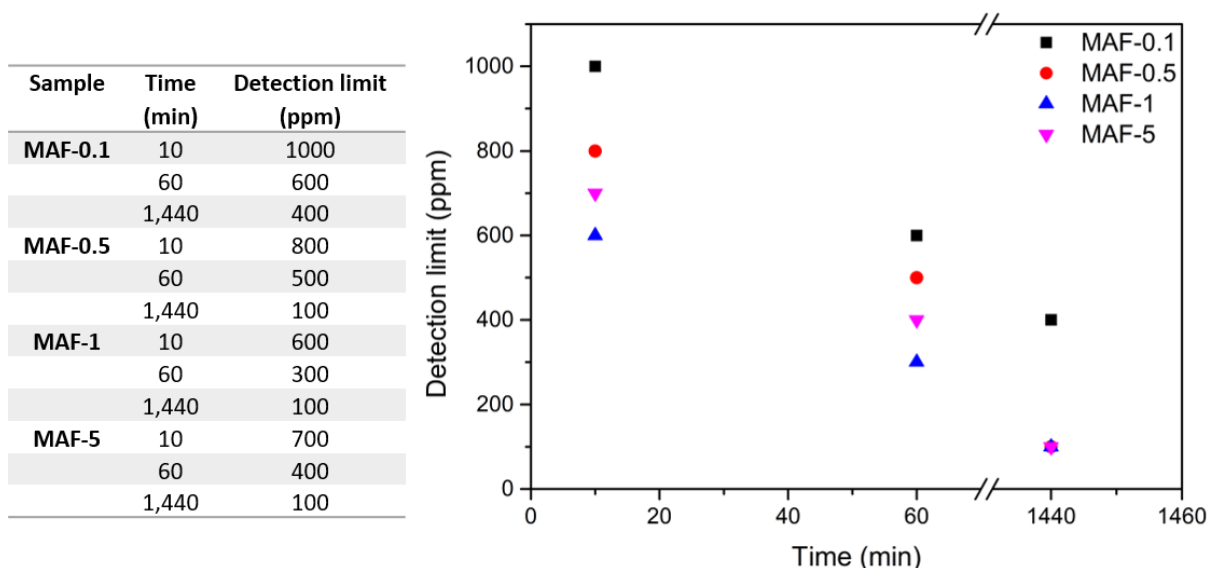
Figure 2-17 – The detection limits of PDMS-MAF composites, during each examined time period, tabulated (left) and plotted (right).

With detection limits established, the next course of action was to compare image analysis and UV-Vis spectroscopy as techniques for determining this metric. Both techniques were used to examine the behaviour of MAF-0.5, the established detection limits from these are recorded in Table 2.3.

Table 2.3 – The determined detection limits of MAF-0.5, with regards to diethylamine, at certain time periods of exposure.

Time (min)	UV-Vis (ppm) [a]	Image analysis (ppm) [b]
0	N/A	N/A
10	>1000	800
20	>1000	N/A
30	1000	N/A
40	900	N/A
50	700	N/A
60	700	500
120	500	N/A
180	400	N/A
1,440	300	100

[a] estimated through visual observation of the data provided in Figure 2-13, [b] calculated through use of CIELAB values discussed in section 2.4.4.

91

Comparison of the data reveals that the image analysis technique had elucidated lower detection limits throughout each shared time period. What was strikingly clear was that UV-Vis spectroscopy was unable to discern any indication of amine until at least 30 minutes into exposure, whereas image analysis required only 10 minutes. The inability for UV-Vis spectroscopy to detect a reaction so early was consequential of the large magnitude of absorption in the region below 400 nm, which was likely eclipsing the emergence of smaller peaks of interest. This large absorption was caused by light scattering; something that could perhaps have been avoided by analysing samples of smaller thickness. It was therefore concluded that image analysis was a better analytical technique for this system.

The sensitivity of these composites has very little meaning without context, which can be provided through comparison with previously-reported systems. The diethylamine detection limit of the PDMS-MAF elastomer doesn't rival that of MAF utilised alone, or the previously-reported poly(oxanorbornene)-based polymer. A 20 mM solution of MAF in THF reportedly displayed a limit of 0.4 ppm within 1 hour, and the 29-31% active-site poly(oxanorbornene) system responded at as low as 20 ppm in aqueous media, within 3 minutes.[40,42] However, PDMS-MAF elastomers hold the advantage of improved stability when compared to MAF itself; MAF-loaded filter paper will decolourise within a matter of minutes when submerged in aqueous solution. Furthermore, the poly(oxanorbornene) architecture cannot perform efficiently under ambient conditions, requiring temperatures in excess of 75 °C in order to rapidly respond at such low concentrations. With respect to both cases, the concentration of analyte-responsive material in PDMS-MAF elastomers was far lower, too, so a higher detection limit is not surprising. Although the sensitivities are less impressive, the PDMS-MAF elastomers are a relatively-stable scaffold for amine-sensing, which function under ambient conditions.

Before concluding this section, it is important to note that evidence of leaching from the PDMS-MAF squares was found. During the study, some surrounding aqueous solutions had adopted a pale-yellow colouration, indicating that the leaching of moieties into the environment had

occurred. An example of this is included as Figure 2-18. This was unexpected, as it was believed that the aqueous environment would not permeate the hydrophobic PDMS network. It was initially believed that this could have been a result of diethylamine-swelling encouraged diffusion. Therefore, a square of MAF-5 was immersed in D_2O for 24 hours and subsequently subjected to ^1H NMR analysis before and after, the results are included as Figure 2-19.


Figure 2-18 – Photographs of MAF-5 suspended in a 1000 ppm diethylamine solution after 24 hours.
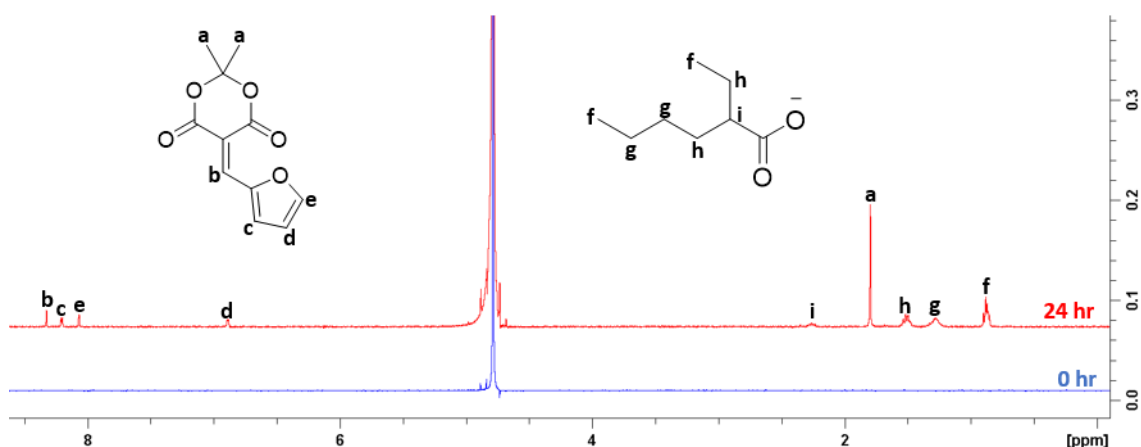
Figure 2-19 – Overlay of the ^1H NMR spectra of the D_2O-diethylamine solution, at 0 hours and 24 hours.

The spectrum confirmed that, over a 24-hour immersion period, a MAF-5 square would leach MAF and 2-ethylhexanoate, or 2-ethylhexanoic acid, from the organotin catalyst complex. The fully characterised ^1H NMR spectra of MAF and the catalyst complex in D_2O can be found in section 2.9 – appendix 2C. As such, it is likely that the yellow colouration shown in Figure 2-18 was a result of leached DASA isomers. This limits the applicability of PDMS-MAF composites in

solution-based environments. However, this is not significant for the context of amine vapour detection – the intended applicational route for this colourimetric sensor.

To conclude, the ability of PDMS-MAF to detect an amine was quantitatively demonstrated by image analysis. Concurrently with section 2.4.3, it was found that, generally, a greater amine or MAF concentration led to a faster response and greater colour change. The lowest detection limit within a practical time period was 300 ppm, from MAF-1. Image analysis was limited in examination of MAF-0.05 samples, due to uncontrolled lighting factors. However, this technique proved to be a more effective means of colour change indication than UV-Vis spectroscopy, in general. As such, image analysis was chosen as the quantitative measure for proof-of-concept experiments, detailed in further sections.

2.4.5 Preliminary amine exposure experiment

Following quantification of the amine-responses of PDMS-MAF composites, their applicational proof-of-concept had to be examined. A preliminary study was conducted whereby MAF-0.5 and a standard PDMS elastomer were exposed to the vapours of two amines. Trimethylamine, dimethylamine and ammonia are three products of microbial degradation, and are commonly utilised analytes for the detection of meat and fish spoilage.[4–6] As such, two amines were selected for this investigation: ammonia and diethylamine, the latter was chosen as dimethylamine was not available at the time and it was thought that this would act as a suitable analogue. Trimethylamine was not used as it does not bear a reactive secondary, or primary, amine. Therefore, the secondary amine and ammonia were decidedly sufficient in providing a proof-of-concept. The PDMS elastomers were included as blank samples, to demonstrate that the amine reactivity was a consequence of MAF incorporation. MAF-0.5 was selected for this study as it was the lowest-loaded network that did not appear to be so adversely affected by lighting conditions (section 2.4.4). Photographs of the experimental setups have been included as Figure 2-20 and Figure 2-22.
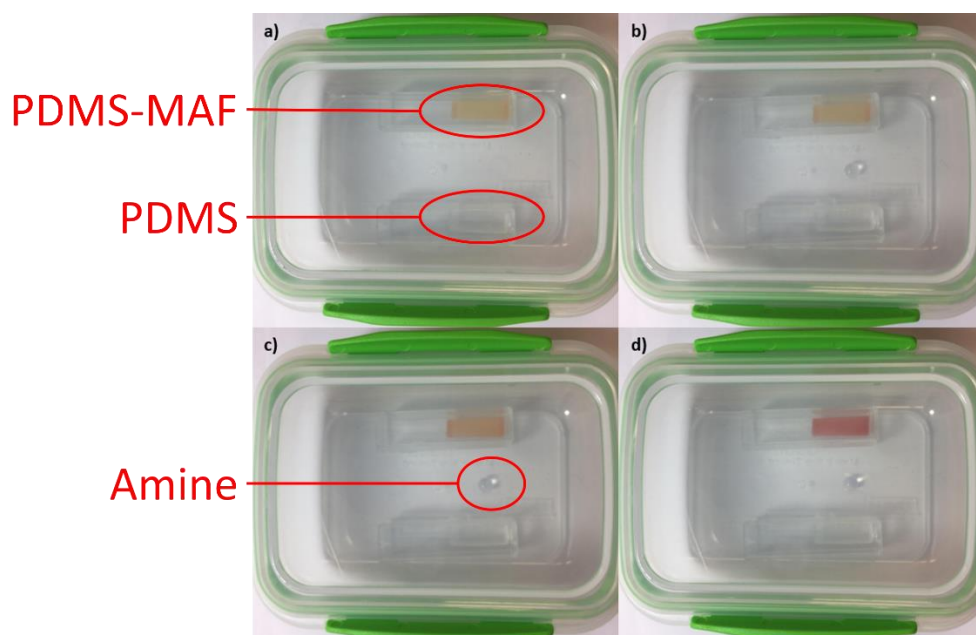
Figure 2-20 - Photographs of the experimental set-up for MAF-0.5 exposure to vapour from a saturated ammonia solution at: a) before addition of solution, b) immediately following addition, c) 1 minute post-addition, d) 10 minutes post-addition.

Figure 2-20 depicts the experimental setup for the ammonia solution experiment. Approximately 20 µl of concentrated ammonia solution was deposited using a Pasteur pipette between two plastic cuvettes, one containing the PDMS-MAF composite and the other a standard PDMS elastomer. As can be seen, there was little visual difference in colour until 1-minute post-deposition of ammonia solution, with a 10-minute interval providing an obvious pink colouration. The photographs were analysed using MATLAB, obtaining RGB colour values, which were then converted to CIELAB values. The CIELAB values were used to calculate ΔE*, a quantification of the change in colour between the initial state (before addition of amine) and the subject time period.[40,55,56] All values have been included in Table 2.4 and Table 2.5, section 2.10 – appendix 2D. The calculated ΔE* values of the MAF-0.5 composite and the blank PDMS network have been plotted together, as Figure 2-21. The ΔE* values for the 1-minute and 10-minute exposures were 10.33 and 27.30, respectively. As these values were above 5, the colour differences were classed as being distinguishable by the human eye.[40,55,56] This data provided confirmation that the composite MAF-0.5 was responsive to, at least, a concentrated solution

of aqueous ammonia. The next test consisted of the same setup but with deposition of diethylamine, photos are displayed as Figure 2-22 and data plotted as Figure 2-23. This experiment was documented for a shorter period of time as the objective was only to record what appeared to be a full external reaction. Subsequently, it was clear that within 1 minute the exterior of the composite had responded to the presence of diethylamine vapour. Evident by Figure 2-22b, the reaction took place instantaneously, appearing as a wave of pink colouration forming across the composite. These findings were a result of a faster reaction rate in contrast to ammonia exposure, agreeing with literature,[40] likely partially caused by the compatibility that diethylamine has with PDMS networks.[57] Colour analysis of photographs was performed on the pixel space that was approximated to be in the centre of the PDMS-MAF composite, hence the immediate photograph measurement had caught the formation of pink colouration. The magnitude of ΔE^* for the composite was above 5, a quantifiable agreement with what was visually apparent.
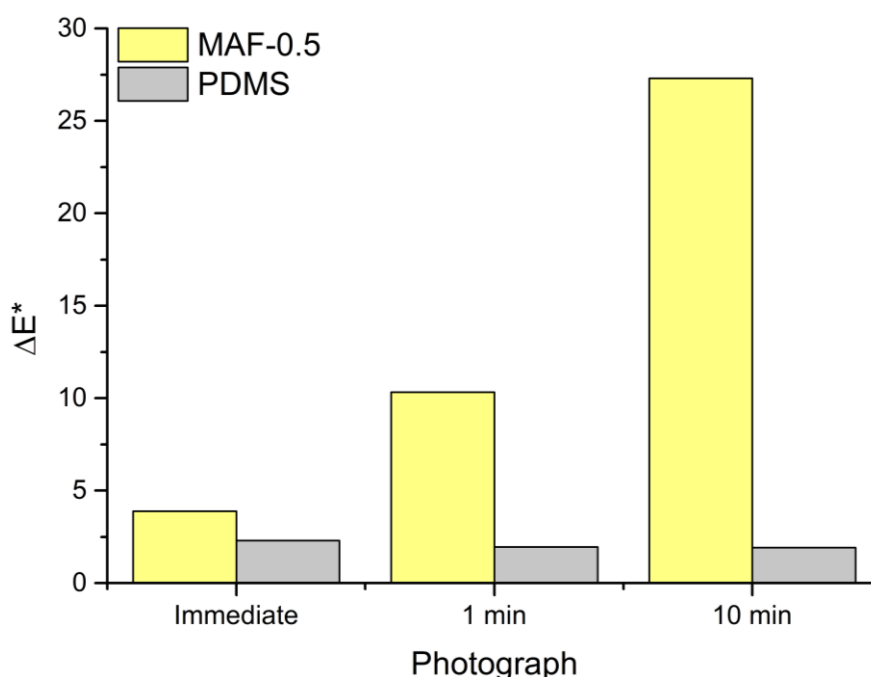

Figure 2-21 – Bar chart of the ΔE^* values obtained from photographs of MAF-0.5 and a blank PDMS network exposed to ammonia vapours, at different time intervals.
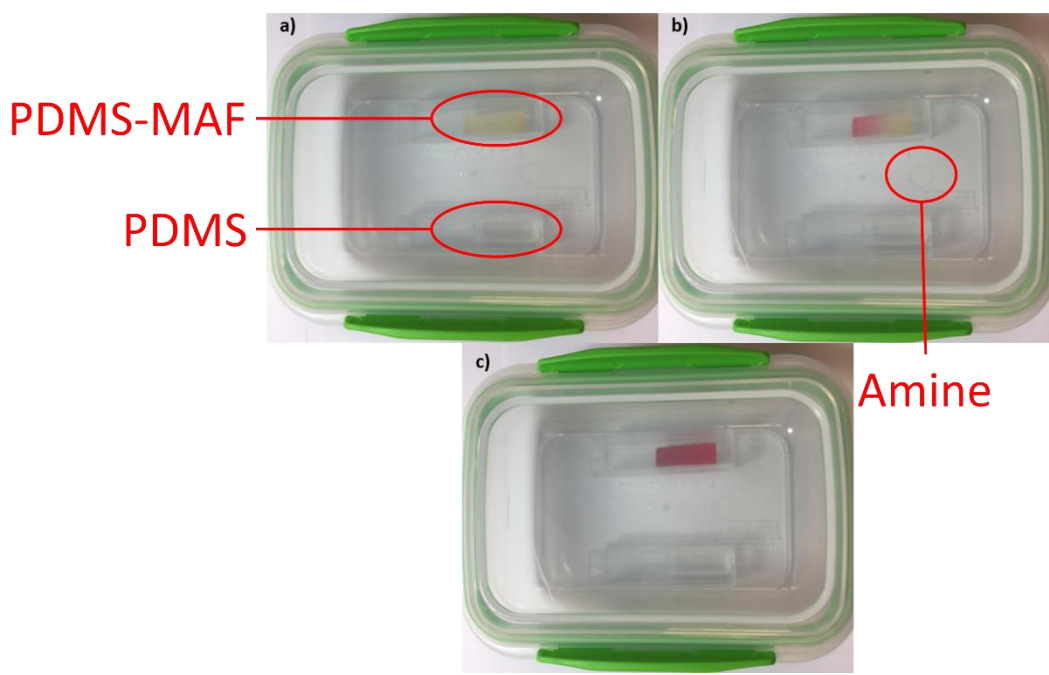
Figure 2-22 - Photographs of the experimental set-up for MAF-0.5 exposure to diethylamine vapour at: a) before addition of solution, b) immediately following addition, c) 1-minute post-addition.
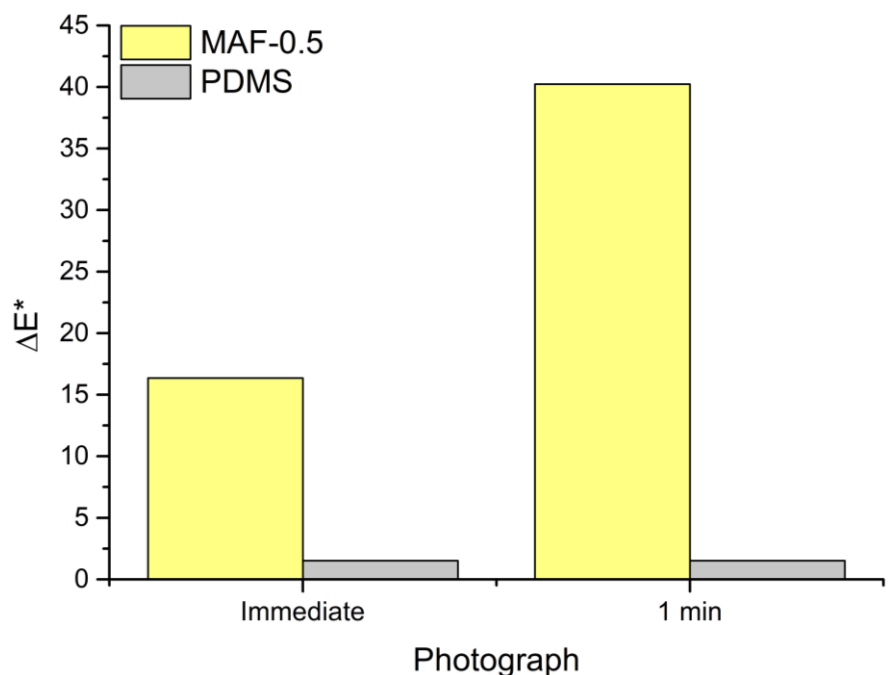

Figure 2-23 - Bar chart of the ΔE* values obtained from photographs of MAF-0.5 and a blank PDMS network exposed to diethylamine vapours, at different time intervals.

2.4.6 Cod decomposition experiment

2.4.6.1 Image quantification of amine-sensitivity

The previous section detailed the exposure of PDMS-MAF composites to diethylamine and concentrated ammonia solution. A demonstrable reaction was caused by the presence of diethylamine and ammonia, indicating a degree of food decomposition responsivity, however these were concentrated vapours and so a practical example had to be investigated. Therefore, cod fillets were sourced from a local Fishmonger, cut into smaller portions with a heat-treated scalpel blade on an ethanol-cleaned surface and frozen, within one hour of purchase. Upon requirement for experimentation, a single portion was removed from the freezer and left to defrost in a fridge for 2 hours, following which it was subjected to the experimental procedure that was described in section 2.2.8. Photographs of the setup were taken upon container sealing and 24 hours later, included as Figure 2-24.
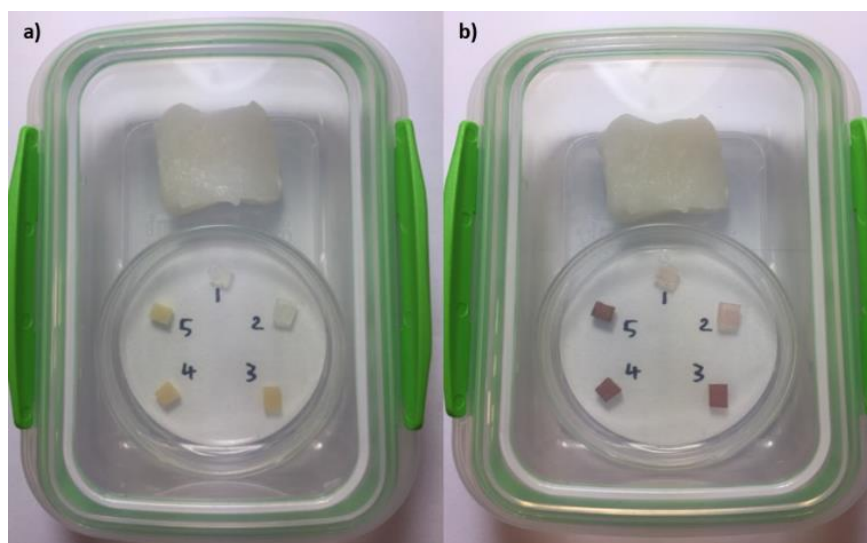
Figure 2-24 - Photographs of the experimental set-up for amine-detection in the presence of a cod fillet, a) immediately after sealing, b) 24 hours later.

Figure 2-24a depicts the experimental setup at time 0 hr; unreacted composites were placed in a petri dish and labelled 1 to 5, denoting the increasing concentration of MAF. Beside the dish (above, in the photograph) was the cod portion, both the dish and cod were sealed in a Sistema® food container and placed on a benchtop over a 24-hour period under dark, ambient conditions.

The state of the experiment after the 24-hour period is shown as Figure 2-24b, whereby it was visually clear that at least samples 3 to 5 (MAF-0.5, MAF-1 and MAF-5) had undergone a colour change within that time. The reaction of 1 and 2 was more subtle but could still be distinguished with careful observation. As with the previous amine tests, the imagery was analysed with MATLAB to obtain quantifiable proof of colour change, those values have been plotted as Figure 2-25. Raw data has been included in Table 2.6, section 2.10 – appendix 2D.
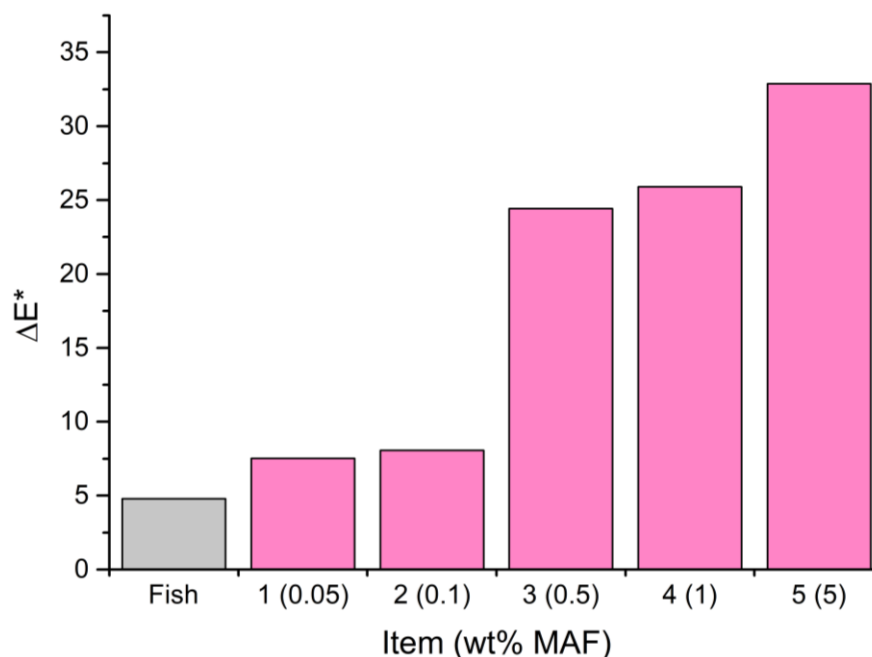

Figure 2-25 - Bar chart of the ΔE* values obtained from photographs of PDMS-MAF composites after 24 hours of exposure to a decaying cod sample.

The data shows that a larger colour change was observed for those with higher loadings of MAF, which is logical as a greater quantity of MAF should lead to a greater quantity of coloured DASA, and so a more vibrant colour would appear. The ΔE* measure for each sample was above 5 and so it was unambiguously determined quantitatively and qualitatively that this reaction was distinguishable by the human eye.[40,56] In conclusion, it appears that the PDMS-MAF composites are well-suited for the detection of fish decomposition; demonstrating its utility in smart packaging applications as a safety and quality assessment tool. Given that meat decomposition leads to similar products, it is assumed that this could be applied to meat packaging, too. Further

experimentation is needed to ascertain whether this system can effectively determine the point of spoilage of a fish sample. Previously conducted research has reported that the spoilage threshold for cod was approximately 18 hours, when kept at 20 °C.[5] Although the spoilage thresholds can vary between species and are subject to treatment,[58] this provides an insight into the timescale required for a response. From the findings of this experiment, it would be ideal to conduct a future study entailing the documentation and recording of time intervals within the 24-hour period, in order to better ascertain the point at which decomposition can be identified. The desirable characteristic that this preliminary architecture has is it's real-time monitoring and immediate interrogatability, when compared with other methods that require the use of secondary equipment.[1,3,5]

2.4.6.2 RFID quantification of amine-sensitivity

The findings of the previous experiment had proved that the PDMS-MAF composites could be used as colourimetric sensors in the identification of cod decomposition, when packaged together. It was then decided to investigate the possibility of utilising stimuli that did not require line of sight with a product; the use of UHF RFID sensing tags. It has been previously reported that RFID sensing is an inexpensive, competitive alternative for the monitoring of foodstuffs, and as such was a driving influence for this section of work.[59–63] As explained in section 2.2.8.2, a film of MAF-0.5 was applied to the reverse of an UHF RFID sensing tag in order to enable the use of the adhesive side. The adhesive was used to apply the tag to the lid of a Sistema® food container so that a cutting of cod could be taped to the base of the setup. This way, the tag would be positioned above the fish, as the reverse could lead to the tape failing and causing the fish to come into direct contact with the tag which would inevitably invalidate the experiment. Photographs of the setup can be seen in Figure 2-26. Firstly, it needed to be proved that a film applied to the reverse side of the tag would not have a detrimental effect on its performance. Therefore, RFID measurements were acquired for two different devices; a tag covered with standard cross-linked PDMS applied to the antenna-side and a tag covered with standard cross-linked PDMS applied to the reverse-side. The data for those measurements have been included

as Figure 2-27a, the variation in sensor value was insignificant. Further measurements were taken which involved the PDMS-MAF tag within the setup, and the tag isolated without the container and fish, that data is included as Figure 2-27b. The data provided a clear indication that the container and fish did not affect sensor values.

Figure 2-26 – Perspective of the fish decomposition experiment from above (left) and below (right), where the RFID tag is adhered to the inside of the lid and the fish portion is taped down to the base of the container.
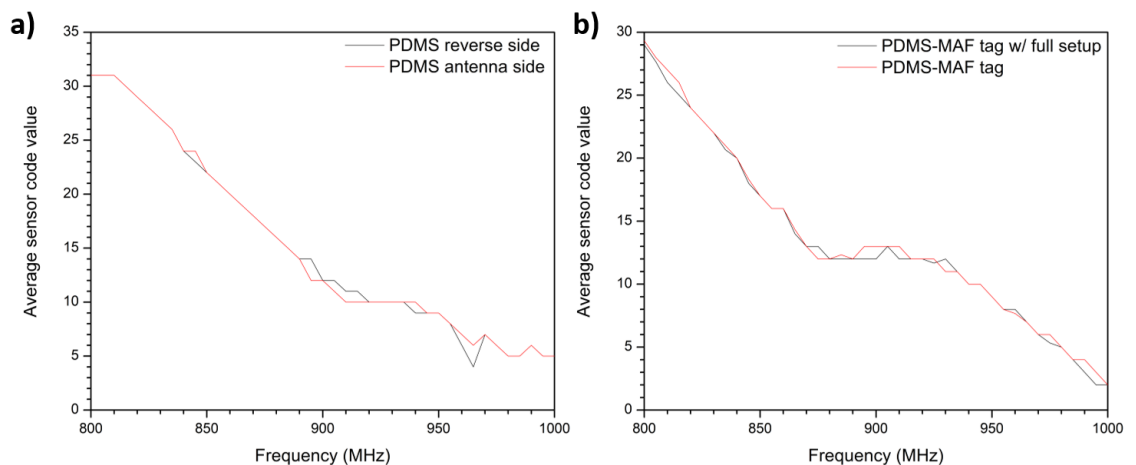

Figure 2-27 - Average sensor code values for a) cross-linked PDMS films that were applied to either the antenna-side of the tag or the reverse-side, b) the PDMS-MAF tag alone and with the rest of the experimental setup.

Consequently, for convenience, the tag was not removed from the experimental setup when the final measurement was taken. Final analysis was conducted 24 hours post-sealing of the food container, the sensor values were compared against initial data and are displayed as Figure 2-28a. There appeared to be very little variation in the data, which is unsurprising as visual inspection revealed that DASA formation did not occur. The PDMS-MAF film was expected to change colour from yellow to dark pink, similar to what had been found previously (Figure 2-24), however it had appeared that the yellow colouration had darkened rather than change altogether. Therefore, there was no clear indication of DASA formation. What's more, small, yellow crystal growths had appeared on the surface of the film. These growths were believed to be MAF crystals, likely seeded by the presence of external microcrystals present after the curing step had finished, which were not washed away with DI H_2O as this step was not taken with the tag-making process. It was not apparent as to why these crystals had not reacted to the decomposition of the cod portion. Photographs of the tag before and after are included Figure 2-28b-d, for comparison.
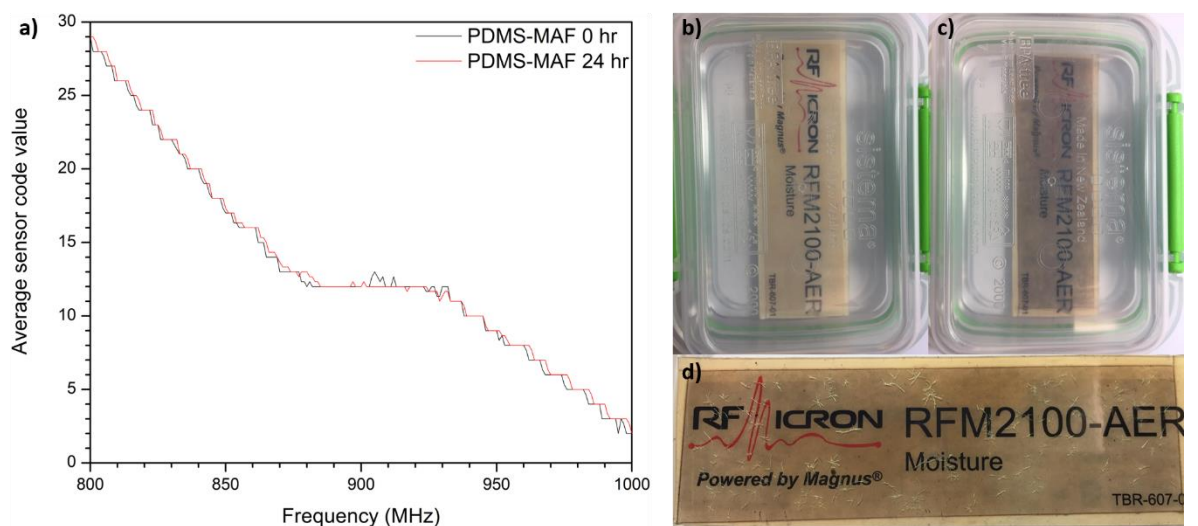

Figure 2-28 – a) A comparison of the sensor code values for the PDMS-MAF exposure to fish experiment at 0 and 24 hours; b) tag immediately before inclusion of the cod sample; c) 24 hours after; d) without the container to provide a clearer perspective of the crystal growth.

Following these findings, it was decided to directly expose this film to an amine in order to ascertain whether it simply was not respondent, or another factor had prevented the reaction. A single drop of concentrated ammonia solution was deposited onto the surface of the PDMS-MAF film, immediately a reaction ensued whereby the dark yellow film was rapidly beginning to develop a pink colouration. A photograph comparison is included as Figure 2-29. Unfortunately, there is no explanation as to why the original exposure had not presented a similar result. To conclude, this experiment was not able to ascertain whether amine-detection can be quantified by RFID sensing analysis. Considering that a reaction to cod decomposition was exhibited by the PDMS-MAF composites in section 2.4.6.1, the result of this experiment is surprising; especially so given that a demonstrable colour change was found upon deposition of concentrated ammonia. Any further investigation regarding this technique should include examination of composites of varying thickness and volume, to see if there is a relationship between thickness and reactivity.

Figure 2-29 – A comparison of the PDMS-MAF tag before (left) and after (right) addition of a single drop of concentrated ammonia solution.

2.5 Conclusions and future work

This chapter of work has introduced an amine-responsive polymeric material consisting of a cross-linked PDMS network doped with the amine-sensitive molecule, MAF. Amine-detection was quantified through UV-Vis spectroscopy and image analysis, and the applicability of the composite was demonstrated by simulation of a food-packaging environment.

The amine-responsivity of a PDMS-MAF elastomer, MAF-0.5, was quantified and assessed using UV-Vis spectroscopy. This was enacted by immersing composites in aqueous diethylamine solutions of various concentrations and subjecting them to spectroscopic scans at various time intervals. A general trend was found whereby increasing the amine concentration resulted in a larger, more rapid colour change response. Furthermore, longer exposure times were required for solutions of low amine concentration, as expected. The fastest recordable response was within 30 minutes, at 1000 ppm diethylamine exposure, however visual observation indicated that a colour change was apparent before this. It was determined that initial response signals would be overshadowed by the light-scattering distortion of the baseline and the large absorbance signal centred around 400 nm. This limited the applicability of UV-Vis spectroscopy as a quantitative technique to measure amine-detection. As such, following investigations were evaluated through a combination of qualitative visual observation and quantitative image analysis.

Image analysis of PDMS-MAF composites entailed a similar methodology to the UV-Vis spectroscopy experiment; samples were immersed in aqueous diethylamine solutions for a certain period of time and examined at various intervals. Amine-detection was quantified through colour change of the composites, using ΔE* as an evaluative metric. Visual observation was required to validate what was found by ΔE* changes; to eliminate the possibility of false-positives, caused by lighting variables. Data for MAF-0.05 was affected by the aforementioned factors and was therefore deemed unreliable and unusable. As was the case previously, it was found that a greater amine concentration would lead to larger colour changes, more rapidly.

The same effect was found with increasing MAF-loading, too. The detection limits determined through image analysis were found to be lower than that elucidated by UV-Vis spectroscopy. This was a consequence of UV-Vis absorbance baseline distortion caused by light scattering. Subsequently, it was shown that image analysis was a better quantitative technique for the evaluation of amine-detection. From this analysis, it was found that the lowest detectable concentrations of diethylamine within 10-minute and 1-hour periods, were 800 and 500 ppm, respectively. These limits were much higher than those previously-reported when using MAF itself, and a covalently-bound poly(oxanorbornene) derivative.[40,42] However, the PDMS-MAF elastomers are more stable than MAF alone and are able to operate under ambient conditions, unlike the poly(oxanorbornene) system.

Following quantification of the amine-detection process, the applicability of the PDMS-MAF elastomers was demonstrated, initially through a preliminary amine-exposure experiment. This experiment entailed the examination of a MAF-0.5 composite, a cross-linked PDMS network and 20 µl of concentrated ammonia solution, or diethylamine, within a sealed container. The setup was designed to simulate a food-packaging environment whereby amine-detection could be easily interpreted without the need for removal of the sensing material. Photographs were taken before, immediately after, 1 minute later and 10 minutes later. They were then evaluated with the same metrics as previous image analysis measurements. It was found that both ammonia and diethylamine would produce a readable response, with the latter being faster. Success of this experiment influenced a further iteration that utilised cod fillets, rather than concentrated amine solutions. The cod decomposition experiment employed all MAF-loadings, revealing that each would exhibit a colour change within a 24-hour exposure period. As expected, the magnitude of colour change increased with MAF-loading. This experiment demonstrated the practical applicability of the PDMS-MAF elastomers as colourimetric sensors in food packaging. Finally, a third packaging experiment was performed that involved attempted quantification of amine-detection, through RFID sensing. A MAF-0.5 film was applied to an RFID sensing tag, which was subsequently adhered to the inside of a food-container. This setup also included a

cod fillet as a source of amines. However, the film did not appear to react within the 24-hour period, reasoning for this is not known. Deposition of a concentrated ammonia solution onto the tag, post-exposure, did yield a colourimetric response. Therefore, it is possible that the concentration of amine released during cod decomposition was too low to yield a response from the film.

Future investigation would entail more thorough examination of the elastomers during fish decomposition; to evaluate colour change at different time periods through the 24-hour exposure. This would provide a better approximation of how soon a response can be seen. It would be desirable to either increase the loading of MAF in the PDMS networks or covalently attach it, thereby increasing amine-sensitivity and stability. However, this would require balancing synthetic accessibility with amine-detection efficiency. Currently, the elastomer is in a position where it produces the desired response, with synthetic and economic accessibility.

2.6 References

1   Z. Li and K. S. Suslick, *ACS Sensors*, 2016, **1**, 1330–1335.

2   Y. Hu, X. Ma, Y. Zhang, Y. Che and J. Zhao, *ACS Sensors*, 2016, **1**, 22–25.

3   H. Li, Q. Chen, J. Zhao and Q. Ouyang, *Anal. Methods*, 2014, **6**, 6271–6277.

4   U. Khulal, J. Zhao, W. Hu and Q. Chen, *RSC Adv.*, 2016, **6**, 4663–4672.

5   A. Pacquit, K. T. Lau, H. McLaughlin, J. Frisby, B. Quilty and D. Diamond, *Talanta*, 2006, **69**, 515–520.

6   B. Kuswandi, Jayus, A. Restyana, A. Abdullah, L. Y. Heng and M. Ahmad, *Food Control*, 2012, **25**, 184–189.

7   T. Lin, Y. Wu, Z. Li, Z. Song, L. Guo and F. Fu, *Anal. Chem.*, 2016, **88**, 11022–11027.

8   K. L. Bicker, S. L. Wiskur and J. J. Lavigne, *Chemosensors: Principles, Strategies and Applications*, John Wiley & Sons, Inc., Hoboken, 2011.

9   L. Feng, C. J. Musto, J. W. Kemling, S. H. Lim and K. S. Suslick, *Chem. Commun.*, 2010, **46**, 2037–2039.

10   K. E. Secor and T. E. Glass, *Org. Lett.*, 2004, **6**, 3727–3730.

11   T. Fan, W. Xu, J. Yao, Z. Jiao, Y. Fu, D. Zhu, Q. He, H. Cao and J. Cheng, *ACS Sensors*, 2016, **1**, 312–317.

12   J. Jaworski, K. Yokoyama, C. Zueger, W. J. Chung, S. W. Lee and A. Majumdar, *Langmuir*, 2011, **27**, 3180–3187.

13   X. Sun, Y. Wang and Y. Lei, *Chem. Soc. Rev.*, 2015, 44, 8019–8061.

14   E. Coronado, J. R. Galán-Mascarós, C. Martí-Gastaldo, E. Palomares, J. R. Durrant, R. Villar, M. Gratzel and M. K. Nazeeruddin, *J. Am. Chem. Soc.*, 2005, **127**, 12351–12356.

15   W. S. P. Carvalho, M. Wei, N. Ikpo, Y. Gao and M. J. Serpe, *Anal. Chem.*, 2018, 90, 459–479.

16   H. N. Kim, W. X. Ren, J. S. Kim and J. Yoon, *Chem. Soc. Rev.*, 2012, 41, 3210–3244.

17   G. Preti, J. N. Labows, J. G. Kostelc, S. Aldinger and R. Daniele, *J. Chromatogr. B Biomed. Sci. Appl.*, 1988, **432**, 1–11.

18   R. Simenhoff, M; Burke, J; Saukkonen, J; Ordinario, A; Doty, *N. Engl. J. Med.*, 1977, **297**, 132–135.

19   S. Bhadra, C. Narvaez, D. J. Thomson and G. E. Bridges, *Talanta*, 2015, **134**, 718–723.

20   S. F. Liu, A. R. Petty, G. T. Sazama and T. M. Swager, *Angew. Chemie - Int. Ed.*, 2015, **54**, 6554–6557.

21   G. A. Sotzing, J. N. Phend, R. H. Grubbs and N. S. Lewis, *Chem. Mater.*, 2000, **12**, 593–595.

22   G. J. Mohr, C. Demuth and U. E. Spichiger-Keller, *Anal. Chem.*, 1998, **70**, 3868–3873.

23   J. Kumpf and U. H. F. Bunz, *Chem. - A Eur. J.*, 2012, **18**, 8921–8924.

24   A. R. Longstreet, M. Jo, R. R. Chandler, K. Hanson, N. Zhan, J. J. Hrudka, H. Mattoussi, M. Shatruk and D. T. McQuade, *J. Am. Chem. Soc.*, 2014, **136**, 15493–15496.

25   S. Rochat and T. M. Swager, *Angew. Chemie - Int. Ed.*, 2014, **53**, 9792–9796.

26   M. Gao, S. Li, Y. Lin, Y. Geng, X. Ling, L. Wang, A. Qin and B. Z. Tang, *ACS Sensors*, 2016, **1**, 179–184.

27   P. A. Peixoto, A. Boulangé, M. Ball, B. Naudin, T. Alle, P. Cosette, P. Karuso and X. Franck, *J. Am. Chem. Soc.*, 2014, **136**, 15248–15256.

28   Y. Shen, M. Kuang, Z. Shen, J. Nieberle, H. Duan and H. Frey, *Angew. Chemie - Int. Ed.*, 2008, **47**, 2227–2230.

29   S. W. Thomas, G. D. Joly and T. M. Swager, *Chem. Rev.*, 2007, 107, 1339–1386.

30   X. Wang, T. W. Chang, G. Lin, M. R. Gartia and G. L. Liu, *Anal. Chem.*, 2017, **89**, 611–615.

31   H. N. Kim, Z. Guo, W. Zhu, J. Yoon and H. Tian, *Chem. Soc. Rev.*, 2011, 40, 79–93.

32   A. T. Hoang, Y. B. Cho, J. S. Park, Y. Yang and Y. S. Kim, *Sensors Actuators, B Chem.*, 2016, **230**, 250–259.

33   N. A. Rakow, A. Sen, M. C. Janzen, J. B. Ponder and K. S. Suslick, *Angew. Chemie - Int. Ed.*, 2005, **44**, 4528–4532.

34   H. Xiao-Wei, L. Zhi-Hua, Z. Xiao-Bo, S. Ji-Yong, M. Han-Ping, Z. Jie-Wen, H. Li-Min and M. Holmes, *Food Chem.*, 2016, **197**, 930–936.

35   S. Helmy, F. A. Leibfarth, S. Oh, J. E. Poelma, C. J. Hawker and J. R. De Alaniz, *J. Am. Chem. Soc.*, 2014, **136**, 8169–8172.

36   S. Helmy, S. Oh, F. A. Leibfarth, C. J. Hawker and J. Read De Alaniz, *J. Org. Chem.*, 2014, **79**, 11316–11329.

37   A. Balamurugan and H. Il Lee, *Macromolecules*, 2016, **49**, 2568–2574.

38   B. P. Mason, M. Whittaker, J. Hemmer, S. Arora, A. Harper, S. Alnemrat, A. McEachen, S. Helmy, J. Read de Alaniz and J. P. Hooper, *Appl. Phys. Lett.*, 2016, **108**, 041906-1–4.

39   D. Zhong, Z. Cao, B. Wu, Q. Zhang and G. Wang, *Sensors Actuators, B Chem.*, 2018, **254**, 385–392.

40   Y. J. Diaz, Z. A. Page, A. S. Knight, N. J. Treat, J. R. Hemmer, C. J. Hawker and J. Read de Alaniz, *Chem. - A Eur. J.*, 2017, **23**, 3562–3566.

41   X. Feng, L. Liu, S. Wang and D. Zhu, *Chem. Soc. Rev.*, 2010, 39, 2411–2419.

42   Q. Chen, Y. J. Diaz, M. C. Hawker, M. R. Martinez, Z. A. Page, S. Xiao-An Zhang, C. J. Hawker and J. Read De Alaniz, *Macromolecules*, 2019, **52**, 4370–4375.

43   N. Bosq, N. Guigo, J. Persello and N. Sbirrazzuoli, *Phys. Chem. Chem. Phys.*, 2014, **16**,

7830–7840.

44   J. N. Lee, C. Park and G. M. Whitesides, *Anal. Chem.*, 2003, **75**, 6544–6554.

45   J. Karovičová and Z. Kohajdová, *Chem. Pap.*, 2005, 59, 70–79.

46   A. Naila, S. Flint, G. Fletcher, P. Bremer and G. Meerdink, *J. Food Sci.*, 2010, **75**, 139–150.

47   F. Bedia Erim, *Trends Anal. Chem.*, 2013, **52**, 239–247.

48   C. V Rumens, M. A. Ziai, K. E. Belsey, J. C. Batchelor and S. J. Holder, *J. Mater. Chem. C*, 2015, **3**, 10091–10098.

49   C. Liewhiran and S. Phanichphant, *Sensors*, 2007, **7**, 650–675.

50   M. M. Lerch, W. Szymański and B. L. Feringa, *Chem. Soc. Rev.*, 2018, 47, 1910–1937.

51   F. Bigi, S. Carloni, L. Ferrari, R. Maggi, A. Mazzacani and G. Sartori, *Tetrahedron Lett.*, 2001, **42**, 5203–5205.

52   F. Rubio, J. Rubio and J. L. Oteo, *Spectrosc. Lett.*, 1998, **31**, 199–219.

53   D. E. Clark, *Spectrosc. Lett.*, 1992, **25**, 201–220.

54   M. M. Lerch, M. Di Donato, A. D. Laurent, M. Medved, A. Iagatti, L. Bussotti, A. Lapini, W. J. Buma, P. Foggi, W. Szymański and B. L. Feringa, *Angew. Chemie Int. Ed.*, 2018, **58**, 8063–8068.

55   A. R. Robertson, *Color Res. Appl.*, 1977, **2**, 7–11.

56   G. Sharma, W. Wu and E. N. Dalal, *Color Res. Appl.*, 2005, **30**, 21–30.

57   Q. W. Yuan and J. E. Mark, *Macromol. Chem. Phys.*, 1999, **200**, 206–220.

58   L. Byrne, K. T. Lau and D. Diamond, *Analyst*, 2002, **127**, 1338–1341.

59   Z. Meng and Z. Li, *Meas. Sci. Rev.*, 2016, **16**, 305–315.

60   D. Nguyen, G. Phan, T. Pham and N. Le, in *Progress In Electromagnetics Research*

Symposium, 2013, pp. 583–587.

61   R. A. Potyrailo, N. Nagraj, Z. Tang, F. J. Mondello, C. Surman and W. Morris, *J. Agric. Food Chem.*, 2012, **60**, 8535–8543.

62   L. K. Fiddes, J. Chang and N. Yan, *Sensors Actuators, B Chem.*, 2014, **202**, 1298–1304.

63   K. H. Eom, M. C. Kim, S. Lee and C. W. Lee, *Int. J. Distrib. Sens. Networks*, 2012, **8**, 1–6.

2.7 Appendix 2A
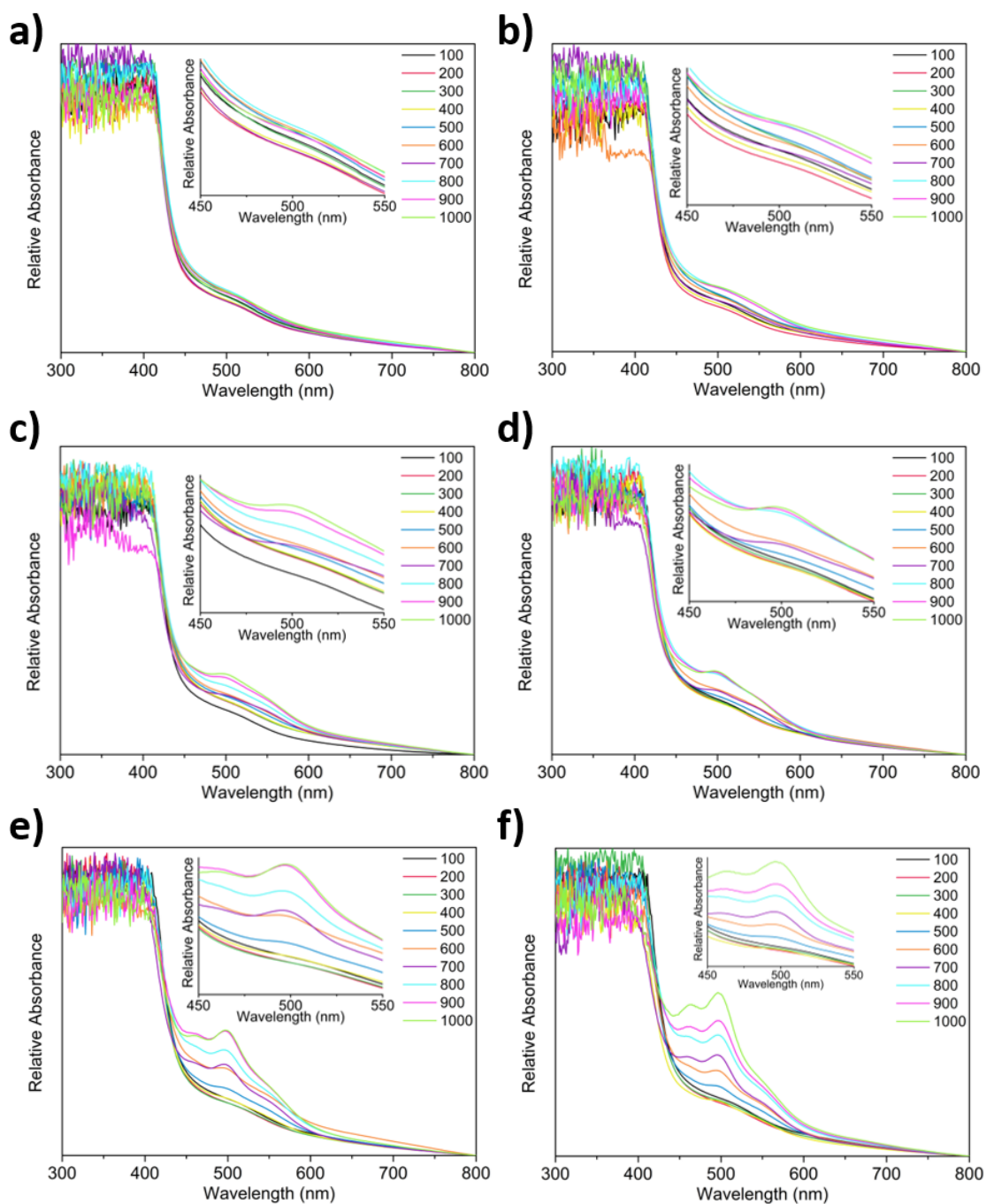
Figure 2-30 – UV-Vis spectra of MAF-0.5 immersed in DI H$_2$O after treatment with aqueous diethylamine solutions, at concentrations of 100 to 1000 ppm, at a) 10 minutes, b) 20 minutes, c) 40 minutes, d) 50 minutes, e) 120 minutes, and f) 180 minutes.

2.8 Appendix 2B
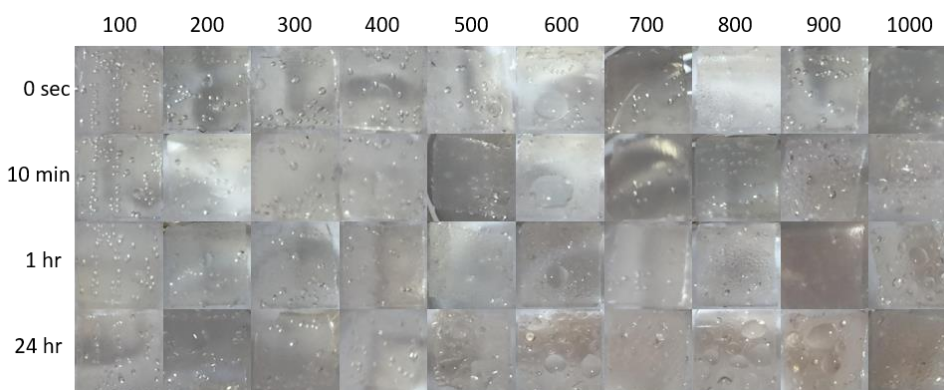
Figure 2-31 – Photograph matrix of MAF-0.05 suspended in an aqueous solution of diethylamine, at various time periods, over a concentration range of 100 to 1000 ppm.
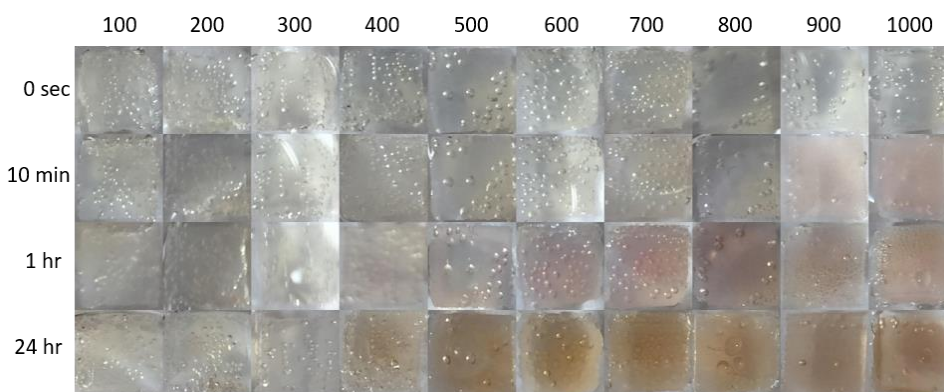

Figure 2-32 - Photograph matrix of MAF-0.01 suspended in an aqueous solution of diethylamine, at various time periods, over a concentration range of 100 to 1000 ppm.
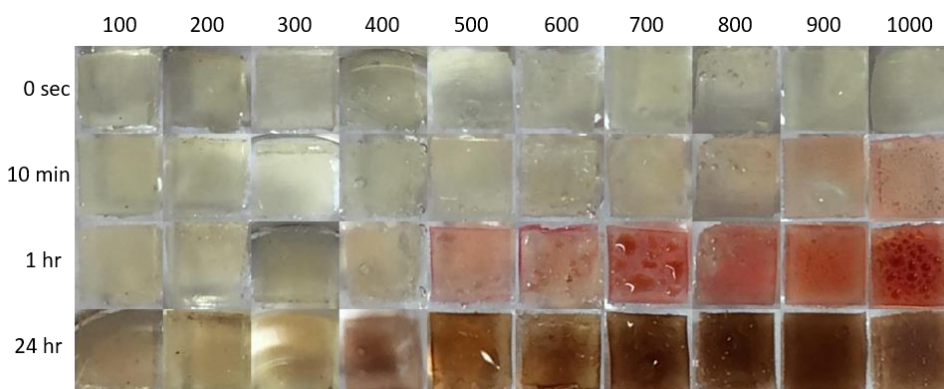
Figure 2-33 - Photograph matrix of MAF-0.5 suspended in an aqueous solution of diethylamine, at various time periods, over a concentration range of 100 to 1000 ppm.
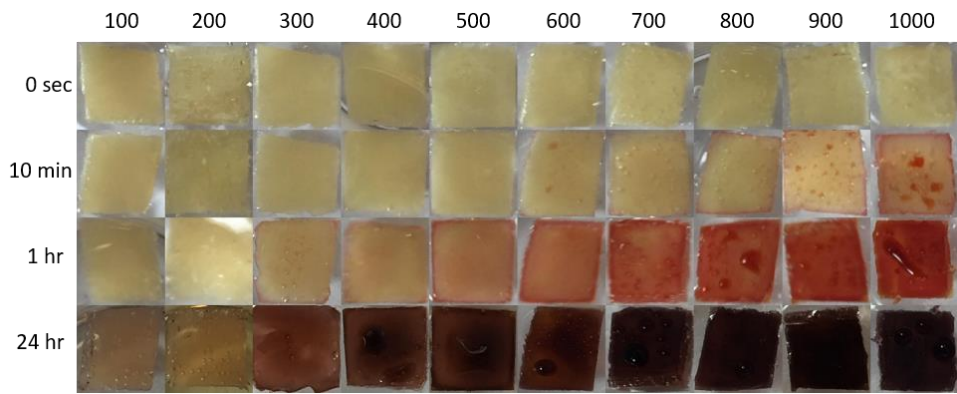
Figure 2-34 - Photograph matrix of MAF-1 suspended in an aqueous solution of diethylamine, at various time periods, over a concentration range of 100 to 1000 ppm.
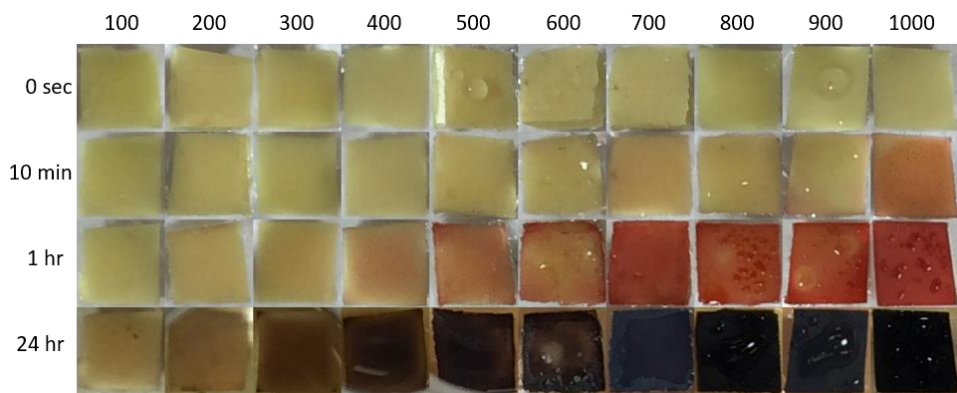
Figure 2-35 - Photograph matrix of MAF-5 suspended in an aqueous solution of diethylamine, at various time periods, over a concentration range of 100 to 1000 ppm.
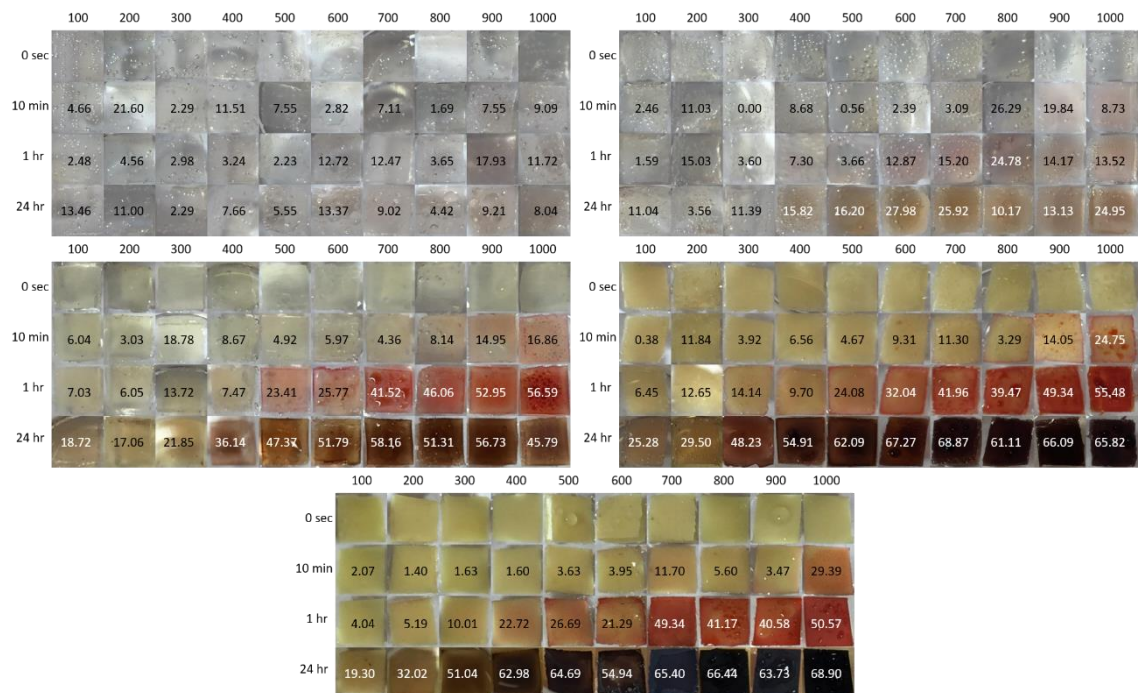

**Figure 2-36 – A combination of the previous photograph matrices, with ΔE* values added.**

2.9 Appendix 2C
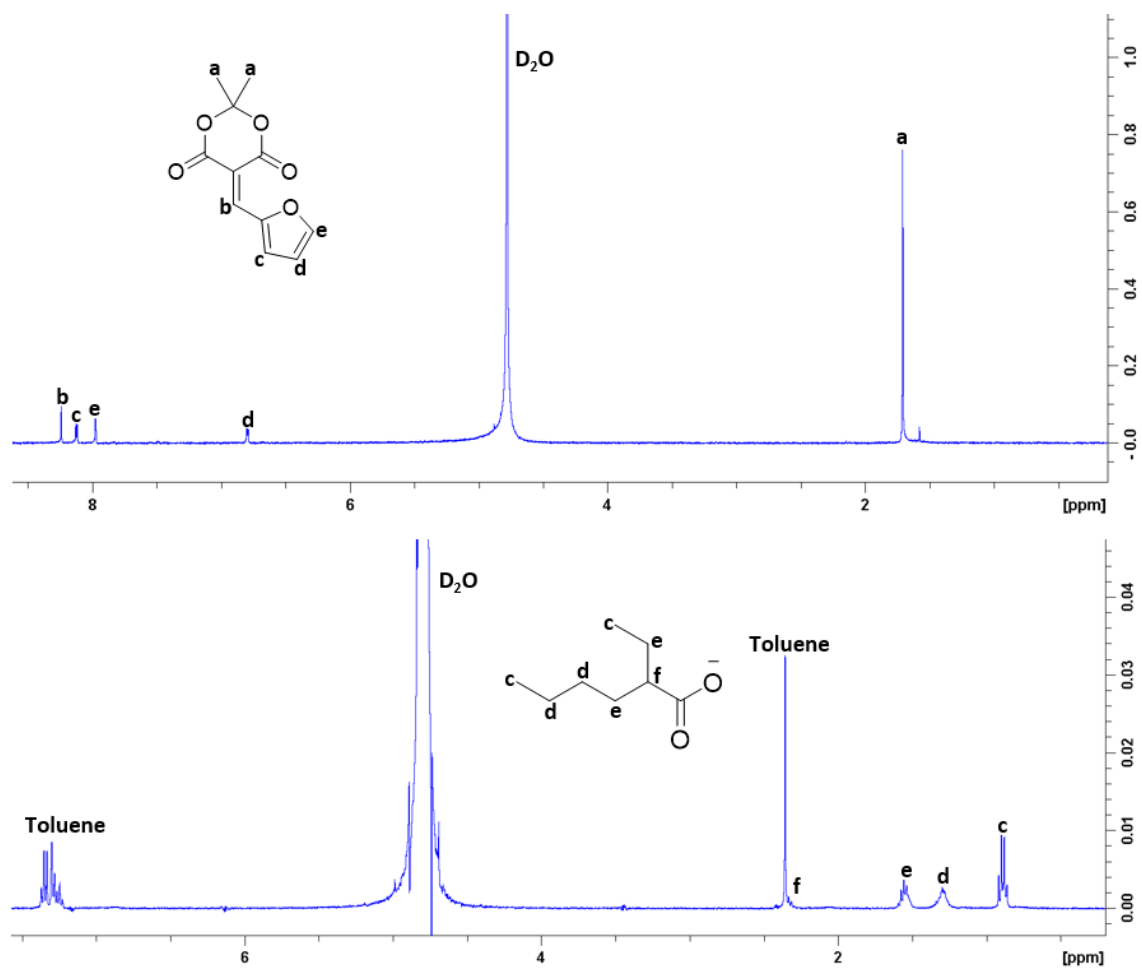
Figure 2-37 -Characterised ^{1}HMR of MAF (top) and the Sn(II) 2-ethylhexanoate-toluene solution (bottom), both acquired in D_2O.

2.10 Appendix 2D

Table 2.4 – Colour metrics for the ammonia solution experiment. Photograph column corresponds to various time periods concerning ammonia deposition.

Photograph	Item	R	G	B	L*	a*	b*	ΔE*
Before	MAF-0.5	160	147	113	61.25	-0.63	19.79	N/A
	PDMS	141	143	140	59.16	-1.32	1.34	N/A
Immediate	MAF-0.5	154	139	110	58.47	0.94	17.59	3.88
	PDMS	147	149	146	61.46	-1.31	1.33	2.30
1 min	MAF-0.5	152	126	103	54.63	6.48	16.28	10.33
	PDMS	146	147	142	60.72	-1.32	2.51	1.95
10 min	MAF-0.5	147	96	92	46.1	20.24	10.84	27.30
	PDMS	146	148	145	61.08	-1.31	1.33	1.92

Table 2.5 – Colour metrics for the diethylamine experiment. Photograph column corresponds to various time periods concerning diethylamine deposition.

Photograph	Item	R	G	B	L*	a*	b*	ΔE*
Before	MAF-0.5	155	155	129	63.34	-4.6	13.67	N/A
	PDMS	145	147	144	60.69	-1.31	1.33	N/A
Immediate	MAF-0.5	160	130	120	56.88	9.91	9.75	16.36
	PDMS	149	151	148	62.22	-1.3	1.32	1.53
1 min	MAF-0.5	135	75	85	39.31	26.58	5.31	40.24
	PDMS	149	151	148	62.22	-1.3	1.32	1.53

Table 2.6 – Colour metrics for PDMS-MAF composites and the cod portion, at time equals 0 and 24 hours.

Photograph	Item	R	G	B	L*	a*	b*	ΔE*
0 hr	Fish	166	162	153	66.71	-0.2	5.19	N/A
	1	174	173	169	70.7	-0.39	2.18	N/A
	2	159	159	147	65.18	-2.21	6.26	N/A
	3	151	132	100	56.09	2.26	19.96	N/A
	4	155	136	106	57.67	2.48	18.77	N/A
	5	154	145	104	60	-3.21	23.01	N/A
24 hr	Fish	161	155	139	64.07	-0.65	9.17	4.80
	1	164	155	146	64.49	1.68	5.89	7.52
	2	164	146	136	61.85	4.99	7.74	8.07
	3	119	85	84	39.68	13.97	6.18	24.42
	4	114	85	87	39.18	12.35	3.52	25.92
	5	110	85	88	38.75	10.86	2.23	32.88

Chapter 3:

Physical blending of donor-acceptor Stenhouse adducts into cross-linked siloxane networks

3.1 Introduction

Over the years, photoswitches have garnered a large amount of interest regarding the unique properties that they exhibit when isomerising under exposure to light; including their ability to change polarity, size and shape.[1–5] What makes them so attractive is the potential for spatiotemporal external control over inducing microscopic changes in various architectures.[6–8] The most commonly studied photoswitches are the azobenzenes, spiropyrans and diarylethenes, which have been shown to be instrumental throughout a host of applications, such as; logic gates,[9] sensor materials,[10–12] memory storage,[13–15] drug delivery systems[5,16,17] and many more.[18–21] These photoswitches operate through absorbance of high-energy UV light, which unfortunately hinders their applicational development, as UV light can damage biological and materials systems, and yields very little penetrative depth.[22–25] As such, measures have been taken to prevent the use of UV light and instead utilise the visible to infrared region of the spectrum.[26–31] Parallel to these attempts, was the introduction of the donor-acceptor Stenhouse adduct (DASA) as a visible light photoswitch, in 2014, by Read de Alaniz and his group.[32,33]
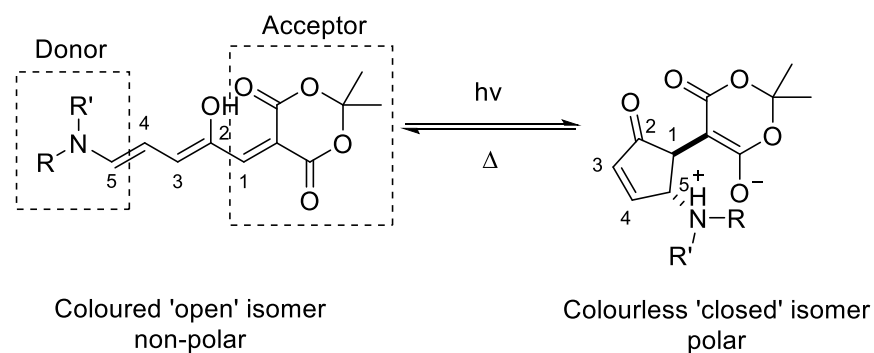

Figure 3-1 – The open and closed forms of a first-generation DASA utilising the Meldrum's acid acceptor group, where R and R' belong to an alkyl amine donor.

DASAs are a class of negative photochromes that respond to visible light; upon exposure they will isomerise from a brightly coloured, highly conjugated, open triene form, to a colourless, more polar, cyclopentenone.[32] Structurally, they consist of a donor amine group connected to a carbon acid acceptor, through a conjugated triene bridge. It has been found that the wavelength

of absorbance and polarity of these moieties can be finely tuned through modification of the donor and acceptor groups, leading to what have been labelled as 'second' and 'third generation' species.[34,35] Furthermore, the impressive fatigue resistance of DASAs is a major advantage over other more commonly used photochromes,[32,36–39] where in some cases 1000 cycles can pass before a 50% photodegradation degree is seen.[40] The photoswitching mechanism of DASAs has been elucidated over a number of in-depth studies and has been shown to consist of a Z/E photoisomerisation, followed by a thermally-dependent electrocyclization, with the formation of a number of transient intermediates along the way.[40–47] Further studies have highlighted the importance of the triene hydroxyl group and established a concentration-dependent effect that DASAs are subject to.[40,48–50] Since their advent, there has been a great deal of interest in these new photoswitches, thanks to their facile preparation, high molar absorptivity, and tailorable response to chemical and thermal stimuli.[51] Consequently, a wide variety of envisioned applications for the photochromes have been suggested; such as sensing platforms,[52–56] drug carriers,[57,58] photopatterning architectures,[59] the monitoring of photochemical reactions,[60] and more.[61–64]

Polydimethylsiloxane (PDMS) is a widely-used, commercially available, cost-effective silicone which is greatly-favoured for its low toxicity, low glass transition temperature (T_g), low reactivity, high flexibility and, most importantly for this body of work, it's optical transparency.[65,66] Owing to these unique properties, it has seen continuous use in the fields of surface patterning,[67–70] and microfluidic channel devices.[71–74] It has also been the subject of photochrome non-covalent incorporation on multiple occasions, providing a facile, cost-effective preparation of photoresponsive materials.[75–78] Yet surprisingly, of the few DASA/polymer blends that have been previously reported, PDMS does not feature as the doped matrix.[34,49,50,54,62,79] Therefore, this chapter of work aimed to contribute to the expansion of photochromic PDMS materials by introducing the incorporation of a first-generation DASA into a cross-linked PDMS network, through facile preparation.[80]

Herein, the forward photoisomerisation and backward thermal reversion of PDMS-DASA networks were followed through solid-state uv-vis spectroscopy, with an attempt to characterise the kinetic process using exponential regression analysis and a previously reported simple two-state model.[49] A focus was taken on the effects of DASA concentration variation, with the determination of evaluative parameters such as the photostationary state (PSS), half-lives and rates of the photochemical and thermal reactions. Further investigations conducted on the lowest concentration iteration entailed examination of the fatigue resistance, the effect of solvent swelling on photoswitching, and the potential detection of open to closed isomerisation by characterised by a function of RFID sensor code value.

3.2 Experimental

3.2.1 Materials and apparatus

Silanol terminated polydimethylsiloxane (DMS-S31) (M_w 26,000, Gelest), tin (II) 2-ethylhexanoate (95%, Sigma-Aldrich), tetraethylorthosilicate (99%, Sigma-Aldrich), dichloromethane (99%, Fisher Scientific), isopropylidene malonate (Meldrum's acid) (98%, Alfa Aesar), 2-furaldehyde (99%, Sigma-Aldrich), diethylamine (99+%, Acros Organics) and dihexylamine (99+%, Acros Organics) were used as received. RFMicron RFM3200-AFR temperature sensing tags were used as bought. The equal dispersion of reagents for the development of PDMS elastomers was made possible through use of a SpeedMixer™ DAC 150.1 FVZ-K bought from Synergy Devices Limited. Application of PDMS films to tags was performed using an automatic precision film applicator CX4 from mtv messtechnik, with a height-adjustable doctor blade.

3.2.2 Synthesis of 5-(furan-2-ylmethylene)-2,2-dimethyl-1,3-dioxane-4,6-dione (MAF)

The synthetic procedure of **MAF**, modified in regards to literature,[32,81] has been explained in Chapter 2, section 2.2.2.

3.2.3 Synthesis of 5-((2Z,4E)-5-(dihexylamino)-2-hydroxypenta-2,4-dien-1-ylidene)-2,2-dimethyl-1,3-dioxane-4,6-dione (HexDASA)

The synthesis of **HexDASA** was carried out by following procedures previously established by literature[32]. **MAF** (1.00 g, 4.5 mmol) was dissolved in THF (10 ml), with stirring. To this, the dihexylamine (1044 µl, 4.5 mmol) was added dropwise, the red solution was allowed to stir at room temperature for 10 minutes, and 0 °C for 20 minutes. The resultant precipitate was isolated through vacuum filtration and washed with cold diethyl ether (50 ml), yielding purple

crystals precipitate (1.07 g, 58.4 %). The final product was analysed using 1H NMR, 13C NMR and FTIR, spectroscopic values match that of known literature.[32]

^{1}H NMR (400 MHz, CDCl$_3$, room temperature) found ppm δ: = 0.90 [**m, 6H** N(CH$_2$CH$_2$CH$_2$CH$_2$CH$_2$**CH$_3$**)$_2$], 1.32 [**m**, 8H N(CH$_2$CH$_2$CH$_2$**CH$_2$CH$_2$**CH$_3$)$_2$], 1.67 [**m, 8H** N(CH$_2$**CH$_2$CH$_2$**CH$_2$CH$_2$CH$_3$)$_2$], 1.71 [**s, 6H (CH$_3$)$_2$**C(OOR)$_2$], 3.39 [**4H** N(**CH$_2$**CH$_2$CH$_2$CH$_2$CH$_2$CH$_3$)$_2$], 6.03 [**t,** J = 12.1 Hz,**1H triene**], 6.68 [**dd,** J = 12.5**,** 1.3 Hz, **1H triene**], 7.1 [**s, 1H triene**], 7.18 [**d,** J = 12.49 Hz,**1H triene**], 11.43 [**m, 1H** (CH$_3$)$_2$C(OOC)$_2$C=CHC**(OH)**R].

^{13}C NMR (CDCl$_3$, room temperature) found ppm δ: = 14.02, 22.55 (multiplet), 26.14, 26.74 (multiplet), 27.12, 29.03, 31.39 (multiplet), 49.70, 57.78, 90.66, 102.18, 103.55, 139.23, 144.95, 151.10, 157.59, 165.36, 167.15.

FTIR (cm^{-1}) HexDASA: 2926 (R-CH$_2$, CH str.); 2853 (R-CH$_2$, CH str.); 1717 (C=O, str.); 1570 (C=O, str.); 1338 (O-H, bend); 1260 (R-N(R')$_2$, C-N str.); 1117 (R-C(OH)=R', C-O str.).

3.2.4 Synthesis of 5-((2Z,4E)-5-(diethylamino)-2-hydroxypenta-2,4-dien-1-ylidene)-2,2-dimethyl-1,3-dioxane-4,6-dione (EtDASA)

The synthesis of **EtDASA** was carried out by following procedures previously reported by literature[32]. **MAF** (1.00 g, 4.5 mmol) was dissolved in THF (10 ml), with stirring. To this, the diethylamine (466 µl, 4.5 mmol) was added dropwise, the red solution was allowed to stir at room temperature for 10 minutes, and 0 °C for 20 minutes. The resultant precipitate was isolated through vacuum filtration and washed with cold diethyl ether (50 ml), yielding a fine, red powder (0.40 g, 28.8 %). The final product was analysed using 1H NMR, 13C NMR and FTIR, spectroscopic values match that of known literature.

^{1}H NMR (400 MHz, CDCl$_3$, room temperature) found ppm δ: = 1.32 [**dt,** J = 19.7, 7.3 Hz, **8H** N(CH$_2$**CH$_3$**)$_2$], 1.71 [**s, 6H (CH$_3$)$_2$**C(OOR)$_2$], 3.49 [**m, 4H** N(**CH$_2$**CH$_3$)$_2$], 6.04 [**t,** J = 12.3 Hz, **1H triene**], 6.69 [**dd,** J = 12.4, 1.5 Hz, **1H triene**], 7.09 [**s, 1H triene**], 7.19 [**d,** J = 12.3 Hz, **1H triene**], 11.44 [**m, 1H** (CH$_3$)$_2$C(OOC)$_2$C=CHC**(OH)**R].

^{13}C NMR (CDCl$_3$, room temperature) found ppm δ: = 12.29, 14.57, 26.73, 44.09, 51.88, 90.98, 101.97, 103.50, 139.74, 144.95, 150.91, 156.47, 165.24, 167.10.

FTIR (cm^{-1}) EtDASA: 3069 (HC=CH, CH str.); 2995 (HC=CH, CH str.); 1678 (C=O, str.); 1597 (C=O, str.); 1368 (O-H, bend); 1260 (R-N(R')$_2$, C-N str.); 1126 (R-C(OH)=R', C-O str.).

3.2.5 Sn catalysed cross-linking of silanol terminated PDMS

The synthetic steps for the production of standard cross-linked PDMS elastomers are detailed in Chapter 2, section 2.2.3.

3.2.6 Sn catalysed cross-linking of silanol terminated PDMS-HexDASA physical blends: Air-cured

Silanol terminated PDMS (2.00 g, 76.9 µmol, DMS-S31, M$_w$ 26,000) and the cross-linking agent tetraethyl orthosilicate (0.04 g, 1.92*10^{-4} mol) (molar ratio of SiOH groups in PDMS to SiOR groups in TEOS, 1:4) were added to a plastic beaker and speed-mixed for 60 seconds. Next, catalyst tin (II) 2-ethyl hexanoate (60 µl, 0.6 M solution in toluene) was added to the reaction mixture and speed-mixed for another 60 seconds. Lastly, **HexDASA** (for amounts, see Table 3.1) in a minimum of DCM was added and the mixture speed-mixed for a final 60 seconds. The mixture was poured into square PTFE moulds (width = 2 cm, length = 2 cm, height = 0.2 cm) and allowed to cure in dark, ambient conditions overnight. Figure 3-2 is a diagrammatic representation of the final product.

FTIR (cm^{-1}) PDMS-HexDASA: 2963 (CH$_3$, CH str); 1412 (Si − CH$_3$, CH$_3$ asym def); 1258 (Si − CH$_3$, CH$_3$ sym def); 1080, 1009 (Si − O − Si str); 785 (Si − C str and CH$_3$ rock. Data obtained for each sample were practically identical, additional peaks are included in Table 3.1.
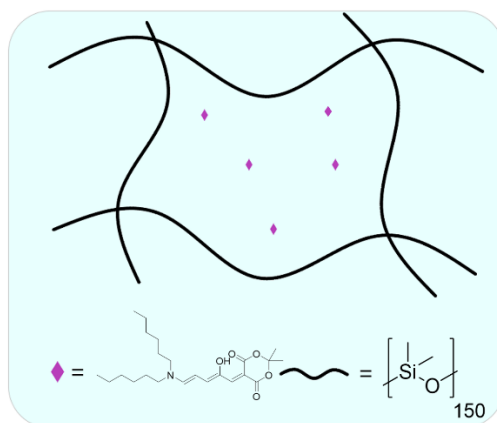
Figure 3-2 - Diagrammatic approximation of the dispersion of DASA between cross-linked PDMS chains.

Table 3.1 - A table depicting the amount of DASA used for each iteration of air-cured composites.

Elastomer	DASA conc.[a] (wt%)	DASA conc. (M)	Mass of DASA used (mg)	DASA moles (mmol)	Additional peaks (cm^{-1})
AC-0.05	0.05	0.0016	1	$2.45*10^{-3}$	N/A
AC-0.1	0.1	0.0032	2	$4.91*10^{-3}$	N/A
AC-0.5	0.5	0.016	10	0.024	2361
AC-1	1	0.032	20	0.049	2369, 1719, 1576
AC-5	5	0.160	100	0.245	1578

[a] with respect to mass of PDMS used.

3.2.7 Sn catalysed cross-linking of silanol terminated PDMS-HexDASA physical blends: sealed atmosphere (SA) cured

Silanol terminated PDMS (2.00 g, 76.9 µmol, DMS-S31, M$_w$ 26,000), cross-linking agent tetraethyl orthosilicate (0.04 g, $1.92*10^{-4}$ mol) (ratio of SiOH groups in PDMS to SiOR groups in TEOS, 1:4), catalyst tin (II) 2-ethyl hexanoate (60 µl, 0.6 M solution in toluene) and **HexDASA** (for amounts, see Table 3.2) in a minimum of DCM were speed-mixed at 3,500 rpm, for a total of 3 minutes. The mixture was poured into square PTFE moulds (width = 2 cm, length = 2 cm, height = 0.2 cm), which were then placed into sealed Sistema® snap-close containers (Figure 3-3). The containers were kept under dark conditions, allowing curing to take place overnight.

FTIR (cm^{-1}) PDMS-HexDASA: 2963 (CH$_3$, CH str); 1398 (Si – CH$_3$, CH$_3$ asym def); 1258 (Si – CH$_3$, CH$_3$ sym def); 1080, 1009 (Si – O – Si str); 785 (Si – C str and CH$_3$ rock). Data obtained for each sample were practically identical, additional peaks included in Table 3.2.

Table 3.2 - A table depicting the amount of DASA used for each iteration of SA cured composites.

Elastomer	DASA conc.[a] (wt%)	DASA conc. (M)	Mass of DASA used (mg)	DASA moles (mmol)	Additional peaks (cm^{-1})
SAC-0.05	0.05	0.0016	1	2.45*10^{-3}	2361, 1655
SAC-0.1	0.1	0.0032	2	4.91*10^{-3}	N/A
SAC-0.5	0.5	0.016	10	0.024	1719, 1572
SAC-1	1	0.032	20	0.049	1719, 1571
SAC-5	5	0.160	100	0.245	1719, 1572

[a] with respect to mass of PDMS used.

Figure 3-3 - A Sistema® snap-close container, used for an alternative curing method.

3.2.8 Sn catalysed cross-linking of silanol terminated PDMS-EtDASA physical blend

Silanol terminated PDMS (2.00 g, 76.9 µmol, DMS-S31, M$_w$ 26,000), cross-linking agent tetraethyl orthosilicate (0.04 g, 1.92*10^{-4} mol) (ratio of SiOH groups in PDMS to SiOR groups in TEOS, 1:4), catalyst tin (II) 2-ethyl hexanoate (60 µl, 0.6 M solution in toluene) and **EtDASA** (1 mg, 2.45*10^{-3} mmol) in a minimum of DCM were speed-mixed at 3,500 rpm, for a total of 3 minutes. The mixture was poured into square PTFE moulds (width = 2 cm, length = 2 cm, height

= 0.2 cm), which were then placed into sealed Sistema® snap-close containers (Figure 3-3). The containers were kept under dark conditions, allowing curing to take place overnight.

FTIR (cm^{-1}) PDMS-EtDASA: 2963 (CH_3, CH str); 1412 (Si – CH_3, CH_3 asym def); 1258 (Si – CH_3, CH_3 sym def); 1080, 1009 (Si – O – Si str); 785 (Si – C str and CH_3 rock).

3.2.9 Film-casting of PDMS-DASA physical blends onto RFID tags

In order to investigate a potential application for light responsivity, RFID tags covered with films of the PDMS-DASA blends were required. The procedure used for tag production was outlined in Chapter 2, section 2.2.5.

3.3 Measurements and Instruments

3.3.1 FT-IR spectroscopic measurements

FTIR spectroscopic analysis was performed on a Shimadzu IRAffinity-1 spectrometer with a Specac Golden Gate™ ATR sampling accessory, under ambient conditions, with 64 scans at a resolution of 4 cm^{-1}. Good optical contact between the sample and the diamond was obtained by clamping of samples via the Golden Gate™, each elastomer was bisected with a clean scalpel, in order to obtain a cross-sectional and surface scans, with each measurement giving identical spectra.

3.3.2 PXRD measurements

PXRD measurements of the samples were taken using a Rigaku Miniflex 600 desktop XRD; scan range of 5 – 40 $^\circ$, 0.02 $^\circ$ step, at 1 $^\circ$ min^{-1}.

3.3.3 UV-vis spectroscopic measurements

UV-Vis analysis was undertaken using a Shimadzu UV-1800 spectrophotometer. Preparation of samples consisted of halving a sample by length with a steel scalpel and mounting it to a quartz slide, using Telesis^{TM} 5 silicone adhesive, this was analysed to determine whether it would interfere with measurements – it provided a blank spectrum. A baseline was established by scanning a "blank" cross-linked PDMS sample, this would ensure that any light absorption could then be characterised to the physically blended DASA moiety. Samples were scanned within the range of 400 to 800 nm.

3.3.4 NMR spectroscopic measurements

^{1}H and ^{13}C NMR data were acquired using a Bruker AVANCE-400 spectrometer, spectra were obtained at 19 $^\circ$C in chloroform-d (d-99.8 atom %, CIL) solution, unless stated otherwise.

3.3.5 UHF-RFID measurements

RFID measurements were performed by Aaron Hillier and Joshua Savage, using Voyantic TagformancePro UHF RFID characterisation apparatus, all tags were scanned in triplicate and average values are reported herein. Each tag was placed at a distance of 30 cm from the apparatus antenna, scanned within a range of 800 to 1,000 MHz. Measurement of film thickness was conducted using Duratool digital Vernier calipers, film thickness was calculated by subtracting the thickness of an RFID tag (average thickness of 50 μm) pre-application from post-application.

3.3.6 Swelling experiments

The mass and volume of each PDMS and PDMS-DASA elastomer was recorded after they were removed from the square PTFE moulds, they were then exposed to a saturated atmosphere of each solvent for a total of 72 hours. Saturated atmospheres were achieved by pouring 25 ml of each solvent into the bottom well of a desiccator and afterwards the metal perforated shelf was placed back into the container, carrying an elastomer sitting in a glass petri dish. In order to provide an air-tight environment the desiccators were smeared with vacuum grease on both top and bottom seals. It was determined that the atmosphere within was saturated with solvent vapour as, after the 72-hour process, each system retained solvent within the bottom well. Post-swelling, the elastomers were weighed and measured again to obtain the difference in volume and mass, allowing for mass and volume-swelling ratios to be calculated. The mass ratio (Q_m) was defined as the difference in swollen and dry masses, divided by the latter. The volume ratio (Q_v) was defined as the difference in swollen and dry volumes, divided by the latter. The swelling experiments were performed in triplicate.

3.3.7 Elastomer photoswitching studies

PDMS-DASA elastomers were stored under dark conditions to prevent switching from extraneous variables i.e. sunlight and/or artificial light. To begin, each sample was mounted atop

a quartz slide and scanned to provide a "0 second" starting point, after this they were placed into a cardboard box to which was attached a 50 W, 6500 K full spectrum LED floodlight (Figure 3-4)**.** The elastomers were exposed to the floodlight through a square cutting, approximately 30 cm above their position. Given this distance, the light intensity was calculated to be 44.21 Wm^{-2}, which equates to 4.42 mW cm^{-2} – using the equation for the surface area of a sphere ($4\pi r^2$) and dividing the total wattage by that value. The inside of the box was lined with reflective foil, in order to disperse the incident light 360 ° in each axis around the subjects, with the assumption that the incident light would lose a negligible amount of energy upon reflection. This resulted in an environment that kept a constant temperature of 34 °C.

Sample exposure times consisted of 30-second intervals, for a total of 600 seconds. Following these measurements, they were left to be exposed until they had reached their photostationary state (PSS), i.e. an appreciable decline in absorbance could no longer be seen. Subsequently, the samples were placed into a lightless oven at 60 °C for 5 minutes intervals, with absorbance measurements being taken ensuing each. This process lasted for a total of 1 hour and was designed to study the process of reverting from the colourless to coloured form. Cycling studies consisted of irradiating PDMS-DASA elastomers with light until they reached their PSS and treating them with a 5-minute oven-reversion step, to then be irradiated again. This process was repeated multiple times.

Figure 3-4 - A custom-made light irradiation box; a 50 W, 6500 K full spectrum LED floodlight attached to a cardboard box lined with reflective foil sheets.

3.4 Results and discussion

3.4.1 Synthesis and characterisation of Meldrum's activated furan (MAF)

MAF was synthesised according to the procedure provided in Chapter 2. Full characterisation of **MAF** can be found in Chapter 2, section 2.4.1, with FT-IR and NMR spectroscopy values matching that of literature.[32,81]

3.4.2 Synthesis and characterisation of HexDASA

HexDASA was produced following the reaction Figure 3-5;[32] the product consisted of dark purple crystals. ^{1}H and ^{13}C NMR and FT-IR (Figure 3-6) of the product confirmed the successful formation of the product and agreed with literature values.[33] Small peaks can be observed emerging from the baseline in the ^{1}H NMR, these are believed to be a combination of the small portion of first-generation DASAs that exist in the cyclic form and the many isomers that can form after the first photoisomerisation step.[40,47] Some assignments in the ^{13}C NMR have the designations **x** and **x'**, these arise from the carbon atoms in question being situated parallel or perpendicular to the delocalised triene system. PXRD of HexDASA (Figure 3-6d) has been included in the characterisation, for comparison with PDMS-DASA composites later in section 2.2.3.1.
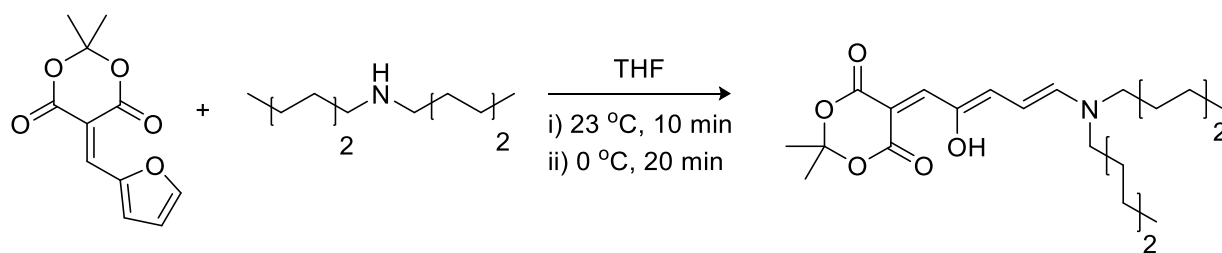

**Figure 3-5 - Synthetic scheme for HexDASA.**
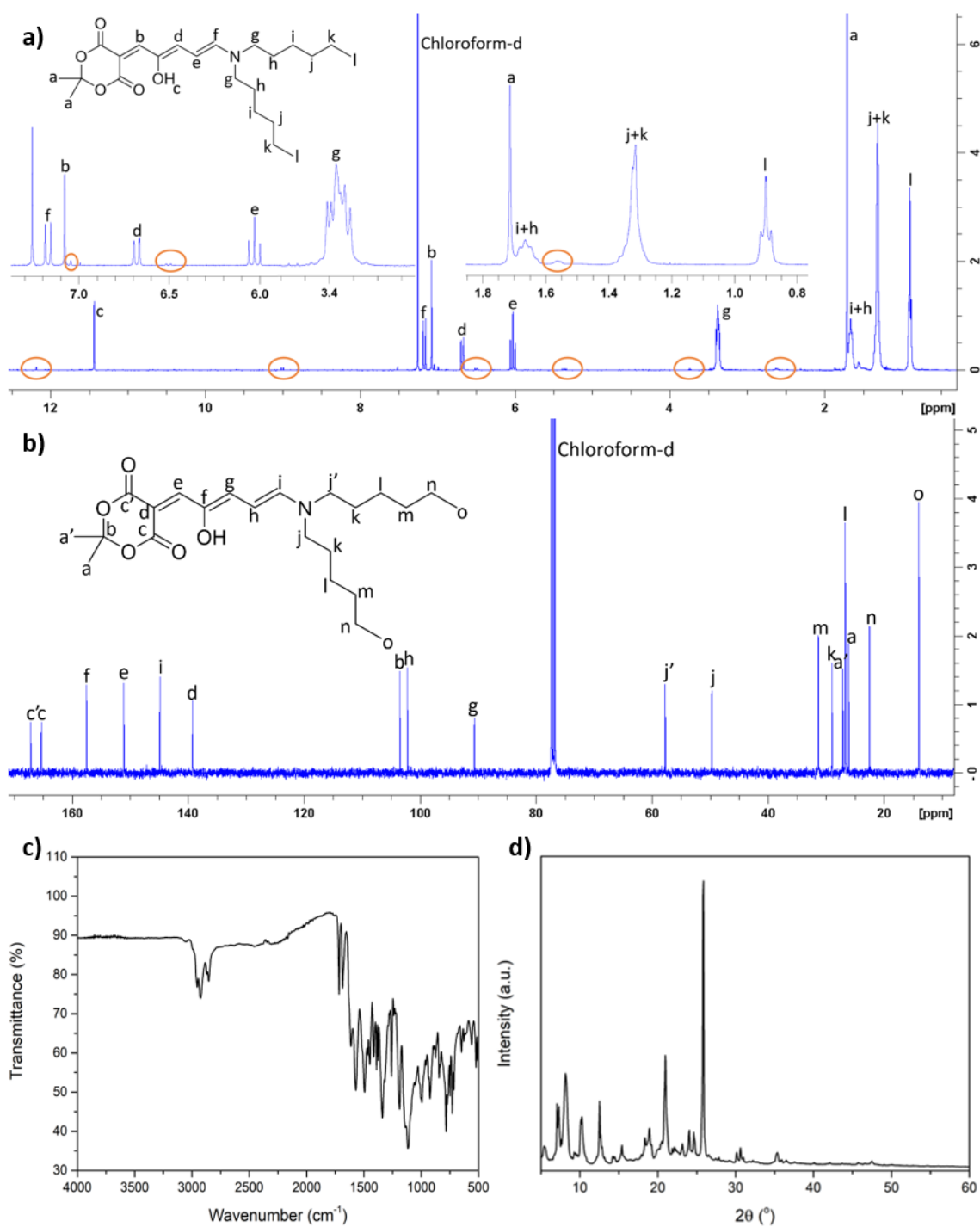
Figure 3-6 – Characterisation of HexDASA: a) ¹H NMR, b) ¹³C NMR, c) FTIR and d) PXRD.

3.4.3 Synthesis and characterisation of EtDASA

The synthetic scheme for EtDASA is provided as Figure 3-7;[32] the product was a fine, red powder.

¹H NMR, ¹³C NMR and FTIR confirmed the successful formation of the product and agreed with

literature values (Figure 3-7).[33] Small peaks can be observed emerging from the baseline in

Figure 3-7c, these are believed to be characteristic of the small portion of EtDASA that exists in

the cyclic form, likely in combination with the multitude of isomers that can form following the first photoisomerisation step.[40,47] Some assignments in both NMR spectra have the designations **x** and **x'**, these arise from the carbon atoms in question being situated parallel or perpendicular to the delocalised triene system.
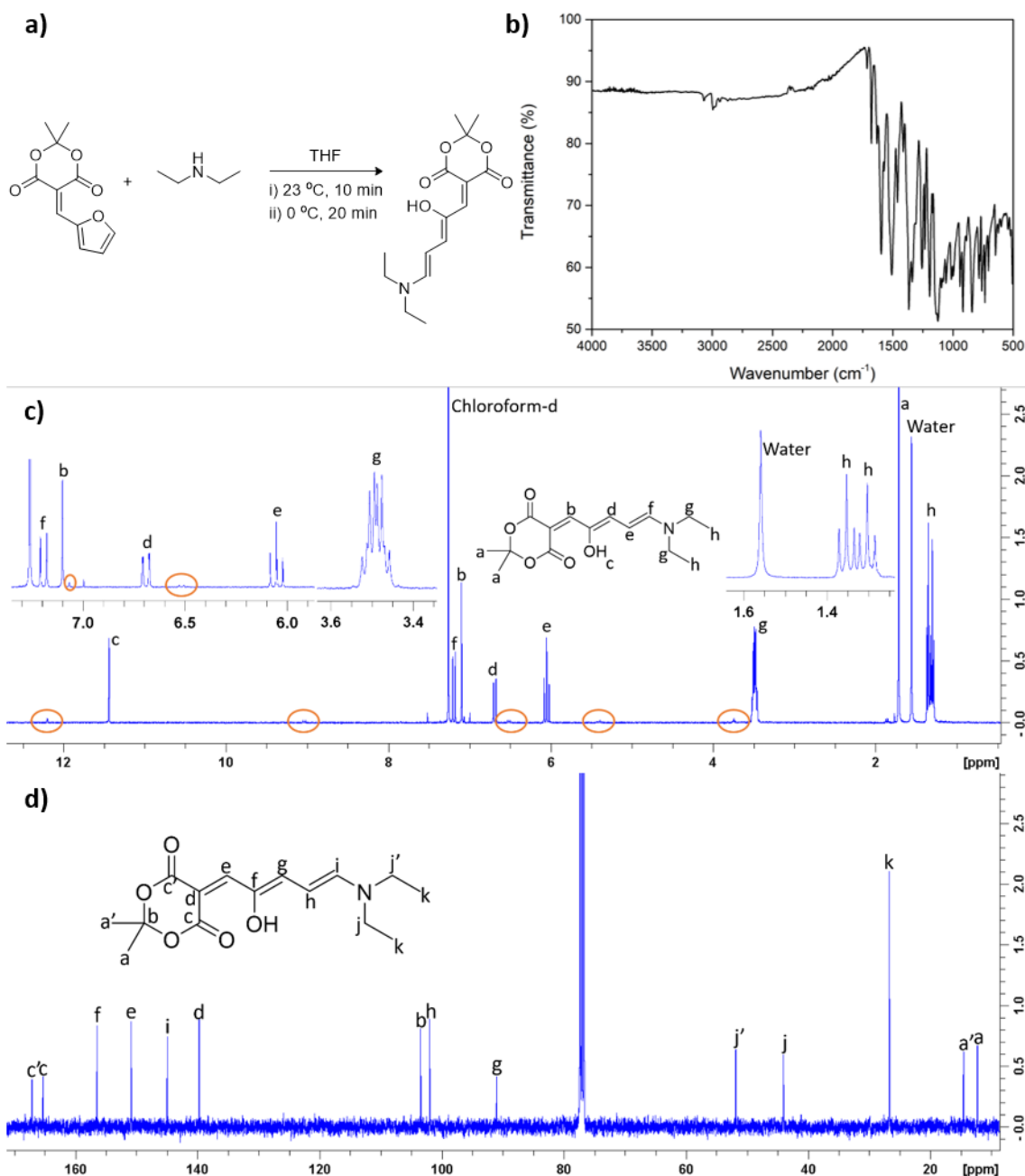

Figure 3-7 – Characterisation and reaction scheme of EtDASA: a) scheme, b) FTIR, c) ¹H NMR, and d) ¹³C NMR.

3.4.4 Synthesis and characterisation of cross-linked PDMS elastomers and PDMS-DASA elastomers

3.4.4.1 Cross-linked PDMS elastomers

Standard cross-linked PDMS elastomers were synthesised according to the procedure laid out in Chapter 2. Characterisation of the elastomers can be found in Chapter 2, section 2.4.2.1. The standard PDMS elastomer was subjected to PXRD analysis (Figure 3-8); producing a spectrum that contains no well-defined peaks. The data infers that the PDMS network is an amorphous species, this will be used later for comparison against the PDMS-DASA composites to investigate the presence of DASA crystallisation.
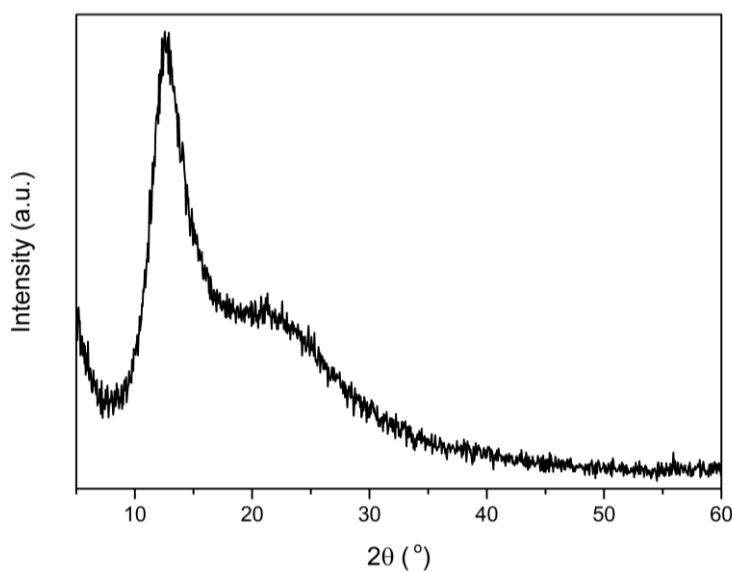

Figure 3-8 - PXRD of a cross-linked PDMS elastomer.

3.4.4.2 PDMS-DASA composites

The aim of this project was to develop a photosensitive elastomeric material that could be applied to a wide variety of applications, through a facile procedure (Figure 3-9). The method used is a minor modification on a previously reported synthetic procedure.[80]

Previous literature has shown that DASAs dissolved within elastomers will exhibit switching properties similar to those which can be achieved in the solution state.[54] It was believed that

dissolving a DASA in solution and dispersing it within a nexus of cross-linked PDMS would produce a similar effect.
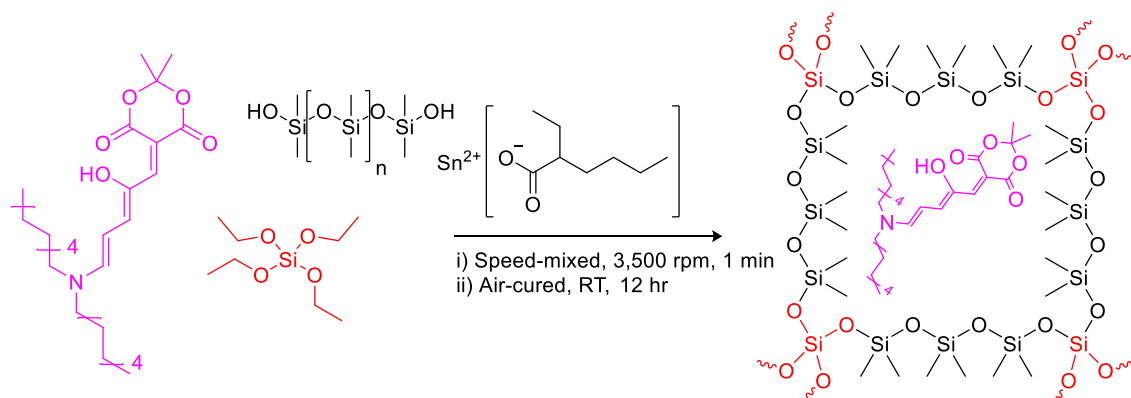

Figure 3-9 - A schematic representation of the production of the PDMS-DASA elastomers.

DCM was chosen as the medium for incorporation of the DASAs into the networks, as both EtDASA and HexDASA were found to be compatible with this solvent, and its high vapour pressure coupled with a low boiling point enabled easy removal, post-curing. As mentioned previously in sections 2.2.4 and 3.2.7, two methods were used for the curing of PDMS-HexDASA composites: air-curing and SA curing. Air-curing consisted of allowing the post-speed mixed reaction mixture to cure in the PTFE moulds under dark, ambient conditions. Whereas SA curing involved placing those moulds inside a Sistema® food container (Figure 3-3), under dark conditions. This direction was taken as it was thought that solvent evaporation during the cross-linking process promoted crystallisation of the HexDASA, as this moiety was not soluble in PDMS or TEOS alone. Therefore, curing the composites in a sealed container would produce a DCM/ethanol-rich atmosphere preventing rapid loss of solvent from the system. It was postulated that once cross-linking had fully occurred, it would be less likely for crystallisation of the DASA to occur. Crystallisation of this species is unwanted as DASAs do not switch in the solid-state.[32] A preliminary test was conducted to confirm this, Figure 3-10 shows photographs of the HexDASA powder before and after a 12-hr light irradiation step. The powder appears to have lightened by a very small degree over this time, however no significant change was apparent.
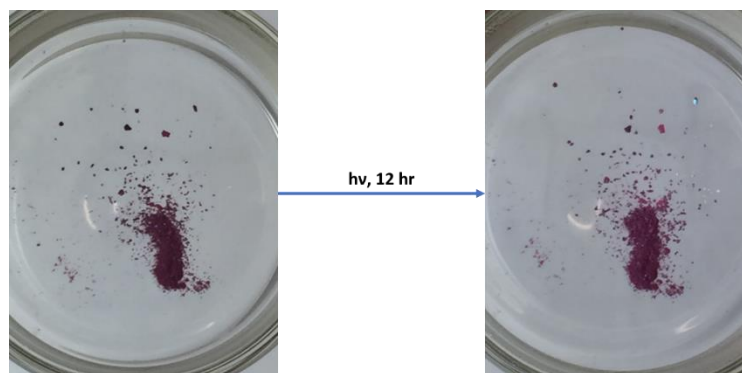
Figure 3-10 - HexDASA powder before (left) and after (right) light irradiation for 12 hours.

After successful curing, each elastomer was subjected to analysis through visual inspection, FT-IR and PXRD. Following these steps, preliminary photoswitching studies were conducted for each sample and if those studies proved successful i.e. the elastomer was able to reversibly decolourise, then a further full photoswitching study was conducted. Full photoswitching studies consisted of the time-lapse of a decolourisation and reversion cycle, through uv-vis spectroscopy. A flow diagram has been included depicting the steps taken during the production, characterisation and analysis of composites in this chapter, as Figure 3-11.

The following sections will discuss the characterisation of various samples, through FT-IR and PXRD, with the results of preliminary photoswitching examinations. The FT-IR spectra shown are that of cross-sections of their respective products; surface and cross-section spectra were practically identical.
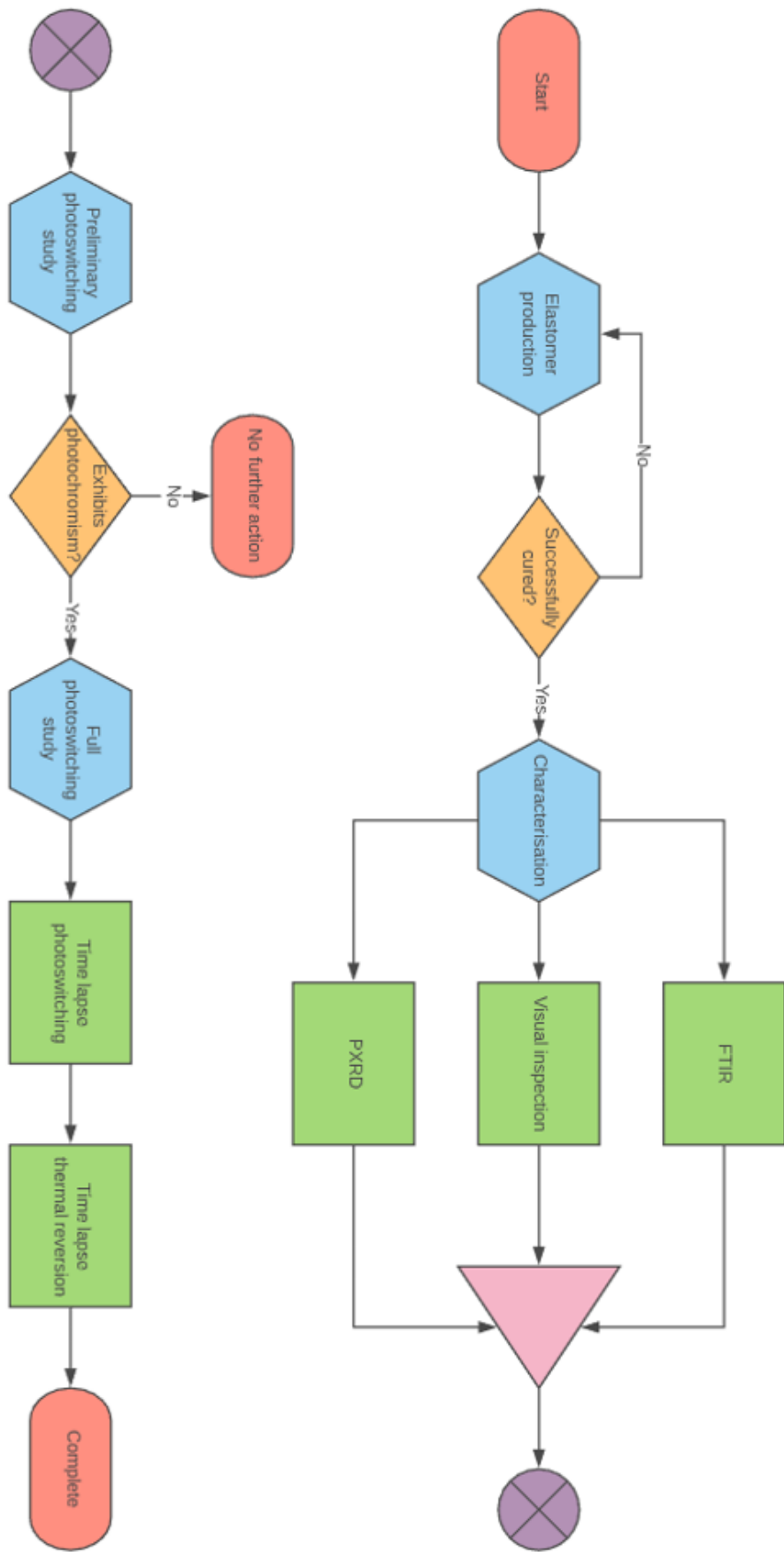
Figure 3-11 - A flowchart depicting the production, characterisation and analysis process for a

PDMS-DASA composite.

3.4.4.2.1 PDMS-EtDASA

This section discusses the characterisation of the PDMS-DASA composite that incorporated EtDASA, classified as PDMS-EtDASA. Diethylamine and dihexylamine were the two readily available donors for the synthesis of DASA moieties at the time of this study and they had both been found to exist as a large portion (> 95%) of open isomer in dark equilibria.[40] This was seen as desirable as it was thought a large contrast in dark and light equilibria would be best, in order to be able to evaluate photoswitching efficiency. In order to decide which alkyl amine donor would be more suitable for further investigation, a preliminary comparison study was conducted, which is detailed in section 3.4.5. The elastomer PDMS-EtDASA was produced according to the procedure laid out in section 3.2.8, whereby a DASA concentration of 0.05 wt% was utilised. Just as with the PDMS elastomers from section 2.4.2.1, these elastomers had a rubber-like texture, however they were instead opaque with an orange colouration. Examination of the FTIR spectra of these new elastomers was unsurprisingly very similar to that of the blank PDMS networks; the TEOS stretch (2289 cm^{-1}) was absent, indicating that cross-linking had taken place. A comparison of the FT-IR spectra of cross-linked PDMS and this PDMS-EtDASA composite showed that they are practically identical and, as expected, no signals arise from the presence of the photoswitch – likely due to incorporating such a low concentration.
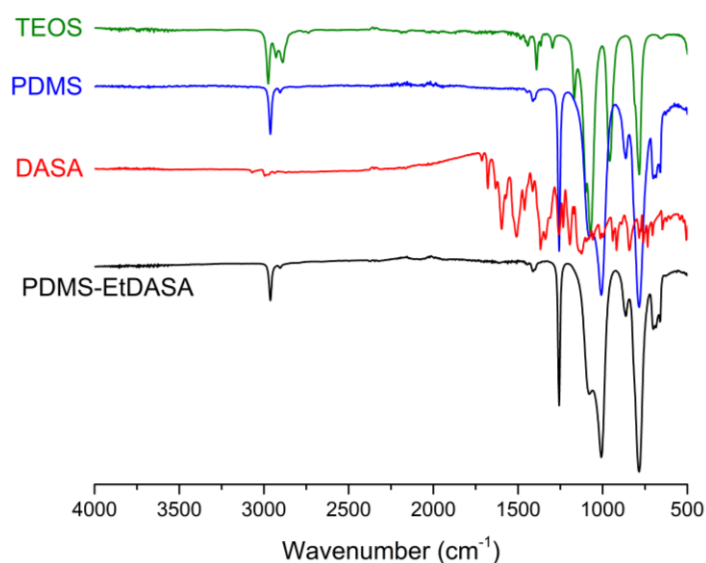

Figure 3-12 - FT-IR overlay of TEOS, silanol terminated PDMS, EtDASA and PDMS-EtDASA.

3.4.4.2.2 Air-cured elastomers (AC-X)

Five different concentrations of HexDASA were incorporated into these composites, they were as follows: 0.05, 0.1, 0.5, 1 and 5 wt%, with respect to the mass of PDMS used for the reaction. The products followed the naming convention of AC-X where X = concentration. With a mass of 2.00 g of silanol terminated PDMS being used, a DASA concentration of 0.05 wt% would consist of 1 mg. Preparation of the DASA moieties consisted of using a minimum amount of DCM, with sonication to ensure solvation, as the DASA was not soluble in PDMS alone. All solutions were added to the PDMS curing mixture after addition of catalyst and cross-linking agent, in the hope that cross-linking would occur before crystallisation of DASA.

All systems cured successfully, each with a pink colouration, of which darkened with increasing concentration. FT-IR analysis (Figure 3-13) provided almost identical spectra to PDMS-EtDASA (Figure 3-12) and the regular cross-linked PDMS samples from Chapter 2, additional peaks are displayed in Table 3.1, section 2.2.4. All spectra were identical but for the gradual emergence of peaks characteristic to the Meldrum's acid acceptor unit; C=O stretches centred around 1719 and 1572 cm^{-1}, the intensity of these signals appeared to positively correlate with loading of DASA.

Upon close visual inspection, it was found that samples with a darker hue (from the batch AC-5) would glisten when the incident angle of light was changed, indicating a large degree of DASA crystallisation within the networks. A comparison was made between AC-0.5 and 5 by use of a Leica MC170 5MP HD microscope camera, to highlight the visual difference (Figure 3-14). The image for AC-0.5 shows very few crystals close to the surface of the composite. However, AC-5 appears to have a high concentration of crystals. This crystal problem led to the curing of elastomers in sealed Sistema® food containers, as it was believed that the retention of solvent during curing would discourage crystallisation.
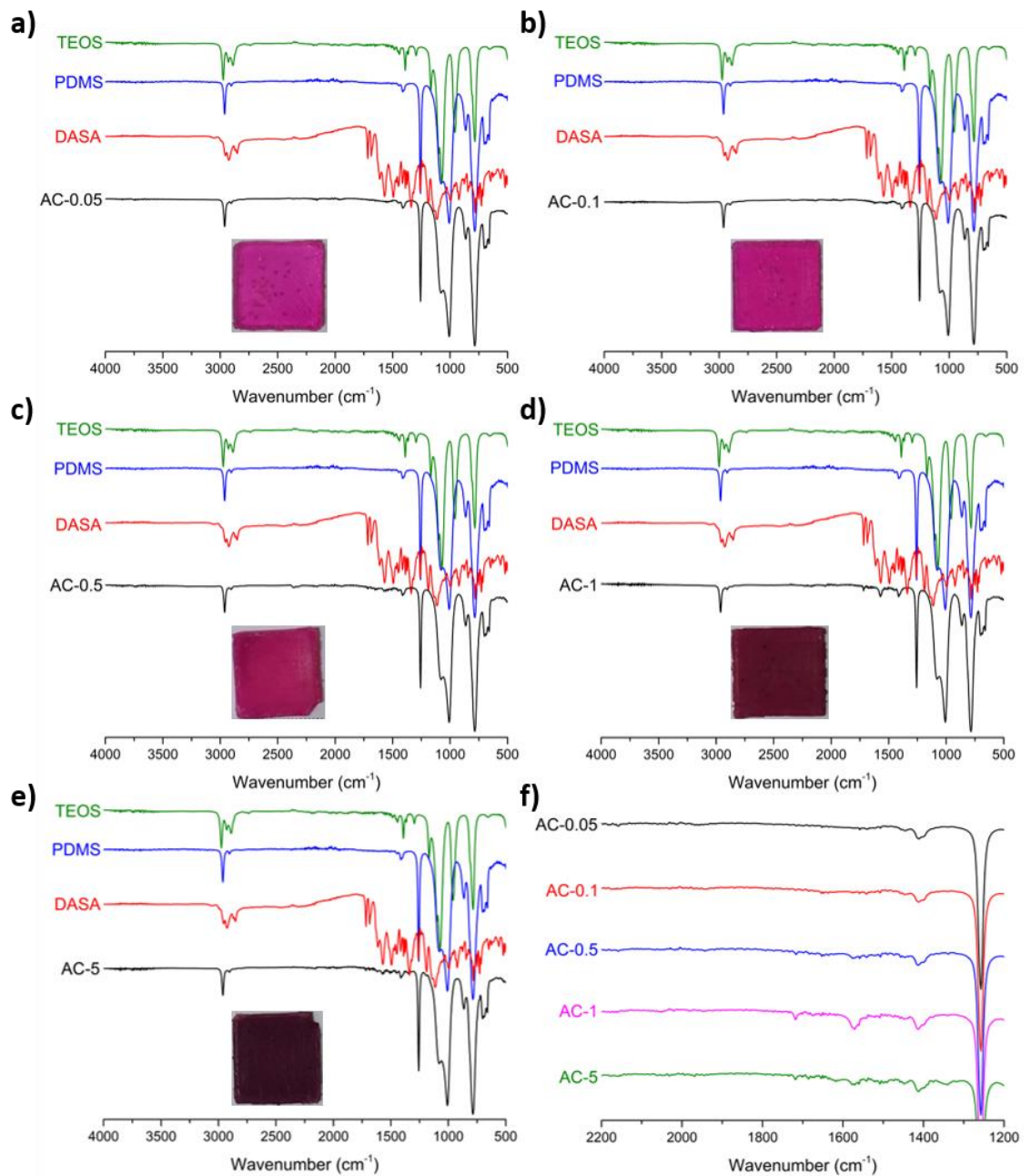
Figure 3-13 - FT-IR overlays of air-cured PDMS-DASA composites, inset with photographs of samples: a) AC-0.05, b) AC-0.1, c) AC-0.5, d) AC-1, e) AC-5 and f) an expansion of an overlay of all elastomers, highlighting the emergence of peaks centred around 1719 and 1572 cm^{-1}.
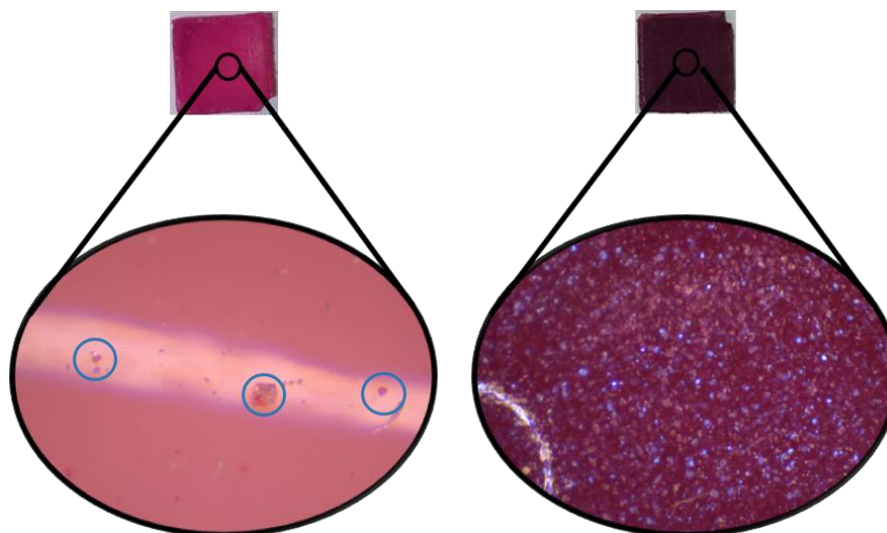
Figure 3-14 - Microscope images (200x) of AC-0.5 (left) and AC-5 (right), apparent crystallites are highlighted with blue circles, for AC-0.5.

PXRD analysis was conducted on each PDMS-DASA composite. The results have been overlaid as Figure 3-15, displaying the spectrum for each sample, 2θ values plotted on the x-axis against normalised intensity as the y-axis. The intensity values varied between samples, therefore each set was normalised separately and given an offset value as to enable clear display and comparison of the data. As expected, the data shows that the polymer networks are amorphous and largely resemble a cross-linked PDMS sample. Orange ellipses have been inserted to highlight the presence of sharp peaks emerging, for samples AC-5 and AC-1, due to crystalline HexDASA (Figure 3-16). There is a small gap, 0.4 $^\circ$, between the peaks of AC-5 and HexDASA which are encompassed by the orange ring; a result of the height difference between samples as HexDASA was in powder form and AC-5 consisted of a small slice of approximately 0.5 mm thickness. The data obtained from this investigation was quantitative proof that DASA crystallisation had developed within the networks of at least AC-5 and AC-1. It was believed that recrystallisation of the DASA was resulting from the rapid evaporation of DCM from the system, during the curing process. Therefore, slowing this evaporation until post-curing was the aim of this procedural modification and so these networks were cured within sealed Sistema® food containers to allow a DCM-saturated atmosphere to develop.
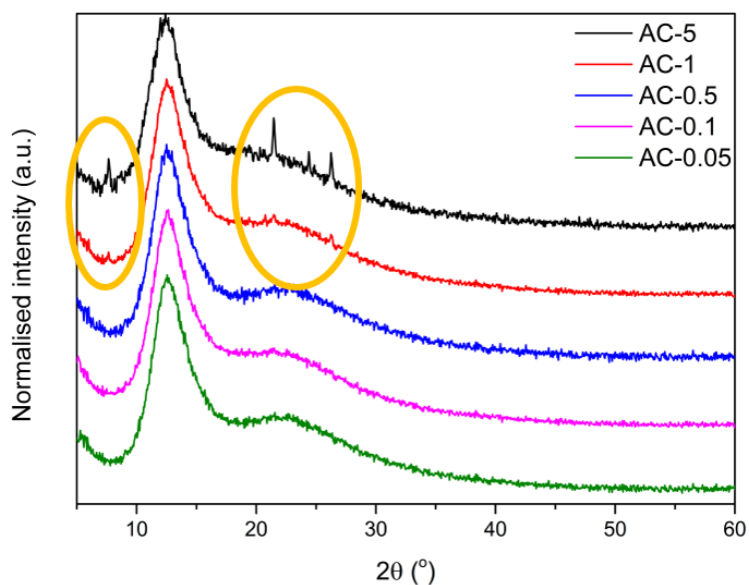
Figure 3-15 - An overlay of the PXRD spectra of air-cured networks, with orange ellipses denoting the peaks characteristic of HexDASA, visible for AC-5 and AC-1.
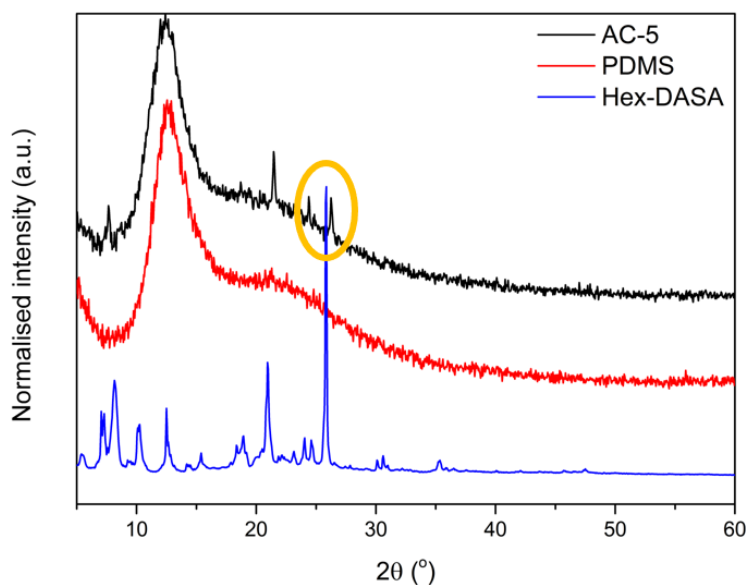

Figure 3-16 - An overlay of the PXRD spectra of AC-5, a cross-linked PDMS elastomer and HexDASA. Orange ring highlights the small 2θ value difference between AC-5 and HexDASA.

3.4.4.2.3 Sealed atmosphere (SA) cured elastomers (SAC-X)

All samples cured successfully and were subjected to visual, FT-IR and PXRD analysis. The FT-IR spectra are provided as Figure 3-17, they are practically identical to the air-cured samples from the previous section. Sample SAC-1 had a noticeably lighter colouration when compared to AC-

1. In contrast, the 5 wt% counterpart; SAC-5 retained the dark purple hue that was displayed by AC-5, both samples are visually identical. Visual inspection suggested that the SA curing process was partially successful, so PXRD analysis was subsequently conducted. Displayed as Figure 3-18, an overlay of the data for each sample is provided. Parallel to the results gathered from the air-cured samples, those from SA curing are largely amorphous; practically identical to cross-linked PDMS. The spectrum for SAC-1 appears to lack signals indicative of the HexDASA powder, but the aforementioned are clearly present for SAC-5.
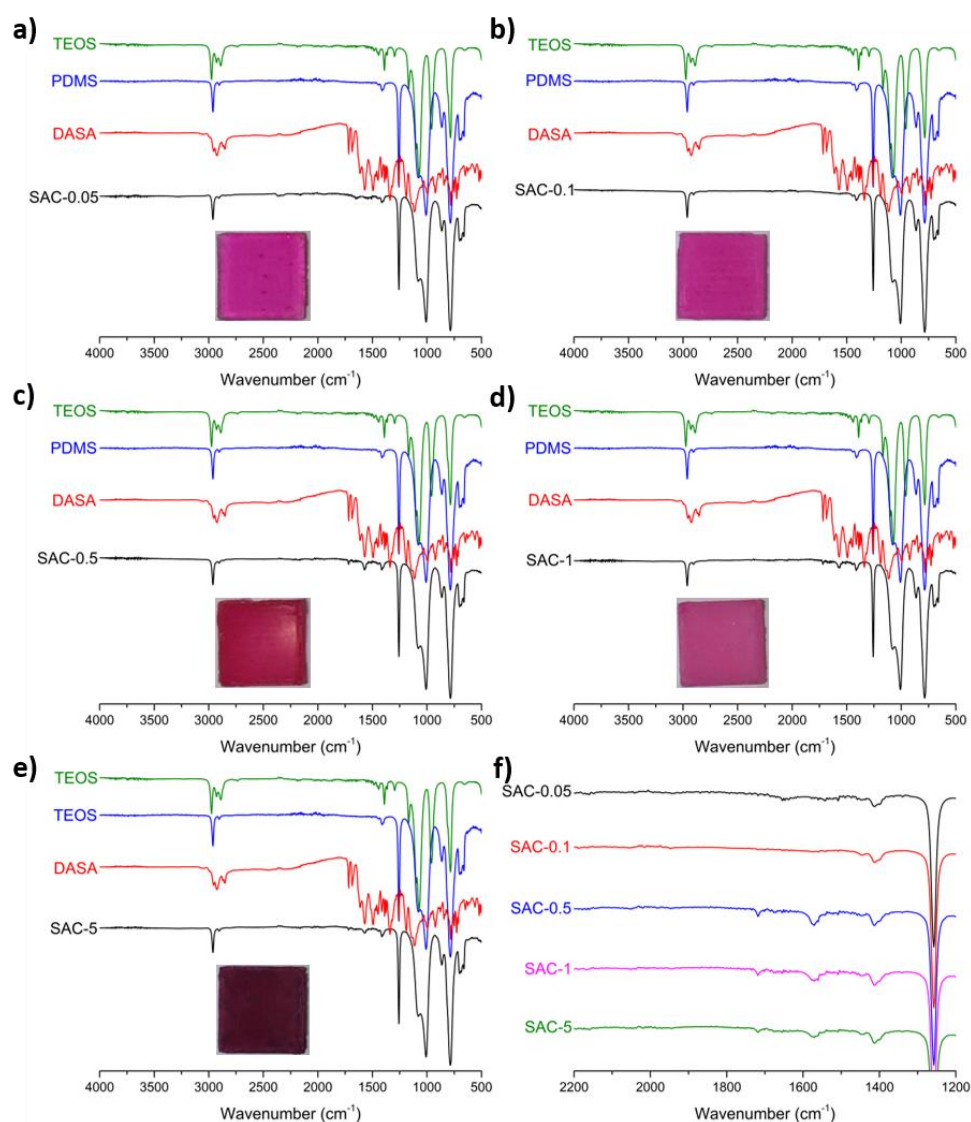

Figure 3-17 - FT-IR overlays of SA cured PDMS-DASA composites: a) SAC-0.05, b) SAC-0.1, c) SAC-0.5, d) SAC-1, e) SAC-5 and f) an expansion of an overlay of all elastomers, highlighting the emergence of peaks centred around 1719 and 1572 cm⁻¹.
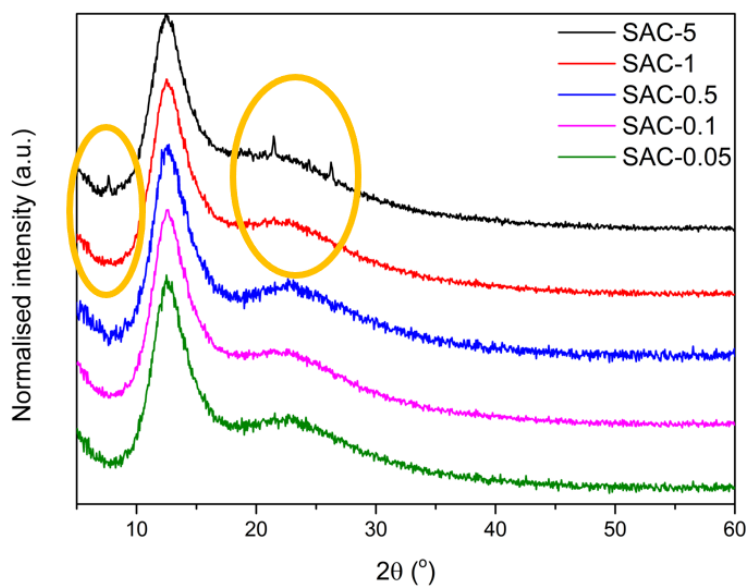
Figure 3-18 - An overlay of the PXRD spectra of SA cured networks, with orange ellipses denoting the peaks characteristic of HexDASA – note that SAC-1 appears to lack these.

At first glance, it appears that those peaks emerging from the main body of SAC-5 are of lower relative intensity when compared to those found in the spectrum of AC-5, and so all four spectra have been overlaid for clarity, as Figure 3-19. Comparing samples AC-5 and SAC-5, it is visually clear that there is a size discrepancy between the signals that are characteristic of DASA crystallisation, more specifically those belonging to the latter have a smaller relative intensity. In light of this, it is likely that the SA curing process has reduced the reachable concentration of crystallisation throughout the network, something that is not entirely apparent from visual inspection alone. For samples AC-1 and SAC-1, there is a clear lack of those characteristic peaks due to HexDASA, for the latter. It is clear from this that the modified curing process has resulted in a decrease of DASA crystallisation, it has not necessarily eliminated the problem entirely, only so much so that it can no longer be visually identified or quantitatively measured through this method.
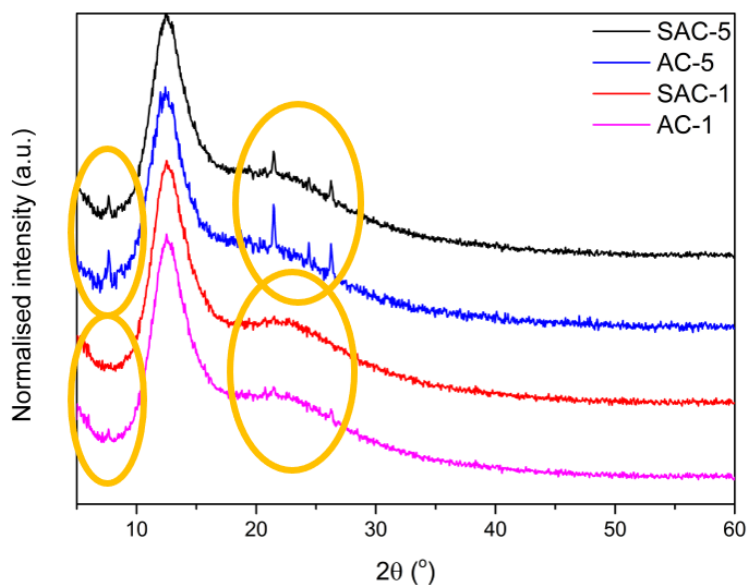
Figure 3-19 - Overlay of the PXRD spectra of AC-5 and 1, and SAC-5 and 1. Note: the orange rings highlighting the presence of DASA crystallite signals, or lack thereof.

Finally, the same conclusion had to be reached as that which was provided with visual inspection alone; the SA curing process was effective in preventing crystallisation for DASA loadings up to, and including, 1 wt%.

3.4.5 Preliminary comparison of the photoswitching rate of PDMS-EtDASA and PDMS-HexDASA

As noted in section 3.4.4.2.1, two alkyl amine donors were readily available for the synthesis of DASAs and subsequent PDMS-DASA elastomers; diethylamine and dihexylamine. The objective of this work was to focus only on one amine donor, that which would exhibit a faster rate of photoswitching. In order to determine that, the elastomers designated PDMS-EtDASA and PDMS-HexDASA were produced, containing the same concentration of their respective DASA; 0.05 wt% with respect to the mass of PDMS used. The elastomers were then compared through a short study. This experiment entailed placing both into the light box of which future photoswitching studies were to take place (section 3.3.7, Figure 3-4) and photographically recording their appearance before and 1 hour after visible light irradiation. It was found that the composite which incorporated HexDASA would switch faster (Figure 3-20).
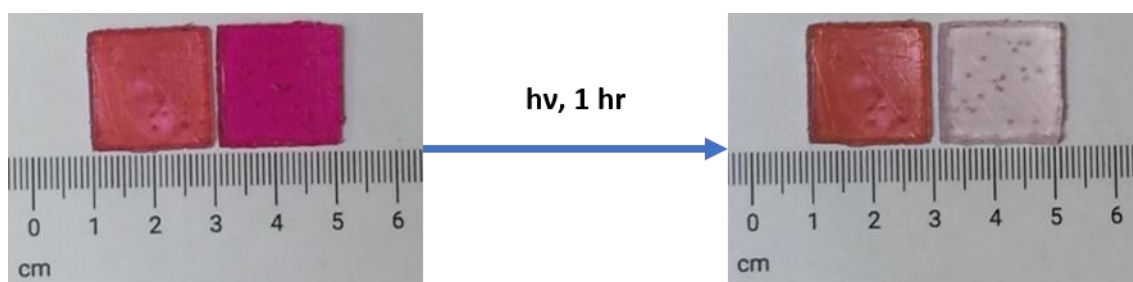
Figure 3-20 - PDMS-EtDASA (left) and PDMS-HexDASA (right) at: a) experiment start and b) 1 hour of light irradiation.

This was an unexpected result, as it has been recently reported that steric hindrance (longer chains) can exacerbate the ring-closure step, post-photoisomerisation, producing a slower switching process for first-generation DASAs.[47] In contrast, an older investigation found that when creating a biphasic mixture of toluene and water (organic and aqueous), short chain alkyl-based DASAs (diethyl amine and dibutyl amine) would near-quantitatively transfer from the organic to aqueous when exposed to visible light. However, the cyclic derivatives of those with longer alkyl chains (dioctyl amine) were found to remain within the organic phase.[33] With regards to those findings, it was believed that it was more energetically favourable for the EtDASA moiety to shift its PSS equilibrium closer to the coloured, open triene form – in such a way that it conforms to the hydrophobic nature of its environment, PDMS. The faster switching of HexDASA was attributed to the comparative hydrophobicity that the dihexyl amine donor holds, in relation to that of diethyl amine. Thereby affording the PDMS-HexDASA elastomer a comparatively easier photoswitching process, hence a significant difference in the observed switching rate between the two composites was found. The findings of this experiment were the deciding factor for incorporating HexDASA in all future elastomer production.

3.4.6 Photoswitching studies

The main aim of this chapter was to produce a reversibly photo-responsive polymeric system, to quantify this, uv-vis spectroscopy was conducted on the PDMS-DASA composites. Samples were subjected to 30-second periods of light irradiation, up to a total of 600 seconds of

exposure, using the setup established in 3.3.7, and subsequently analysed with a uv-vis spectrometer (Figure 3-21). Subsequently, samples were placed into an oven (60 °C) to induce thermal reversion and rapidly reach a dark equilibrium,[40] with uv-vis scans taking place every 300 seconds, for a total of 1 hour.
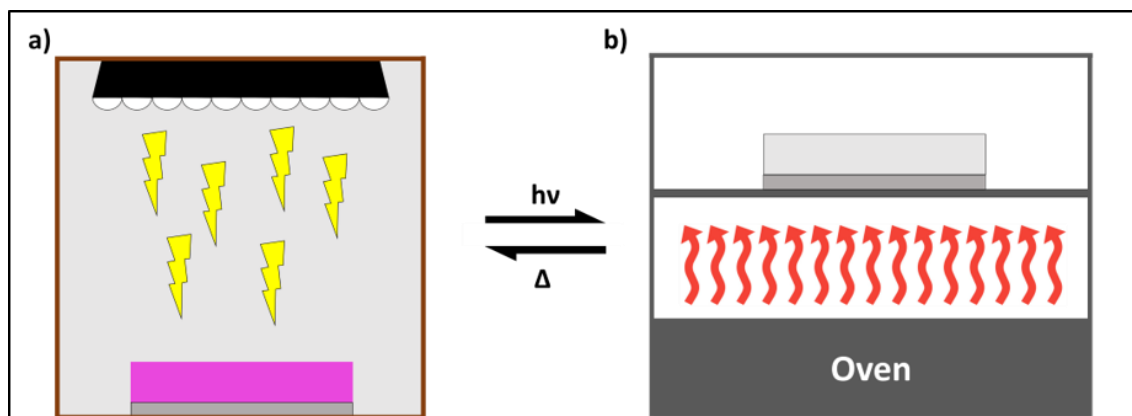

Figure 3-21 - Graphic representation of photoswitching (left) and oven-reversion (right). The photoswitching consists of placing the sample inside a cardboard box which has an LED lamp attached to the ceiling.

The data is presented as relative absorbance vs. wavelength (y, x) and the λ_{max} (538 nm) values were plotted against time to depict the rate of absorbance loss. As these samples were translucent solids, the baseline absorbance values for each scan experienced drift (Figure 3-22), similarly to what has been found in literature. It was thought this drift was light scattering caused by the presence of DASA microcrystals, so the data had to first be corrected in order to make comparisons later. The absorbance value for 600 nm was subtracted from every other value in each spectrum, so all spectra would have a reference point of x = 600 nm, y = 0. As can be seen from Figure 3-22, this brought all spectra in-line with each other. The wavelength of 600 nm was an arbitrary choice, it was deemed far enough away from the maxima to minimise interference with data analysis.
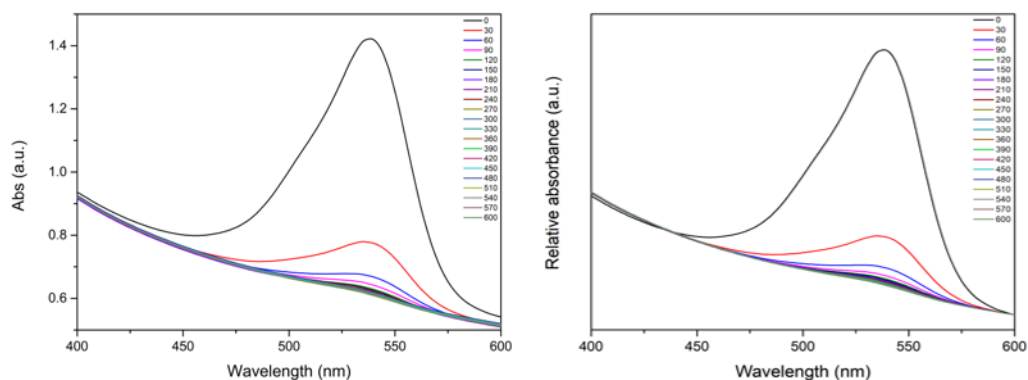
Figure 3-22 - UV-vis spectrum of AC-0.05 before data processing (left) and post-changes (right).

As a consequence of this data processing it was decided that the y-axis should be labelled as 'relative absorbance' rather than just 'abs.' – the following discussion is based around how the data changes in relation to its previous state(s), therefore discrete values were considered unnecessary. Following a completed 30-second time-lapse study, each sample was left exposed to the light source until the absorption value would no longer decrease, i.e. it had reached its PSS, these steps would last between 1 to 3 hours where UV-vis scanning would occur at various times – as opposed to strict 30-second intervals, out of practicality. This was done in order to establish the time window in which the sample would fully switch. The minimum absorption values are retroactively used as "0%" guides, for the 30-second time-lapse data. In other words, assuming that a sample is exhibiting "100%" absorbance at 0 seconds and that the minimum is provided as a "0%" marker, an absorbance value at 600 seconds can then be displayed as a relative percentage. Finally, a reversion study took place where the sample was placed into a dark oven, set to 60 °C, for 300-second intervals preceding absorption value measurements, this would last for a total of 1 hour. The oven-reversion data experienced the same treatment as shown in Figure 3-22.

3.4.6.1 Photoswitching mechanism of DASAs

The photoswitching mechanism for DASAs has been extensively investigated over the last few years, starting with the proposal of a transient intermediary species.[41] Investigations included

147

computational,[42,43] surface[44] and gas-phase studies,[45] transient absorption spectroscopy,[46] NMR analysis[40] and rapid-scan FTIR spectroscopy.[47] Each of these have contributed toward furthering the understanding of how these negative photochromes behave in the presence of light and heat. Photoswitching of DASAs can be described overall by three major steps: Z/E photoisomerisation, followed by thermal electrocyclization and a concomitant proton transfer.[47] In reality, the procedure is not so clear-cut and can fall prey to unwanted side-products through unproductive isomerisation (refer to figure 1.13, Chapter 1). Nevertheless, multiple investigations have been able to adequately characterise the behaviour of these photoswitches, in solution and the solid-state alike.[35,40,49,55] A common method is to employ exponential fitting to the forward and backward reactions, with the assumption that they adhere to first order kinetics. Although this may not be entirely correct, it is a convenient way of characterising the process. The data described here has been treated in a similar fashion to a previously reported method,[49] and exponential regression fitting function.[40] Through these methods, the switching process can be depicted as Figure 3-23. This combination allows for convenient quantification of forward and backward reaction rates, and the overall quantum yield of the reaction through uv-vis spectroscopy. The method largely neglects the existence of intermediary species that have been highlighted in the past (**Error! Reference source not found.**), theoretically limiting the accuracy of derived quantities. Whereas other methods can provide more expansive and detailed mechanistic explanations of the switching process; however, they require more specialised techniques or the use of NMR – neither of which were accessible for this chapter of work. This two-state model has demonstrated success with characterising DASA/polymer blends, with the need for only one analytical technique - uv-vis spectroscopy – establishing itself as the ideal method for understanding the PDMS-DASA blends discussed herein.
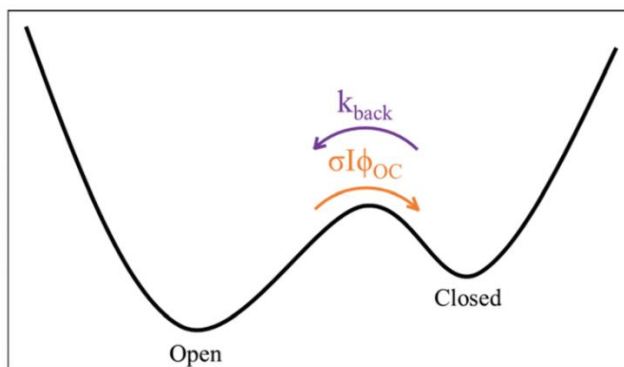
Figure 3-23 – A previously reported two-state model that describes the photoisomerisation of DASAs.[49] **The forward reaction rate is dependent on the absorption cross-section *σ*, the intensity of light being absorbed *I* and the net quantum yield of isomerising from the open to closed form, Φ_{oc}. The backward reaction rate is denoted as k_{back}.**

It has been shown in the past that DASAs exist as both open and closed isomers, even when subjected to a dark equilibrium.[40] It was postulated that long-chain alkyl-based DASAs tend to exist as >99.9% linear isomers. Given the inaccessibility of NMR analysis for the PDMS-DASA elastomers, it was not possible to identify the equilibrium at which HexDASA would sit – within this network – under dark conditions. The ^{1}H NMR spectrum shown earlier (section 3.4.2, Figure 3-6a) showed a large majority of the linear form under dark equilibrium. Given that chloroform and PDMS have relatively similar dielectric constants, the assumption was taken throughout these studies that, before light irradiation, the DASA consisted of 100% linear isomers.[82,83] This method provided an opportunity for comparison with DASA/PMMA blends, bringing context to the performance of the PDMS-DASA elastomers.

3.4.6.2 Preliminary study

All products required preliminary examinations before initiation of full photoswitching studies. They were placed into the custom-made light box (3.3.7) and left exposed to the LED white light for 1 hour. The results of those examinations are displayed as Figure 3-24. The SA cured composites were PDMS-DASA pads that were cured within Sistema® food containers (3.2.7, Figure 3-3), with the aim of preventing crystallisation that had visibly formed within AC-5 and

shown minor emergence in AC-1. Other than during the curing process, these samples had been treated in an identical manner to the air-cured batches. Air-cured elastomers AC-0.05, 0.1 and 0.5 appeared to switch fully within the 1-hour window, but AC-1 and AC-5 did not. It was believed that partial switching had occurred with the heavier-loaded samples, hence the subtle lightening of their colouration. It was found that SAC-0.05, 0.1, 0.5 and 1 had all decolourised within the time window. This result, coupled with the evidence that SA curing had eliminated or partially halted crystal growth (3.4.4.2.3, Figure 3-19), indicated that the initial switching problem experienced by AC-1 was a result of crystallite interference. Unfortunately, SAC-5 did not switch entirely, although it is clear from the image that partial switching did occur. Despite the lack of complete switching for some, all samples were pushed forward for a full photoswitching study as it was thought that a useful comparison could still be drawn between lighter and heavier-loaded composites. Elastomers that had displayed full-switching were subjected to oven reversion for 1 hour, as a study of the kinetics of the colour loss couldn't be performed if there was very little colour to begin with. Subsequently, AC-1 and AC-5 were used 'as is', because they appeared to retain a large concentration of the open-isomer DASA. Following these examinations, each sample underwent a full photoswitching study.
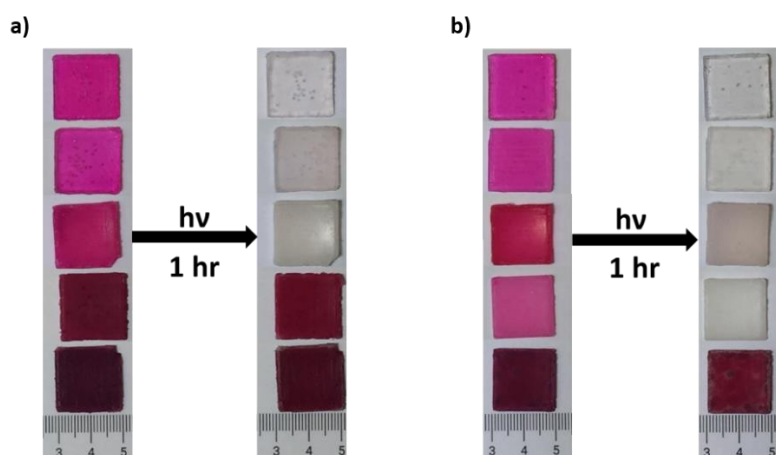

Figure 3-24 - Photographs of a) air-cured and b) sealed atmosphere-cured samples, before (left) and after (right) a 1-hour period of light irradiation, Concentration of DASA increases as the picture descends, from 0.05 wt% (top), to 5 wt% (bottom).

3.4.6.3 Extensive photoswitching study

As previously explained, this section shall detail and discuss the findings of more in-depth photoswitching experiments, which incorporated irradiation of samples with an LED white light (section 3.3.7). Characterisation of the photoswitching kinetics was the aim for this investigation, entailing the identification of certain parameters such as half-lives, reaction rates, and the change in absorbance at the photostationary state (PSS). Changes in absorbance were recorded through uv-vis spectroscopic scanning every 30 seconds up to a final 600 seconds. Following this samples were left to be exposed until a final measurement was taken at 3,600 seconds. This measure was taken as not all samples would fully decolourise within the 600 second time window. Immediately afterward, thermal reversion at 60 ^{o}C took place within an oven, with further scans every 300 seconds. Data sets were plotted as functions of the change in absorbance over time; for the purposes of kinetics calculations, the λ_{max} absorbance values were presumed to be directly related to the concentration of the coloured species of DASA (open isomer). Therefore, from here on, concentration and absorbance should be considered as one and the same. It was found that after 2 hours of visible light irradiation, samples AC-5 and SAC-5 exhibited too large a degree of absorption to produce meaningful data (Figure 3-43 and Figure 3-44, section 3.7 – appendix 3A). This was thought to be caused by a combination of the crystallisation discussed in section 3.4.4.2.2 and the inherently high molar absorptivity of DASAs,[32] as such, further analysis was abandoned. From here on, the data acquired for samples AC-0.05 to AC-1, and SAC-0.05 to SAC-1 shall be discussed. Plots for each elastomer consist of a time-lapse for both the forward and backward reactions, beside the change in λ_{max} over time. This discussion shall feature all investigated elastomers, but in the interest of variety only the data for sample AC-0.05 is displayed here, as Figure 3-25. Spectra for other elastomers have been placed in sections 3.8 and 3.9 – appendices 3B and 3C, respectively. Each PDMS-DASA elastomer displayed clear absorbance at the beginning of their respective studies, peaking at 538 nm, an expected wavelength from these first-generation switches.[32,33] Upon exposure to a white light source (section 3.3.7), a steady decrease in absorbance was evident (Figure 3-25a),

with an indication of greater loss per time interval for the less-concentrated samples. This decrease continued until reaching what was believed to be the photostationary state, where the forward reaction rate was almost balanced by the thermal reverse rate.[49] Essentially, the PSS was qualitatively determined through inspection of the data. It has been found in the past, that a transient, red-shifted absorption band can form upon irradiation in non-polar media.[41,46,84] No such signals appeared in any spectra recorded for this experiment, it was expected that they would be found at approximately 600 nm.[84] Following the photoisomerisation step, thermal reversion took place (Figure 3-25b). The data clearly indicated a reformation of the original, coloured isomer, by an increase in absorbance, centred around 538 nm. The λ_{max} absorbance values from both halves of the study were plotted against time as a single graph. This graph was then resized and contextualised in order to highlight the two different experiments and has been included as Figure 3-25c and d. Figure 3-25c depicts the first 600 seconds of visible light exposure. Figure 3-25d encompasses both sets of data, that from the light irradiation step is highlighted by a grey rectangle and has been compressed, such that it allows for convenient display of the thermal reversion data. The data sets were fitted with an exponential regression model, plotted in Origin9, in accordance with previously reported investigations.[40,41,46,49,84] Fitting the data enabled the approximation of forward (photochemical) and backward (thermal) reaction rates, and half-lives; hereby referred to as $k_{forward}$ and k_{back}, and $t^P_{1/2}$ and $t^T_{1/2}$, respectively. These metrics shall be discussed later in this section. In order to conveniently compare the change in absorbance over time for each sample, the data sets were collated and have been plotted as Figure 3-26.
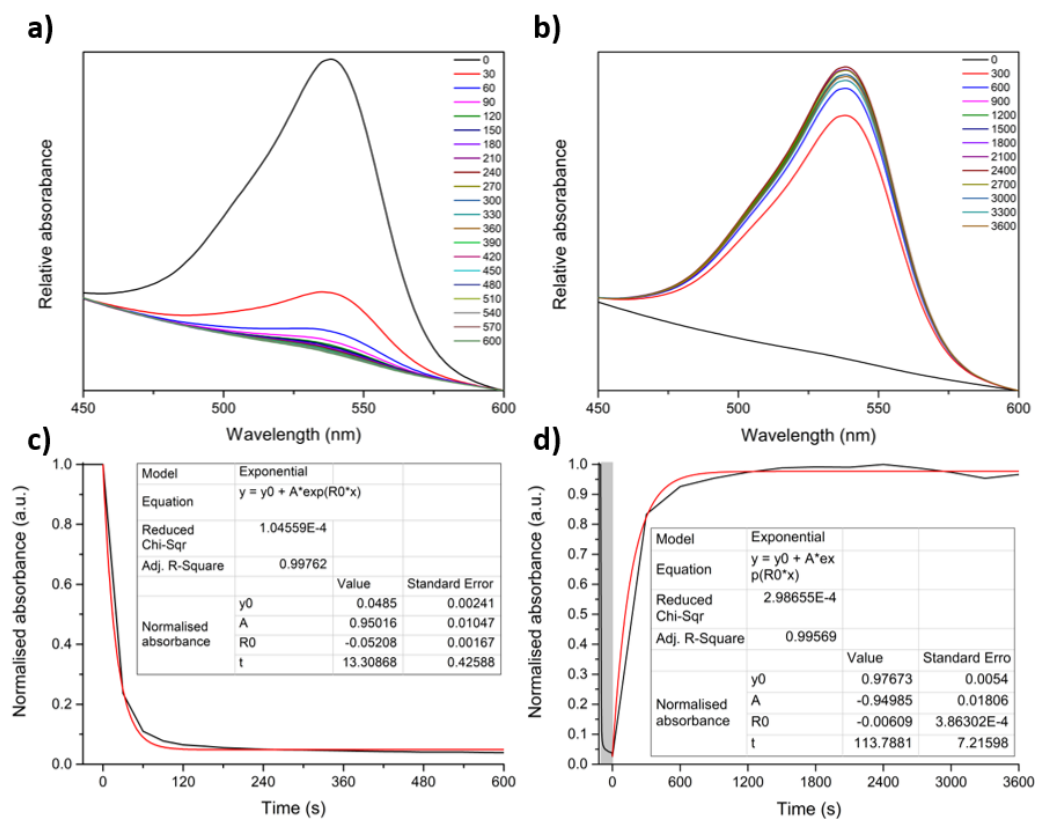
Figure 3-25 - UV-vis data acquired for AC-0.05, consisting of a) a time lapse of the forward photoswitching reaction, b) the thermal reversion, and c+d) the change in λ_{max} over time, for the forward and backward reactions, respectively.
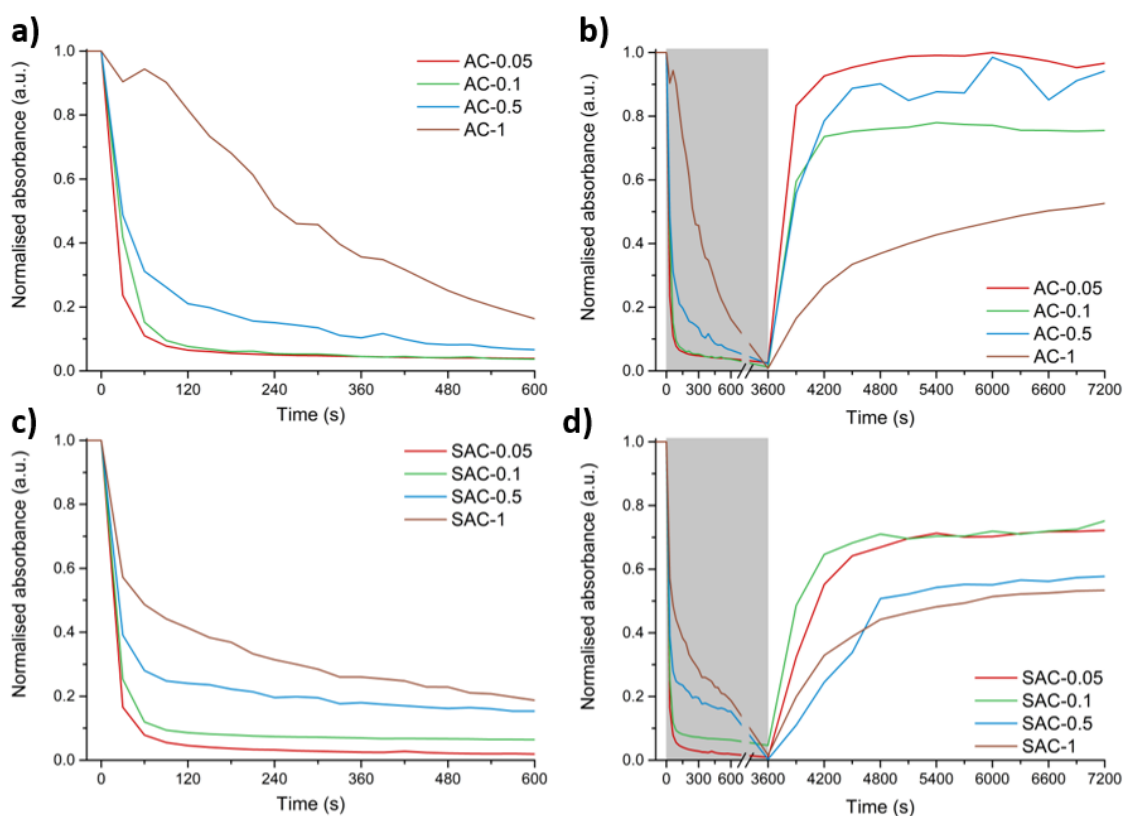
Figure 3-26 – Plots of the change in absorbance over time for the a) AC photoisomerisation, b) AC thermal reversion, c) SAC photoisomerisation, and d) SAC thermal reversion experiments.

Immediately, it was apparent that a larger concentration of DASA lead to a slower rate of photoisomerisation, made apparent by initial comparison of the line-shapes in Figure 3-26a. The photoisomerisation process for AC-1 presented an almost linear-like relationship between absorbance and exposure time, this is believed to be symptomatic of DASA crystallisation. Data corresponding to SAC-1 confirmed that hypothesis (Figure 3-26c), as it was found earlier that crystallisation had been largely prevented in this sample (section 3.4.4.2.3). The data for thermal reversion is included as Figure 3-26b and d, where the grey rectangle indicates visible light irradiation. Similarly, to the forward reaction, it seemed that thermal reversion was also affected; a fall in reversion rate with increasing concentration was witnessed. Reversion data for the sample AC-0.5 fluctuated greatly, it is thought that this was caused by the scattering of light encouraged by DASA microcrystals. Overall, the data suggested that the forward photoisomerisation and backward thermal reversion were both hampered by concentration

effects. This was not unexpected, as a previous investigation entailed the analysis of various DASA concentrations in solution and as DASA/polymer blends.[49] It was found that an increase in DASA concentration, in solutions such as toluene or chloroform, would inhibit the forward reaction and destabilise the cyclic form, translated as a drop in quantum yield and an increase in thermal reversion rate. It was noted that both effects consequentially inhibited net photoproduct formation. However, with a polymer, such as PMMA, it was found that a larger decrease in quantum yield would occur, paired with a slower reversion rate. Overall, this still led to an exacerbation of the photoswitching process. Metrics from the acquired data, such as the time taken to reach a PSS, or the absorbance loss over the duration of the study, are tabulated as Table 3.3.

Table 3.3 – A table containing metrics such as the approximated PSS time, and the calculated absorbance loss at varying time intervals.

Sample	DASA conc. (M)	PSS (s)	ΔA at PSS (%)	ΔA at 600 s (%)	$k_{forward}$ (x10^{-3}) (s^{-1})	k_{back} (x10^{-3}) (s^{-1})	*A* recovery (%)
AC-0.05	0.0016	90	92.2	96.2	52	6.1	100
AC-0.1	0.0032	90	90.5	96.3	33	5.1	75.6
AC-0.5	0.016	120	79.0	93.4	23	3.2	98.5
AC-1	0.032	600	83.7	83.7	2	1	52.7
SAC-0.05	0.0016	90	94.5	98.1	63	2.3	72.2
SAC-0.1	0.0032	90	90.6	93.6	53	3.3	74.3
SAC-0.5	0.016	120	75.4	84.6	41	1.2	57.7
SAC-1	0.032	300	71.5	81.2	13	1.5	53.4

To reiterate, the PSS times have been qualitatively determined, based upon inspection of λ_{max} differences between time periods; decisions were dependent on the moment that it appeared that absorbance losses were no longer significant. As such, further losses were assumed to be from photodecomposition.[40] Unsurprisingly, the PSS times and concentration were directly proportional, such that an increase in the latter was an increase for both. As mentioned earlier (section 3.4.6.1) the DASA is assumed to exist as 100% linear isomers before light exposure, therefore it can be said with certainty based on that assumption, that the absorbance at the PSS is a direct ratio of open to closed forms. As such, the data largely confirmed that an increase in DASA concentration would lead to a lower photoswitching efficiency, in this case photoswitching

efficiency depended on the amount of absorbance lost once a PSS was reached. The only exception to this rule was AC-1; most likely consequential of the presence of DASA crystals. Acquisition of the exact forward and backward reaction rates confirmed earlier speculation (Figure 3-25) that the former decreases with a rise in concentration and the latter appears to increase. The reasoning for this phenomenon is not entirely clear and is believed to be an effect of steric interference by other nearby DASA molecules.[49] This correlation, however, did not apply overall; it was found that for the SAC elastomers, reversion rate didn't bear a relationship with concentration. There appears to be no logical reason for this and is considered to be just an anomaly. Finally, no discernible trend could be found when inspecting the absorbance recoveries, post-thermal reversion. The absorbance recovery is defined as the percentage of initial absorbance that was reached within 1 hour of thermal reversion. The average loss in absorbance was 27%, as of yet there appear to be no studies regarding this area of kinetics for DASA/polymer blends, whereas it has been seen to be possible with covalently-attached analogues.[51,64,85] It is postulated that this large drop in re-obtainable absorbance is a matter of photodecomposition.[40,54]

Thus far, an insight into the kinetic characteristics of these elastomers has been provided. However, comparisons need to be made, in order to provide context to the data at hand. It is difficult to be able to do so with other previously established DASA/polymer blends, as many factors that affect the photoswitching process must be taken into account; such as light source intensity, DASA concentration, DASA acceptor/donor nature, experimental conditions, material dimensions, chemical nature of the material, etc. Most importantly, there are very few published studies that have investigated DASA/polymer blends, two of which do not provide a great amount of detail as to their switching kinetics,[34,62] leaving three other cases to be considered.[49,50,54] Herein, Hooper et.al produced a first-generation DASA-containing polyurethane which was capable of localised temperature mapping.[54] It was found that a cylindrical sample of 2.2 mm thickness and 10 mm length would require 80 hours to fully decolourise; an extremely slow process in comparison to the composites described in this

chapter. However, this is an unfair comparison as the intended application required the promotion of linear isomer stability, to prevent immediate reformation of the cyclic form.[54] The next case to be considered was regarding the blending of DASA into PS films, for an investigation into photoinduced deadhesion applications.[50] It was found that an 8 wt% loading of DASA into a PS film would take 14 hours to fully decolourise, but would not exhibit reversion, likely due to polymer chain steric interference, as a dissolution of said film into DCM yielded a rapid reversion of the photoswitch. It is likely that the high T_g of the polymer film had a role to play in this inhibition of thermal reversion, similarly to a previously reported investigation.[85] A low glass transition temperature is a strong advantage that PDMS has over other previously used polymer analogues. Another other example of DASA/polymer blends, of which will be the prime literature comparison for the work described here, consisted of incorporating a third generation photochrome into PMMA and PS films, with the main focus of the investigation being placed on the former.[49] It was found that films containing 0.01 and 0.008 M DASA would lose 75 and 82% of their absorbance within 600 s, respectively, indicating a slower rate of switching when compared to what has been demonstrated by AC-0.5 (Table 3.3). A comparison of k_{back} values revealed that the PMMA/DASA blend thermal reversion reaction was slower in contrast to the architecture described in this work, suggesting that cyclic stability is lower in PDMS-DASA networks. The difference in perceived reversion is somewhat expected, as the high glass transition of PMMA[86] has been found to inhibit the ring-opening process in the past.[85] However, this has less of a detrimental effect on second generation DASAs, and presumably those of the third generation, too.

As mentioned previously, exponential regression was performed on the absorbance vs. time data sets for each sample, displayed in Figure 3-25. This fitting model, including variations, has been used throughout various studies of DASA switching behaviour.[40,41,46,49,84] It brings with it an assumption that the photochromes behave under first order kinetics. Although this may not be strictly accurate, as it is already established that the kinetic pathway of DASAs is complex, it does provide a convenient route for characterisation of the process through isomer half-life

determination. The thermal half-life of the species in question is an important characteristic for evaluation of itself as a photoswitching platform.[87] As such, the half-lives for each sample were determined by:[88]

$$t_{\frac{1}{2}} = \frac{\ln{(0.5)}}{k}$$ **Equation 1**

Where *k* is the rate of reaction calculated through the regression analysis. From this, half-lives were determined, tabulated (Table 3.4) and displayed as Figure 3-27, where $t^P_{1/2}$ and $t^T_{1/2}$ correspond to the photochemical (forward) and thermal (backward) processes. It was found that for both AC and SAC elastomers, forward half-life would increase along with DASA concentration, as expected because this translates as a slower photoisomerisation reaction.
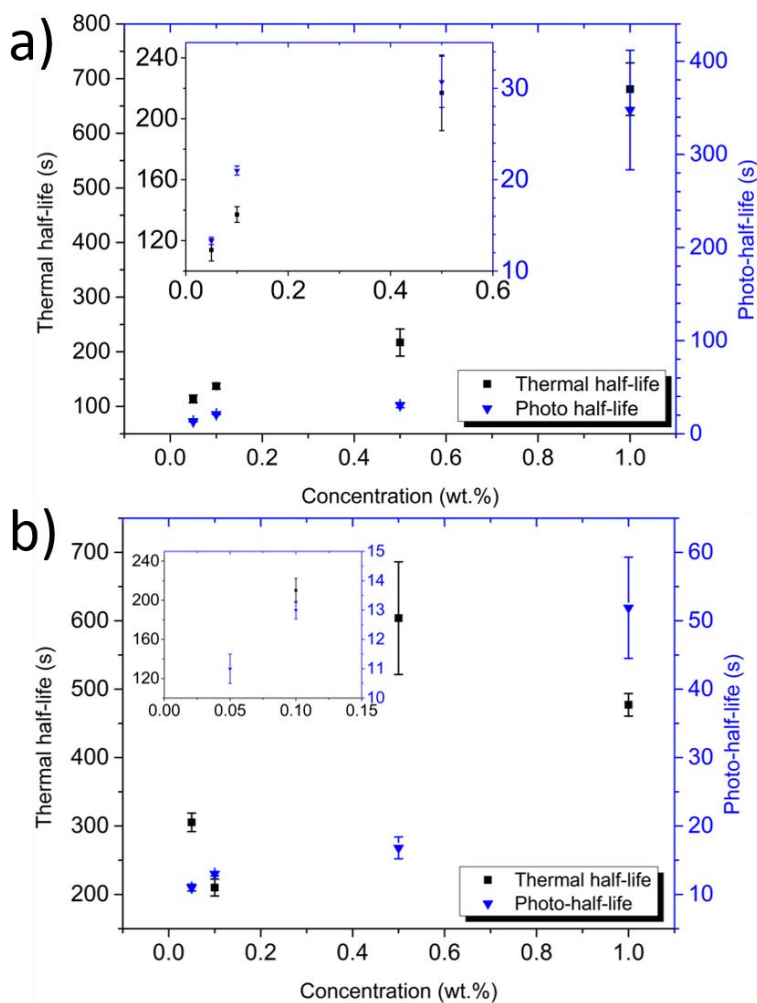

Figure 3-27 – Photochemical and thermal half-lives for a) AC and b) SAC elastomers, calculated through exponential regression.

Similarly, the same trend was seen for thermal reversion of the AC samples whereby the reaction is inhibited with increasing concentrations.[49] Whereas, the SAC samples did not exhibit an overall trend; mirroring their performance shown in Figure 3-26d. Interestingly, as with the forward reaction rates, it appeared that SAC $t^P_{1/2}$ values were indicative of a faster photoisomerisation, in comparison to the AC analogues. On the other hand, the AC elastomers demonstrated shorter reversion half-lives. Overall, suggesting that the AC samples have a less stable cyclic isomer, possibly explainable by the presence of DASA crystals that may not have been distinguishable through PXRD analysis (section 3.4.4.2.2). A focus on half-life determination for DASA/polymer blends has not been found in the literature and as such a direct comparison with other architectures is not possible.

Table 3.4 – A table of the calculated half-lives and molar absorptivity coefficients, for each elastomer.

Sample	DASA conc. (M)	$t^P_{1/2}$ (s)[a]	$t^T_{1/2}$ (s)[a]	ε (M^{-1} cm^{-1}) [b]
AC-0.05	0.0016	13.3 ± 0.4	113.8 ± 7.2	6122
AC-0.1	0.0032	21.0 ± 0.5	137.1 ± 5.1	4798
AC-0.5	0.016	30.7 ± 2.8	217.0 ± 24.8	1209
AC-1	0.032	347.6 ± 64.1	680.7 ± 48.0	546
SAC-0.05	0.0016	11.0 ± 0.5	305.4 ± 13.5	4433
SAC-0.1	0.0032	13.0 ± 0.3	210.1 ± 12.3	3108
SAC-0.5	0.016	16.8 ± 1.6	603.9 ± 82.3	1184
SAC-1	0.032	51.9 ± 7.9	477.2 ± 16.5	484

[a] **calculated by exponential regression,** [b] **path length of 0.2 cm.**

Along with isomer half-lives, the molar absorptivity coefficients were tabulated. The intention was to use these to calculate the efficiency of the forward photoswitching reaction; the quantum yield. The molar absorptivity can be obtained by a rudimentary rearrangement of the Beer-Lambert law:

$$A = \varepsilon c l \qquad \textbf{Equation 2}$$

$$\varepsilon = \frac{A}{cl} \qquad \textbf{Equation 3}$$

Where A is the measured absorbance of a sample, c is the concentration (M) and l is the path length (cm). As such, ε values were calculated for each PDMS-DASA elastomer and are provided in Table 3.4. A comparison of these values with those of other DASAs and another DASA/polymer blend elucidated how small they really are; the ε for DASAs has been shown to vary between at least 50,000 and 176,000 M^{-1} cm^{-1}.[32,40,89] A previous study into the concentration effects akin to DASAs showed that at solution concentrations such as 1×10^{-3} M, a path length of 15 μm needed to be used, in order to achieved absorbance values of c.a. 0.3 or less.[49] This concentration almost mirrors that of the perceived concentration of samples such as AC-0.05 and SAC-0.05; assuming that they would share similar molar absorptivity (c.a. 100,000 M^{-1} cm^{-1})[32] this should have provided absorbance values of at least 3.2 a.u., but of course did not. Furthermore, the molar absorptivity of HexDASA in toluene was determined to be 75,000-80,000 M^{-1} cm^{-1} calculated from two absorbance measurements. With this in mind, it is likely that the resulting low magnitude of molar absorptivity values (Table 3.4) was caused by a combination of low linear isomer concentration and light scattering-affected absorbance. Unfortunately, investigating the former was not practical and therefore the assumption of 100% open isomer had to stand. Consequently, any calculated quantum yields would be inherently inaccurate, making the process unnecessary.

To summarise what has been gleaned in this section; it would appear that sealed-atmosphere curing produced elastomers that were able to decolourise faster than that of the air-cured variety, but in contrast demonstrated slower thermal reversion (Table 3.3, Figure 3-26). It is postulated that this difference was caused by the inhibition of crystal growth in the SAC elastomers; crystal formation likely hampered the forward switching process and favoured linear isomerisation, similarly to the behaviour of azobenzene photoswitches.[90] This work has also confirmed that PDMS-DASA blends suffer from the concentration effect that was previously reported, such that drops in photoisomerisation rate and thermal reversion with rising concentration were apparent.[49] As such, the half-lives for corresponding reactions were also affected (Figure 3-27).

3.4.7 Cycling study of AC-0.05

In order to probe the reusability of the previously synthesised PDMS-DASAs, a photoswitching cycling study was undertaken using a sample from the AC-0.05 batch. DASAs are well known for their high fatigue resistance which is of course key for reversible systems.[43,46,49,51,84] As explained in section 3.3.7, the cycling study consisted of measuring the absorbance of a sample after a 5-minute visible light exposure instance and a 5-minute oven-reversion step, these values were then plotted as Figure 3-28. The data indicates that over multiple cycles, photodecomposition occurs; the maximum attainable absorbance degrades by 51.3%. Degradation was calculated by normalising the λ_{max} (538 nm) values such that the maximum was equal to 1 and the minimum, 0. The value that becomes 0 was assumed to be the state at which 100% of the DASA had cyclised – from this percentage values could be inferred.
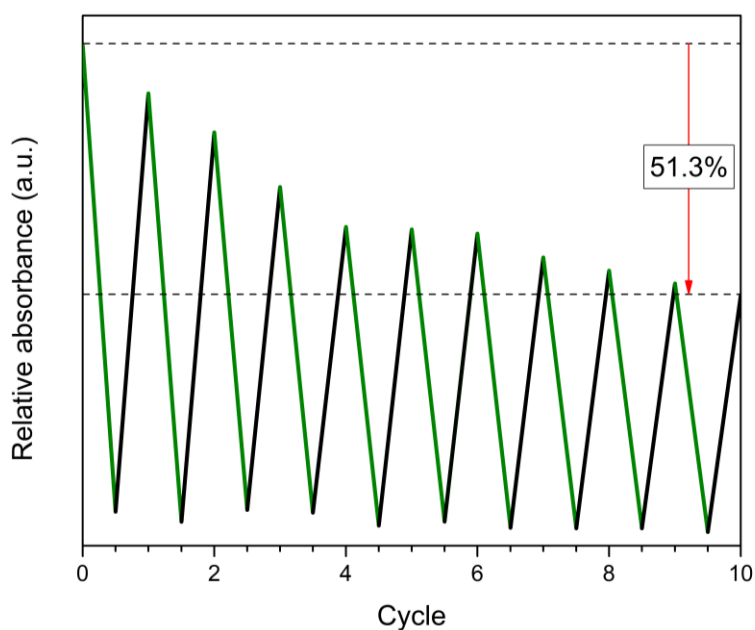

Figure 3-28 - UV-vis cycling study of AC-0.05, showing a 51.3 % decrease in absorbance post-oven reversion, within 10 cycles. Cycles constituted a 5-minute light exposure step, followed by a 5-minute oven-reversion period – designated '5x5'.

It was thought that the inherent non-polarity[65] of the PDMS network would encourage the equilibrium to favour the linear, open form of DASA as it too has no net charge. Instead, it

appears that the equilibrium gradually shifted toward the zwitterionic, closed form, something that has been reported in previous literature.[54] Known studies of DASA-polymer blends haven't provided cycling metrics, making it difficult to directly compare this data. There are however examples of DASA-polymer conjugation that hold an impressive degree of resistance,[91,92] whereas some appear to lose a great deal even after a single cycle.[93] Although, this was likely due to utilising such longer irradiation times; it was found that, for molecular DASAs in solution at least, a longer light exposure time can lead to a marginal decrease in fatigue resistance.[40] A decision was made to investigate whether the gradual fatigue of photo-responsivity could be affected by the length of time elastomers would spend under visible light exposure. A second elastomer pad from the AC-0.05 batch was subjected to a cycling study in much the same way as the first, except this time the light exposure intervals were 15 minutes long, and the oven reversion steps were kept the same (5 minutes). The results of a 10-cycle experiment are displayed as Figure 3-29.
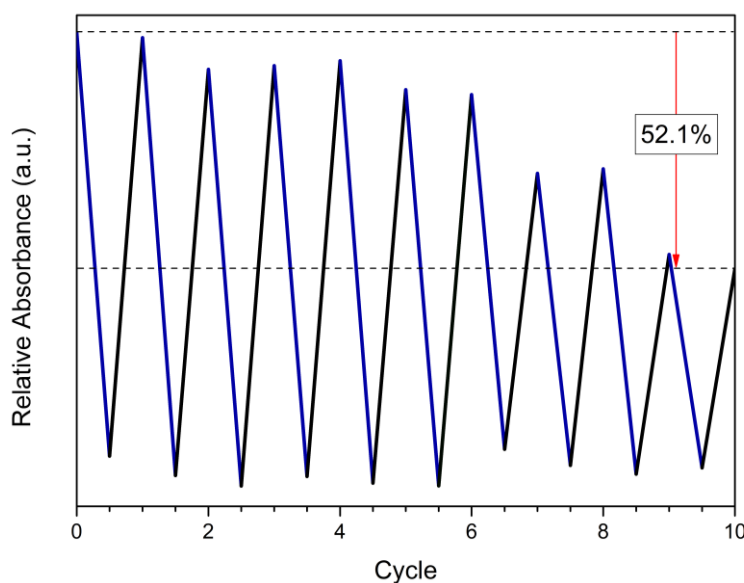

Figure 3-29 - UV-vis cycling study of AC-0.05, showing a 52.1 % decrease in absorbance post-oven reversion, within 10 cycles. Cycles constituted a 15-minute light exposure step, followed by a 5-minute oven-reversion period – designated '5x15'.

From here on, the first study shall be referred to as '**5x5**' and the second as '**5x15**', denoted by green and blue plot colours, respectively. As shown by Figure 3-29, the decomposition of photoswitch was calculated to be 52.1%, an insignificant difference when compared to the original 5x5 study which displayed a loss of 51.3%. Upon comparison of both plots, it was clear that 5x5 constantly experienced a negative change in absorbance maxima, in other words, the efficiency in reversibility was continuously decreasing. Whereas, for 5x15 it was found that on at least 3 occasions, the absorbance maxima would experience a positive change, the reason for this is unknown. In fact, it was expected that reversion would be comparatively less efficient, given that the sample had spent longer periods under visible light exposure. It was believed that a longer exposure time would cause further drops in absorbance recovery, due to photodecomposition. In light of this, it was concluded that up to, and including, a three-fold increase in exposure time did not affect photoswitch decomposition. The normalised maxima were plotted beside the percentage changes per cycle, for each study, to elucidate any kind of correlation (Figure 3-30). The percentage changes in maxima for both studies appeared to follow no discernible pattern, in other words they were statistically random (Figure 3-30b).
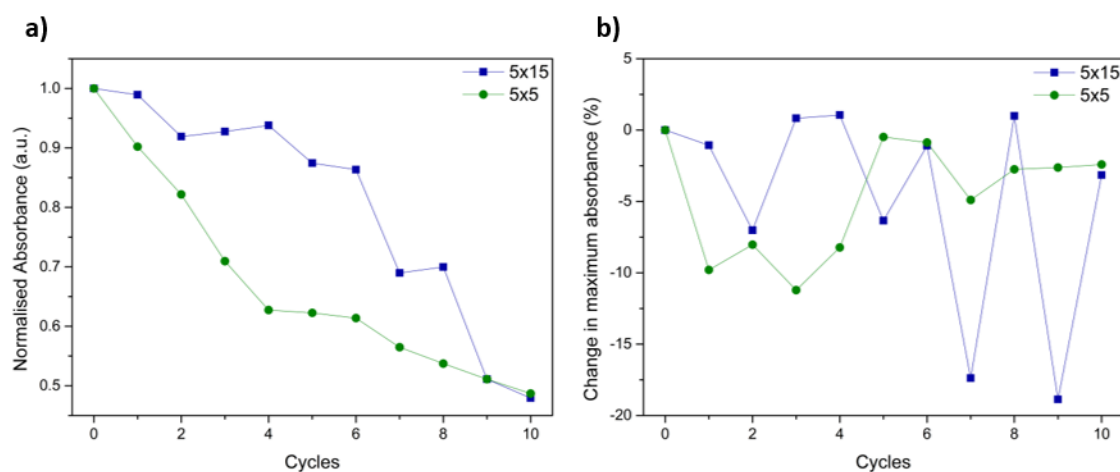

Figure 3-30 - Plots of a) the maxima of both cycling studies, normalised for convenient comparison, and b) the percentage changes in said maxima.

There was an approximate 50% loss in recoverable absorbance over 10 cycles for both studies, and from this it was hypothesised that complete degradation of the photoswitching species

could occur within a total of 20 cycles. As such, it was decided that an extended 20 cycle study was to be performed. As the 5x15 experiment had been recently undertaken, extending this alone to 20 cycles seemed like the most convenient course of action. Earlier, data showed little difference between the two, so it was decided that this single 20 cycle study could be representable for both. The extended study has been included as Figure 3-31. The overall degradation of photoswitch was found to be 81.1%, after a 20-cycle study. From this, it was concluded that the process of degradation appeared to be asymptotic, in other words, the magnitude of decomposition lessened over an increasing number of cycles. Although, a much longer study would have been necessary to unequivocally confirm this hypothesis. Further from these findings, a final extension was made to this study whereby 5 more cycles were undertaken. This time, the sample would experience a 10-minute oven reversion step. The reasoning behind this experiment was to determine whether the loss in absorbance found so far was actually a result of irreversible decomposition of DASA, or if this process could be reversed by applying further heating. The data for this experiment has been displayed as Figure 3-32. The extra 5 cycles, which consisted of 15-minute light exposure and 10-minute oven reversion, have been coloured in red for to enable clear and convenient distinction from the rest of the previously conducted study.

As can be seen, the first 10-minute reversion period rejuvenated a large amount of absorbance, more so than what was initially held by the composite. This result was promising as it showed that the loss of absorbance experienced over previous cycling studies was not irreversible. Therefore, the decrease in DASA activity could not have been caused by photodecomposition. It seems that with each cycle, a small portion of DASA would reside in the cyclic form, rather than revert back to the linear isomer. Lengthening the heating time must have supplied the required amount of energy to traverse the thermal reversion barrier more easily. A previous report in which DASAs were dissolved into PS films found a similar phenomenon; dissolution of a composite which could not revert, led to an immediate reformation of the linear isomer.[50] Further examination of the data revealed the total reduction in recoverable absorbance maxima

experienced during the during the final 5 cycles was almost equal to that of which was displayed during the first 20 cycles (Figure 3-32). This shows that the benefit of prolonged heating is relatively short-lived. On the other hand, this could be seen as a positive characteristic as it indicates that pre-treatment through multiple switching cycles can lead to accumulation of the stabilised cyclised isomer, which has found use in thermal-sensing.[54]
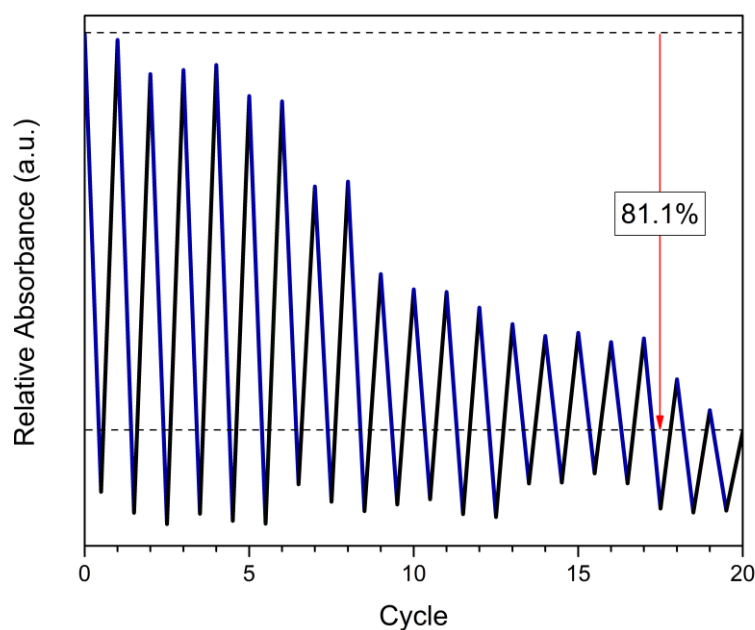

Figure 3-31 - Extension of cycling 5x15, to 20 cycles. Examination of maxima shows an overall decomposition of 81.1% of photoswitching species.
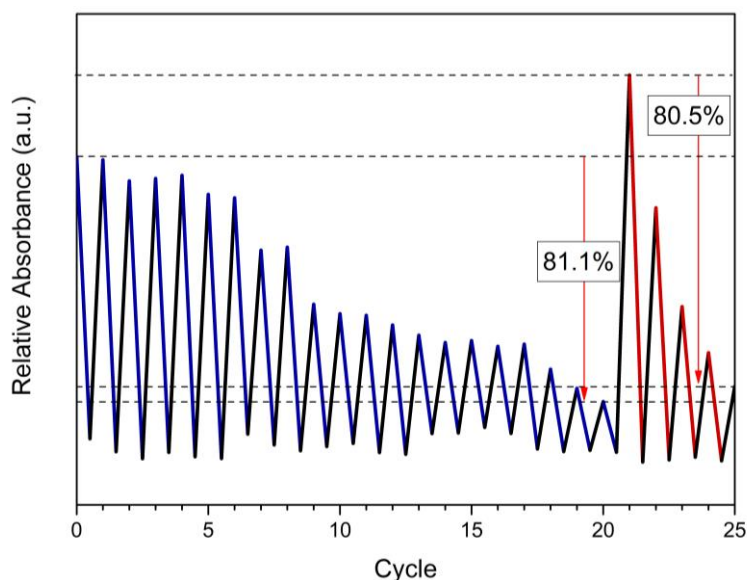
Figure 3-32 - The 5x15 study further extended by 5 cycles, to include oven-reversion steps of 10 minutes.

In conclusion, it has been found that these PDMS-DASA composites show little fatigue resistance, at least in comparison to other frameworks established in literature[91] and molecular DASAs themselves.[40,94,95] Although the decay of DASA activity can be reversed, this benefit is only transient, therefore the recyclability of these physically blended networks has to be classed as limited. Given that these cycling studies were only performed on samples from the batch AC-0.05, it was found previously that this loading of DASA provided the most efficient reversion process (section 3.4.6.3, Figure 3-26, Table 3.3), and so it can be surmised that those with heavier loadings would likely exhibit a larger magnitude of decay within fewer cycles. This phenomenon could prove to be a problem when attempting implementation into a framework that requires on/off switching, with set stimuli exposure times. Despite this, it does appear to hasten the forward switching process, which can be seen as advantageous.

3.4.8 Effect of solvent swelling on photoresponsivity

As has been shown in the past, polymer networks can act as media for the photoswitching of DASAs, either through covalent bonding[56,91,96] or physical blending/suspension,[34,54] but, solution-state switching produces a more rapid isomerisation process.[49] The purpose of this experiment

was to investigate whether solvent swelling of a PDMS-DASA elastomer could accelerate the photoswitching process. The intention was to produce an encapsulated gel matrix that displayed the advantages of solution-state switching and the versatility of solid-state materials. Encapsulation of elastomers could be easily facilitated by the incorporation into solvent-resistance, vacuum-sealable pouches. AC-0.05 (2.2.4) and blank cross-linked PDMS elastomers synthesised under the procedure laid out in 2.2.3 were subjected to solvent vapour swelling; the latter to provide reference data for the former. The swelling procedure, originating from literature[80] and described in 3.3.6, consisted of placing each elastomer into a glass desiccator, on an internal perforated metal shelf and allowing them to sit in a saturated atmosphere of target solvent for 72 hours. The solvent range provided examples of polar protic, aprotic and non-polar media, such as: acetone; dichloromethane (DCM); N, N-dimethylformamide (DMF); diethyl ether; ethanol; ethyl acetate; propan-1-ol; tetrahydrofuran (THF); and toluene. The mass and volume of each sample were taken before and after swelling, and used to calculate the swelling ratio of both variables. The experiment was conducted in triplicate, providing an average swelling ratio for mass, Q_m, and volume, Q_v, plotted as Figure 3-33a and b, respectively. Error bars represent standard deviation of the mean.
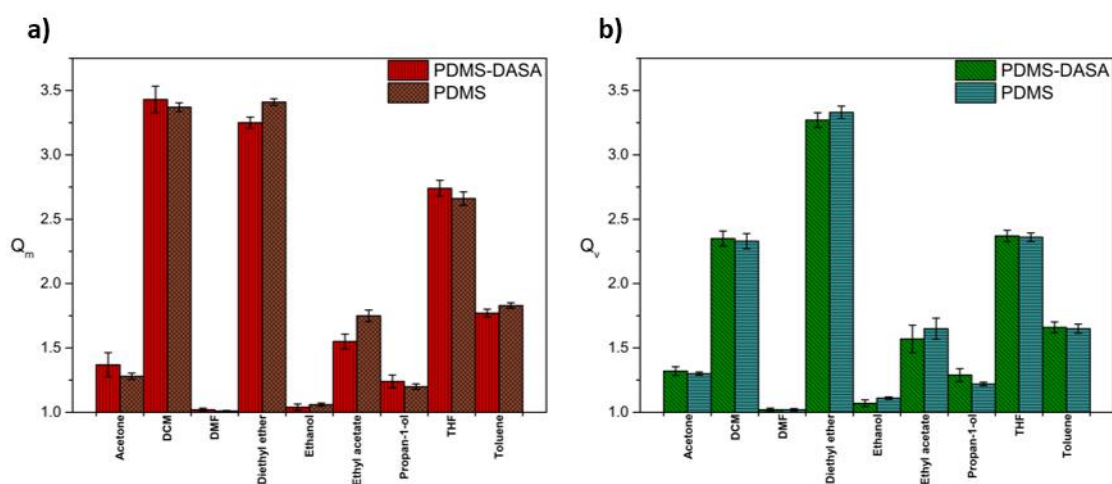

Figure 3-33 – Comparison of a) the Q_m and b) Q_v values for regular PDMS and AC-0.05.

A side-by-side comparison of the Q_m and Q_v values for both data sets revealed a large degree of similarity. As expected, those vapours with a greater relative polarity (ethanol, DMF, propan-1-

ol) proved to be incompatible with PDMS, and those with a lack of polarity (toluene, diethyl ether) or a comparatively small dipole moment (DCM, THF) seemed to be favourable for absorption.[65] It appeared that the PDMS-DASA network also held a high affinity for the less polar and more non-polar solvents; no significant swelling difference was seen between the two architectures. The swelling degrees for volume were largely identical for most solvents, with the exception of diethyl ether and ethyl acetate, and those pertaining to mass showed a slightly larger variation across the range, however that is to be expected when utilising a gravimetric determination of swelling.[65] It was evident that the DASA yielded little significance toward these parameters. After discerning the swelling parameters of the PDMS-DASA composites, the focus shifted to investigating how much, if at all, the presence of solvent would affect the process of photoswitching. Each sample was removed from its respective desiccator after the 72-hour exposure period had ended and immediately subjected to a photoswitching study. This consisted of the same procedure laid out in section 3.3.7, a 30-second time-lapse study, whereby samples would be exposed to visible light for 30-second periods and subsequently scanned with a uv-vis spectrometer. This discussion will detail the analysis of data for elastomers swelled in acetone and DCM vapours, and overall results will be tabulated later. The uv-vis time-lapse for the acetone swelling study is provided as Figure 3-34a, where each spectral line accounts for a 30-second period of visible light exposure. It was immediately apparent that this overlay of spectra was strikingly similar to that of the photoswitching for AC-1 (section 3.8- appendix 3B, Figure 3-48a), suggesting that the swelling of acetone into the network had caused a great decrease in the rate of photoswitching.
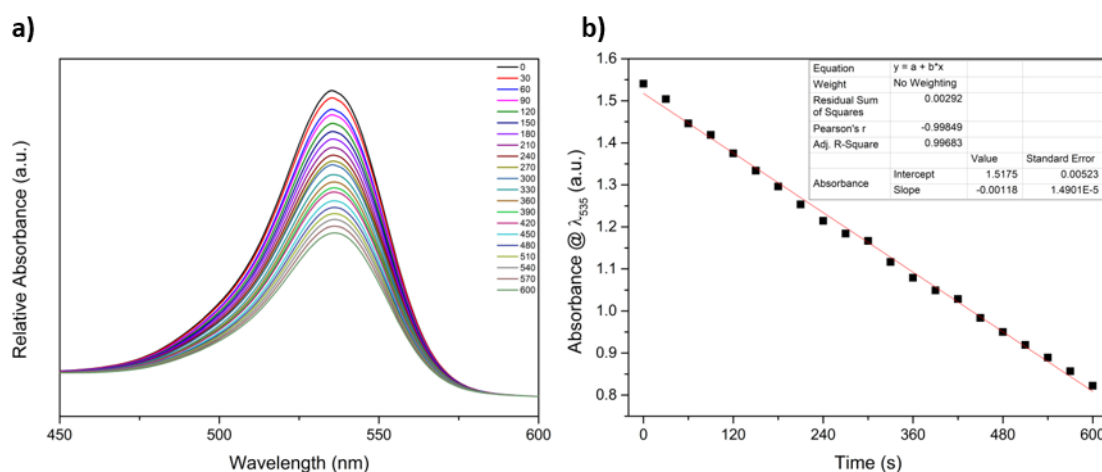
Figure 3-34 – a) UV-vis time-lapse of AC-0.05 swelled by acetone vapours, b) the absorbance values of λ_{max} = 535 nm, during each 30-second period.

Examining the absorbance maxima over time (Figure 3-34b) confirmed the rate loss; vapour swelling had transformed from what was initially seen as an exponential change in absorbance, to a linear function. Similarly to previous analysis of solid uv-vis samples (3.4.6, Figure 3-22), the data acquired in this study experienced baseline drift which was caused by the diffuse transmission of light, owing to the presence of microcrystals in the elastomer, in combination with solvent effects. For the network swelled by acetone vapour, this was easily corrected, enabling accurate comparison of the spectra during each time period. On the other hand, this was not the case for all systems tested, specifically that featuring DCM. Although all won't be shown in detail here, the baseline drift exhibited by the DCM-based study was of the greatest degree, and so it is featured as Figure 3-35a. The uv-vis spectra for all other swollen elastomers can be found in section 3.10 – appendix 3D. Absorbance values at various timestamps (450-600 s) experienced large shifts in magnitude and so provided an unreliable picture of the photoswitching process – observed more clearly in the range of 400 to 450 nm. Therefore, those points were not included in the fitting of data, as shown by Figure 3-35b/c.
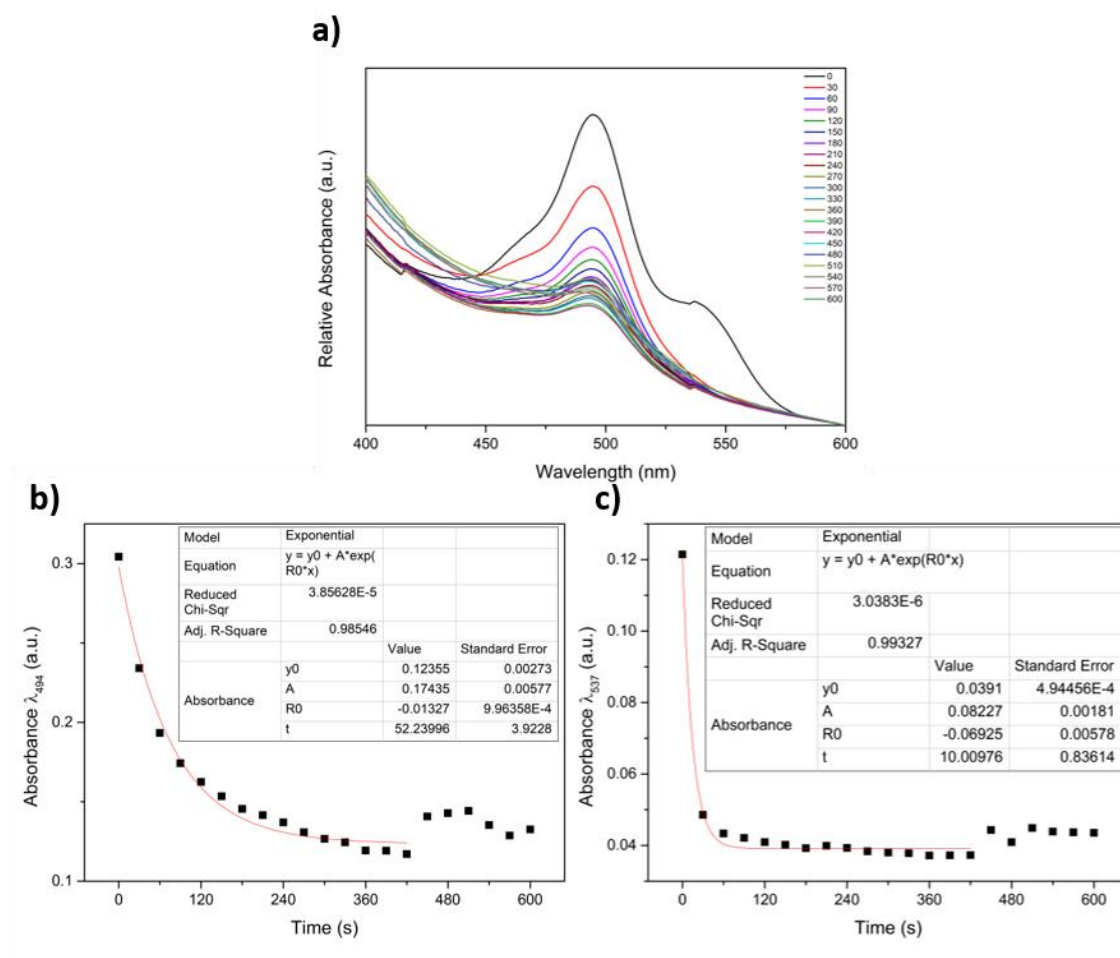
Figure 3-35 - a) UV-vis time-lapse of AC-0.05 swelled by DCM vapours – note the large baseline drift, b) the absorbance values of λ_{max} = 494 nm, during each 30-second period, c) the absorbance values of λ_{max} = 537 nm, during each 30-second period.

It was clear from this data that the DCM-swollen elastomer exhibited photoswitching faster than the analogue that had absorbed acetone, at least initially, as it resembled an exponential decay. In fact, the acetone-swollen elastomer had demonstrated the lowest switching efficiency, shown in Table 3.5. It was expected that each solvent would produce a varying effect on the efficiency of the reaction, as this has been continuously shown in the past.[43,49,84,89] Other than for acetone, each uv-vis profile consisted of two significant peaks situated in the ranges of 494-501 nm and 532-543 nm; designated as "peak 2" and "peak 1", respectively. The intensity ratio between these two signals varies; peak 1 is dominant for diethyl ether, ethyl acetate, propan-1-ol and toluene, and peak 2 is dominant for DMF, ethanol, THF and DCM. The maxima of peak 2 for

diethyl ether was almost indistinguishable from peak 1, therefore an accurate value could not be obtained and has not been reported.

Table 3.5 – Tabulated data for the uv-vis spectroscopy of the swollen AC-0.05 elastomers.

Solvent [a]	Type	Polarity [b] index	Peak 1 (nm) [c]	Abs. @ 600 s (%)	Peak 2 (nm) [d]	Abs. @ 600 s (%)
DMF	Polar aprotic	6.4	535	0	494	33
Acetone	Polar aprotic	5.1	535	51	N/A	N/A
Ethyl acetate	Polar aprotic	4.4	536	2	496	4
Ethanol	Polar protic	4.3	532	0	499	36
THF	Polar aprotic	4	539	4	498	14
Propan-1-ol	Polar protic	4	532	41	495	38
DCM	Polar aprotic	3.1	537	8	494	19 [e]
Diethyl ether	Non-polar	2.8	539	1	N/A	N/A
Toluene	Non-polar	2.4	543	1	501	39
N/A [f]	N/A	N/A	538	4	N/A	N/A

[a] Solvent in which the elastomer was swelled; [b] acquired from literature;[97] [c] signal within 532-543 nm range; [d] signal within 494-501 nm range; [e] absorbance value taken at 420 seconds; the last reliable data point; [f] refers to data obtained for AC-0.05 (section 3.4.6.3, Figure 3-25).

As this study was conducted with swollen samples that were continually losing solvent to the environment, it was decided that leaving the photoswitches to reach a PSS outside of the 600-second period would be unnecessary. There was no guarantee that any solvent would be left trapped within the elastomers by the time a PSS had been reached, given the volatility of said solvents and the constant temperature of 34 °C in the light box. Therefore, in order to visualise the absorbance values as percentages of open-form DASA, the "0%" marker would have to be approximated. To do this, a line of best fit had to be drawn between two points on what was considered the baseline for the overlay spectra of each solvent – examples for acetone and DCM are shown in Figure 3-36. The disadvantage of this approach is such that it assumes the spectra to display linear-shaped baselines, which is not characteristic of the uv-vis data of PDMS-DASA elastomers, so far. Nevertheless, it allowed for a convenient evaluation of the photophysical reaction. With an insight into data treatment provided, the discussion shall now focus on the

nature of the two peaks that have appeared for most systems. After that, the photoswitching kinetics shall be compared against the solution-state and an unswollen elastomer.
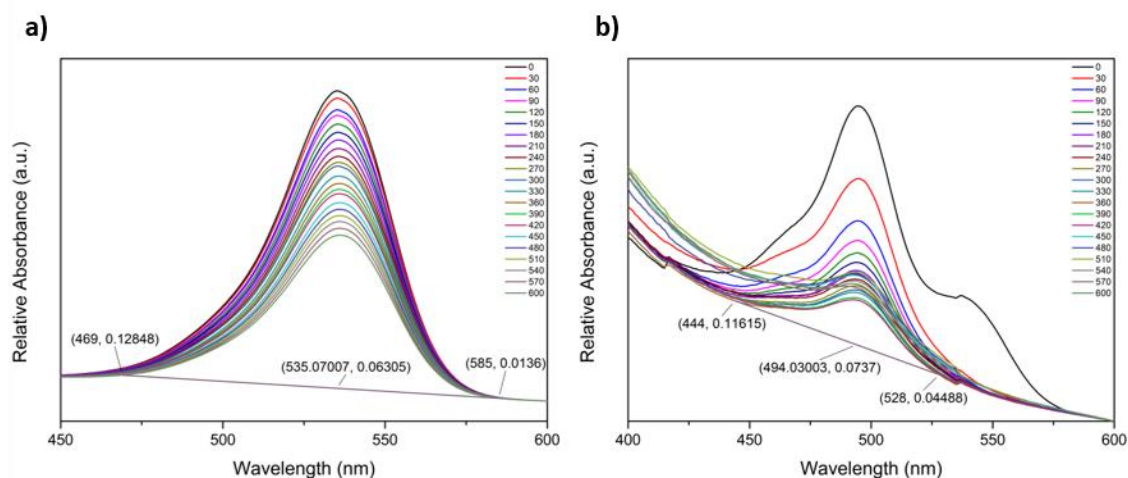
Figure 3-36 – A line of best fit plotted between two points for approximation of a 0% absorbance value, on the uv-vis spectral overlays of a) acetone and b) DCM.

Firstly, it is important to note that the λ_{max} for an unswollen PDMS-DASA sample was observed at 538 nm. Solvent swelling had altered this position and, in most cases, produced a second unknown peak. To identify the origins of both peaks, the first step was to discount this as being a consequence of DASA being divided between suspension inside the network and solvation within the solvent; such that both states would produce discrete bandwidths. Focussing on the peak 1 range; these likely originated from a blue- or red-shift of the original 538 nm signal, produced by solvatochromism. This theory is corroborated when examining the relationship between polarity index and λ_{max} (Table 3.5); an overall trend is seen where λ_{max} within the peak 1 range increases with decreasing solvent polarity, with DCM being the only outlier. It has been previously demonstrated that DASAs exhibit negative solvatochromism – a blue-shift in absorbance with increasing polarity, especially so with polar protic media.[51] Hence, ethanol and propan-1-ol do not fit the established trend. The existence of the 532-543 nm range being consequential of solvent interaction is further supported by values reported in various previously published articles, shown in Table 3.6. Although, the reported values all pertain to

different first-generation DASAs, it is known that dialkylamine-based DASAs vary very little in terms of their absorbance profiles.[33,40] As such, these values are comparative. The reported λ_{max} for THF originates from a barbituric acid derived DASA, it has been previously stated that these switches experience a 25 nm bathochromic shift, relative to Meldrum's acid-based species.[33] Therefore, the assumption has been taken that for a Meldrum's acid-based DASA the wavelength of absorption would have been centred around 537 nm – close to what has been found experimentally, here.

Table 3.6 – Tabulated observed "peak 1" wavelengths and those reported in literature, for each solvent.

Solvent	Polarity index	Observed Peak 1 (nm)	Reported λ_{max} (nm) [a]
DMF	6.4	535	531 [98]
Acetone	5.1	535	530 [84]
Ethyl acetate	4.4	536	N/A [b]
Ethanol	4.3	532	522 [55]
THF	4	539	562 [c 79]
Propan-1-ol	4	532	524 [d 84]
DCM	3.1	537	539 [41]
Diethyl ether	2.8	539	N/A [b]
Toluene	2.4	543	545 [32]
N/A [e]	N/A	538	N/A

[a] **Values reported in various academic reports;** [b] **no available data;** [c] **corresponds to a barbituric acid-based acceptor species;** [d] **propan-2-ol;** [e] **refers to data obtained for AC-0.05 (section 3.4.6.3, Figure 3-25).**

As the values reported in literature are closer to the peak 1 range than they are peak 2, it has been concluded that the former was consequential of solvatochromism. The discussion shall now focus on the origin of the signals designated as "peak 2". Initially, it seemed possible that peak 2 was indicative of the linear DASA species itself and that peak 1 was characteristic of the thermally unstable *Z-E* photoisomerisation product, A' (section 3.4.6.1, **Error! Reference source n ot found.**).[41,42,44–47,99] The A' moiety is characterised by a transient red-shifted absorption band, which persists at lower temperatures, but will disappear under ambient conditions; either by reversion to A or a forward reaction to B, within a short amount of time – i.e. less than 30 seconds. However, it is far more likely that peak 1 was a solvatochromic product, given the

reported absorption maxima of each solvent (Table 3.6). Subsequently, peak 2 was determined to be a blue-shifted signal relative to what was expected from the PDMS-DASA elastomer, and therefore could not be characteristic to A' nor the linear DASA, itself. A phenomenon like this has been reported to affect spiropyran/polymer blends and azobenzene self-assembled monolayers.[100–103] It has been reported that at certain photoswitch concentrations a blue-shifted signal can appear; concomitant with an inhibition of the photoswitching process. This slowing of photoswitching is believed to take place either through excitonic coupling or steric hindrances, during weak aggregation of the photochromes, known as H-aggregation.[104,105] Furthermore, DASA/PS blends drop-cast by Bardeen et al. reportedly experienced a similar effect.[49] They found a blue-shift broadening of spectral signature with increasing DASA concentration, believing it to be a case of H-aggregation. However, they noted that this did not occur in the solution-state or PMMA blends and that the action behind it was unknown. Furthermore, the DASA concentration they required to produce a visual shift of the PS films was on the order of 10^{-2} M, orders of magnitude higher than what has been featured in this chapter. Therefore, it cannot be definitively said whether the blue-shifted signal found here was consequential of DASA H-aggregation or some other unknown effect. What is clear is that solvent-swelling was required, as this was not found to occur within the dry PDMS-DASA elastomers. It is possible that the swelling encouraged partial-diffusion and therefore aggregation of DASA across the network, through intermolecular packing. Although the only evidence to support this supposition is qualitative. Additionally, it is not known why this phenomenon was not present in the spectral profile for acetone (Figure 3-34).

Although a definitive origin of both peaks has not been found, their photoswitching kinetics could still be compared. To provide context on the performance of the swollen elastomers, and even the dry elastomer itself, a solution-state study had to be conducted with HexDASA. Therefore, the DASA was dissolved in two example solvents; DCM and toluene. The concentrations were identical to the effective concentration of DASA in the PDMS-DASA elastomer. The effective concentration of the elastomer was 3.2 x 10^{-4} M; the intended

concentration was 1.6 x 10^{-3} M but the path length was only 0.2 cm. As such, solutions of 3.2 x 10^{-4} M were subjected to white light irradiation for a total of 120 s, each. The resultant spectra are included as Figure 3-37.
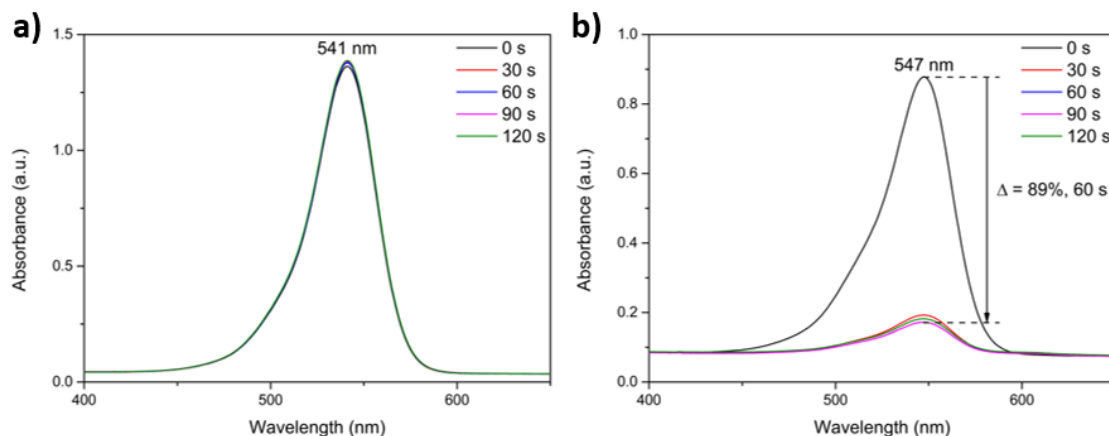

Figure 3-37 – UV-vis spectra over time, during white light irradiation of HexDASA in: a) DCM and b) toluene.

The spectra provided absorption wavelength maxima of 541 and 547 nm, in DCM and toluene, respectively. These wavelength values were very close to that of peak 1 for both specific cases of swelling and a dry elastomer (Table 3.5). This further supported the hypothesis that peak 1 originated from a solvatochromic shift in the original elastomer signal. As has been demonstrated in the past with similar analogues,[40] the bulky HexDASA was unable to switch in DCM and so further comparison with this solvent was abandoned. Toluene however, displayed approximately 89% bleaching upon reaching the PSS, which took 60 seconds. Following the 60-second mark, there were no significant decreases in absorption, hence the study was halted. Naturally, the performance of a dry elastomer, a toluene-swollen elastomer, and the toluene-HexDASA solution then had to be compared. As the solution-state study had reached a PSS within 60 s, this was the point in time at which all three systems were compared. Therefore, the absorbance data for each swollen elastomer, the dry elastomer, and HexDASA in toluene were normalised and converted to percentage bleaching values; displayed as Figure 3-38a/b. Taking an initial focus on peak 1 bleaching, the solution state and AIR-0.05 were practically equal in

performance with 89%, but slightly outperformed by DCM, THF and toluene-swollen systems – reaching 93, 98 and 93%, respectively. This suggested that solvent-swelling was beneficial, in that it appeared to slightly accelerate the photoswitching process. Toluene and THF are known to encourage photoswitching in first-generation DASAs,[32,79] however it was surprising that DCM produced a similar effect given it's inhibiting properties.[40,84]
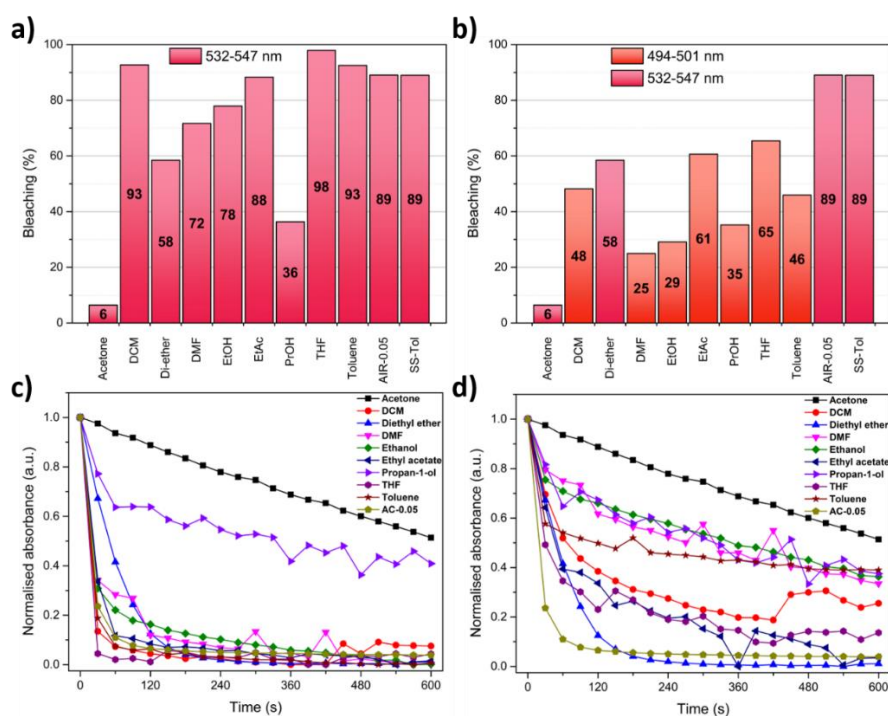

Figure 3-38 – Attained percentage photobleaching after 60 s of a) peak 1 and b) peak 2, for each swollen elastomer, a dry elastomer and the solution state (toluene). Where di-ether = diethyl ether; EtAc = ethyl acetate; PrOH = propan-1-ol. Normalised absorbance for c) peak 1 and d) peak 2, over time.

It is possible that the presence of DCM was not enough to inhibit the switching process, but that raises the question as to why other solvents such as propan-1-ol and acetone had more of a profound effect; especially since they were less-compatible with the PDMS matrix. Switching in acetone and methanol has been reported with other analogues in the past, it is assumed therefore that it can occur in propan-1-ol, too.[84] It was expected that the most polar solvents would inhibit photoisomerisation.[47] However, there did not appear to be a trend between

polarity and switching efficacy; the disparities between toluene (polarity index: 2.4, bleaching: 93%) and diethyl ether (2.8, 58%), and propan-1-ol (4, 36%) and THF (4, 98%), highlighted this. Additionally, there was no clear relationship between the amount of solvent taken in and switching efficacy; poor-swelling solvents like acetone and propan-1-ol led to reduced bleaching, but the same was found with the most compatible solvent, diethyl ether. As such, the relationship that influenced switching efficacy was a not a simple correlation and was most likely a combination of the amount of solvent taken up and the ability for the DASA to switch in said media. Concerning the bleaching of peak 2, it was evident that the average bleaching percentage was far lower for this signal, explainable by potential H-aggregation. Although acetone, AIR-0.05 and solution-state toluene didn't have secondary peaks, and diethyl ether calculable maxima, they were still included for comparison. A slightly clearer trend of polarity inhibiting the switching process was found, however outliers did exist, such as ethyl acetate and THF. The plotting of both absorbance maxima over time, as Figure 3-38c/d, highlights how much slower the switching process was for the 494-501 nm signal range.

To conclude, it is apparent that a gel system composed of DCM, THF or toluene was able to accelerate the photoswitching process somewhat. This acceleration cannot be reduced to a single factor such as polarity as no clear trend exists; it is likely that multiple factors were contributing to this. The other solvents employed in this experiment seemed to provide an inhibiting effect, especially so for the case of acetone. However, there was also the problem of the interference of a second signal that still caused product colouration. The definitive origin of this is unknown, but it is believed to be a consequence of H-aggregation. No matter the cause, it is clear that it severely inhibited the photoswitching process and as such is a major disadvantage. Therefore, at present it has been found that the swelling of a PDMS-DASA elastomer does not improve overall photoswitching kinetics.

3.4.9 Light sensor RFID measurements

This was a preliminary application study concerning the photoresponsivity of PDMS-DASA. It consisted of applying a thin film of the composite to an RFMicron RFM3200-AFR temperature sensing tag and investigating whether a significant difference in sensor value could be caused by switching with visible light. The RFMicron tag used was a passive tag as it didn't require a dedicated power source, it was in fact powered by radio waves that it received. The tag receives and reflects radio waves from and to an RFID reader, attempting to match what is called impedance values. When this impedance value is mismatched, it results in a change in the backscattered power of the tag. A mismatch in impedance can be caused by changes of certain stimuli in the sensing material, such as temperature.[106] In this case, the sensing material was the PDMS-DASA film and the stimuli was to be permittivity. Permittivity is essentially a measure of the polarizability of a material when an electric field is applied, therefore something with a high permittivity value can store more energy from an applied field. It was thought that the polarity changes in a first-generation DASA caused by photoswitching would in turn affect the permittivity of the film, and therefore produce a variation in the analogue response of the tag. The film application procedure was identical to that detailed in Chapter 2 of this work, with the exception of DASA implementation, as opposed to MAF. The solution was dispersed evenly across the tag surface via a doctor blade and an mtv messtechnik film applicator with the height set to apply at 500 μm. Producing a PDMS-DASA covered tag, with a DASA loading of 0.05 wt% (Figure 3-39). The backscatter power of the tag was then read by a Voyantic TagformancePro UHF RFID characterisation apparatus, before and after visible light exposure, three times. The average sensor values have been plotted against frequency, in Figure 3-40.
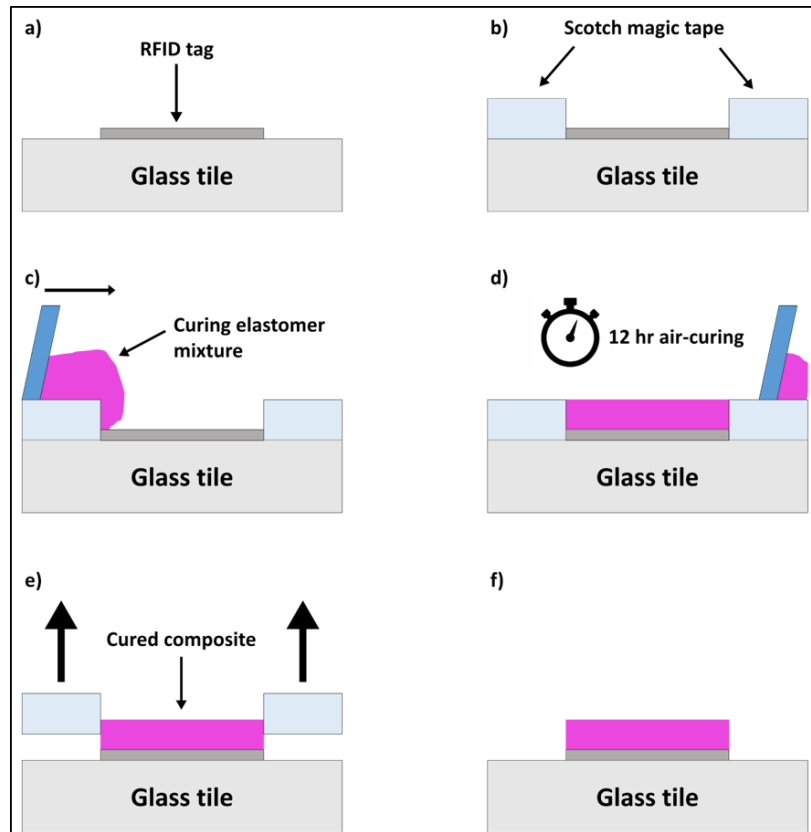
Figure 3-39 – A modified diagrammatic representation of film-casting, using the Scotch tape-well method:[107] a + b) A UHF RFID tag is taped to a glass substrate using Scotch magic tape; c + d) the speed-mixed elastomer mixture is applied using a doctor blade and allowed to air-cure overnight, in a dark environment; e) removal of tape; f) finished product.
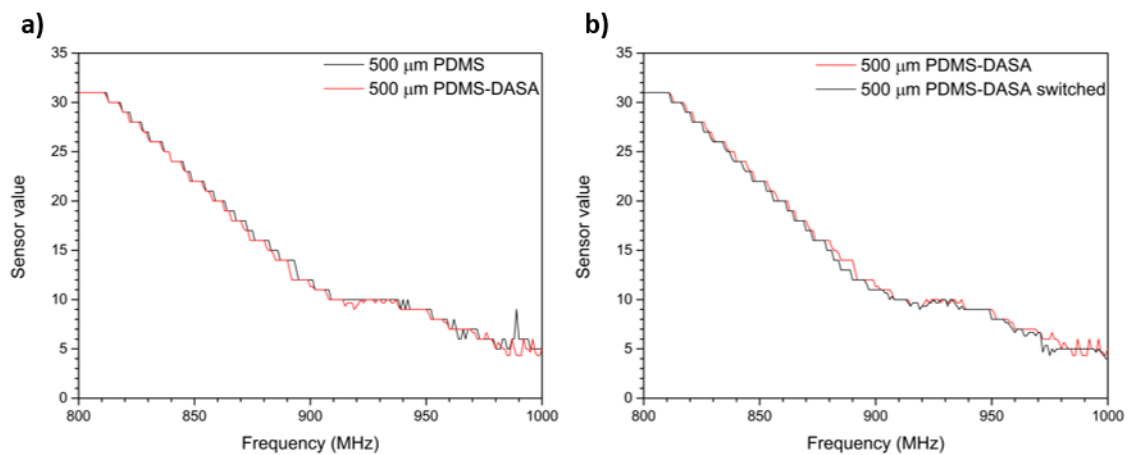

Figure 3-40 – Plots of backscattered power as sensor values, against frequency, for RFMicron tags covered with 500 μm films of: a) PDMS and PDMS-DASA, b) PDMS-DASA open and closed.

Figure 3-40a is a comparison of the sensor values across the 800-1,000 MHz bandwidth, for a PDMS-covered tag and PDMS-DASA covered tag. The black line corresponds to the PDMS-covered tag, and the red to the PDMS-DASA analogue. As can be seen, the values varied very little with no clear significant difference. It was expected that there would be some variation in the signals, as the DASA likely has a different relative permittivity to PDMS. Regardless, the film of the tag was then encouraged to undergo photoswitching, in order to see if the change from the open, non-polar isomer to the closed, zwitterionic form would affect the signal received by the tag. This consisted of placing the tag into the appropriate setup (3.3.7) and leaving it exposed to visible light for 1 hour. The irradiation period appeared to have worked, denoted by a pink to colourless colour change. The result of this colour change is displayed as Figure 3-40b; the tag before irradiation denoted by a red signal, and after, by black. Although a significant difference isn't abundantly clear, when comparing three analysis cycles of the same tag in the same state, it can be seen that standard signal variation is smaller (Figure 3-41). It could be stipulated that there was a small impedance shift but this would require corroboratory evidence. A previously reported investigation has found that a less than 500 µm-thick film was required in order to begin to prevent a well of water from producing an unmatchable impedance.[108] As they had found that above this thickness was the boundary at which the tag signal could no longer be flooded by water, it was then thought that a less than 500 µm-thick layer was required in order to increase sensitivity for this light-sensitive application. With that in mind, 250 µm PDMS-DASA films of the same loading were applied to new tags and these new analogues were treated in an identical manner to the previous, the results of which are included as Figure 3-42. From the variation between signals corresponding to the PDMS and PDMS-DASA films (Figure 3-42a), it was clear that they did not share similar relative permittivity, indicating that a lessening of film thickness had indeed increased the sensitivity of the device, as expected. The data outputs from before and after switching told a similar story (Figure 3-42b) in that the tag then recognised that there had been a change in permittivity. The difference may not seem large, but when

comparing this to the signal output of a 500 μm film there was a clear increase in signal distinction. This is corroborative evidence for what was stipulated earlier regarding Figure 3-40b.
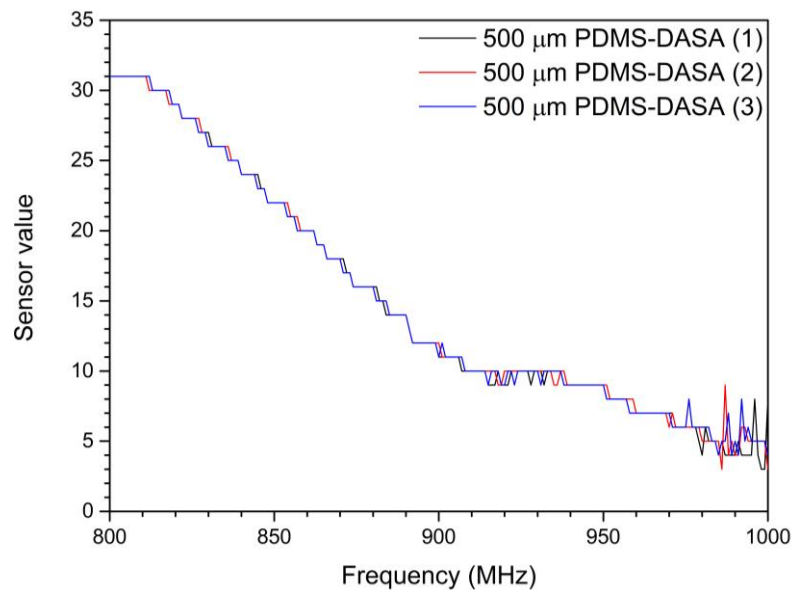

Figure 3-41 – Plots of backscattered power as sensor values, against frequency, for three runs of an RFMicron tag covered with a 500 μm-thick PDMS-DASA film (coloured).
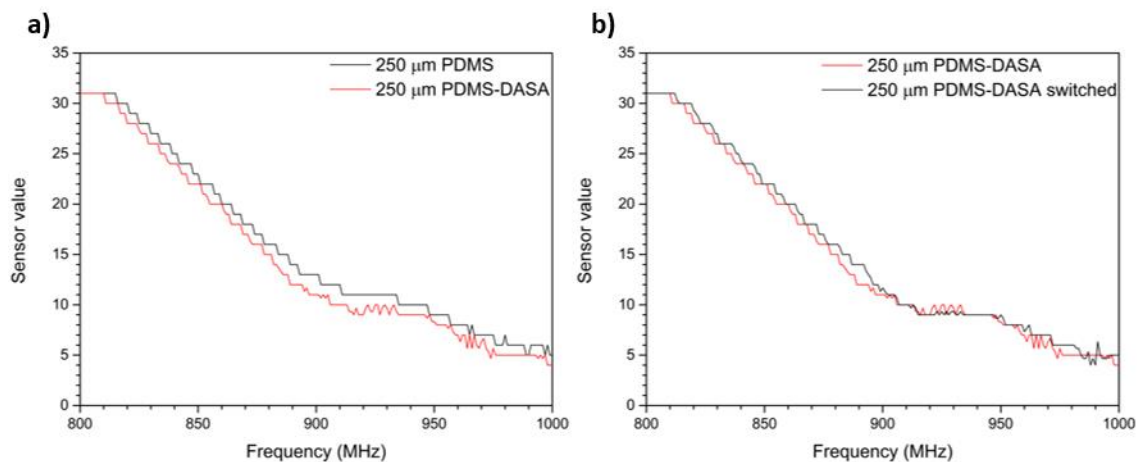

Figure 3-42 - Plots of backscattered power as sensor values, against frequency, for RFMicron tags covered with 250 μm films of: a) PDMS, b) PDMS-DASA.

In conclusion, it has been found that decreasing the thickness of sensing material led to a marginal difference in sensor values. It is now thought that had a higher loading of DASA been implemented, a more distinct relationship would have been seen. Although this appeared to

show that passive UHF RFID can be used to distinguish between the open and closed forms of first-generation DASAs, further studies would need to be conducted before this hypothesis could be definitively confirmed.

3.5 Conclusions and future work

With regards to the SA curing process, in an ideal situation crystallisation that affected AC-1 and AC-5 would be prevented, and in that event increase the efficiency of both moieties. PXRD analysis plotted as Figure 3-19 (section 3.4.4.2.3), revealed that this procedural modification did indeed prevent crystallisation in the 1 wt% samples, and appeared to reduce the degree within those of 5 wt%. The preliminary photoswitching study performed supported this, as it was found that SAC-1 would decolourise with 1 hour of light exposure, something AC-1 could not do (Figure 3-24). Data from uv-vis spectroscopy further corroborated this theory when it was found that SAC-1 displayed a greater photoisomerisation rate, lower half-life and lower minimum attainable absorbance, when compared to data gathered from AC-1 (Figure 3-26, Table 3.3 and Table 3.4).

It was hypothesised that the PDMS-DASA networks with the lowest amount of DASA loading would prove to be more efficient at photoswitching and reverting, i.e. both processes would be quicker with smaller concentrations of DASA.[49] Examination of the absorbance maxima at each time interval for the AC elastomers revealed that as DASA loading increased across samples, the absorbance loss, and the forward reaction rate would both be hindered (section 3.4.6.3, Figure 3-26a/c). The investigation into SA cured samples provided extra proof to support the theory that DASA concentration would affect the efficiency of photoswitching; forward rate would decrease and minimum absorbance increase (Figure 3-26b/d). Furthermore, it was found that overall, the SAC samples exhibited faster photoisomerisation but slower thermal reversion rates when compared to those of the AC method. It is postulated that this was caused by a decrease in the concentration of DASA crystallisation, which subsequently favoured a forward reaction. Exponential regression analysis enabled the determination of the half-lives for both forward and backward reactions for each sample. As expected, the half-lives would increase for both reaction pathways as DASA concentration increased, this effect was seen for the AC elastomers (Table 3.4). Although, SAC networks exhibited thermal reversion rates and half-lives that did not appear

to bear a relationship with concentration. This was thought to be anomalous however, considering the effect that concentration had exhibited with the photoisomerisation reaction. As such, it was thought that these anomalous results were caused by light scattering during sample scans. In relation to this problem, it was made apparent that only a fraction of the linear DASA isomer was present at the beginning of each study, despite dark equilibrium having taken place. This was found through determination of the molar absorptivity coefficients, ε (Table 3.4), where it was seen that they were significantly lower than they should have been.[32,49,89] Unfortunately, the determination of isomer concentrations was not practically investigable during the study, further work would perhaps entail the use of magic angle spinning NMR to elucidate those ratios.[109,110] Overall, it appears that AC composites would be better suited for applications that require reusability, whereas the SAC networks would be more suitable employed for tamper systems which consist of only single usage.

The cycling study experiment aimed to evaluate the fatigue resistance of AC-0.05 (section 3.4.7). It was initially found that a 51.3% overall loss of absorbance would result from 10 cycles of 5 minutes of light exposure and thermal reversion, each (Figure 3-28). The irradiation time for a second sample was then increased to 15 minutes with the expectation that longer exposure would result in a greater loss in recoverable absorbance. However, this led to a similar total absorbance loss of 52.1% within the same number of cycles, indicating up to a three-fold increase in exposure time wouldn't cause photoswitch decomposition (Figure 3-30). Analysis of this data elucidated that a 50% loss in recoverable absorbance had occurred, therefore a decision was taken to enact a further 10 cycles in order to see if this correlation would ensue. It was found that an 81.1% drop in recoverable absorbance was reached within the extra 10 cycles, suggesting more of an asymptotic loss over time (Figure 3-31). As a final investigation, 5 further cycles were conducted whereby the oven reversion interval was increased to 10 minutes in an attempt to see whether the drop in recovery was consequential of photoswitch decomposition or simply a requirement of greater energy (Figure 3-32). Indeed, it was found that the drop in recoverable absorbance was reversible, producing a much higher absorbance value than what

the sample had demonstrated at the beginning of cycling. Although this benefit did not last for long, as it was found that the loss of recoverable absorbance over 5 cycles was approximate to that exhibited by the previous 20. Future studies regarding this topic would encompass the entire concentration range of PDMS-DASAs, rather than just what has been shown here. A framework would be laid out in which samples from each batch would be subjected to reversion at temperatures other than 60 °C, building a profile that enables the identification of the ideal thermal reversion conditions for this architecture.

The solvent swelling experiment was designed to determine whether the swelling of a PDMS-DASA elastomer would accelerate the forward photoswitching process. It was found that swelling in THF, toluene or DCM would have the desired effect; up to a 9% increase in bleaching within 60 s could be attained. On the other hand, examples such as acetone or propan-1-ol would severely hinder the process (Table 3.5 and Figure 3-38). The absorption profiles consisted of two peaks; that characteristic to the PDMS-DASA elastomer (peak 1) and a second peak of indefinite origin (peak 2). Peak 1 was situated between 532 and 543 nm, produced by a solvatochromic shift of the PDMS-DASA absorbance. Peak 2 is believed to be a consequence of H-aggregation between DASA molecules, made possible by diffusion through swelling. There is no definitive proof for this hypothesis and acquisition of such is beyond the scope of this thesis. Future work could encompass the swelling of PDMS-DASA elastomers of greater concentrations, too. It has been previously reported that an increase in photoswitch concentration, at least with spiropyrans, can lead to larger spectral blue-shifting during H-aggregation.[100] This method could perhaps provide further qualitative confirmation of H-aggregation appearing in the DASA/polymer blends studied here.

As a preliminary applicational study, a PDMS-DASA film (0.05 wt%) was applied to the antenna side of an RFMicron RFM3200-AFR temperature sensing tag. The desired outcome was to see a change in sensor value, which corresponded to the photoisomerisation of the DASA species. Initially, no difference was found between the open and closed states, in a 500 µm film (Figure

3-40). A previous investigation of film thickness profiles showed that a 500 μm film was required in order to measure the impedance caused by a well of water on its surface; films of lower thickness could not match the impedance brought by the solution. As such, it was then decided to produce a film of half the previous thickness – 250 μm. This effort appeared successful as clear difference could then be seen between a regular PDMS film and the open form PDMS-DASA film (Figure 3-42). This further translated into an appreciable change in sensor value after photoisomerisation (Figure 3-42b). Providing promise for the incorporation of PDMS-DASA films in light and heat sensing applications. Future work regarding RFID studies would employ the use of larger DASA concentrations, in an attempt to boost the difference in sensor value that can be seen upon photoswitching. Of course, a film has a far larger surface area for solvent evaporation when compared with the traditional PDMS-DASA pads, likely meaning that crystallisation would quantitatively appear in lower concentrations of DASA. This could likely be prevented by employing DASAs with different amine donors, such as N-methoxyaniline. As it has been found before that bulkier side groups can prevent the crystallisation of azobenzenes, it is believed that the same rule may be applied here.[90] Naturally, the selection of this aniline derivative would mean incorporation of a second generation DASA and these species are known to exist as a more even ratio of linear to closed isomers.[35] Therefore, it may be more prudent to change the acceptor unit to pyrazolone, as third generation DASAs exist near-quantitatively in the linear form.[49]

3.6 References

1   M. Irie, *Chem. Rev.*, 2000, **100**, 1685–1716.

2   H. Tian and S. Yang, *Chem. Soc. Rev.*, 2004, **33**, 85–97.

3   A. Natansohn and P. Rochon, *Chem. Rev.*, 2002, **102**, 4139–4175.

4   G. Berkovic, V. Krongauz and V. Weiss, *Chem. Rev.*, 2000, **100**, 1741–1753.

5   W. A. Velema, W. Szymanski and B. L. Feringa, *J. Am. Chem. Soc.*, 2014, **136**, 2178–2191.

6   V. I. Minkin, *Molecular Switches*, Wiley-VCH, Weinheim, Second Edition, 2011.

7   C. Brieke, F. Rohrbach, A. Gottschalk, G. Mayer and A. Heckel, *Angew. Chemie - Int. Ed.*, 2012, **51**, 8446–8476.

8   N. Ankenbruck, T. Courtney, Y. Naro and A. Deiters, *Angew Chem Int Ed Engl*, 2018, **57**, 2768–2798.

9   J. Andréasson and U. Pischel, *Chem. Soc. Rev.*, 2015, 44, 1053–1069.

10   X. Xie, G. Mistlberger and E. Bakker, *J. Am. Chem. Soc.*, 2012, **134**, 16929–16932.

11   M. Qin, Y. Huang, F. Li and Y. Song, *J. Mater. Chem. C*, 2015, **3**, 9265–9275.

12   A. Abdollahi, Z. Alinejad and A. R. Mahdavian, *J. Mater. Chem. C*, 2017, **5**, 6588–6600.

13   T. Fukaminato, T. Doi, N. Tamaoki, K. Okuno, Y. Ishibashi, H. Miyasaka and M. Irie, *J. Am. Chem. Soc.*, 2011, **133**, 4984–4990.

14   B. L. Feringa, W. F. Jager and B. de Lange, *Tetrahedron*, 1993, **49**, 8267–8310.

15   D. Majumdar, H. M. Lee, J. Kim, K. S. Kim and B. J. Mhin, *J. Chem. Phys.*, 1999, **111**, 5866–5872.

16   J. Broichhagen, J. A. Frank and D. Trauner, *Acc. Chem. Res.*, 2015, **48**, 1947–1960.

17   G. Petriashvili, L. Devadze, T. Zurabishvili, N. Sepashvili and K. Chubinidze, *Biomed. Opt.*

Express, 2016, **7**, 442.

18   Y. He, Y. Yamamoto, W. Jin, T. Fukushima, A. Saeki, S. Seki, N. Lshii and T. Aida, *Adv. Mater.*, 2010, **22**, 829–832.

19   C. Qin, Y. Feng, W. Luo, C. Cao, W. Hu and W. Feng, *J. Mater. Chem. A*, 2015, **3**, 16453–16460.

20   Y. He, Y. Zhu, Z. Chen, W. He and X. Wang, *Chem. Commun.*, 2013, **49**, 5556–5558.

21   J. Wang, B. Wu, S. Li, G. Sinawang, X. Wang and Y. He, *ACS Sustain. Chem. Eng.*, 2016, **4**, 4036–4042.

22   P. Avci, A. Gupta, M. Sadasivam, D. Vecchio, Z. Pam, N. Pam, M. R. Hamblin and S. Cutan Med Surg Author manuscript, *Low-level laser (light) therapy (LLLT) in skin: stimulating, healing, restoring*, 2013, vol. 32.

23   M. Dong, A. Babalhavaeji, M. J. Hansen, L. Kálmán and G. A. Woolley, *Chem. Commun.*, 2015, **51**, 12981–12984.

24   J. Broichhagen, J. A. Frank, N. R. Johnston, R. K. Mitchell, K. Šmid, P. Marchetti, M. Bugliani, G. A. Rutter, D. Trauner and D. J. Hodson, *Chem. Commun.*, 2015, **51**, 6018–6021.

25   J. Olejniczak, C. J. Carling and A. Almutairi, *J. Control. Release*, 2015, **219**, 18–30.

26   M. Dong, A. Babalhavaeji, S. Samanta, A. A. Beharry and G. A. Woolley, *Acc. Chem. Res.*, 2015, **48**, 2662–2670.

27   A. A. Beharry, O. Sadovski and G. A. Woolley, *J. Am. Chem. Soc.*, 2011, **133**, 19684–19687.

28   T. Fukaminato, T. Hirose, T. Doi, M. Hazama, K. Matsuda and M. Irie, *J. Am. Chem. Soc.*, 2014, **136**, 17145–17154.

29   A. Cnossen, L. Hou, M. M. Pollard, P. V Wesenhagen, W. R. Browne and B. L. Feringa, *J.*

Am. Chem. Soc., 2012, **134**, 17613–17619.

30   F. Cheng, R. Yin, Y. Zhang, C. C. Yen and Y. Yu, *Soft Matter*, 2010, **6**, 3447–3449.

31   D. Bléger and S. Hecht, *Angew. Chemie - Int. Ed.*, 2015, **54**, 11338–11349.

32   S. Helmy, F. A. Leibfarth, S. Oh, J. E. Poelma, C. J. Hawker and J. R. De Alaniz, *J. Am. Chem. Soc.*, 2014, **136**, 8169–8172.

33   S. Helmy, S. Oh, F. A. Leibfarth, C. J. Hawker and J. Read De Alaniz, *J. Org. Chem.*, 2014, **79**, 11316–11329.

34   J. R. Hemmer, S. O. Poelma, N. Treat, Z. A. Page, N. D. Dolinski, Y. J. Diaz, W. Tomlinson, K. D. Clark, J. P. Hooper, C. Hawker and J. Read De Alaniz, *J. Am. Chem. Soc.*, 2016, **138**, 13960–13966.

35   J. R. Hemmer, Z. A. Page, K. D. Clark, F. Stricker, N. D. Dolinski, C. J. Hawker and J. Read De Alaniz, *J. Am. Chem. Soc*, 2018, **140**, 18.

36   R. Klajn, *Chem. Soc. Rev.*, 2014, **43**, 148–184.

37   M. Irie, T. Fukaminato, K. Matsuda and S. Kobatake, *Chem. Rev.*, 2014, **114**, 12174–12277.

38   X. Li, J. Li, Y. Wang, T. Matsuura and J. Meng, *J. Photochem. Photobiol. A Chem.*, 2004, **161**, 201–213.

39   C. Petermayer, S. Thumser, F. Kink, P. Mayer and H. Dube, *J. Am. Chem. Soc.*, 2017, **139**, 15060–15067.

40   N. Mallo, E. D. Foley, H. Iranmanesh, A. D. W. Kennedy, E. T. Luis, J. Ho, J. B. Harper and J. E. Beves, *Chem. Sci.*, 2018, **9**, 8242–8252.

41   M. M. Lerch, S. J. Wezenberg, W. Szymanski and B. L. Feringa, *J. Am. Chem. Soc.*, 2016, **138**, 6344–6347.

42   A. D. Laurent, M. Medve and D. Jacquemin, *ChemPhysChem*, 2016, **17**, 1846–1851.

43   C. García-Iriepa, M. Marazzi and D. Sampedro, *ChemPhotoChem*, 2019, **3**, 866–873.

44   A. Belhboub, F. Boucher and D. Jacquemin, *J. Mater. Chem. C*, 2017, **5**, 1624–1631.

45   J. N. Bull, E. Carrascosa, N. Mallo, M. S. Scholz, G. Da Silva, J. E. Beves and E. J. Bieske, *J. Phys. Chem. Lett.*, 2018, **9**, 665–671.

46   M. Di Donato, M. M. Lerch, A. Lapini, A. D. Laurent, A. Iagatti, L. Bussotti, S. P. Ihrig, M. Medved, D. Jacquemin, W. Szymański, W. J. Buma, P. Foggi and B. L. Feringa, *J. Am. Chem. Soc.*, 2017, **139**, 15596–15599.

47   H. Zulfikri, M. A. J. Koenis, M. M. Lerch, M. Di Donato, W. Szymański, C. Filippi, B. L. Feringa and W. J. Buma, *J. Am. Chem. Soc.*, 2019, **141**, 7376–7384.

48   M. M. Lerch, M. Medved, A. Lapini, A. D. Laurent, A. Iagatti, L. Bussotti, W. Szymański, W. J. Buma, P. Foggi, M. Di Donato and B. L. Feringa, *J. Phys. Chem. A*, 2018, **122**, 955–964.

49   B. F. Lui, N. T. Tierce, F. Tong, M. M. Sroda, H. Lu, J. Read De Alaniz and C. J. Bardeen, *Photochem. Photobiol. Sci.*, 2019, **18**, 1587–1595.

50   S. H. Mostafavi, W. Li, K. D. Clark, F. Stricker, J. R. De Alaniz and C. J. Bardeen, *Macromolecules*, 2019, **52**, 6311–6317.

51   M. M. Lerch, W. Szymański and B. L. Feringa, *Chem. Soc. Rev.*, 2018, **47**, 1910–1937.

52   A. Balamurugan and H. Il Lee, *Macromolecules*, 2016, **49**, 2568–2574.

53   Y. J. Diaz, Z. A. Page, A. S. Knight, N. J. Treat, J. R. Hemmer, C. J. Hawker and J. Read de Alaniz, *Chem. - A Eur. J.*, 2017, **23**, 3562–3566.

54   B. P. Mason, M. Whittaker, J. Hemmer, S. Arora, A. Harper, S. Alnemrat, A. McEachen, S. Helmy, J. Read de Alaniz and J. P. Hooper, *Appl. Phys. Lett.*, 2016, **108**, 041906-1–4.

55   D. Zhong, Z. Cao, B. Wu, Q. Zhang and G. Wang, *Sensors Actuators, B Chem.*, 2018, **254**,

385–392.

56   Q. Chen, Y. J. Diaz, M. C. Hawker, M. R. Martinez, Z. A. Page, S. Xiao-An Zhang, C. J. Hawker and J. Read De Alaniz, *Macromolecules*, 2019, **52**, 4370–4375.

57   S. O. Poelma, S. S. Oh, S. Helmy, A. S. Knight, G. L. Burnett, H. T. Soh, C. J. Hawker and J. Read De Alaniz, *Chem. Commun.*, 2016, **52**, 10525–10528.

58   T. Senthilkumar, L. Zhou, Q. Gu, L. Liu, F. Lv and S. Wang, *Angew. Chemie - Int. Ed.*, 2018, **57**, 13114–13119.

59   S. Singh, K. Friedel, M. Himmerlich, Y. Lei, G. Schlingloff and A. Schober, *ACS Macro Lett.*, 2015, **4**, 1273–1277.

60   N. D. Dolinski, Z. A. Page, F. Eisenreich, J. Niu, S. Hecht, J. Read de Alaniz and C. J. Hawker, *ChemPhotoChem*, 2017, **1**, 125–131.

61   S. Jia, J. D. Du, A. Hawley, W. K. Fong, B. Graham and B. J. Boyd, *Langmuir*, 2017, **33**, 2215–2221.

62   F. Y. Tang, J. N. Hou, K. X. Liang, Y. N. Y. Liu, L. Deng and Y. N. Y. Liu, *New J. Chem.*, 2017, **41**, 6071–6075.

63   H. Zhao, X. Qin, L. Zhao, S. Dong, L. Gu, W. Sun, D. Wang and Y. Zheng, *ACS Appl. Mater. Interfaces*, 2020, **12**, 8960.

64   O. Rifaie-Graham, S. Ulrich, N. F. B. Galensowske, S. Balog, M. Chami, D. Rentsch, J. R. Hemmer, J. Read De Alaniz, L. F. Boesel and N. Bruns, *J. Am. Chem. Soc.*, 2018, **140**, 8027–8036.

65   J. N. Lee, C. Park and G. M. Whitesides, *Anal. Chem.*, 2003, **75**, 6544–6554.

66   J. C. Lötters, W. Olthuis, P. H. Veltink and P. Bergveld, *J. Micromechanics Microengineering*, 1997, **7**, 145–147.

67   C. Zhong, A. Kapetanovic, Y. Deng and M. Rolandi, *Adv. Mater.*, 2011, **23**, 4776–4781.

68   X. Duan, Y. Zhao, A. Perl, E. Berenschot, D. N. Reinhoudt and J. Huskens, *Adv. Funct. Mater.*, 2010, **20**, 663–668.

69   W. Chen, R. H. W. Lam and J. Fu, *Lab Chip*, 2012, **12**, 391–395.

70   K. A. Heyries, C. A. Marquette and L. J. Blum, *Langmuir*, 2007, **23**, 4523–4527.

71   I. Yoo, S. Song, B. Yoon and J. M. Kim, *Macromol. Rapid Commun.*, 2012, **33**, 1256–1261.

72   K. W. Oh, K. Lee, B. Ahn and E. P. Furlani, *Lab Chip*, 2012, **12**, 515–545.

73   H. Wu, T. W. Odom, D. T. Chiu and G. M. Whitesides, *J. Am. Chem. Soc.*, 2003, **125**, 554–559.

74   G. M. Whitesides, *Nature*, 2006, **442**, 368–373.

75   Z. Zhao and J. Tian, *J. Appl. Polym. Sci.*, 2017, **134**, 1–9.

76   M. E. Genovese, A. Athanassiou and D. Fragouli, *J. Mater. Chem. A*, 2015, **3**, 22441–22447.

77   P. Tannouri, K. M. Arafeh, J. M. Krahn, S. L. Beaupré, C. Menon and N. R. Branda, *Chem. Mater.*, 2014, **26**, 4330–4333.

78   Y. S. Nam, I. Yoo, O. Yarimaga, I. S. Park, D. H. Park, S. Song, J. M. Kim and C. W. Lee, *Chem. Commun.*, 2014, **50**, 4251–4254.

79   M. Nau, D. Seelinger and M. Biesalski, *Adv. Mater. Interfaces*, 2019, **6**, 1–5.

80   C. V Rumens, M. A. Ziai, K. E. Belsey, J. C. Batchelor and S. J. Holder, *J. Mater. Chem. C*, 2015, **3**, 10091–10098.

81   F. Bigi, S. Carloni, L. Ferrari, R. Maggi, A. Mazzacani and G. Sartori, *Tetrahedron Lett.*, 2001, **42**, 5203–5205.

82   J. D. Cauwood and W. E. S. Turner, *J. Chem. Soc. Trans.*, 1915, **107**, 276–282.

83   P. Du, X. Lin and X. Zhang, in *2011 16th International Solid-State Sensors, Actuators and Microsystems Conference*, IEEE, 2011, pp. 645–648.

84   M. M. Lerch, M. Di Donato, A. D. Laurent, M. Medved, A. Iagatti, L. Bussotti, A. Lapini, W. J. Buma, P. Foggi, W. Szymański and B. L. Feringa, *Angew. Chemie Int. Ed.*, 2018, **58**, 8063–8068.

85   S. Ulrich, J. R. Hemmer, Z. A. Page, N. D. Dolinski, O. Rifaie-Graham, N. Bruns, C. J. Hawker, L. F. Boesel and J. Read De Alaniz, *ACS Macro Lett.*, 2017, **6**, 738–742.

86   M. Ashby, *Materials Selection in Mechanical Design*, Elsevier, Burlington, Third Ed., 2005.

87   H. Tian and J. Zhang, *Photochromic Materials*, Wiley-VCH, Weinheim, 2016.

88   R. Chang, in *Physical Chemistry for the Chemical and Biological Sciences*, eds. J. Kromm and A. McGuire, University Sciences Books, Sausalito, Third edit., 2000, pp. 446–458.

89   N. Mallo, P. T. Brown, H. Iranmanesh, T. S. C. MacDonald, M. J. Teusner, J. B. Harper, G. E. Ball and J. E. Beves, *Chem. Commun.*, 2016, **52**, 13576–13579.

90   C. Pakula, C. Hanisch, V. Zaporojtchenko, T. Strunskus, C. Bornholdt, D. Zargarani, R. Herges and F. Faupel, *J. Mater. Sci.*, 2011, **46**, 2488–2494.

91   G. Sinawang, B. Wu, J. Wang, S. Li and Y. He, *Macromol. Chem. Phys.*, 2016, **217**, 2409–2414.

92   B. Wu, T. Xue, W. Wang, S. Li, J. Shen and Y. He, *J. Mater. Chem. C*, 2018, **6**, 8538–8545.

93   J. E. Yap, N. Mallo, D. S. Thomas, J. E. Beves and M. H. Stenzel, *Polym. Chem.*, 2019, **10**, 6515–6522.

94   S. Yang, J. Liu, Z. Cao, M. Li, Q. Luo and D. Qu, *Dye. Pigment.*, 2018, **148**, 341–347.

95   Y. De Cai, T. Y. Chen, X. Q. Chen and X. Bao, *Org. Lett.,* 2019, **21**, 7445–7449.

96   S. Singh, P. Mai, J. Borowiec, Y. Zhang, Y. Lei and A. Schober, *R. Soc. Open Sci.*, 2018, **5**, 1–7.

97   L. R. Snyder, *J. Chromatogr. Sci.*, 1978, **16**, 223–234.

98   J. Ahrens, T. Bian, T. Vexler and R. Klajn, *ChemPhotoChem*, 2017, **1**, 230–236.

99   C. García-Iriepa and M. Marazzi, *Materials (Basel).*, 2017, **10**, 1025.

100   H. Eckhardt, A. Bose and V. A. Krongauz, *Polymer (Guildf).*, 1987, **28**, 1959–1964.

101   C. Gahl, R. Schmidt, D. Brete, E. R. McNellis, W. Freyer, R. Carley, K. Reuter and M. Weinelt, *J. Am. Chem. Soc.*, 2010, **132**, 1831–1838.

102   M. Utecht, T. Klamroth and P. Saalfrank, *Phys. Chem. Chem. Phys.*, 2011, **13**, 21608–21614.

103   C. Cocchi, T. Moldt, C. Gahl, M. Weinelt and C. Draxl, *J. Chem. Phys.*, 2016, **145**, 1-11

104   E. Titov and P. Saalfrank, *J. Phys. Chem. A*, 2016, **120**, 3055–3070.

105   F. C. Spano, *Acc. Chem. Res.*, 2010, **43**, 429–439.

106   J. Virtanen, L. Ukkonen, T. Björninen, L. Sydaňheimo and A. Z. Elsherbeni, *SAS 2011 - IEEE Sensors Appl. Symp. Proc.*, 2011, 312–317.

107   C. Liewhiran and S. Phanichphant, *Sensors*, 2007, **7**, 650–675.

108   A. J. R. Hillier, V. Makarovaite, C. W. Gourlay, S. J. Holder and J. C. Batchelor, *IEEE Sens. J.*, 2019, **19**, 5389–5395.

109   T. M. Forrest, G. E. Wilson, Y. Pan and J. Schaefer, *J. Biol. Chem.*, 1991, **266**, 24485–24491.

110   S. Van Vlierberghe, B. Fritzinger, J. C. Martins and P. Dubruel, *Appl. Spectrosc.*, 2010, **64**, 1176–1180.

3.7 Appendix 3A
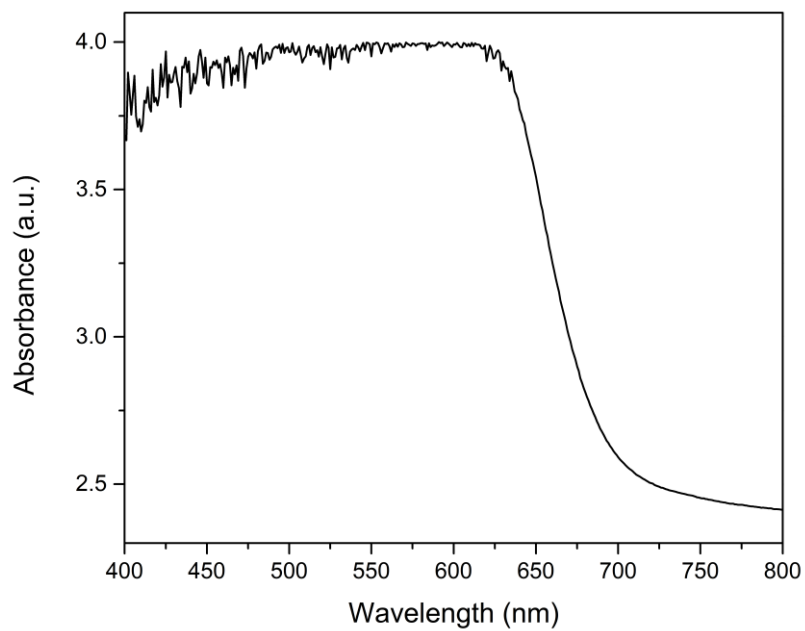
Figure 3-43 - UV-vis plot of AC-5 after 2 hours of light irradiation.
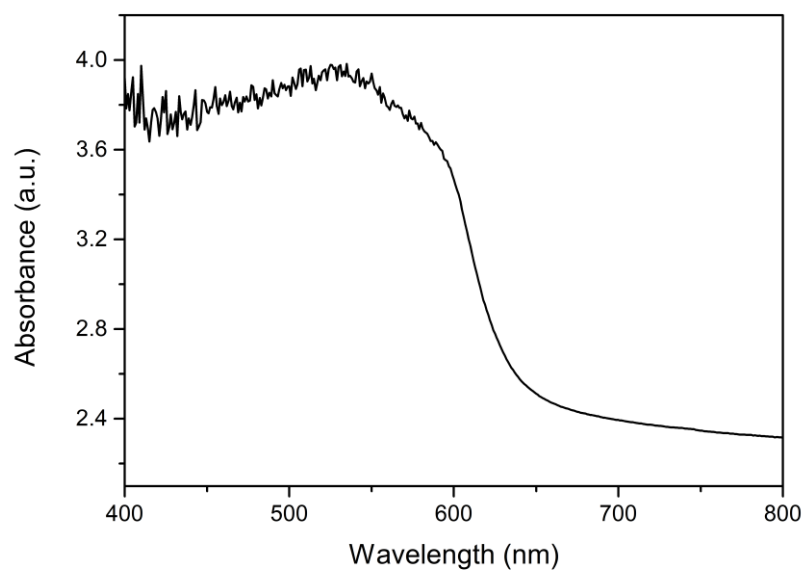
Figure 3-44 - UV-vis plot of SAC-5 after 2 hours of light irradiation.

3.8 Appendix 3B
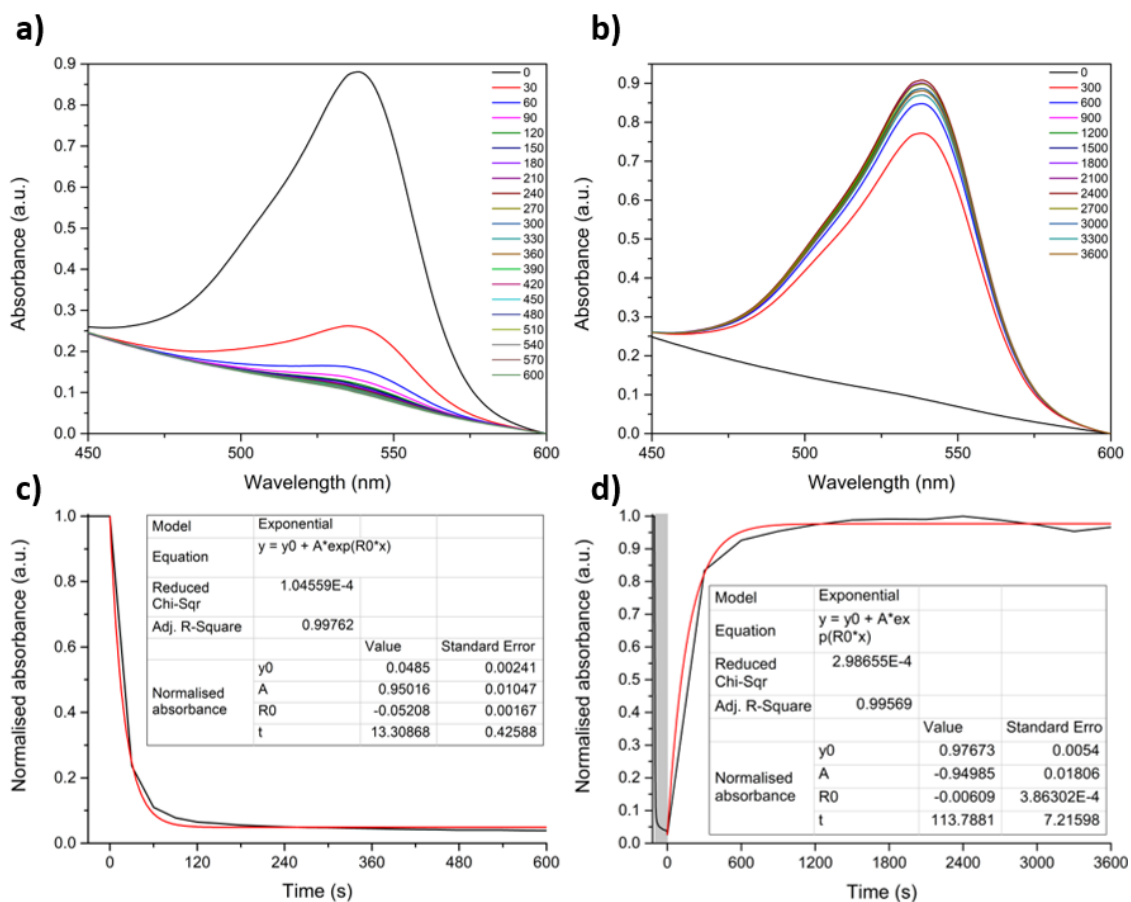
Figure 3-45 - UV-vis data acquired for AC-0.05, consisting of a) a time lapse of the forward photoswitching reaction, b) the thermal reversion, and c+d) the change in λ_{max} over time, for the forward and backward reactions, respectively.
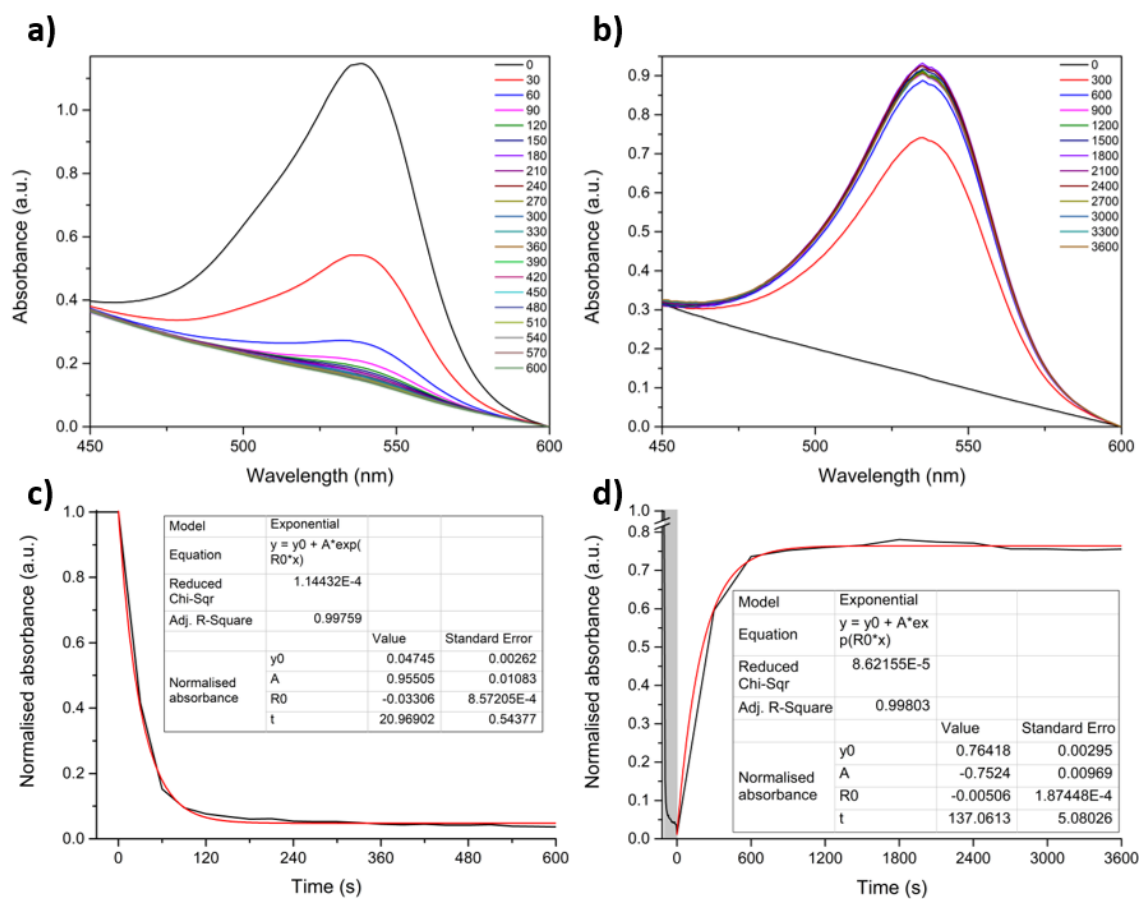
Figure 3-46 - UV-vis data acquired for AC-0.1, consisting of a) a time lapse of the forward photoswitching reaction, b) the thermal reversion, and c+d) the change in λ_{max} over time, for the forward and backward reactions, respectively.
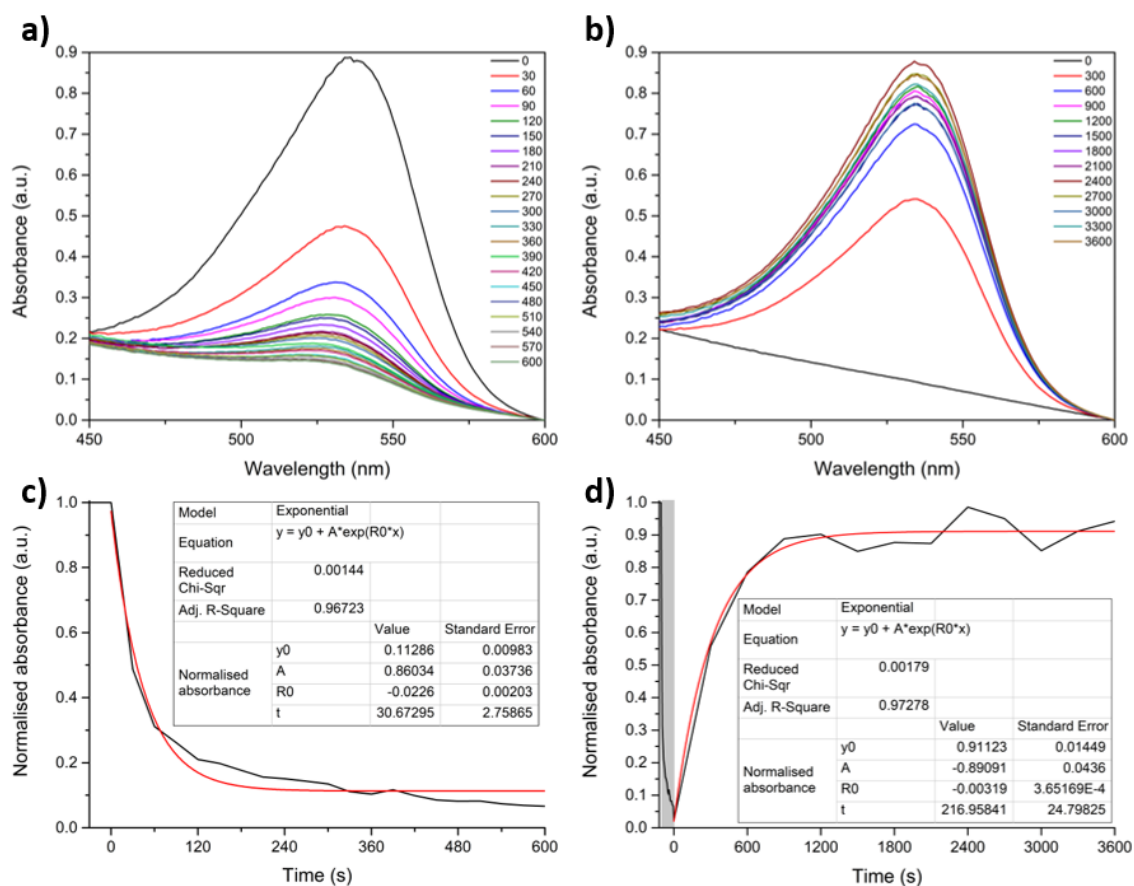
Figure 3-47 - UV-vis data acquired for AC-0.5, consisting of a) a time lapse of the forward photoswitching reaction, b) the thermal reversion, and c+d) the change in λ_{max} over time, for the forward and backward reactions, respectively.
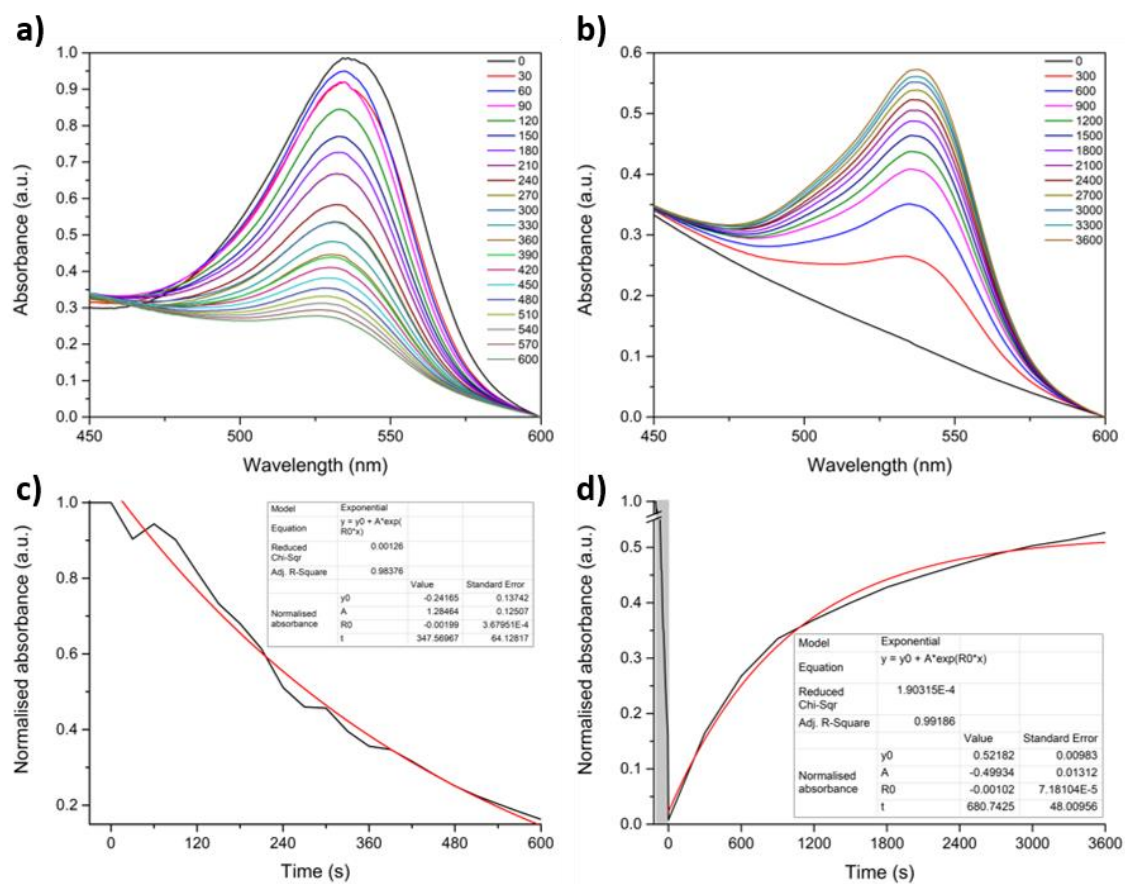
Figure 3-48 - UV-vis data acquired for AC-1, consisting of a) a time lapse of the forward photoswitching reaction, b) the thermal reversion, and c+d) the change in λ_{max} over time, for the forward and backward reactions, respectively.

3.9 Appendix 3C
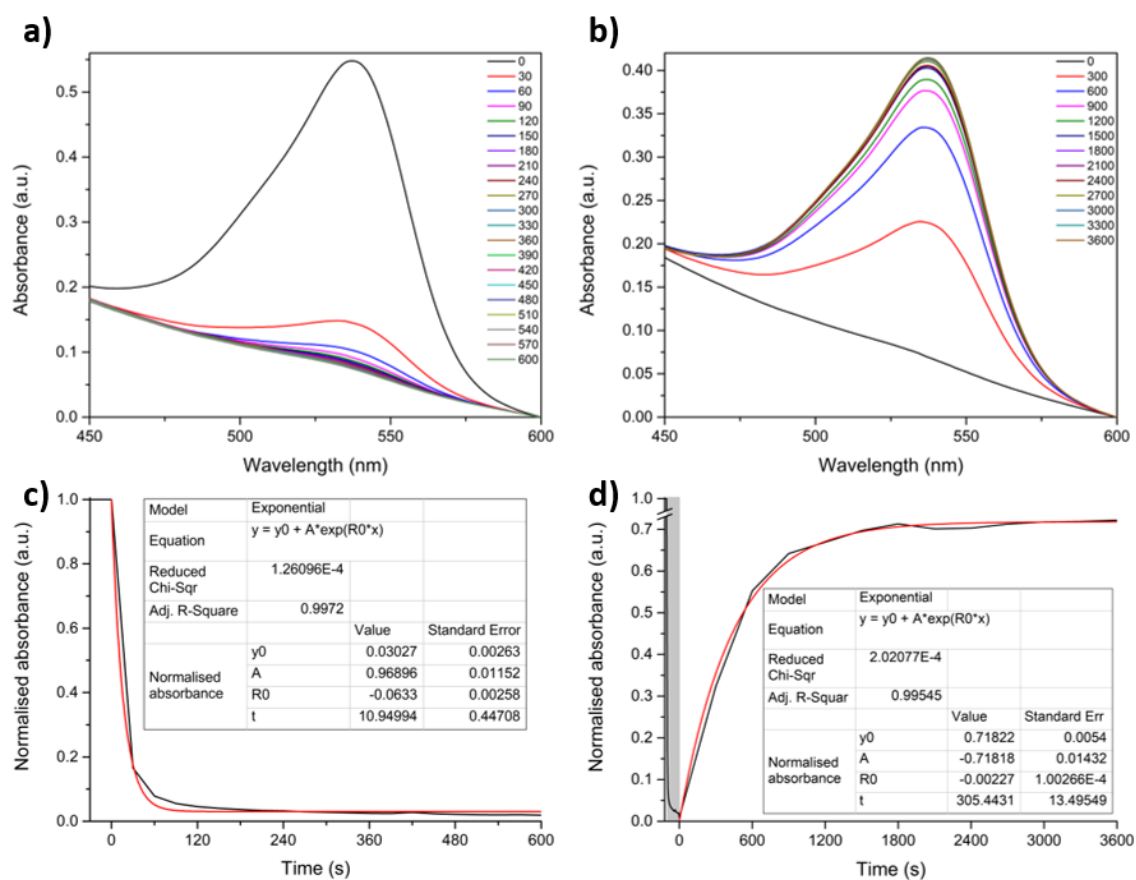
Figure 3-49 - UV-vis data acquired for SAC-0.05, consisting of a) a time lapse of the forward photoswitching reaction, b) the thermal reversion, and c+d) the change in λ_{max} over time, for the forward and backward reactions, respectively.
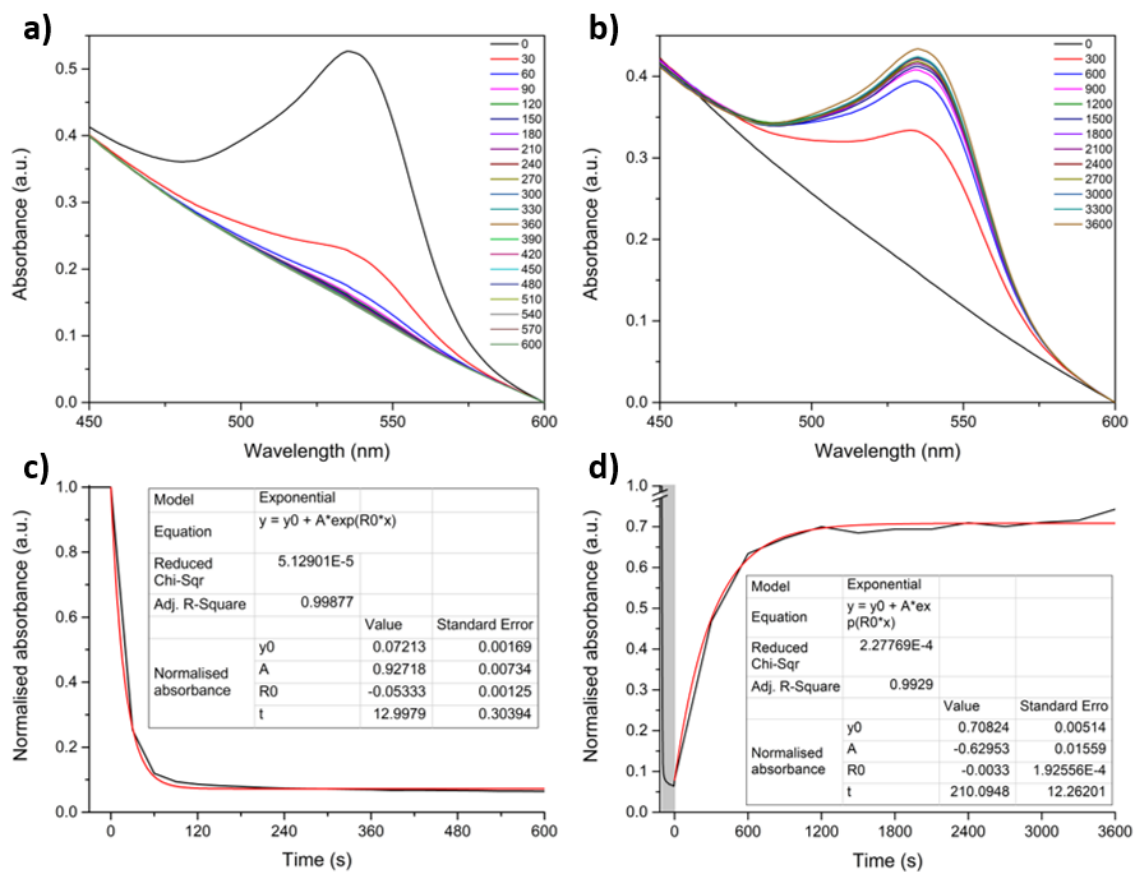
Figure 3-50 - UV-vis data acquired for SAC-0.1, consisting of a) a time lapse of the forward photoswitching reaction, b) the thermal reversion, and c+d) the change in λ_{max} over time, for the forward and backward reactions, respectively.
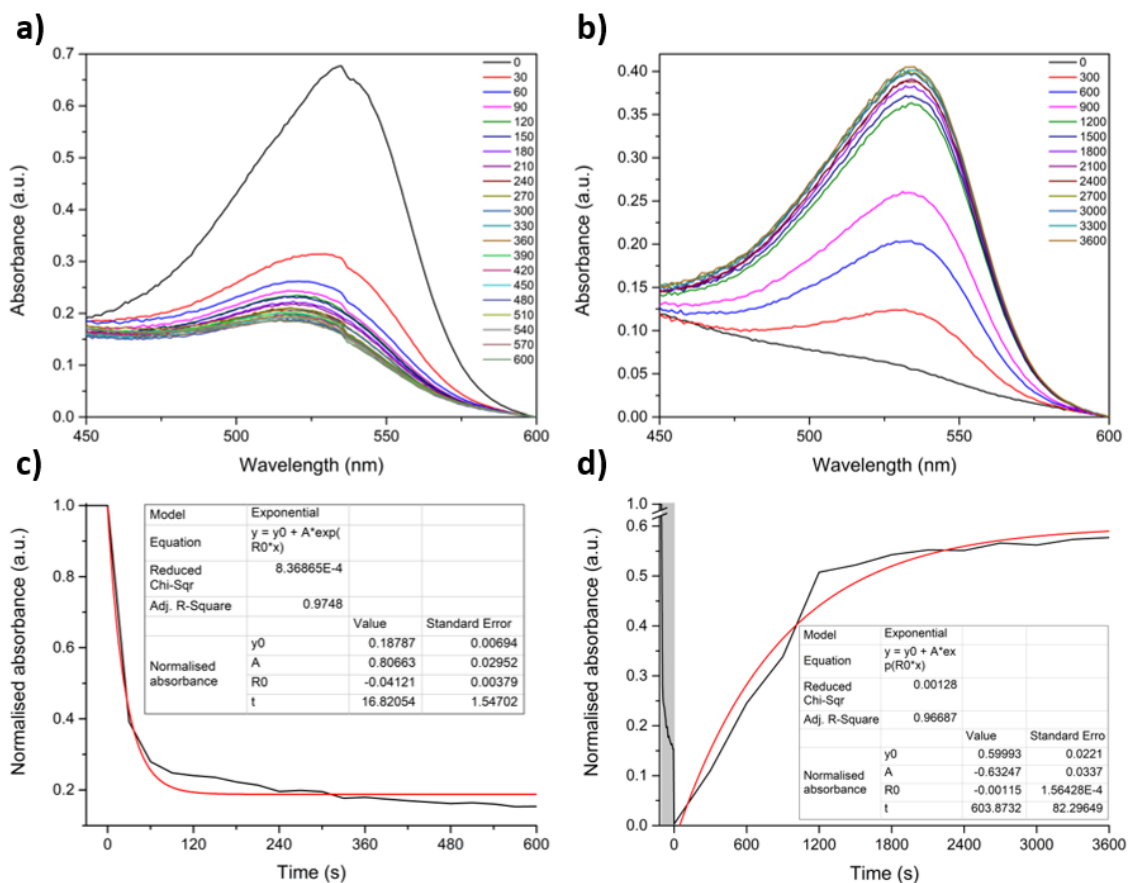
Figure 3-51 - UV-vis data acquired for SAC-0.5, consisting of a) a time lapse of the forward photoswitching reaction, b) the thermal reversion, and c+d) the change in λ$_{max}$ over time, for the forward and backward reactions, respectively.
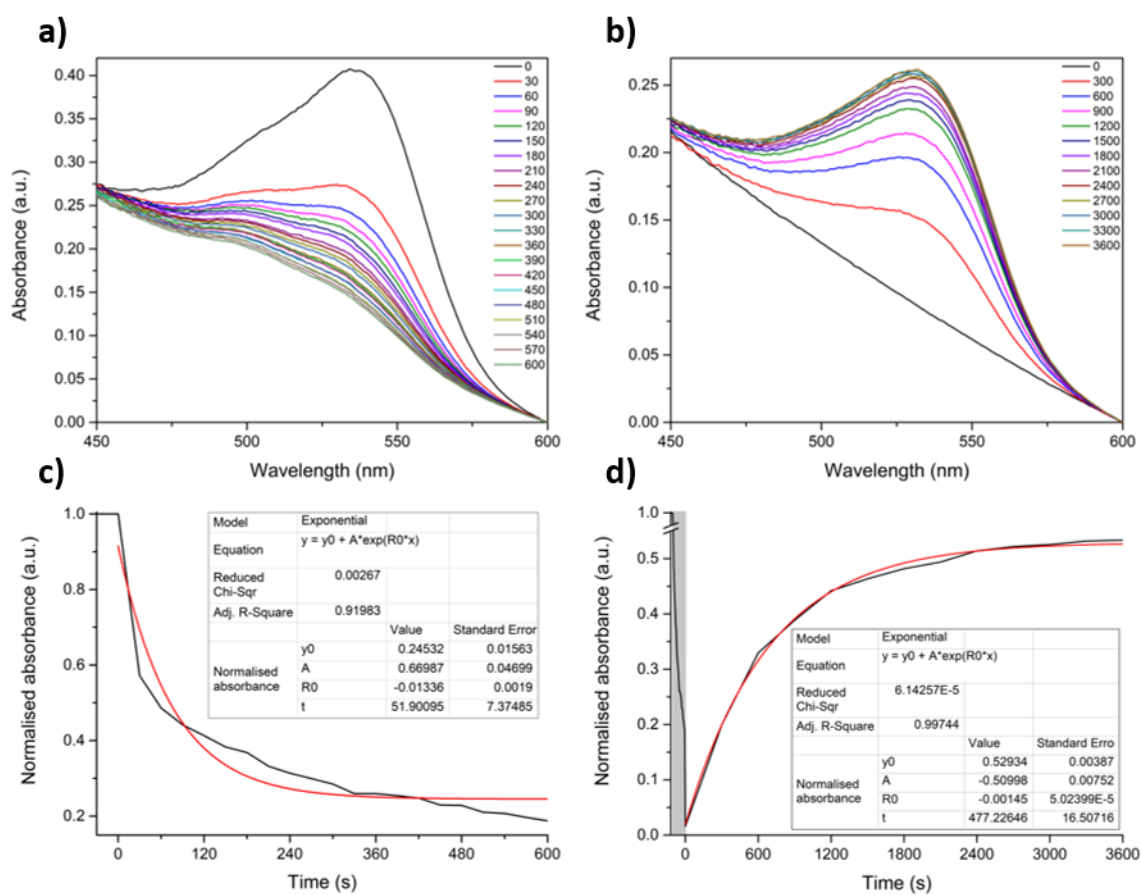
Figure 3-52 - UV-vis data acquired for SAC-1, consisting of a) a time lapse of the forward photoswitching reaction, b) the thermal reversion, and c+d) the change in λ_{max} over time, for the forward and backward reactions, respectively.

3.10 Appendix 3D
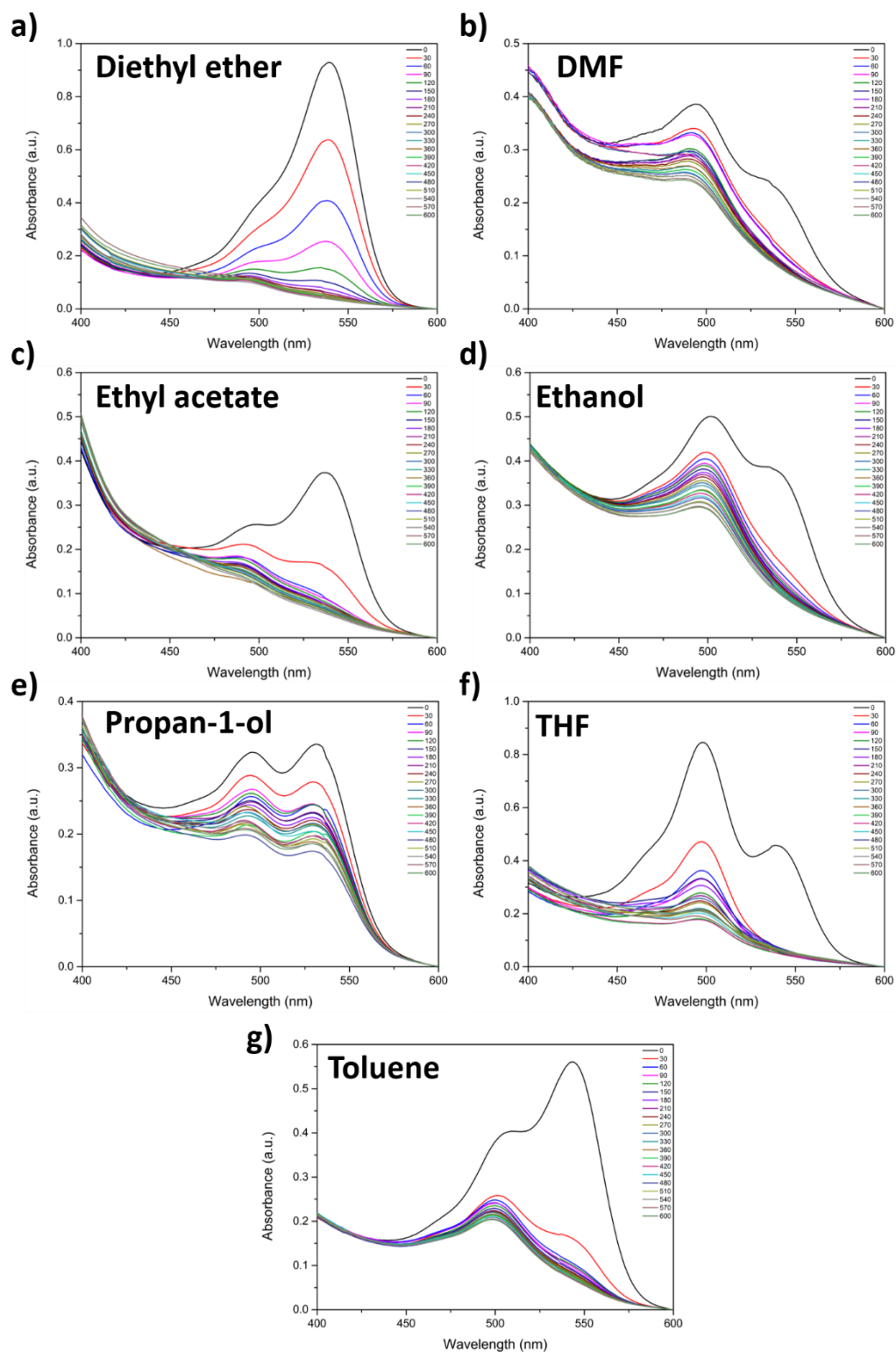
Figure 3-53 – UV-vis time-lapse data for AC-0.05 elastomer swollen by: a) diethyl ether, b) DMF, c) ethyl acetate, d) ethanol, e) propan-1-ol, f) THF, g) toluene.

Chapter 4:

Routes toward DASA-appended

polymers

4.1 Introduction

The incorporation of photoswitches into polymeric materials allows for light-dependent, spatiotemporal control over macroscopic properties. This has been previously demonstrated by drug delivery systems,[1–3] photoactuators[4–6] and various "smart" materials.[7–9] DASAs are a relatively new class of visible light photoswitches, which exhibit negative photochromism and provide facile access to light-controlling species.[10] Since their advent in 2014,[11] DASAs have received a great deal of attention, pertaining to the benefits they can provide to polymeric architectures.[12] The transformation from a non-polar to a more polar state through visible light irradiation, makes them ideal candidates for molecular delivery systems,[13–15] surface wettability switches[16–18] and implementation into deadhesion applications.[19] Furthermore, this transformation comes with a complete colour loss, providing them with popularity for photopatterning applications[20,21] and sensing devices.[22,23] As such, DASAs have already established a wide-range polymer application base, which is likely to continue growing within the coming years. Chapter 3 of this thesis described a method by which DASAs could be incorporated within PDMS elastomers, through non-covalent means. However, this method was limited by crystallisation at high photoswitch concentrations. Therefore, the covalent attachment of DASAs was the logical step forward; providing a greater degree of DASA functionalisation, without the limiting effects of crystallisation. Theoretically, a greater degree of functionalisation should lead to a larger magnitude of change in macroscopic properties. Covalent attachment of DASAs has been previously demonstrated on polymeric backbones such as: poly(ethylene glycol),[13,14] polystyrene,[16] acrylate/methacrylate polymers,[15,21,23,24] polyethyleneimine,[20,25] polydopamine[17] and poly(oxa-norbornene).[26] Popular routes toward covalent DASA-polymer conjugates consist of amino-functionalisation of PEG chains by way of Click chemistry;[13,14] activated ester-amino coupling in acrylate and methacrylates;[15,21] or a simple reaction of the DASA precursory species with an already available amino functional group.[17,25]

This chapter describes a multitude of experiments that were performed in the pursuit of the covalent appendation of a DASA to polymeric backbones, whether through grafting onto a chain or incorporation as a repeating unit, itself. The syntheses reported here focused on three different methods toward covalent DASA-functionalisation, they were: exploiting the availability of secondary amines innate to a polyethyleneimine (PEI) chain; constructing a polymeric chain consisting of barbituric acid-derived DASA precursor monomers; and grafting amino-functionality onto a polysiloxane chain, for subsequent further reaction. Although not all investigations were successful or completed, the findings reported here will be informative for future work.

4.2 Experimental

4.2.1 Materials and apparatus

Polyethyleneimine (branched: M_w 600, linear: M_w 2,500 and 10,000), hexamethylenediamine (98%, Sigma Aldrich), hexamethylene diisocyanate (>99.0%, Sigma Aldrich), butyl isocyanate (98%, Sigma Aldrich), diethyl malonate (99+%, Acros Organics), barbituric acid (99+%, Acros Organics), sodium metal (99.9%, Sigma Aldrich), hydrochloric acid (37%, Fisher Chemical), poly(methylhydrosiloxane-*co*-dimethylsiloxane) (HMS-071, Gelest, M_w 1,900-2,000), platinum(0)-1,3-divinyl-1,1,3,3-tetramethyldisiloxane complex in xylene(0.1 M, Pt ≈ 2%, Sigma Aldrich), ethanol (99+%, Fisher Chemical), dimethyl sulphoxide (99.9%, Alfa Aesar), diethyl ether (99+%, Acros Organics), methanol (99.8+%, Acros Organics), tetrahydrofuran (99.8%, Acros Organics), toluene (99+%, Fisher Chemical) and Celite® 545 (Sigma Aldrich) were all used as received. *N*-allyl aniline (95%, Sigma Aldrich) was stripped of its inhibitor, using a silica micro-column.

4.2.2 Synthesis of 5-(furan-2-ylmethylene)-2,2-dimethyl-1,3-dioxane-4,6-dione (MAF)

MAF was synthesised following the procedure given in Chapter 2, section 2.2.2.[11,27]

4.2.3 Synthesis of PEI-DASA (PEI M_w 600, 10 mol% DASA) (Compound 1)

The synthetic procedure described here was adapted from a previously-reported method.[25] Branched PEI (0.38 g, 8.8 mmol, M_w 600) and MAF (0.20 g, 0.88 mmol) were dissolved separately in EtOH (5 ml each). The dissolved PEI was added to the MAF solution, the resultant mixture was stirred under ambient conditions, for 15 minutes. Reaction progression was denoted by a colour change of yellow to pink. Following this, the reaction mixture was precipitated into cold, stirring THF (50 ml). A red solid was obtained (0.25 g, 43%) and analysed using ^{1}H NMR.

^{1}H NMR (400 MHz, DMSO-d_6, room temperature) found ppm δ: = 1.35-1.60 [**m, 6H (CH$_3$)$_2$**C(OOR)$_2$], 1.35-1.60 [**m, 1H** -CH$_2$-**NH**-CH$_2$-], 1.35-1.60 [**m, 2H** -CH$_2$-**NH$_2$**], 2.30-2.90 [**m, 2H** -RN-**CH$_2$**-CH$_2$-], 2.30-2.90 [**m, 2H** -CH$_2$-**CH$_2$**-NH], 2.30-2.90 [**m, 2H** -HN-**CH$_2$**-CH$_2$-], 2.30-2.90 [**m, 2H** -CH$_2$-**CH$_2$**-NH$_2$-], 3.12-3.95 [**m, 2H** -RN-**CH$_2$**-CH$_2$-], 3.12-3.95 [**m, 2H** -CH$_2$-**CH$_2$**-RN-], 5.77 [**s, 1H triene**], 6.13-6.43 [**m, 1H triene**], 6.13-6.43 [**m, 1H triene**], 7.20-7.42 [**m, 1H triene**].

4.2.4 Synthesis of PEI-DASA (PEI M$_w$ 10,000, 100 mol% DASA) (Compound 2)

Linear PEI (0.10 g, 2.3 mmol, M$_w$ 10,000) and MAF (0.80 g, 3.6 mmol) were dissolved separately in EtOH (5 ml each). The dissolved PEI was added to the MAF solution, the resultant mixture was stirred under ambient conditions, for 15 minutes. Reaction progression was denoted by a colour change of yellow to pink and eventually the formation of a red polymeric suspension. Following this, the red solid (0.39 g, 40%) was isolated via vacuum filtration. The product was insoluble in a large range of solvents: acetone, chloroform, DCM, diethyl ether, DMSO, ethanol, ethyl acetate, hexane, THF, toluene and water. The product was subsequently dried in a vacuum oven (60 °C) for 24 hours and analysed using FTIR spectroscopy.

FTIR (cm^{-1}): 2990 (R-CH$_2$, CH str.); 2828 (R-CH$_2$, CH str.); 1560 (C=O, str.); 1340 (O-H, bend); 1196 (C-O, str.); 1111 (R-C(OH)=R', C-O str.); 772 (N-H, wag).

4.2.5 Synthesis of PEI-DASA (PEI M$_w$ 10,000, 20 mol% DASA) (Compound 3a/b)

Linear PEI (0.50 g, 11.6 mmol, M$_w$ 10,000) and MAF (0.52 g, 2.3 mmol) were dissolved separately in EtOH (5 ml each). The dissolved PEI was added to the MAF solution, the resultant mixture was stirred under ambient conditions, for 15 minutes. Reaction progression was denoted by a colour change of yellow to pink. During the reaction, a precipitate began to form at the ethanol-glassware interface. This initial, red precipitate had a viscous consistency, was isolated through filtration and dried overnight (0.57 g, 56%, 3a). The remaining orange ethanolic-solution was

dropped into cold, stirring diethyl ether, producing an orange powder ($\approx$ 50 mg, 5%, 3b). The orange powder was analysed using ^{1}H NMR spectroscopy. The initial red precipitate was insoluble in a large range of solvents: acetone, chloroform, DCM, diethyl ether, DMSO, ethanol, ethyl acetate, hexane, THF, toluene and water. Subsequently, it was analysed using FTIR spectroscopy, only. Products 3a/b were dried in a vacuum oven (60 °C) for 24 hours.

^{1}H NMR (400 MHz, CD$_3$OD, room temperature) found ppm δ: = 1.61 [**s, 6H (CH$_3$)$_2$**C(OOR)$_2$], 1.97-4.56 [**m, 2H** -RN-**CH$_2$**-CH$_2$-], 1.97-4.56 [**m,** 2H -CH$_2$-**CH$_2$**-NH-], 1.97-4.56 [**m, 2H** -NH-**CH$_2$**-CH$_2$-], 1.97-4.56 [**m, 2H** -CH$_2$-**CH$_2$**-R-], 6.00-6.75 [**m, 1H triene**], 6.00-6.75 [**m, 1H triene**], 7.07-7.87 [**m, 1H triene**], 7.93-8.32 [**m, 1H triene**].

FTIR (cm^{-1}): 2990 (R-CH$_2$, CH str.); 2833 (R-CH$_2$, CH str.); 1560 (C=O, str.); 1396 (O-H, bend); 1258 (C-O, str.); 1200 (C-O, str.); 1142 (C-N, str.); 1111 (R-C(OH)=R', C-O str.); 775 (N-H, wag).

4.2.6 Synthesis of PEI-DASA (PEI M$_w$ 10,000, 10 mol% DASA) (Compound 4)

Linear PEI (0.51 g, 11.8 mmol, M$_w$ 10,000) and MAF (0.28 g, 1.3 mmol) were dissolved separately in EtOH (5 ml each). The dissolved PEI was added to the MAF solution, the resultant mixture was stirred under ambient conditions, for 15 minutes. Reaction progression was denoted by a colour change of yellow to pink. The reaction mixture was then dropped into cold, stirring diethyl ether, precipitating a red powder (0.49 g, 62%). The product was isolated via vacuum filtration, dried in a vacuum oven (60 °C) for 24 hours and analysed using ^{1}H NMR and FTIR spectroscopy.

^{1}H NMR (400 MHz, CD$_3$OD, room temperature) found ppm δ: = 1.63 [**s, 6H (CH$_3$)$_2$**C(OOR)$_2$], 2.31-4.49 [**m, 2H** -RN-**CH$_2$**-CH$_2$-], 2.31-4.49 [**m, 2H** -CH$_2$-**CH$_2$**-NH-], 2.31-4.49 [**m, 2H** -NH-**CH$_2$**-CH$_2$-], 2.31-4.49 [**m, 2H** -CH$_2$-**CH$_2$**-R-], 6.44 [**s, 1H triene**], 6.54 [**s, 1H triene**], 6.93 [**s, 1H triene**], 7.58 [**s, 1H triene**].

FTIR (cm^{-1}): 2978 (R-CH$_2$, CH str.); 2826 (R-CH$_2$, CH str.); 1557 (C=O, str.); 1387 (O-H, bend); 1256 (C-O, str.); 1200 (C-O, str.); 1145 (C-N, str.); 1111 (R-C(OH)=R', C-O str.); 745 (N-H, wag).

4.2.7 Synthesis of PEI-DASA (PEI M$_w$ 2,500, 10 mol% DASA) (Compound 5)

Linear PEI (0.5 g, 12 mmol, M$_w$ 2,500) and MAF (0.30 g, 1.2 mmol) were dissolved separately in MeOH (5 ml each). The dissolved PEI was added to the MAF solution, the resultant mixture was stirred under ambient conditions, for 15 minutes. Reaction progression was denoted by a colour change of yellow to pink. Following this, the reaction mixture was precipitated into cold, stirring diethyl ether (50 ml), forming a fine, pink suspension. The suspension was subsequently centrifuged, over three 20-minute periods, to yield a colourless diethyl ether supernatant and a red sediment. The red solid (0.54 g, 67%) was isolated by decanting, re-dissolving in MeOH and drying under vacuum, overnight. The product was analysed using ^{1}H and ^{13}C NMR.

^{1}H NMR (400 MHz, CD$_3$OD, room temperature) found ppm δ: = 1.58 [**s, 6H (CH$_3$)$_2$**C(OOR)$_2$], 2.08-4.02 [**m, 2H** -RN-**CH$_2$**-CH$_2$-], 2.08-4.02 [**m, 2H** -CH$_2$-**CH$_2$**-NH-], 2.08-4.02 [**m, 2H** -NH-**CH$_2$**-CH$_2$-], 2.08-4.02 [**m, 2H** -CH$_2$-**CH$_2$**-R-], 5.17 [**s, 1H triene**], 6.40 [**s, 1H triene**], 6.51 [**s, 1H triene**], 7.54 [**s, 1H triene**].

^{13}C NMR (CD$_3$OD, room temperature) found ppm δ: = 24.80 (multiplet), 45.6 (multiplet), 51.3 (multiplet), 59.1 (multiplet), 75.17, 101.69, 110.17, 167.68 (multiplet).

4.2.8 Synthesis of PEI-DASA (PEI M$_w$ 2,500, 100 mol% DASA) (Compound 6)

Linear PEI (0.16 g, 3.7 mmol, M$_w$ 2,500) and MAF (1.02 g, 4.6 mmol) were dissolved separately in DMSO (5 ml each). The dissolved PEI was added to the MAF solution, the resultant mixture was stirred under ambient conditions, for 15 minutes. Reaction progression was denoted by a colour change of yellow to pink. Following this, the reaction mixture was precipitated into cold, stirring diethyl ether (50 ml) and isolated via vacuum filtration. The product, a red solid (0.39 g, 33%), was dried in a vacuum oven (60 °C) for 24 hours and analysed using ^{1}H NMR.

^{1}H NMR (400 MHz, DMSO-d_6, room temperature) found ppm δ: = 1.10-1.79 [**m, 6H (CH$_3$)$_2$**C(OOR)$_2$], 1.10-1.79 [**m, 1H** -CH$_2$-**NH**-CH$_2$-], 1.87-4.02 [**m, 2H** RN-**CH$_2$**-CH$_2$], 1.87-4.02 [**m,**

2H -CH$_2$-**CH$_2$**-NH], 1.87-4.02 [**m, 2H** -HN-**CH$_2$**-CH$_2$-], 1.87-4.02 [**m, 2H** -CH$_2$-**CH$_2$**-R-], 5.70-6.55 [**m, 1H triene**], 5.70-6.55 [**m, 1H triene**], 7.20-7.80 [**m, 1H triene**], 7.20-7.80 [**m, 1H triene**].

4.2.9 Synthesis of poly(N, N'-Bis[propyl]urea) (Compound 7)

Hexamethylenediamine (0.69 g, 5.9 mmol) was dissolved in dry THF (4 ml). To this solution, hexamethylene diisocyanate (1.00 g, 5.9 mmol) was added dropwise, with cooling to 0 °C and stirring. Immediately, a white foam began to form, the reaction was left to stir for 15 minutes. Post-reaction, the white precipitate was isolated and washed in DCM, by sonication. Finally, the product (0.57 g, 42.2%) was dried under vacuum and subjected to FTIR analysis.

FTIR (cm^{-1}): 3323 (N-H, str.); 2932 (C-H, str.); 2857 (C-H, str.); 2259 (N=C=O, asym. str); 1612 (C=O, str.); 1250 (C-N, str.).

4.2.10 Synthesis of hexamethylene bis(butylurea) (Compound 8)

Hexamethylenediamine (20 mg, 0.17 mmol) was dissolved in dry THF (2 ml). To this solution, butyl isocyanate (40 mg, 0.40 mmol) was added dropwise, with cooling to 0 °C and stirring. Immediately, a white precipitate began to form, the reaction was left to stir for 15 minutes. The white solid was then filtered off and washed with DCM, by sonication. The product (10.6 mg, 18%) was isolated, dried and subjected to ^{1}H NMR, ^{13}C NMR and FTIR analysis.

^{1}H NMR (400 MHz, CD$_3$OD, room temperature) found ppm δ: = 0.94 [**t,** J = 7.4 Hz, **6H** -CH$_2$-**CH$_3$**], 1.36 [**m, 4H** -CH$_2$-**CH$_2$**-CH$_3$], 1.45 [**m, 4H** -CH$_2$-**CH$_2$**-CH$_2$], 3.10 [**t,** J = 6.9 Hz, **4H** -NH-**CH$_2$**-CH$_2$], 5.83 [**s, 4H** -CH$_2$-**NH**-C=O].

^{13}C NMR (CD$_3$OD, room temperature) found ppm δ: = 12.74, 19.62, 26.16, 29.90, 32.13, 39.32, 39.45.

FTIR (cm^{-1}): 3321 (N-H, str.); 2932 (C-H, str.); 2857 (C-H, str.); 1614 (C=O, str.); 1244 (C-N, str.).

4.2.11 Synthesis of hexamethylene bis(N-butylbarbituric acid) (Compound 9)

Sodium metal (4.24 mg) was placed into a round bottom flask, attached to a reflux condenser. To this, ethanol (2 ml) was added, a vigorous reaction ensued. Following the completion of this reaction, diethyl malonate (9.6 mg, 0.06 mmol) was added to the reaction mixture, along with an ethanolic solution (2 ml) of compound 8 (10.6 mg, 0.03 mmol). The reaction was refluxed at 110 °C, with stirring, for 2 hours. After 2 hours, hot DI H_2O (50 °C, 5 ml) was added to the reaction mixture, followed by the addition of conc. HCl, until the reaction was acidified. The solution was filtered, the filtrate left to cool in a fridge overnight and then filtered a second time, to obtain a white solid. The white solid (8.2 mg, 61%) was washed with DI H_2O and dried in a vacuum oven (60 °C), overnight. Compound 8 was subjected to ^{1}H and ^{13}C NMR analysis.

^{1}H NMR (400 MHz, CD$_3$OD, room temperature) found ppm δ: = 0.93 [**t,** *J* = 7.6 Hz, **6H** -CH$_2$-**CH$_3$**], 1.34 [**m, 4H** -CH$_2$-**CH$_2$**-CH$_3$], 1.46 [**m, 4H** -CH$_2$-**CH$_2$**-CH$_2$], 3.10 [**t,** J = 6.8 Hz, **4H** -CH$_2$-**CH$_2$**-NH].

^{13}C NMR (CD$_3$OD, room temperature) found ppm δ: = 12.74, 19.61, 26.14, 29.87, 32.11, 39.32, 39.44.

4.2.12 Synthesis of poly(methyl[propylaniline]siloxane-*co*-dimethylsiloxane) (Compound 10)

Poly(MHS-DMS) (1 g, 13.6 mmol) was dissolved in toluene (10 ml) and stirred at 80 °C. To this hot solution, *N*-allyl aniline (0.127 g, 0.95 mmol), was added. Following this, platinum(0)-1,3-divinyl-1,1,3,3-tetramethyldisiloxane complex (25 μl, 0.1 M in xylene) was added to the reaction mixture. The reaction was stirred and kept at 80 °C for 24 hr, after which, the product was precipitated into cold, stirring methanol and isolated via vacuum filtration. The product was subsequently redissolved in hexane and filtered through a bed of Celite® 545, to remove residual platinum contaminants. The product (0.52 g, 63%) was dried through rotary evaporation and subjected to ^{1}H NMR, and FTIR, spectroscopic analyses.

^{1}H NMR (400 MHz, CDCl$_3$, room temperature) found ppm δ: = 0.08 [**s, 12H** -Si-**CH$_3$**], 0.82 [**m, 2H** -Si-**CH$_2$**-CH$_2$-], 1.66 [**m, 2H** -CH$_2$-**CH$_2$**-CH$_2$-], 3.08 [**s, 2H** -CH$_2$-**CH$_2$**-NH-], 3.63 [**s, 1H** -CH$_2$-**NH**-C$_6$H$_5$], 4.68 [**m, 1H** -Si-**H**], 6.58 [**m, 2H phenyl**], 6.67 [**m, 1H phenyl**], 7.15 [**m, 2H phenyl**].

FTIR (cm^{-1}): 2963 (C-H, str.); 1602 (C-C str.); 1504 (C-C str.); 1258 (Si-CH$_3$ scissor); 1072 (Si-O-Si asym. str.); 1011 (Si-O-Si asym. str.); 787 (Si-O-Si scissor).

4.3 Measurements and Instruments

4.3.1 FT-IR spectroscopic measurements

FTIR spectroscopic analysis was performed on a Shimadzu IRAffinity-1 spectrometer with a Specac Golden Gate™ ATR sampling accessory, under ambient conditions, with 64 scans at a resolution of 4 cm^{-1}. Good optical contact between the sample and the diamond was obtained by clamping of samples via the Golden Gate™.

4.3.2 NMR spectroscopic measurements

^{1}H and ^{13}C NMR data were acquired using a Bruker AVANCE-400 spectrometer, spectra were obtained at 19 ^{o}C in methanol-d_4 (d-99.8 atom %, CIL), dimethylsulphoxide-d_6 (d-99.9 atom %, CIL) and chloroform-d (d-99.8 atom %, CIL).

4.4 Results and discussion

4.4.1 Synthesis and characterisation of DASA-functionalised PEI

As secondary amines are innate to its structure, PEI is a natural choice for producing a DASA-appended polymer. This section shall detail and discuss the attempts at synthesising a DASA-functionalised PEI backbone, featuring compounds 1-6. In all cases where possible, precipitation of the product was conducted in cold, stirring diethyl ether, alternative methods of purification were not undertaken. Some compounds retained solvent even after a 24-hour drying period. Compound 1 was synthesised using branched PEI (M_w 600) and MAF, through a procedure adapted from a previously-reported method.[25] This consisted of reacting MAF and PEI in ethanol for 15 minutes, followed by a precipitation into cold, stirring THF and isolation via vacuum filtration. The reaction scheme is included as Figure 4-1. The resultant red solid was analysed using ^{1}H NMR (Figure 4-2a) and compared with a previously-reported example, and PEI-600 itself (Figure 4-2b). The two synthetic procedures were identical, apart from the precipitation process; Wu et al conducted precipitation into THF, from ethanol, three times. It is likely that a significant portion of the yield for compound 1 was lost in the filtrate due to insufficient precipitation, hence only 43% was attained, as opposed to a possible 62%.[25] The successful synthesis of compound 1 was confirmed by ^{1}H NMR; the signals between 8 and 5 ppm closely resembled those which were published previously. Regarding Figure 4-2a, signal c, which should correspond to the DASA hydroxyl group, was not found. This was also the case for the reference product (Figure 4-2b). It was believed that lack of a signal was indicative of inter/intramolecular hydrogen-bonding. The degree of functionalisation could not be accurately calculated, due to the interference of solvent signals such as water, ethanol and DMSO-d_6. Further evidence to support functionalisation was the downfield shift of the PEI-CH$_2$ signals and the reduction of the amino signals.
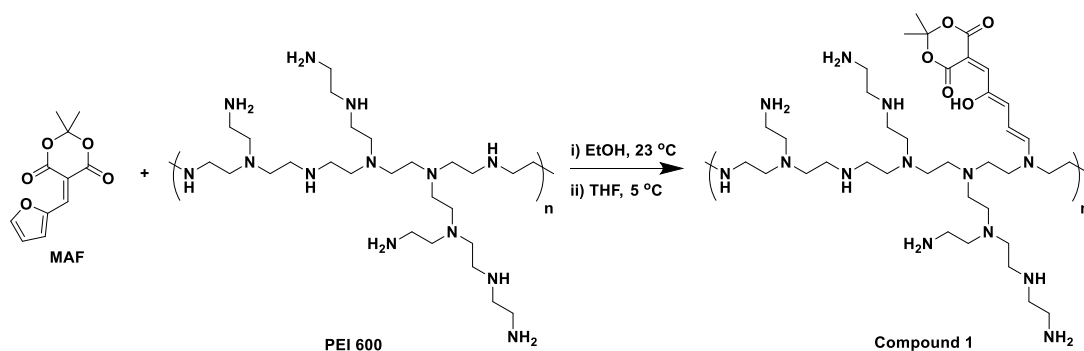
Figure 4-1 – Synthetic scheme for compound 1.
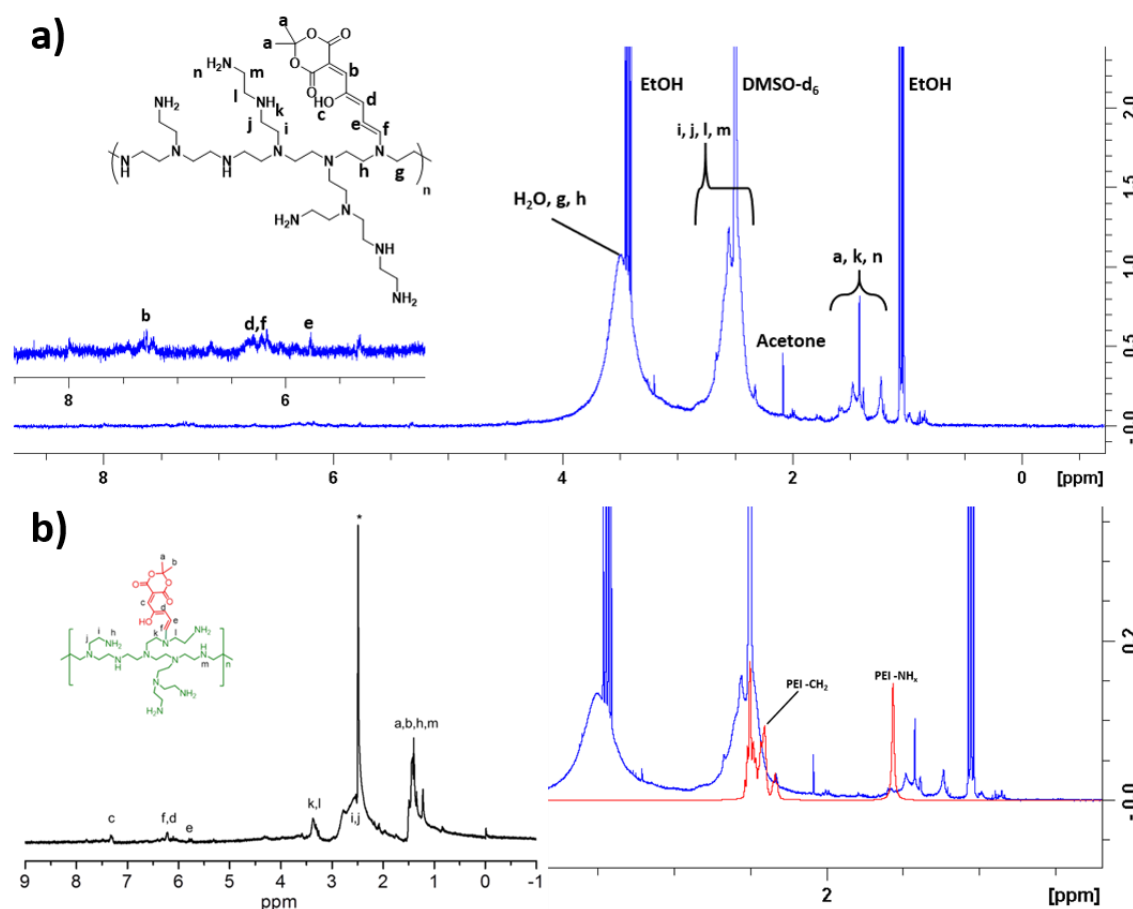
Figure 4-2 – a) ^{1}H NMR spectrum of compound 1, in DMSO-d_6; b) ^{1}H NMR spectra of a previously-reported PEI-DASA example (left)[25] and compound 1 overlaid with PEI-600 (right).

Following successful modification of the branched PEI system, it was decided to continue investigative syntheses with linear analogues, as they are known to be insoluble in water at room temperature.[28,29] The water solubility and subsequent enforced switching, is something that largely limits the applicational use of DASAs in aqueous environments.[12] Although this

disadvantage has been overcome in some circumstances, the synthesis of PEI-DASA – when optimised – will be more facile and accessible.[26,30] There is also the added advantage that linear PEIs are less cytotoxic than their branched counterparts.[31,32] For the purposes of comparison, the ^{1}H NMR and FTIR spectra of the utilised linear PEIs (M_w 10,000 and 2,500) are included in sections 4.7 and 4.8 – appendices 4A/B, respectively. The synthetic scheme for compounds 2-6 is included as Figure 4-3; variations of the procedure are detailed in the table below the scheme.

Compound	Solvent	PEI M_w (gmol^{-1})	DASA (mol%)
2	EtOH	10,000	100
3	EtOH	10,000	20
4	EtOH	10,000	10
5	MeOH	2,500	10
6	DMSO	2,500	100
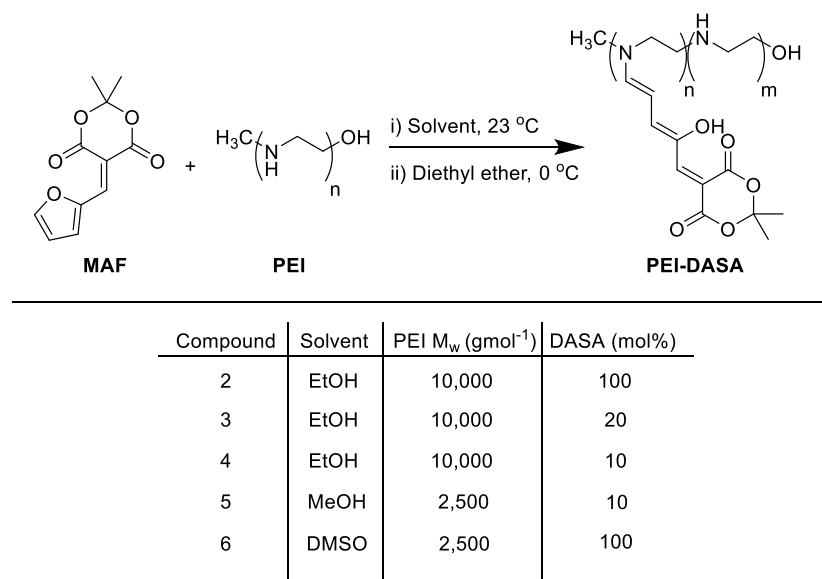
Figure 4-3 – Synthetic scheme for the linear PEI-DASA samples, with a table highlighting the solvent, molecular weight and DASA-loading differences between each.

The synthetic procedure for compound 2 has been described in more detail in section 4.2.4. Upon addition of the dissolved PEI to the ethanolic-MAF solution, a colour change of yellow to pink occurred, indicating the formation of a DASA. The reaction was stirred for 15 minutes, within which a red, polymeric suspension had formed. This precipitate, compound 2 (0.39 g, 40%), was insoluble in a range of polar to non-polar solvents, such as DMSO, water, DMF, DCM, THF, toluene and diethyl ether. It was found to swell in polar organic solvents, therefore the product was swollen in methanol-d_4, to remove residual MAF and investigate whether any soluble PEI-DASA was present. The ^{1}H NMR for that leaching experiment (Figure 4-4a) revealed that swelling the product would release precursory MAF and very little more. This indicated that

any successfully synthesised PEI-DASA was either wholly insoluble, or existed within too dilute concentrations to be quantified. The FTIR spectrum of compound 2 has been overlaid with that of PEI 10,000, included as Figure 4-4b. A secondary amine stretch and an amine wag are prominent at 3213 and 799 cm^{-1}, respectively for PEI. Whereas, compound 2 shows a complete lack of an amine stretch and a large reduction in the intensity of the amine wag region, indicating DASA-functionalisation. Additionally, C=O and C-O stretches can be found at 1560 and 1111 cm^{-1}, respectively – characteristic of the DASA Meldrum's acid acceptor group. It is believed that the insolubility of compound 2 was consequential of high concentrations of intermolecular hydrogen-bonding between polymer chains, illustrated by Figure 4-4c. Linear PEI chains are prone to exhibiting interchain hydrogen-bonding, forming helical chains.[33,34] As such, the hypothesis of interchain hydrogen-bonding is the most probable explanation.
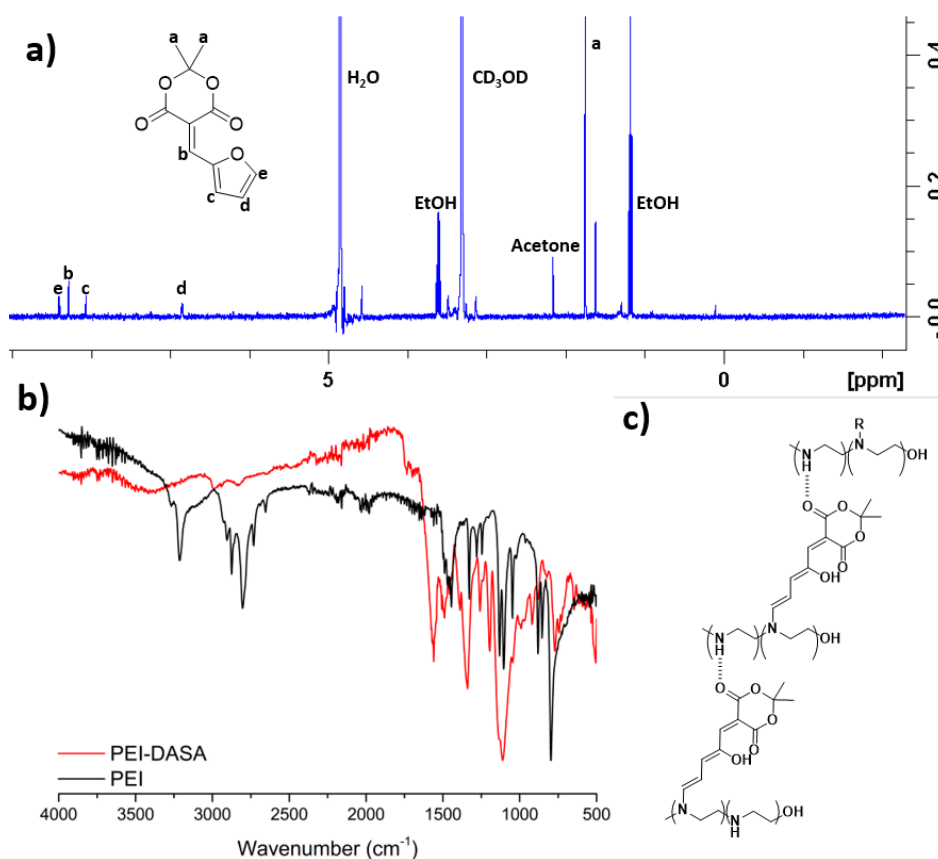

Figure 4-4 – a) ^{1}H NMR spectrum of a methanol-d$_4$ leached solution from compound 2; b) an FTIR spectrum of compound 2, overlaid with that of PEI 10,000; c) a schematic representation of the theorised hydrogen-bonding polymer chain interactions.

With the general insolubility of compound 2, a reduction in DASA loading was attempted, culminating in compounds 3a/b. It was believed that covalent modification of a smaller degree would reduce the concentration of intermolecular hydrogen-bonding, and so, lower the likelihood of an insoluble precipitate. The procedure was an adaption of that used to produce compound 1, and has been described in section 4.2.5; it was found that compound 1 would only precipitate in THF at low temperatures (≤ 5 °C), or would precipitate readily in diethyl ether at room temperature and below, hence the latter proved to be a more effective solvent. The first product, compound 3a (0.57 g, 56%), was a precipitate that had formed during the reaction and was insoluble in all tested solvents, similarly to compound 2. This product was isolated via vacuum filtration, washed and dried. The second product, compound 3b (50 mg, 5%), was the result of precipitation into diethyl ether, from ethanol, producing a fine orange powder. Compound 3a was subjected to FTIR analysis and compared with PEI 10,000, shown by Figure 4-5a. As with compound 2, the FTIR spectrum of compound 3a supported the hypothesis of DASA-functionalisation. There was a lack of N-H stretches within the 3200 cm^{-1} region and a reduction in the intensity of N-H wags, centred around 775 cm^{-1}. Further corroborated by the appearance of C=O and C-O stretches at 1560 and 1111 cm^{-1}. Compound 3b was analysed using ^{1}H NMR, in methanol-d_4, the resultant spectrum is included as Figure 4-5b. Despite the 24-hour drying period under vacuum, some solvents had been retained. Functionalisation of PEI was confirmed by the presence of shifted PEI -CH_2 signals, labelled as f, g and h, and the presence of the characteristic DASA triene peaks b, c, d and e. Accurately determining the degree of functionalisation was not possible, due to the presence of multiple solvent signals within the 2-4 ppm region. However, an approximation was obtained by subtracting the integrals of EtOH and acetone from the signal group 'f, g, h' and then comparing that value to 'a'. This provided a ratio of 31 : 6, indicating an approximate DASA-functionalisation of 16%; less than the desired 20%. To remove residual MAF and isolate more potential compound 3b, compound 3a was swollen in a methanol-d_4 solution – similarly to compound 2. ^{1}H NMR analysis was conducted, yielding a spectrum that was very similar to Figure 4-5b, therefore it had not been included.
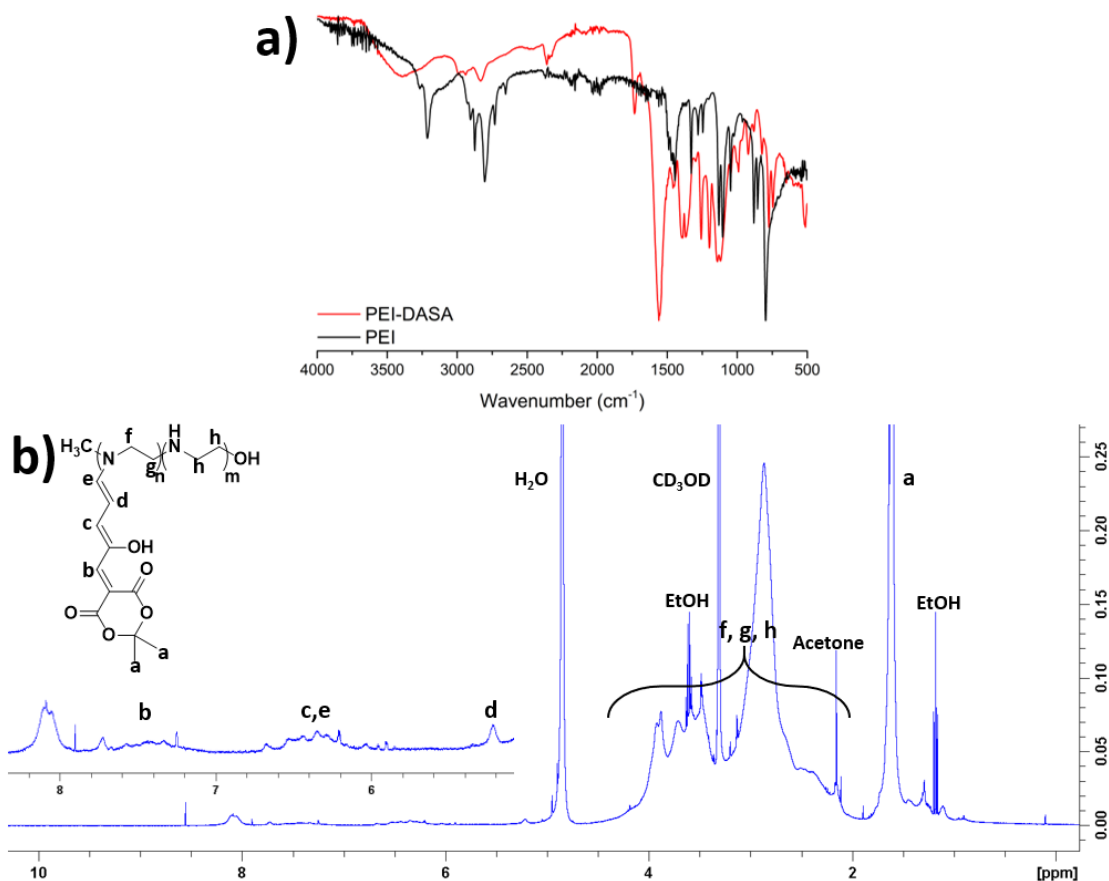
Figure 4-5 – a) FTIR of compound 3a, overlaid with that of PEI 10,000; b) ^{1}H NMR of 3b in methanol-d_4.

Due to the formation of the insoluble compound 3a, the attempted DASA-functionalisation was further lowered to 10 mol%. The synthetic procedure applied here was identical to that of compounds 3a/b and has been described in section 4.2.6. Fortunately, an insoluble material did not form and compound 4 (0.49 g, 62%) was precipitated from cold diethyl ether, as a red powder. Compound 4 was characterised using FTIR and ^{1}H NMR spectroscopy, displayed as Figure 4-6a/b, respectively. Successful modification was confirmed by a lack of secondary amine stretches within the 3200 cm^{-1} region of the FTIR spectrum. Furthermore, the characteristic C=O and C-O stretches of a DASA were present at 1557 and 1111 cm^{-1}, respectively. Examination of the ^{1}H NMR spectrum corroborated what was revealed by the FTIR data; signals indicative of a DASA triene were present between 6 and 8 ppm and the unmodified PEI backbone signals weren't present. This suggested that the PEI chain had indeed been functionalised. Mirroring

the findings from compound 3, the DASA-functionalisation could only be approximated by comparing the peak groups 'f, g, h' and 'a'. The integrals of CD$_3$OD, its ^{13}C satellite peaks and acetone were subtracted from 'f, g, h', providing a ratio of 54 : 6, indicating a DASA-functionalisation of approximately 11%, very close to the desired 10%.
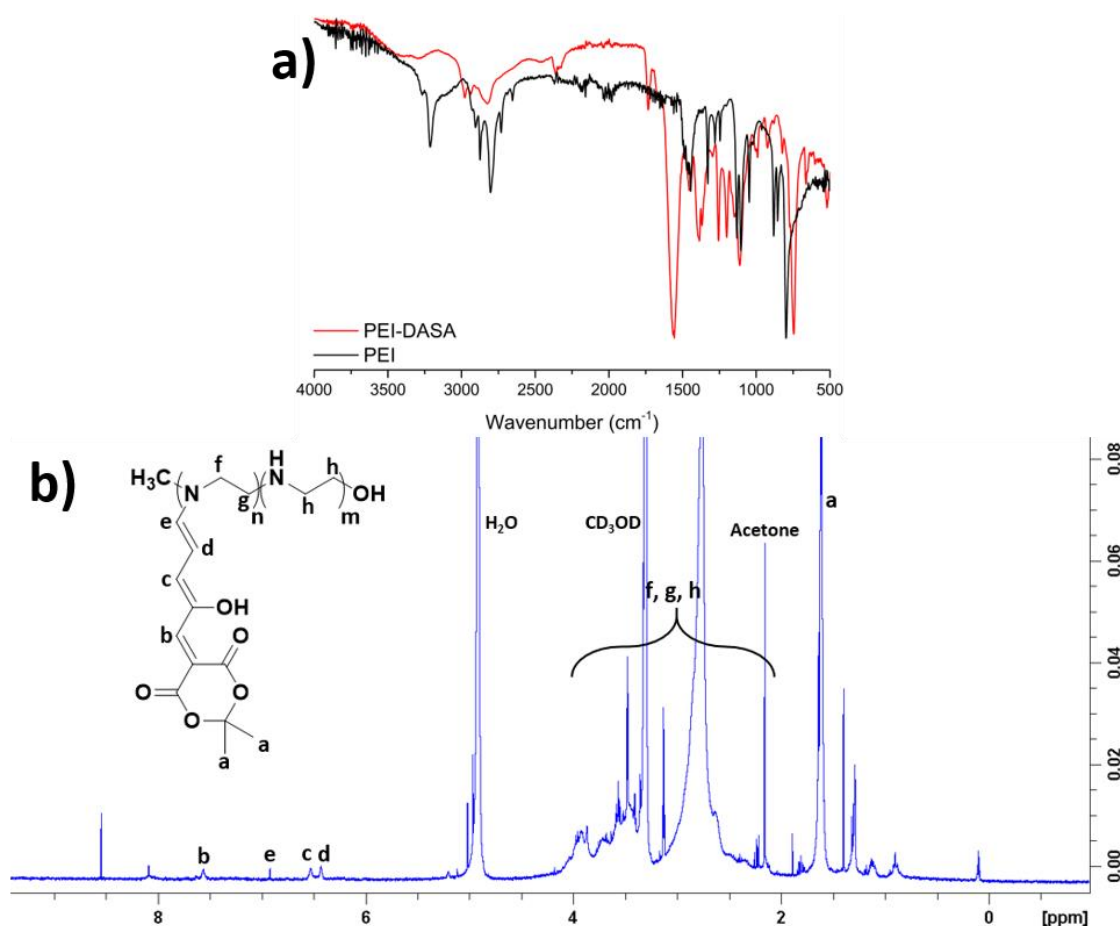

Figure 4-6 – a) FTIR of compound 4, overlaid with that of PEI 10,000; b) ^{1}H NMR of 4 in methanol-d_4.

With the successful appendation of a DASA to PEI 10,000, it was decided to attempt the same method with a lower molecular weight analogue that was readily available – PEI 2,500. The synthetic procedure for compound 5 (0.54 g, 67%) was followed as before, using ethanol in place of methanol and has been described in section 4.2.7. The ^{1}H and ^{13}C NMR, and FTIR spectra of compound 5 have been included as Figure 4-7a-c, respectively. The unassigned peaks between δ = 6 and 8 ppm for the ^{1}H NMR spectrum are believed to be characteristic of the colourless, closed DASA form, and a mixture of both open and closed isomers.
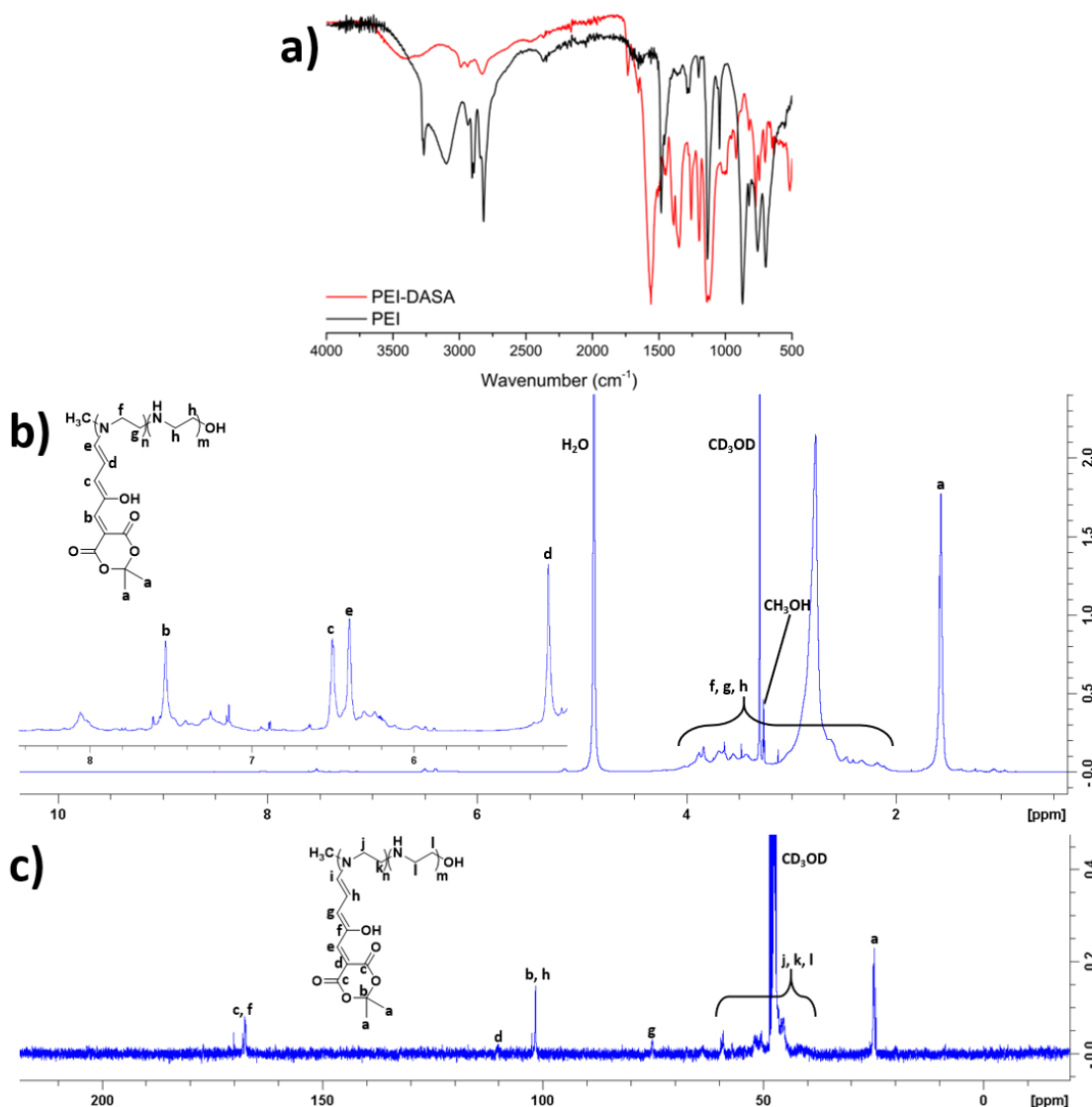
Figure 4-7 – a) FTIR of compound 5, overlaid with that of PEI 2,500; b) ^{1}H NMR of 5 in methanol-d_4; c) ^{13}C NMR of 5 in methanol-d_4.

The product existed predominantly in the open form, this was supported by the lack of a visible ketone carbonyl signal within the region of 200-220 ppm, in the ^{13}C spectrum. This peak would be expected, had the photoswitch predominantly adopted the closed, cyclopentenone structure. The FTIR spectrum of PEI 2,500 indicated the presence of secondary amines, by the single N-H stretch located around 3267 cm^{-1} and the peaks corresponding to an N-H wag within the region of 900-700 cm^{-1}. These signals were either lacking or reduced in the FTIR spectrum for compound 5, indicating a degree of successful DASA-functionalisation. This supposition was further supported by the emergence of C=O and C-O stretches, located at 1560 and 1111 cm^{-1},

respectively. These are characteristic of the Meldrum's acid acceptor group of the DASA species. Accurately calculating the degree of functionalisation wasn't possible, due to interference of deuterated and regular methanol peaks within the 2-4 ppm region of the ^{1}H NMR spectrum. As before with compounds 3 and 4, subtracting the solvent integral allowed for an approximation of the functionalisation, by comparison of signals 'f, g, h' with 'a'. This gave a ratio of 46 : 6, indicating an approximate DASA-functionalisation of 13% of the PEI backbone. This was slightly larger than anticipated (10%). Following the successful synthesis of compound 5, it was decided that an increase in the DASA-functionalisation would be attempted. A larger concentration of photoswitch would theoretically lead to greater changes in macroscopic properties, upon visible light irradiation. Therefore, the aim was to produce a 100% MAF-loaded PEI backbone. The synthesis of compound 2 - which utilised a 100% modification for PEI 10,000 - revealed that a high loading of DASA could lead to a product that was insoluble in a large range of solvents. It was believed that this was consequential of a high concentration of interchain hydrogen-bonding. Polar organic solvents, such as DMSO, caused the product to swell however. As such, it was decided that the synthetic procedure for compound 6 would be performed in DMSO, in the hope that perhaps the product would be soluble. Herein, the product was synthesised according to the method laid out earlier (section 4.2.8), precipitated into diethyl ether and isolated via vacuum filtration. Compound 6 (0.39 g, 33%) was in fact found to be insoluble in a range of polar and non-polar solvents, excluding DMSO. The product was characterised through FTIR and ^{1}H NMR spectroscopy, shown as Figure 4-8a/b. Successful functionalisation was supported by the FTIR spectrum; with a lack of an N-H stretch in the 3200 cm^1 region and the presence of C=O and C-O stretches around 1562 and 1200 cm^{-1}, respectively. As with compound 5, the peak region between δ = 6 and 8 ppm of the NMR spectrum consisted of a mixture of proton signals corresponding to the open triene and closed cyclopentenone DASA isomers. It was apparent that the open form took precedence, based on the magnitude of the assigned peaks and minor appearance of the triene hydroxyl group, 'c'. Once again, an accurate picture of the DASA-functionalisation was not possible, as the characteristic PEI backbone peaks had

merged with a number of solvents and unknown signals. Despite this, using the method discussed for the previous three PEI-DASA compounds, an approximation of the functionalisation was determined. Achieved by subtracting contaminant peaks from the body of 'g, h, j' and comparing to 'a' produced a ratio of 31 : 6, again suggesting a functionalisation of just 16% of the PEI backbone. This was far below what was intended, it is possible that this was the limit of which functionalisation could be achieved, likely due to steric hindrance.
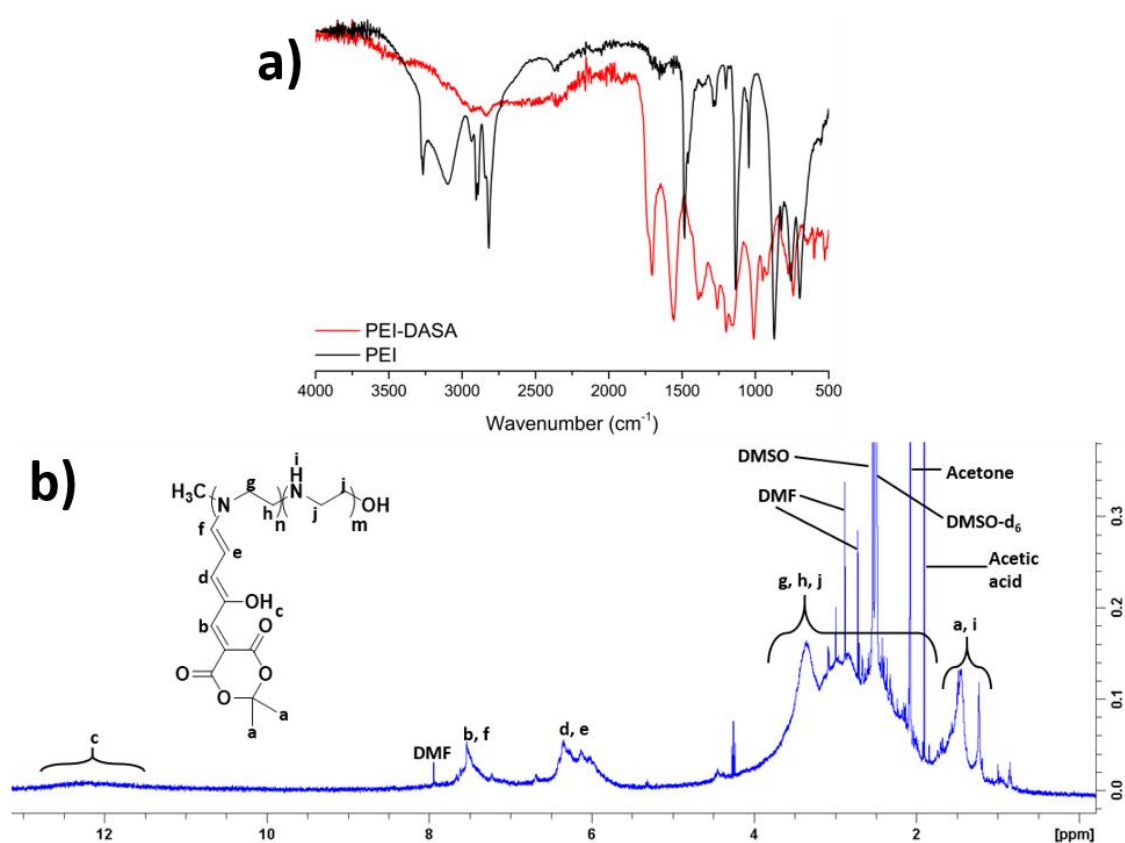

Figure 4-8 – a) FTIR of compound 6, overlaid with that of PEI 2,500; b) ^{1}H NMR of 6 in DMSO-d_6

To conclude, the synthetic route towards linear PEI-DASA needs further optimisation. Further investigation into purification methods should be taken, in order to reduce the amount of product lost during the precipitation step. Ideally, more time would be taken to completely dry the products, in order to accurately assess the level of DASA-functionalisation. However, the overall aim was achieved, in which the successful appendation of a DASA onto PEI was demonstrated.

4.4.2 Syntheses and characterisations toward a barbituric acid-derived DASA polymer

This section will detail the investigation into producing a polymer consisting of DASA monomeric units, the products described here include compounds 7, 8 and 9. The desired end-result for this project was a polymer that could exhibit mechanochromism, whereby photoswitching would cause a macroscopic change in polymer volume. The synthetic roadmap toward the final product is illustrated as Figure 4-9.
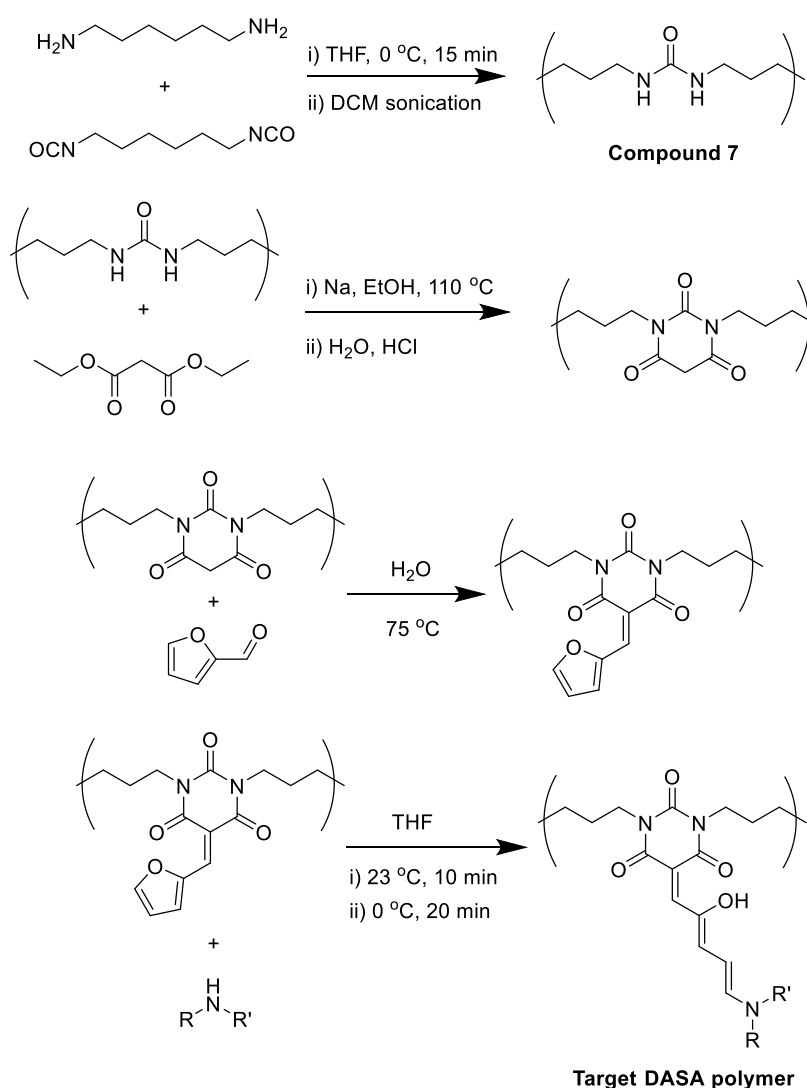
Figure 4-9 - Synthetic roadmap toward the target DASA polymer.

Compound 7 would be formed by the reaction of a diamine and diisocyanate, producing a polyurea-based scaffold. Providing this step was successful, a barbituric acid-derived species

could then be synthesised from this and eventually converted to an activated furan DASA-precursor. All of this would culminate in an end-product DASA polymer, with the hope that the high concentration of DASA in the backbone would encourage large macroscopic changes upon visible light irradiation. The synthetic procedure toward compound 7 has been described in section 4.2.9. It was known that the isocyanate species were liable to react with atmospheric H_2O, despite this the reaction was not performed under an inert atmosphere. The reasoning behind this was to establish a successful synthetic pathway first and optimise later. The addition of hexamethylenediamine to hexamethylene diisocyanate immediately produced an exothermic reaction with a white, foamy precipitate. After 15 minutes, the reaction could no longer progress, as stirring was hindered by the resultant solid. The precipitate was isolated via vacuum filtration, swollen, and sonicated, in DCM, to remove any starting materials. The foam was likely a result of a build-up of CO_2, caused by the isocyanate groups reacting with atmospheric water.[35] The isocyanate groups would convert to primary amines during this process; hence the resultant yield was only 42%. Compound 7 was insoluble in a large range of solvents, including even the most polar, such as water and DMSO. As such, NMR analysis could not be conducted. Instead, compound 7 was subjected to FTIR spectroscopic analysis; Figure 4-10a is an overlay of that data, with analyses of the two starting materials. For the purposes of comparison, the IR spectra for both starting materials - hexamethylenediamine and hexamethylene diisocyanate - can be found in section 4.9 – appendix 4C. Apparent in the product spectrum was a secondary amine N-H stretch (3323 cm^{-1}) and a C=O stretch (1612 cm^{-1}), both suggesting the presence of amides. Furthermore, the wavenumbers of these bands suggested that they were taking part in interchain urea hydrogen-bonding, as has been reported in the past for other polyurea derivatives.[36,37] It has been reported that this ordered form of hydrogen-bonding is indicative of very close packing of chains, which can lead to solubility issues.[38] Therefore, the insolubility of compound 7 was most likely caused by a high concentration of hydrogen-bonding between urea units, as depicted by Figure 4-10b. Additionally, an intense absorption band at 2259 cm^{-1} was present, characteristic of an isocyanate N=C=O stretch. This data strongly indicated the

formation of a chain-extended urea species, likely capped by isocyanate groups, of which had not undergone a complete reaction.[39] This was surprising, as it was thought that those species would have fully reacted with the equimolar amount of amine, or atmospheric H_2O.
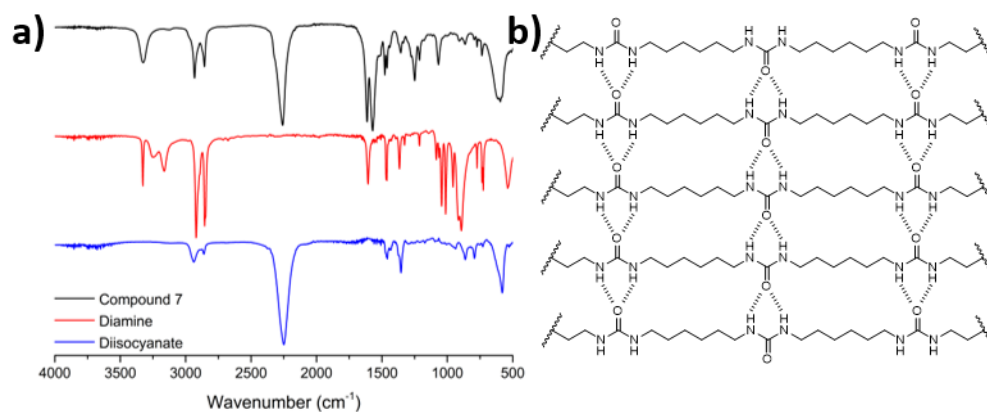

Figure 4-10 – a) FTIR spectral overlay of compound 7, hexamethylenediamine and hexamethylene diisocyanate; b) a representation of the hydrogen-bonding between polymer chains of compound 7.

With the successful synthesis but undesirable insolubility of compound 7, it was decided that a non-polymeric species would be the focus of initial investigations and that success in that area could be used to inform further work. This time, hexamethylenediamine was reacted with butyl isocyanate to produce a diurea species. The synthetic scheme toward compound 8 is illustrated as Figure 4-11.
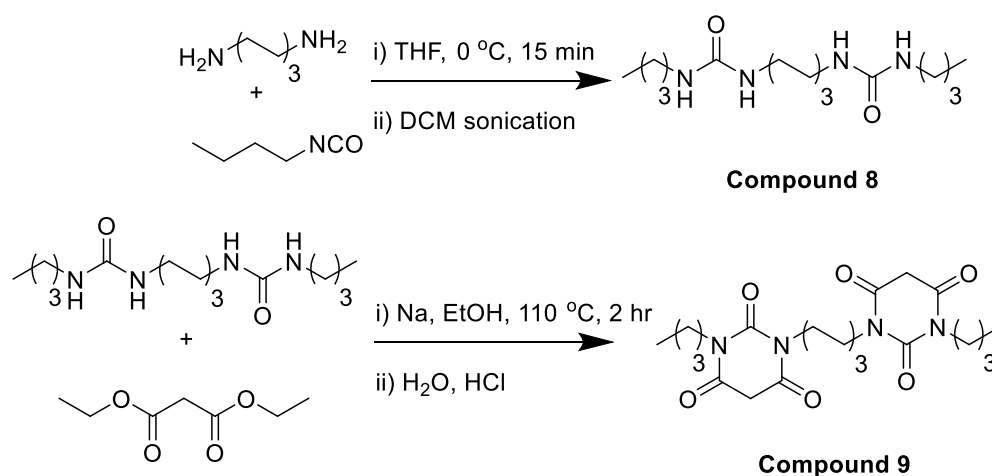
Figure 4-11 – Synthetic routes toward compounds 8 and 9.

As with compound 7, the reaction appeared to proceed immediately, producing a white precipitate. The product was isolated by vacuum filtration and washed in DCM, with sonication. Following this, it was isolated a second time and dried in a vacuum oven overnight. The yield of this compound was very low, at only 18%, it is likely that the reaction was worked up far too early. Compound 8 was analysed using FTIR spectroscopy (Figure 4-12b); immediately clear, was the lack of an isocyanate N=C=O stretch, in the 2200-2300 cm^{-1} region, indicating complete conversion. A secondary amide N-H stretch and an amide C=O stretch were apparent, at 3321 and 1614 cm^{-1}, respectively. Compound 8 was soluble in methanol and was analysed by ^1H and ^{13}C NMR spectroscopy. The data are included as Figure 4-12c/d, spectra of hexamethylenediamine and butyl isocyanate can be found in section 4.9 – appendix 4C. The ^1H spectrum contained an unknown, broad singlet at 4.57 ppm and the ^{13}C spectrum didn't display any expected carbonyl signals in the region of 160-170 ppm. Despite this, both spectra confirmed a successful synthesis. The next step was to further react the diurea species with diethyl malonate, to produce a barbituric acid derivative – compound 9 (Figure 4-11). The synthetic method toward compound 9 was adapted from a previously published textbook procedure.[40] The synthetic scheme for this reaction is illustrated by Figure 4-13a, and the ^1H NMR spectrum of barbituric acid is included in section 4.9 – appendix 4C, as a reference material. Compound 9, a white solid, was obtained with a yield of 61%. The ^1H NMR spectrum of compound 9 (Figure 4-13b) was almost identical to that of compound 8, as they share very similar structures. What was immediately clear was the lack of an amide proton, designated as 'd' for compound 8; an indication of successful condensation between the diethyl malonate and the urea functional groups. Despite this, compound 9 was lacking the heterocycle's methylene proton signal, designated as 'e'. This was expected to appear within the region of 3.5 ppm. A comparison of compound 8 and 9, with barbituric acid, has been included as Figure 4-13c, for clarity. Compound 9 was also subjected to ^{13}C NMR analysis, included as Figure 4-13d. Parallel with compound 8, there was a noticeable lack of carbonyl signals within the region of 160-170 ppm, the cause of this is unknown. Additionally, like with the ^1H spectrum, the signal

characteristic of the methylene carbons of the six-membered ring ('g') was also absent. This signal was expected to be located within the 40-ppm region, nearby to 'f' and 'd', however, the inset expansion of Figure 4-13d revealed only two signals. With these findings, it had to be concluded that the synthesis of compound 9 was unsuccessful. Due to material availability constraints at the time, further syntheses could not be attempted.
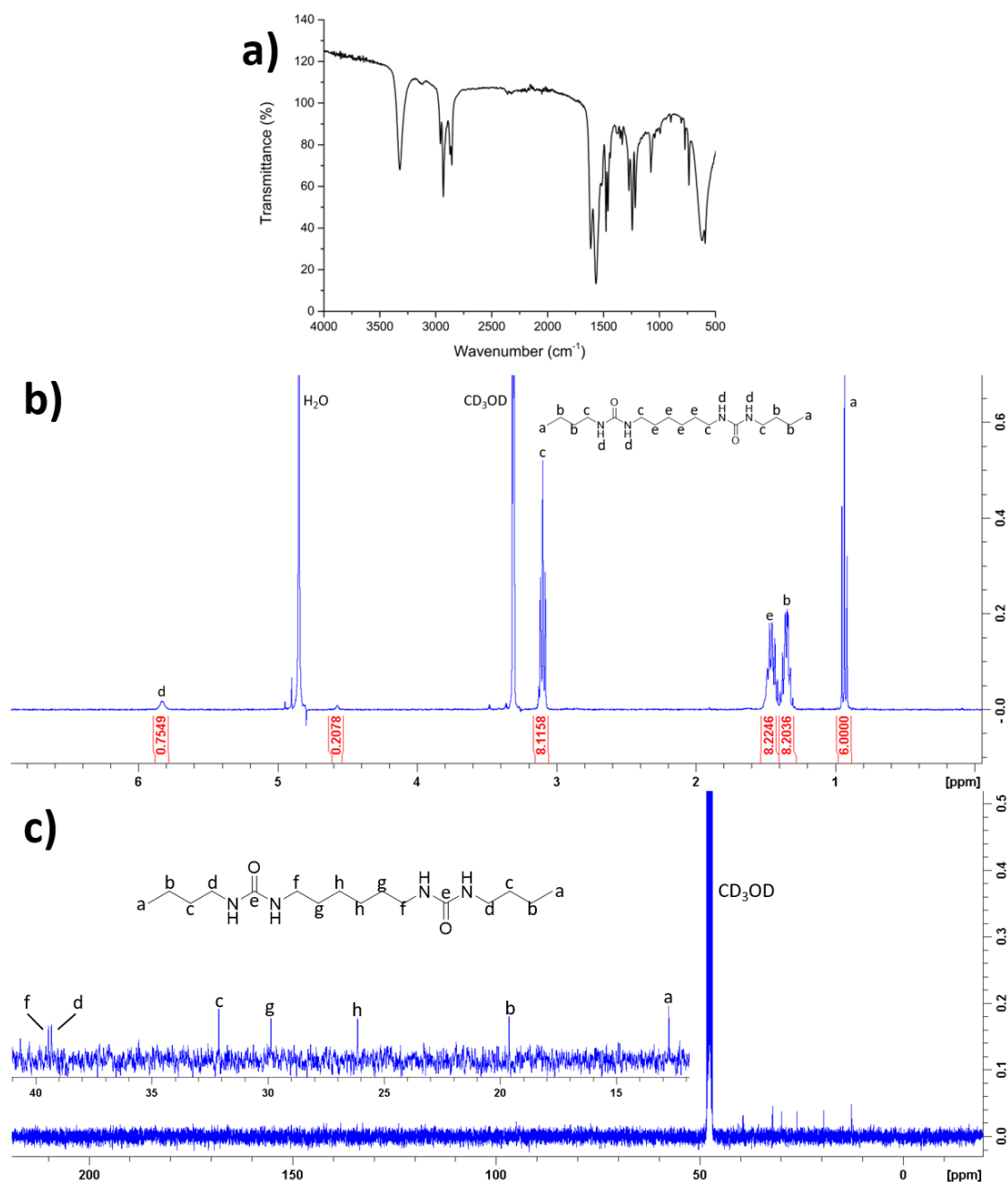

Figure 4-12 - a) FTIR of compound 8; b) ^{1}H NMR of compound 8 in methanol-d_4; c) ^{13}C NMR of 8 in methanol-d_4.
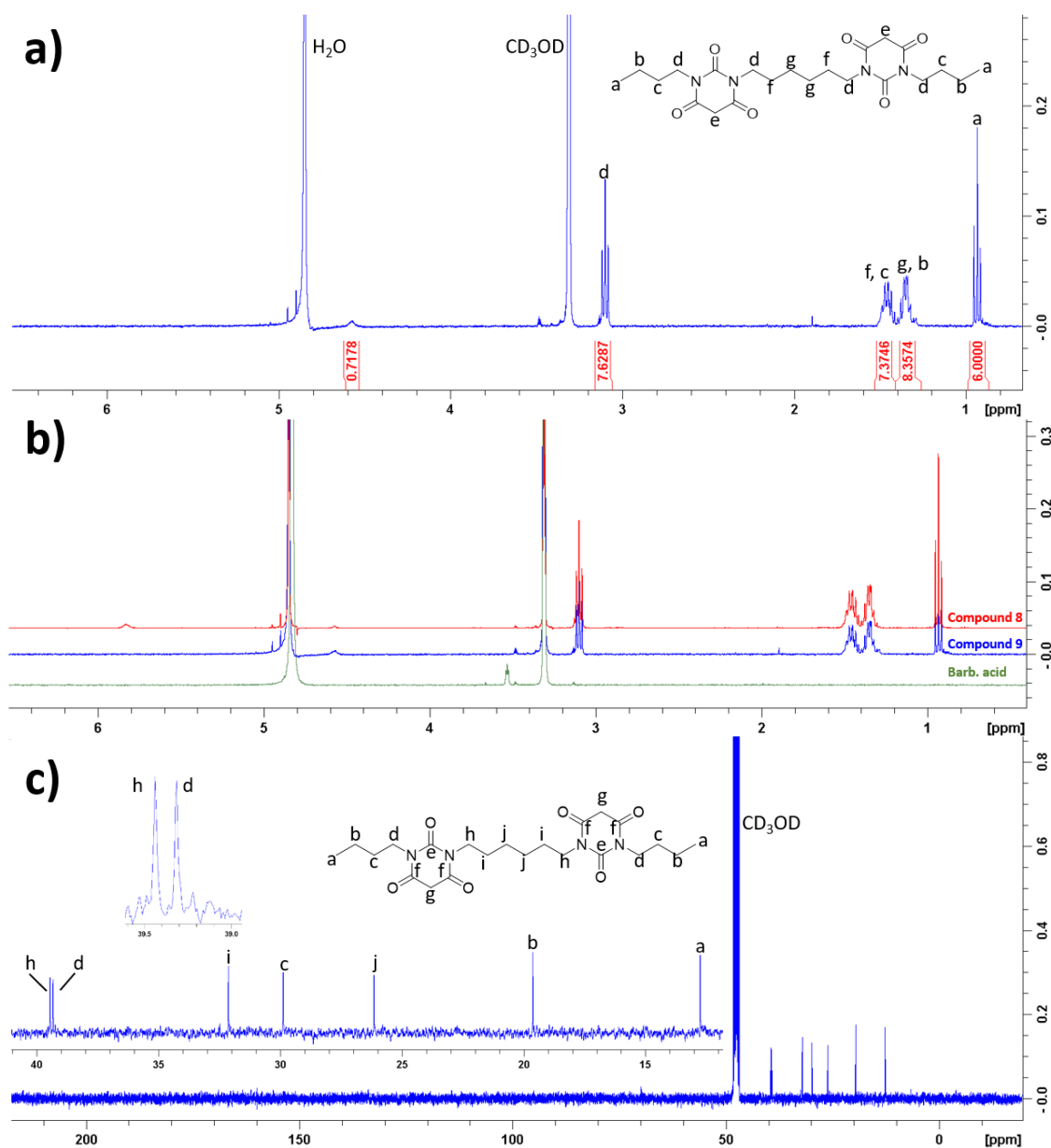
Figure 4-13 - a) ^{1}H NMR of compound 9 in methanol-d_4; b) ^{1}H NMR comparison of compound 8, 9 and barbituric acid; c) ^{13}C NMR of 9 in methanol-d_4.

4.4.3 Syntheses and characterisations toward a DASA-functionalised polysiloxane backbone

This investigation was the natural development of the work described in chapter 3 of this thesis; covalent attachment of a DASA to a polysiloxane, as opposed to the non-covalent doping of a cross-linked network. Covalent attachment of a DASA would allow for a higher photoswitch loading than doping and bypass the potential for crystallisation, altogether. The overall aim was

to provide amino-functionality to a polysiloxane chain, which could then be further reacted with MAF to provide DASA side-chains. The synthetic plan for this is included as Figure 4-14. Firstly, *N*-ally aniline was to be grafted onto a poly(MHS-DMS) chain through Pt-catalysed hydrosilylation. This would be followed by a reaction of the newly-formed secondary amines with an equimolar amount of MAF, to produce the DASA-functionalised polysiloxane. The number of Si-H reactive sites was determined from comparison of the Si-CH3 and Si-H ^{1}H NMR integrals - shown in Figure 4-15. The poly(MHS-DMS) held a 7 mol% concentration of reactive Si-H groups, therefore the product would have a maximum of 7 mol% amino-functionality. As such, compound 10 was produced by a hydrosilylation reaction between *N*-allyl aniline and poly(MHS-DMS), with a 1 : 1 molar ratio of Si-H to *N*-ally aniline. The hydrosilylation reaction was allowed to progress for 24 hours, until taken off, precipitated into cold, stirring methanol and isolated via vacuum filtration. The product was a dark brown oil when isolated from methanol. The dark colouration was believed to be indicative of the residual platinum catalyst, as such it was re-dissolved into hexane from the filter paper, and further filtered through a bed of Celite® 545. The filtering process was performed 5 times, but did not remove all of the residual platinum. Consequently, compound 10 was a dark brown oil, with a yield of 63% (0.52 g). After drying, the product was subjected to FTIR and ^{1}H NMR analysis. A comparison of the FTIR spectra of compound 10 and the precursory poly(MHS-DMS) is included as Figure 4-16a; the spectrum for poly(MHS-DMS) itself is located in section 4.10 – appendix 4D. Both spectra were almost identical; exhibiting the expected siloxane asymmetric stretches of 1072 and 1011 cm^{-1}, and the scissor of 787 cm^{-1}. However, compound 10 lacked the characteristic Si-H stretch at 2158 cm^{-1} and displayed two bands indicative of C-C stretching in aromatic rings, at 1605 and 1506 cm^{-1}, respectively (inset). This data was concomitant with a successful hydrosilylation reaction. Supporting evidence came from the ^{1}H NMR spectrum, as Figure 4-16b.
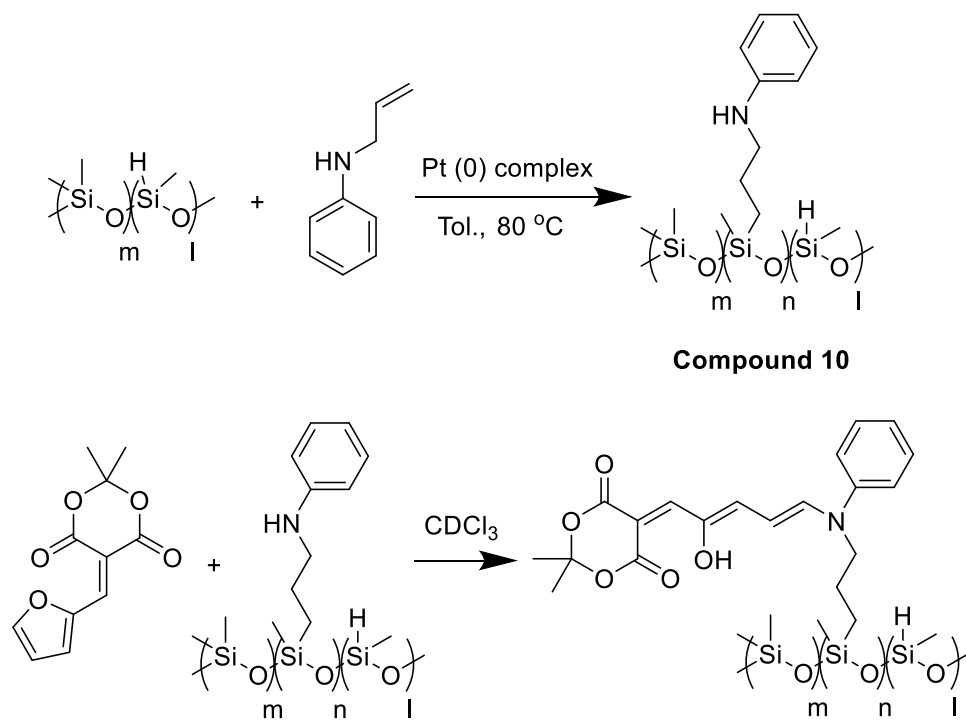
Figure 4-14 – Synthetic schemes toward the production of a DASA-functionalised polysiloxane backbone.


$$87-3 = 84 \text{ H}$$
$$84/6 = 14$$

$$m = 14n$$

❖ Si-CH$_3$: Si-H, 14 : 1, 93% : 7%
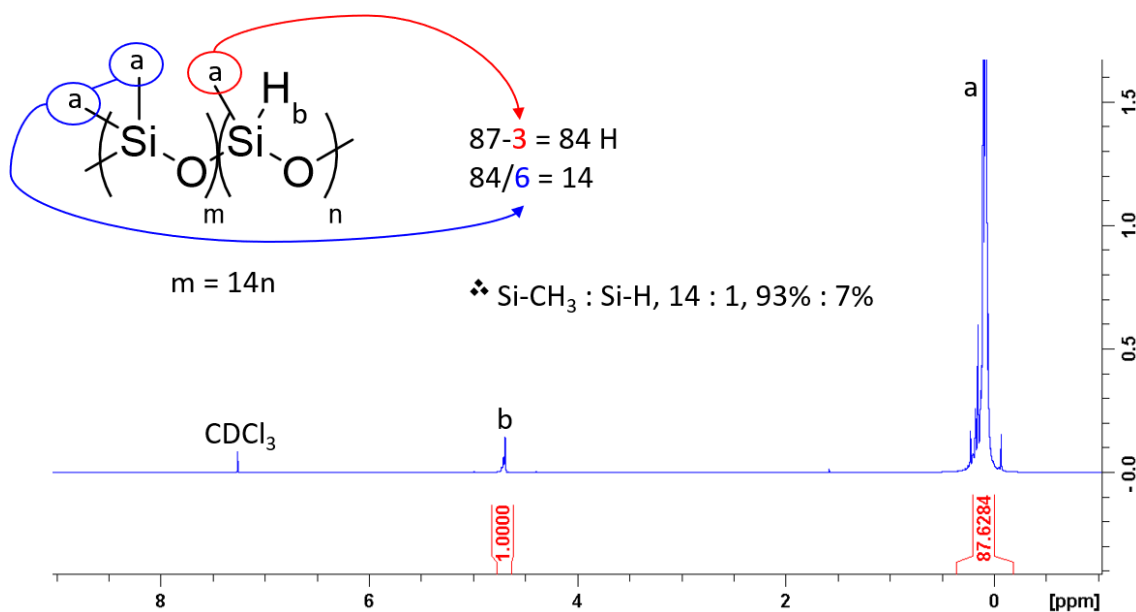
Figure 4-15 – ^{1}H NMR spectrum of poly(MHS-DMS), with calculations toward the determination of reactive Si-H sites.
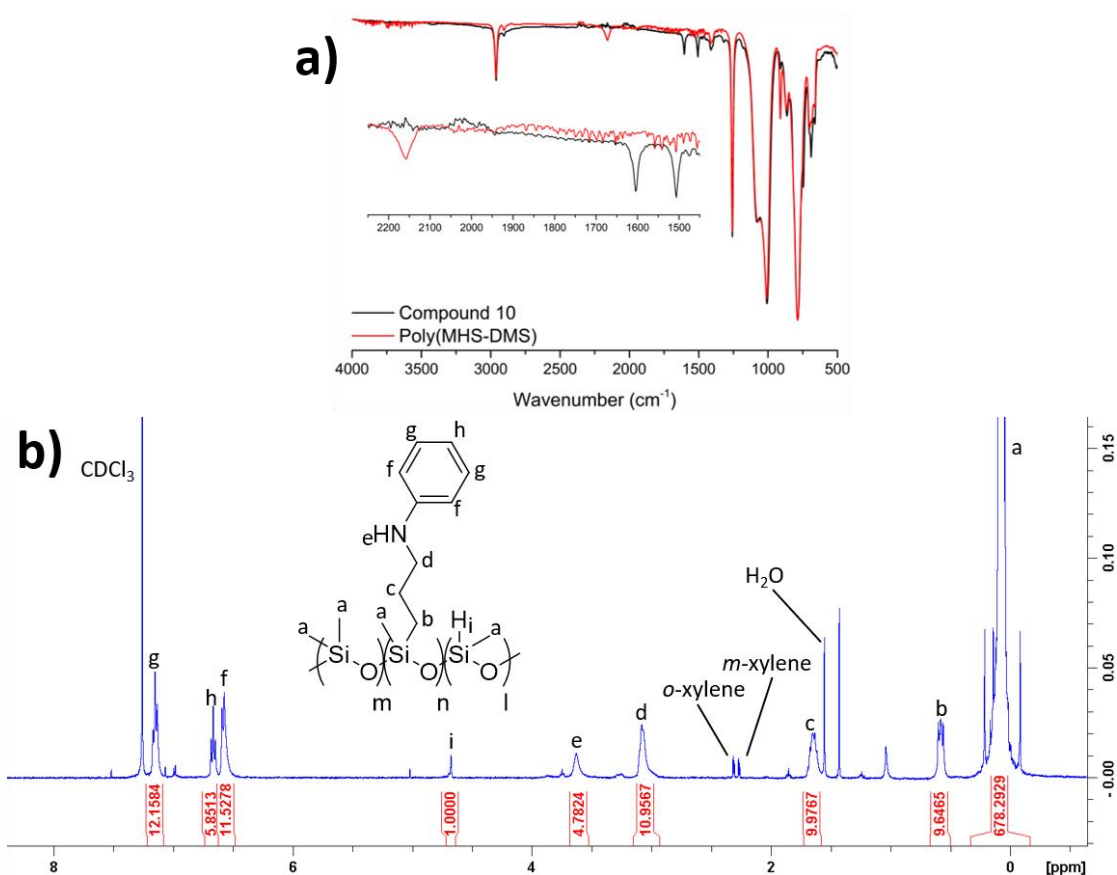
Figure 4-16 – a) FTIR spectrum of compound 10; b) ^{1}H NMR spectrum of compound 10.

Comparison of the Si-H and Si-CH$_3$ integrals suggested an 88% conversion of the Si-H groups, meaning that 6% of the polymer backbone was functionalised with propyl aniline units. The reaction was monitored by ^{1}H NMR, after 4 and 24 hours and both indicated similar degrees of conversion. Therefore, it was concluded that future iterations of this experiment would only require ≤ 4 hr reaction times. Following this, a preliminary experiment was conducted, to assess the viability of producing a DASA from the amino-functionalised polysiloxane. Equimolar amounts of MAF and compound 10 were dissolved in chloroform-*d* and left to react in an NMR tube; the resultant ^{1}H NMR spectrum is included as Figure 4-17a. The integrals of signals 'e' and 'k, o, p, q', were monitored over time; to calculate the degree of DASA-conversion through the change in the ratio between the Si-H (i) and N-H (e), and the MAF (k, o, p, q) and *p*-phenyl (h) peaks. The integral values for each species, at 0, 24, 48, 72 and 168 hours, were plotted as Figure 4-17b.
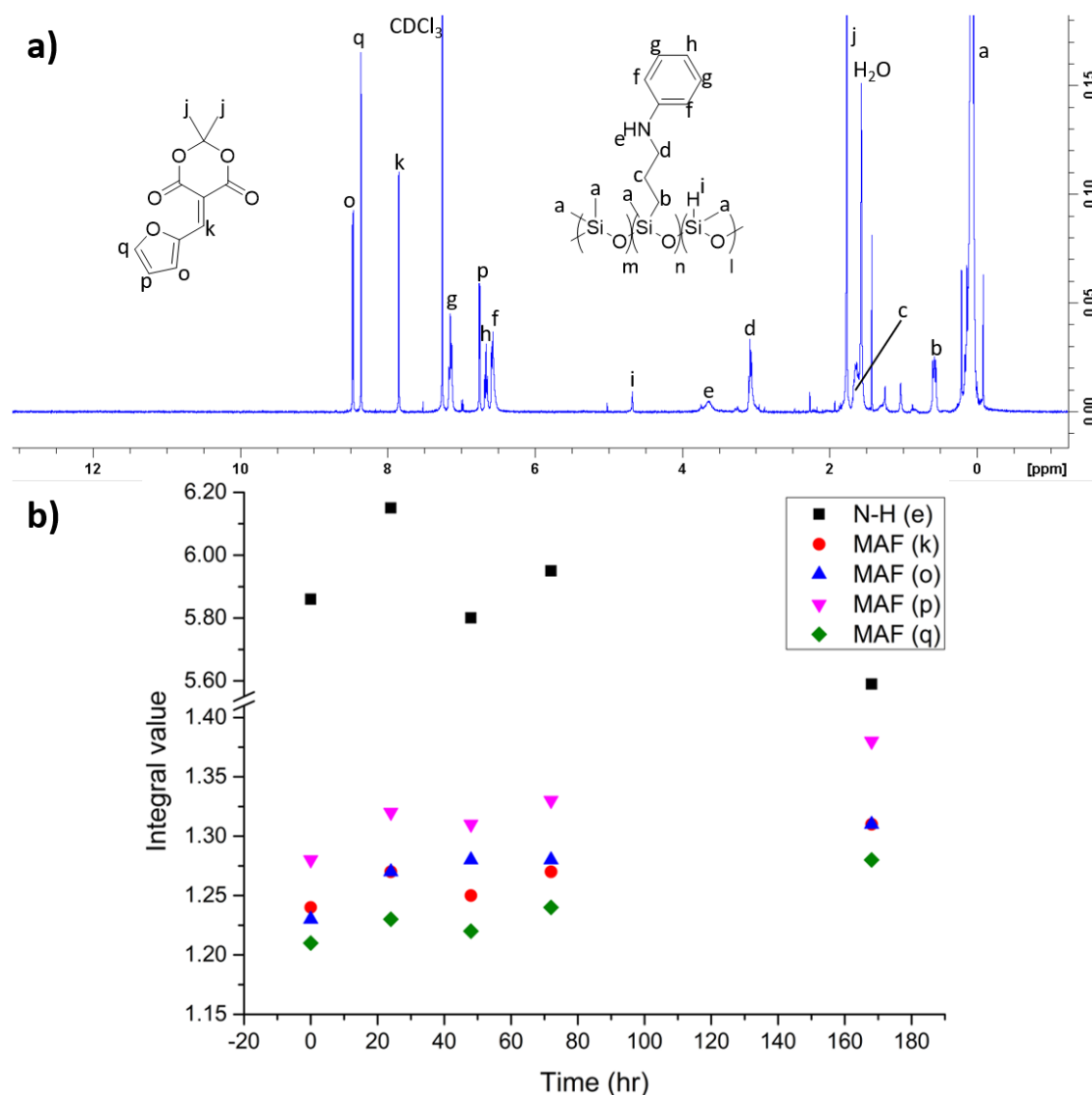
Figure 4-17 – a) ^{1}H NMR of MAF and compound 10, after 168 hrs; b) a plot of the integrals for signals e, k, o, p and q, over time.

It was clear from the data that integration of the signals was unreliable; an overall decrease in N-H concentration had occurred, with fluctuations, but with a net increase of MAF. Ideally, the integral values of both MAF and N-H signals would continually decrease. As such, the only reliable indication of DASA formation was the appearance of a faint pink colouration of the reaction itself; appearing after 24 hours and remaining throughout the study. Nevertheless, this was clearly an extremely slow reaction, lacking in practicality and so it was decided to take measures to speed up the process. The synthesis of second-generation DASAs, those utilising aniline-based donors, has been found to be slower than that of the first generation.[12] It has been

reported that this process can be quickened by adding an excess of amine, heating and/or basifying the media.[41,42] Therefore, the reaction was spiked with triethylamine (TEA), in order to accelerate the DASA formation. As before, a pink colouration was visible throughout the reaction. The reaction was subjected to ^{1}H NMR spectroscopic analysis immediately and 18 hours after addition of the base. The spectra of TEA, 0-hr and 18-hr have been included as Figure 4-18a. After 18 hours of reacting, a large reduction in the characteristic MAF signals was found, highlighted by pink bands, in Figure 4-18a. This reduction was concomitant with the appearance of new signals, especially so within the region of 6 – 9 ppm – the expected area for characteristic DASA triene protons. Characterisation of the 18-hr spectrum can be found in Figure 4-18b/c. From this data, it was apparent that the MAF and product 10 had successfully reacted to produce DASA-functionality and that the new species existed in an equilibrium between linear and cyclic forms. Integration of signals "j and j'" indicated a relationship of linear to cyclic of 38 : 62. This was not surprising, as it has already been reported that an aniline-derived DASA without phenyl-substitution has similarly displayed a ratio of 17 : 83.[42] A portion of the spectrum, from Figure 4-18b, has been highlighted by a blue ring. This highlighted area includes a signal characteristic of the secondary amine belonging to product 10 (see Figure 4-17a), its presence suggested an incomplete DASA-functionalisation of the backbone. An additional signal was present however; a sharp singlet had appeared which is believed to be characteristic of the cyclic DASA isomer, proton "p'". Concerning the cyclic species, protons "o' and i'" were not visible, it was expected that they would in fact appear within the same region as "p'". Final supporting evidence for the formation of the linear DASA isomer, is the emergence of what is believed to be a hydroxyl signal, at approximately 9.6 ppm. As this was only a preliminary investigation, a larger-scale experiment would need to be conducted, in order to ascertain a practicably usable product.
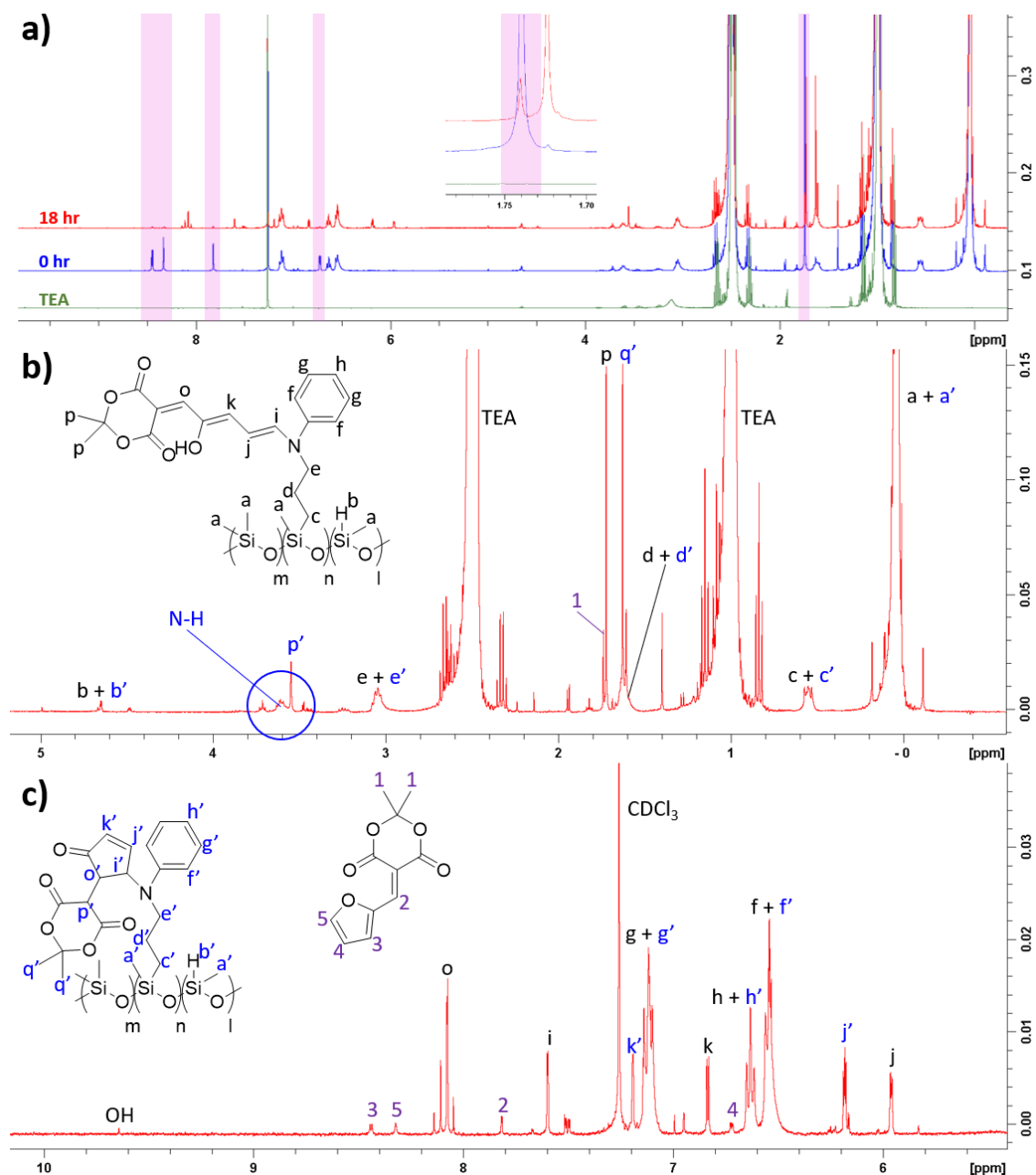
Figure 4-18 – a) ^{1}H NMR spectral overlay of TEA and the tube reaction of product 10 and MAF, at 0 and 18 hours post-TEA addition, MAF signals are highlighted by pink bands; **b + c)** expansions of the 18-hr ^{1}H NMR spectrum, the blue ring highlights signals potentially characteristic of unreacted amine and cyclic DASA protons (see discussion).

4.5 Conclusions and future work

This chapter of work has focused on the covalent modification of polymers by DASA appendation, or the synthesis of a polymeric backbone, consisting of DASA-acceptor units. Failed and somewhat successful syntheses have been reported. These investigative routes are as of yet incomplete, it is hoped that collating current findings shall be of help for future investigations.

Concerning the PEI-DASA polymer project, it was determined that a 10 mol% loading of DASA onto the backbone is the ideal starting point, both for the M_w 10,000 and 2,500 species. Compounds such as 2 and 3a made it clear that a DASA-functionalisation of 20-100 mol% for the M_w 10,000 species, would result in an insoluble precipitate. It is believed that this was a consequence of a high concentration of intermolecular hydrogen-bonding between chains, potentially through unreacted secondary amines interacting with carbonyl units. Although insoluble, these products were successfully appended with DASA units, as determined by examination of their FTIR spectra. This was made evident by C-O/C=O stretches from the Meldrum's acid unit and the disappearance of secondary amine stretches centred around 3200 cm^{-1}. Compounds such as 3b, 4, 5 and 6 were all soluble PEI-DASA samples, characterisation of those was determined through a combination of FTIR and ^{1}H NMR spectroscopy. Accurately calculating the degree of functionalisation for compounds 3b-6 wasn't possible, due to the number of overlapping solvent peaks. However, approximations were attempted by subtracting the interfering signals and comparing that characteristic of the PEI backbone to signals believed to be indicative of Meldrum's acid methyl groups. The resulting approximations, along with yields, are displayed in Table 4.1. The functionalisation percentages for compounds 3b, 4 and 5 were close to their desired values, but it should again be stressed that these were only approximations. The DASA-functionalisation for compound 6 (PEI 2,500) was largely underwhelming, at 16 mol%, as opposed to the desired 100 mol%. Considering that the attempt at 100 mol% for PEI 10,000 (compound 2) led to an insoluble product, including in DMSO, it was expected that the same would occur for compound 6. However, compound 6 was soluble in

DMSO. Additionally, given that both compounds 3b and 6 fell short of their aimed functionalisation, it is possible that DASA-appendation of PEI becomes sterically hindered between 10 and 20 mol%.

Table 4.1 - Tabulated differences between syntheses of compounds 2-6. The far-right column states the experimental DASA-functionalisation.

Compound	Solvent	PEI M_w (gmol^{-1})	DASA (mol%)	Yield (g) [%]	DASA (mol%) [ex]
2	EtOH	10,000	100	0.39 [40]	N/A
3	EtOH	10,000	20	a = 0.57 [56] b = 0.05 [5]	a = N/A b = 16
4	EtOH	10,000	10	0.49 [62]	11
5	MeOH	2,500	10	0.54 [67]	13
6	DMSO	2,500	100	0.39 [33]	16

Future investigations will utilise deuterated solvents other than chloroform-*d*, DMSO-*d$_6$* and methanol-*d$_4$*, as these can potentially cover important signals. It should be noted that none of the PEI-DASA species reported here were soluble in DCM; it would be the ideal solvent, otherwise. Furthermore, it is important to note that it is possible that the conjugates synthesised here, could have existed in equilibrium between the open and closed DASA isomers. The variety of unidentifiable signals emerging from the baseline between 6 and 8 ppm supported this hypothesis.

The second project described here consisted of the construction of a polyurea that was to be further reacted with diethyl malonate, to produce a barbituric acid-based backbone. Subsequently, that would have been modified with furfural to produce a polymeric system that would readily react in the presence of amines. However, it was found that with the reagents used here, hexamethylenediamine and hexamethylene diisocyanate, an insoluble material would form. The condensation of the diamine and diisocyanate led to an insoluble polyurea. It is believed that the long, straight-chain spacer units had a propensity for close-range intermolecular packing, which further encouraged intermolecular urea unit hydrogen-bonding.

As such, compound 7 could only be partially characterised through FTIR spectroscopy. Characteristic isocyanate, secondary amide and amide carbonyl stretches indicated that the synthesis of a urea was successful and that it was capped by isocyanate groups. Due to the insolubility of compound 7, it was decided to instead restrict the investigation to non-polymeric systems until more synthetic progress could be made. The synthesis of a bis(urea) was successful, shown by FTIR, ^{1}H and ^{13}C NMR. However, further reaction with diethyl malonate did not appear to form the desired barbituric acid-based product. As the ^{1}H and ^{13}C NMR spectra of compound 9 were practically identical to that of compound 8, a successful synthesis was ruled out. It is possible that the reaction was not allowed to take its course for long enough, as the literature-derived synthesis was 7-hours long.[40] As such, further investigations will account for this. Furthermore, future attempts at the synthesis of a polyurea shall entail more sterically-hindered reactants such as aromatic ring systems, as they have been found to encourage polyurea solubility in organic solvents.[43] In hindsight, it would have been more prudent to include a polyether within the main chain, to produce what's known as "soft-segments".[44] This would likely help reduce the insolubility of the product.

The final synthetic section of this chapter detailed the attempted DASA-modification of a polysiloxane backbone. A platinum-catalysed hydrosilylation reaction between poly(MHS-DMS) and *N*-allyl aniline was reported. The purpose of this was to create a secondary amine active site, to be further reacted with MAF. Success of the hydrosilylation reaction was shown by the FTIR and ^{1}H NMR spectra of compound 10; the former revealing a disappearance of the characteristic Si-H stretch at 2158 cm^{-1} and the latter elucidated an 88% reduction in Si-H concentration. This translated to approximately 6% of the siloxane backbone, of a possible 7%, being functionalised with *N*-propyl aniline units. Naturally, this was then reacted with MAF in an attempt to produce a DASA-polymer conjugate. An NMR tube reaction took place, running for 168 hours until it was decidedly halted due to being impracticably slow. The formation of DASA could not be identified by NMR analysis as the secondary amine signal integrals would fluctuate and those belong to MAF seemingly increased. The only indication of a reaction was a pale pink

colouration adopted by the solution, 24 hours in and there-on throughout. As such, it was decided to spike the reaction mixture with TEA, to basify it and hopefully accelerate the process. NMR analysis showed that within 18 hours, the MAF signals exhibited a major reduction, suggesting DASA-formation. This was supported by the appearance of signals believed to be characteristic of the linear and cyclic DASA forms. It appeared that they existed in an equilibrium that favoured the cyclic form, unsurprisingly. Given the small scale of this reaction, future work would entail a scale-up of reagents. Additionally, further investigations will pertain to the modification of half of the siloxane backbone, leaving Si-H groups left over for a degree of cross-linking, with tetravinylsilane as an example. The amine-reactivity of this network could then be investigated, in a similar manner to what has been reported in chapter 2 of this thesis. This work would be carried out with aliphatic allyl amines, too, as they may yield a more rapid reaction – not requiring basification of the reaction mixture.

4.6 References

1   Y. Wang, P. Han, H. Xu, Z. Wang, X. Zhang and A. V Kabanov, *Langmuir*, 2010, **26**, 709–715.

2   S. Son, E. Shin and B. S. Kim, *Biomacromolecules*, 2014, **15**, 628–634.

3   G. Petriashvili, L. Devadze, T. Zurabishvili, N. Sepashvili and K. Chubinidze, *Biomed. Opt. Express*, 2016, **7**, 442.

4   A. Koçer, M. Walko, W. Meijberg and B. L. Feringa, *Science (80-.).*, 2005, **309**, 755–758.

5   M. Yamada, M. Kondo, J. I. Mamiya, Y. Yu, M. Kinoshita, C. J. Barrett and T. Ikeda, *Angew. Chemie - Int. Ed.*, 2008, **47**, 4986–4988.

6   H. Zeng, O. M. Wani, P. Wasylczyk, R. Kaczmarek and A. Priimagi, *Adv. Mater.*, 2017, **29**, 1–7.

7   X. Pei, A. Fernandes, B. Mathy, X. Laloyaux, B. Nysten, O. Riant and A. M. Jonas, *Langmuir*, 2011, **27**, 9403–9412.

8   L. Li, S. Pan, X. Pang, H. Chen, D. Hu, L. Ke, Y. Xiong and W. Xu, *Soft Matter*, 2012, **8**, 7357–7360.

9   Y.-N. Zhou, J.-J. Li, Q. Zhang and Z.-H. Luo, *Langmuir*, 2014, **30**, 12236–12242.

10   S. Helmy, S. Oh, F. A. Leibfarth, C. J. Hawker and J. Read De Alaniz, *J. Org. Chem.*, 2014, **79**, 11316–11329.

11   S. Helmy, F. A. Leibfarth, S. Oh, J. E. Poelma, C. J. Hawker and J. R. De Alaniz, *J. Am. Chem. Soc.*, 2014, **136**, 8169–8172.

12   M. M. Lerch, W. Szymański and B. L. Feringa, *Chem. Soc. Rev.*, 2018, **47**, 1910–1937.

13   S. O. Poelma, S. S. Oh, S. Helmy, A. S. Knight, G. L. Burnett, H. T. Soh, C. J. Hawker and J. Read De Alaniz, *Chem. Commun.*, 2016, **52**, 10525–10528.

14   T. Senthilkumar, L. Zhou, Q. Gu, L. Liu, F. Lv and S. Wang, *Angew. Chemie - Int. Ed.*, 2018, **57**, 13114–13119.

15   O. Rifaie-Graham, S. Ulrich, N. F. B. Galensowske, S. Balog, M. Chami, D. Rentsch, J. R. Hemmer, J. Read De Alaniz, L. F. Boesel and N. Bruns, *J. Am. Chem. Soc.*, 2018, **140**, 8027–8036.

16   G. Sinawang, B. Wu, J. Wang, S. Li and Y. He, *Macromol. Chem. Phys.*, 2016, **217**, 2409–2414.

17   H. Zhao, D. Wang, Y. Fan, M. Ren, S. Dong and Y. Zheng, *Langmuir*, 2018, **34**, 15537–15543.

18   M. Nau, D. Seelinger and M. Biesalski, *Adv. Mater. Interfaces*, 2019, **6**, 1–5.

19   S. H. Mostafavi, W. Li, K. D. Clark, F. Stricker, J. R. De Alaniz and C. J. Bardeen, *Macromolecules*, 2019, **52**, 6311–6317.

20   S. Singh, K. Friedel, M. Himmerlich, Y. Lei, G. Schlingloff and A. Schober, *ACS Macro Lett.*, 2015, **4**, 1273–1277.

21   S. Ulrich, J. R. Hemmer, Z. A. Page, N. D. Dolinski, O. Rifaie-Graham, N. Bruns, C. J. Hawker, L. F. Boesel and J. Read De Alaniz, *ACS Macro Lett.*, 2017, **6**, 738–742.

22   B. P. Mason, M. Whittaker, J. Hemmer, S. Arora, A. Harper, S. Alnemrat, A. McEachen, S. Helmy, J. Read de Alaniz and J. P. Hooper, *Appl. Phys. Lett.*, 2016, **108**, 041906-1–4.

23   A. Balamurugan and H. Il Lee, *Macromolecules*, 2016, **49**, 2568–2574.

24   J. E. Yap, N. Mallo, D. S. Thomas, J. E. Beves and M. H. Stenzel, *Polym. Chem.*, 2019, **10**, 6515–6522.

25   D. Zhong, Z. Cao, B. Wu, Q. Zhang and G. Wang, *Sensors Actuators, B Chem.*, 2018, **254**, 385–392.

26 Q. Chen, Y. J. Diaz, M. C. Hawker, M. R. Martinez, Z. A. Page, S. Xiao-An Zhang, C. J. Hawker and J. Read De Alaniz, *Macromolecules*, 2019, **52**, 4370–4375.

27 F. Bigi, S. Carloni, L. Ferrari, R. Maggi, A. Mazzacani and G. Sartori, *Tetrahedron Lett.*, 2001, **42**, 5203–5205.

28 R. Bahulekar, N. R. Ayyangar and S. Ponrathnam, *Enzyme Microb. Technol.*, 1991, **13**, 858–868.

29 J. Hernandez-Montelongo, E. G. Lucchesi, V. F. Nascimento, C. G. França, I. Gonzalez, W. A. A. Macedo, D. Machado, M. Lancellotti, A. M. Moraes, M. M. Beppu and M. A. Cotta, *Mater. Sci. Eng. C*, 2017, **71**, 718–724.

30 R. Saha, A. Devaraj, S. Bhattacharyya, S. Das, E. Zangrando and P. S. Mukherjee, *J. Am. Chem. Soc.*, 2019, **141**, 8638–8645.

31 D. Fischer, T. Bieber, Y. Li, H. P. Elsässer and T. Kissel, *Pharm. Res.*, 1999, 16, 1273–1279.

32 A. C. Hunter, *Adv. Drug Deliv. Rev.*, 2006, **58**, 1523–1531.

33 S. Kobayashi, *Prog. Polym. Sci.*, 1990, **15**, 751–823.

34 J. J. Virgen-Ortíz, J. C. S. Dos Santos, Á. Berenguer-Murcia, O. Barbosa, R. C. Rodrigues and R. Fernandez-Lafuente, *J. Mater. Chem. B*, 2017, 5, 7461–7490.

35 P. C. Painter and M. M. Coleman, *Fundamentals of polymer science: an introductory text*, CRC Press, New York, Second Edi., 1997.

36 M. M. Coleman, M. Sobkowiak, G. J. Pehlert and P. C. Painter, *Macromol. Chem. Phys.*, 1997, **198**, 117–136.

37 J. Mattia and P. Painter, *Macromolecules*, 2007, **40**, 1546–1554.

38 T. Li, T. Zheng, J. Han, Z. Liu, Z. X. Guo, Z. Zhuang, J. Xu and B. H. Guo, *Polymers*, 2019, **11**, 1-18.

39   S. K. Wang and C. S. P. Sung, *Macromolecules*, 2002, **35**, 883–888.

40   B. S. Furniss, A. J. Hannaford, P. W. G. Smith and A. R. Tatchell, *Vogel's textbook of practical organic chemistry*, John Wiley & Sons, Inc., New York, Fifth Edit., 1989.

41   J. R. Hemmer, S. O. Poelma, N. Treat, Z. A. Page, N. D. Dolinski, Y. J. Diaz, W. Tomlinson, K. D. Clark, J. P. Hooper, C. Hawker and J. Read De Alaniz, *J. Am. Chem. Soc.*, 2016, **138**, 13960–13966.

42   N. Mallo, P. T. Brown, H. Iranmanesh, T. S. C. MacDonald, M. J. Teusner, J. B. Harper, G. E. Ball and J. E. Beves, *Chem. Commun.*, 2016, **52**, 13576–13579.

43   M. Joshi, S. Jauhari and K. R. Desai, *Int. J. ChemTech Res.*, 2011, **3**, 29–32.

44   Z. S. Chen, W. P. Yang and C. W. Macosko, *Rubber Chem. Technol.*, 1988, **61**, 86–99.

4.7 Appendix 4A
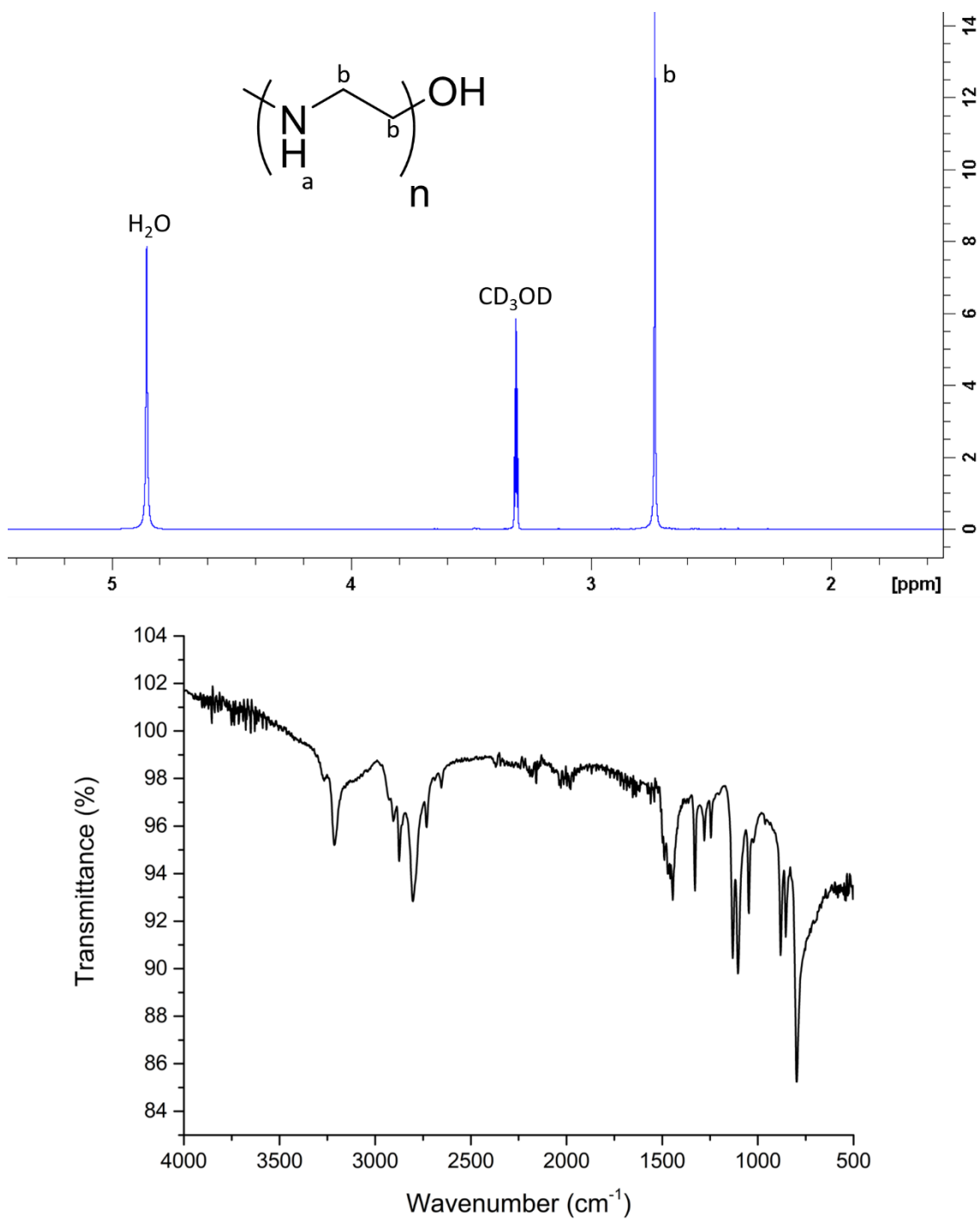
Figure 4.0-19 - ^{1}H NMR of PEI 10,000 in methanol-d$_4$ (top) and its FTIR spectrum (bottom, right).

4.8 Appendix 4B
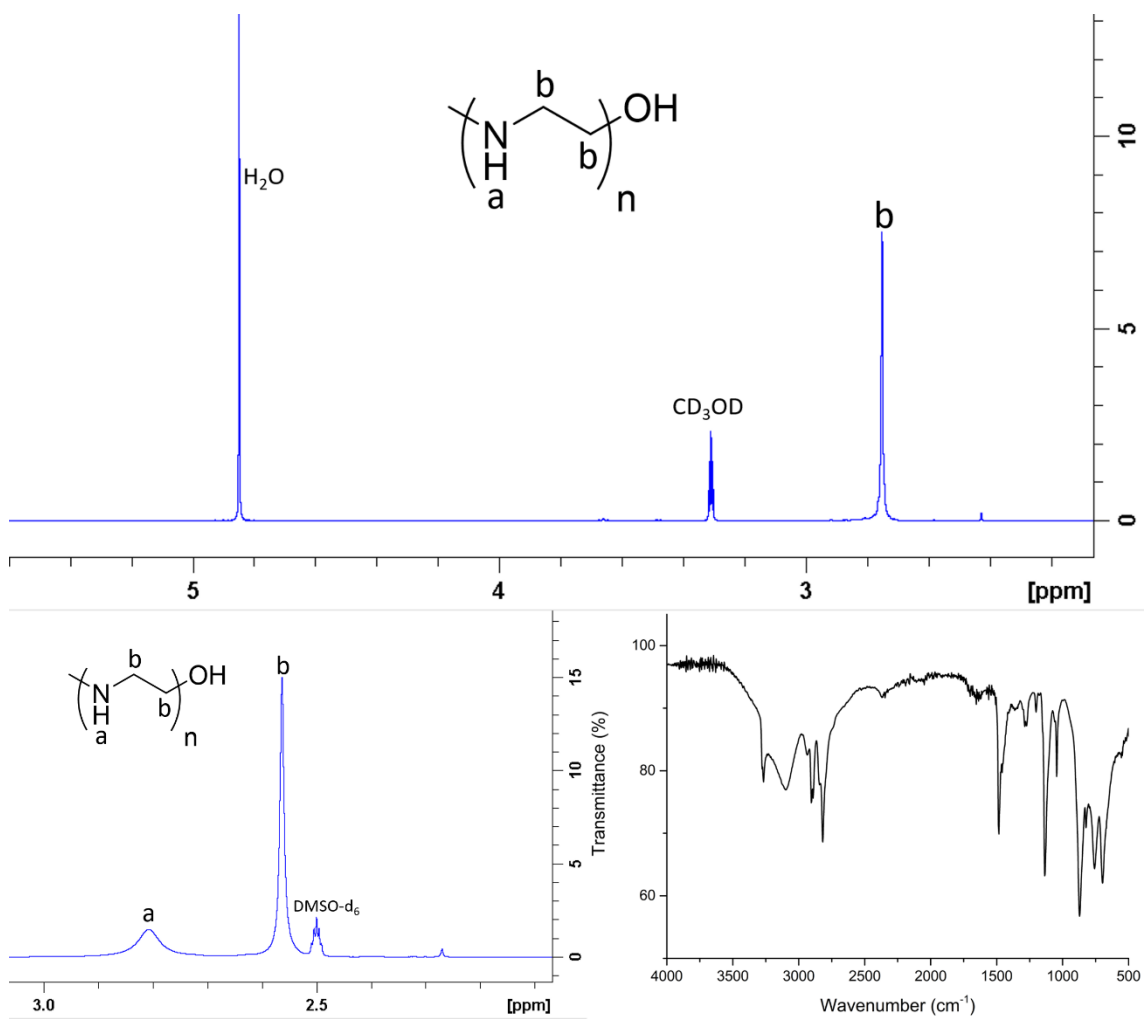
Figure 4.0-20 – ^{1}H NMR of PEI 2,500 in methanol-d$_4$ (top) and DMSO-d$_6$ (bottom, left), alongside its FTIR spectrum (bottom, right).

4.9 Appendix 4C
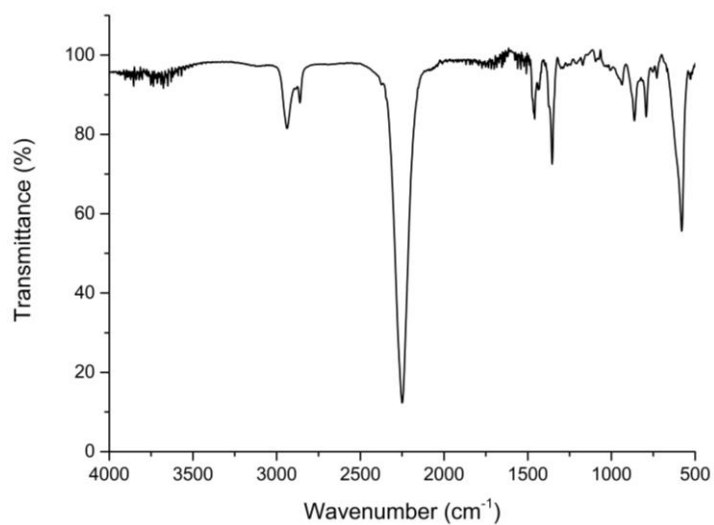
**Figure 4.0-21 – FTIR spectrum of hexamethylene diisocyanate.**
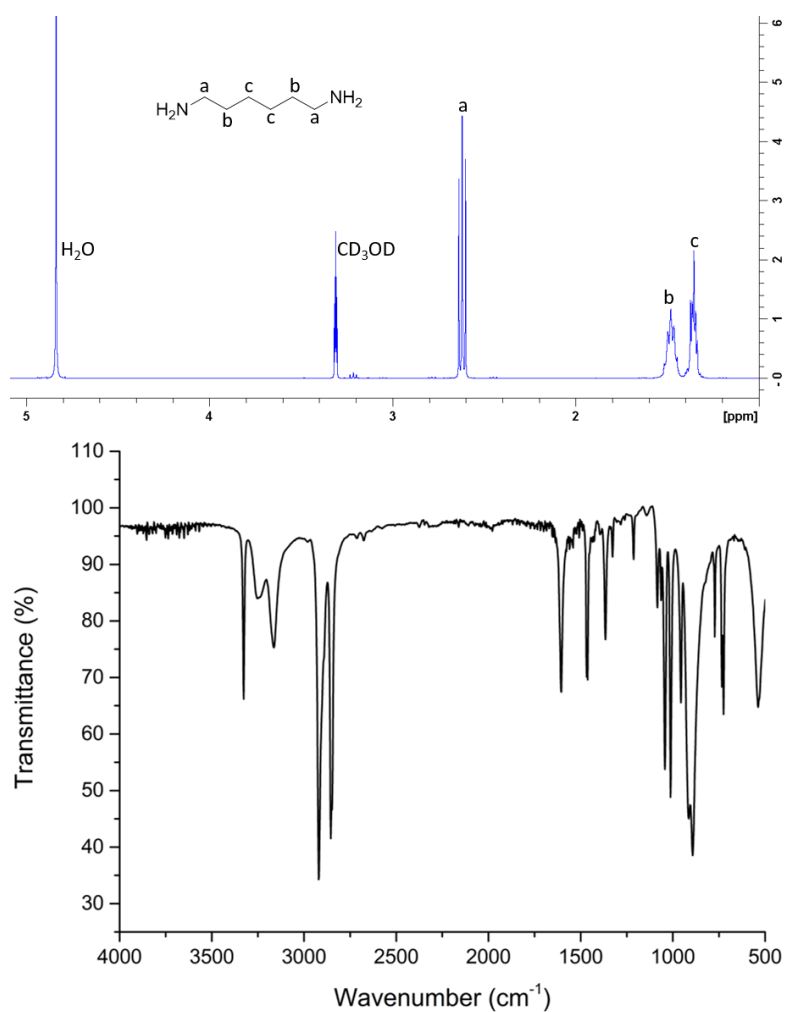
**Figure 4.0-22 – ^{1}H NMR (top) and FTIR (bottom) spectra of hexamethylenediamine.**
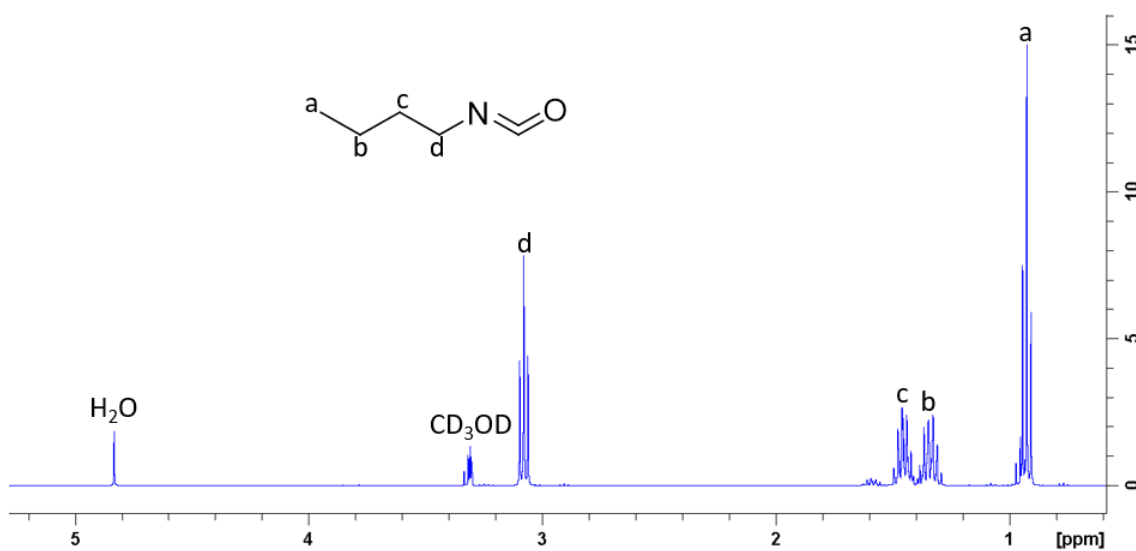
Figure 4.0-23 - ¹H NMR spectrum of butylisocyanate.
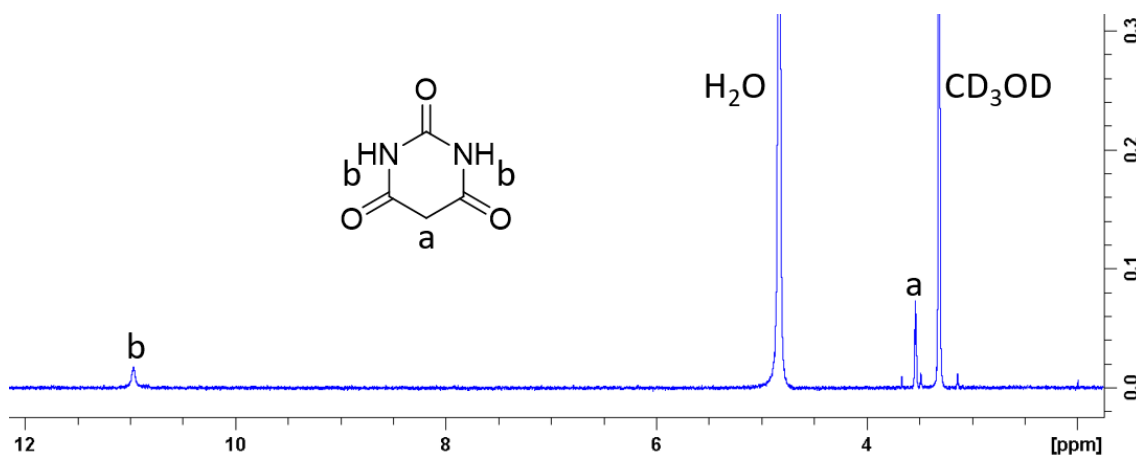
Figure 4.0-24 – ¹H NMR spectrum of barbituric acid.

4.10 Appendix 4D
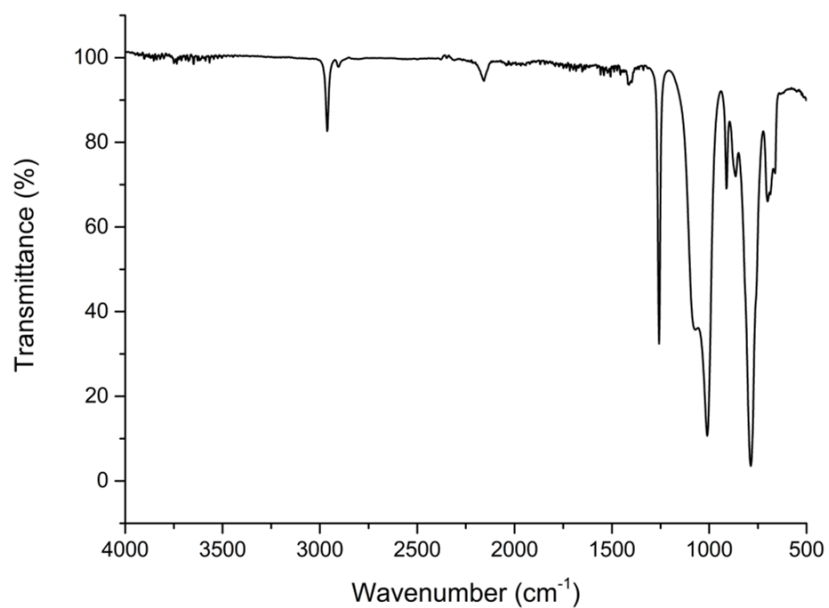
**Figure 4.0-25 – FTIR spectrum of poly(MHS-DMS).**
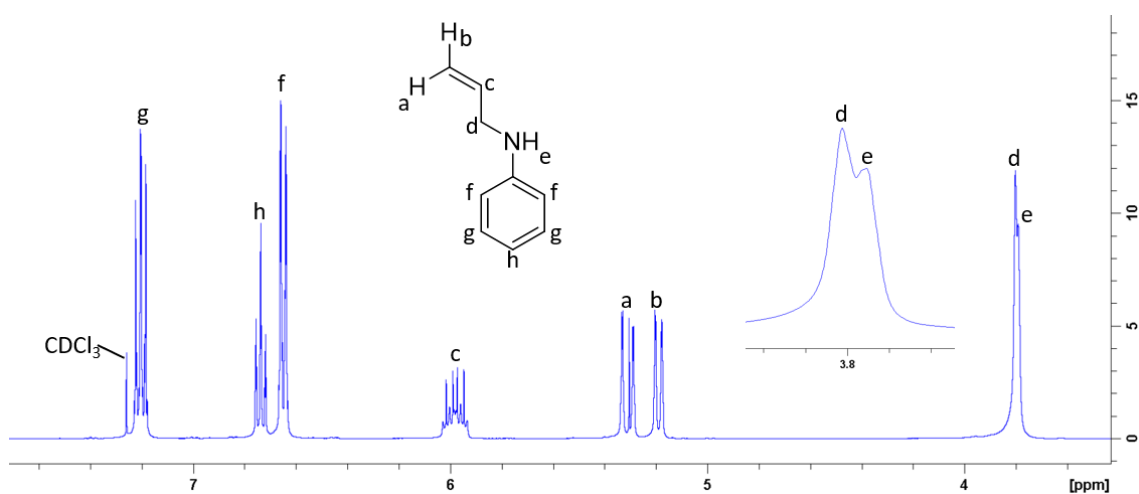
Figure 4.0-26 – ^{1}H NMR spectrum of *N*-allyl aniline, in chloroform-*d*.

Chapter 5:

Final Conclusions

The overarching aim of this thesis has focussed on developing stimuli-responsive polymeric materials, through incorporation of the recently-discovered DASA visible light photoswitches. This included the doping of cross-linked PDMS matrices with amine- and photo-responsive species and attempts at covalently attaching the species to various polymeric backbones.

The second chapter of this thesis introduced the doping of PDMS with MAF, the precursory species to DASA formation. The network consisted of a silanol-terminated PDMS cross-linked using an organotin catalyst complex, with MAF blended into the mixture. The aim was to develop a cost-effective amine-responsive network that could be synthesised through facile means. The mechanism of action exploited the rapid synthetic route to DASAs, through nucleophilic attack of amines. This reaction would produce a vibrant red to purple colouration within the network, hence a fast, easily detectable colourimetric response could be read. Analysis of amine-response performance was conducted through UV-Vis spectroscopy, image analysis and RFID sensor measurements. It was found that the earliest quantifiable response through UV-Vis spectroscopy was within 30 minutes, in a 1000 ppm diethylamine solution, but that visual observation could indicate reactivity much earlier than this. Subsequently, image analysis had shown that the earliest detectable response was within 10 minutes at a diethylamine concentration of as low as 800 ppm. From this, it was determined that image analysis was a better evaluative measure of amine-detectability. Following these studies, a practical example was demonstrated by exposure to concentrated diethylamine and ammonia vapours, which provided preliminary determination of amine-reactivity in a simulated food packaging environment. This practical applicability was further demonstrated by inclusion of fresh cod samples which would inevitably release amines upon decomposition, over time. Finally, it was found that with the current architecture, it was not possible to evaluate the amine-detection response through RFID sensing measures.

The third chapter of this thesis detailed the development of a photo-responsive cross-linked PDMS pad. The elastomer was produced in a similar manner to that featured in chapter 2;

doping of an organotin-crosslinked PDMS network with a stimuli-responsive species. That

species was a visible light photoswitch; dihexyl DASA. At high concentrations of doping (1-5

wt%), the DASA would crystallise, thereby inhibiting the photoswitching process. Subsequently,

it was found that curing within a solvent-rich atmosphere would somewhat hinder DASA

crystallisation, allowing for loadings of at least 1 wt% with minimal crystal formation.

Photoswitching performance of the PDMS-DASA elastomers was evaluated through UV-Vis

spectroscopy, with a focus on the difference imparted by variation of the photoswitch

concentration, and the consequences of using different curing methods – open or sealed

atmospheres. As hypothesised, a general trend was observed whereby an increase in DASA

loading would lead to slower forward and backward photoswitching processes. Comparison of

the data obtained from air-cured (AC) and sealed atmosphere cured (SAC) samples revealed that

the SAC elastomers exhibited a faster forward photoisomerisation reaction, but displayed a

slower thermal reversion rate. It is believed that these differences were consequential of the

presence, or lack thereof, of DASA crystals. Such that, intermolecular interactions with the

crystals would provide a more convenient pathway for thermal reversion, and overall, hinder

the forward switching process. From this, it was concluded that AC elastomers would be best

utilised for applications that required reusability and SAC architectures were better suited for

single-use tamper systems. A further experiment was conducted, investigating the effect that

solvent swelling would have on the forward photoswitching process. It was found that THF,

toluene and DCM would provide minor acceleration, whereas other examples would have the

opposite effect, especially so for acetone and propan-1-ol. Finally, the ability to detect PDMS-

DASA switching through RFID sensing was investigated. A PDMS-DASA film was applied to an

RFID tag, with sensor code values being obtained before and after photoswitching. The acquired

data was promising for a 250 μm film, such that a change in sensor value was found after film

decolourisation.

The fourth chapter of this thesis focused on the covalent modification of polymers by DASA

appendation, or the synthesis of a polymeric backbone, consisting of DASA-acceptor units. Failed

and somewhat successful syntheses were reported. Beginning with the PEI-DASA modification; a 10 mol% loading of DASA onto linear PEI (2,500 and 10,000 M_w) was successful. Increasing this loading to 20 mol% (PEI 10,000) and 100 mol% (PEI 2,500 and 10,000) would lead to largely insoluble products, this was believed to be a consequence of interchain hydrogen-bonding. The second project of covalent modification concerned the synthesis of a DASA-based polymer, beginning from a polyurea derivative. It was found that the reaction between hexamethylenediamine and hexamethylene diisocyanate would produce an insoluble product. Consequently, attention was focused on developing a bis(urea) instead, as a precursory indicator toward future synthetic investigation. The bis(urea) was further reacted with diethyl malonate, with the hope of producing a bis(barbituric acid). It was concluded that this reaction had failed as spectroscopic data did not suggest successful formation of the desired product. The final synthetic investigation concerned appending a DASA to a polysiloxane chain, through Pt-catalysed hydrosilylation and subsequent secondary amine-reactivity. The hydrosilylation of poly(MHS-DMS) and *N*-allyl aniline was successful, evident by FTIR and ^{1}H NMR spectroscopic data, with the latter indicating an *N*-propylaniline functionalisation of 6 mol% (88% of the desired level). The product was further reacted with MAF in chloroform-d, in an NMR tube. DASA-formation was extremely slow; therefore, the reaction was basified, demonstrably accelerating the process.

Overall, the aims of this thesis were met. An amine-sensing polymeric material was facilely-produced through blending of the DASA precursor, MAF, in chapter 2. The product's application as a non-destructive method of colourimetric detection of decaying fish products was demonstrated through simulated packaging experiments. A light-responsive polymeric material consisting of a polysiloxane network doped with a first generation DASA was successfully synthesised, in chapter 3. The performance of the product as a photoswitchable material was evaluated through UV-vis spectroscopic analysis, elucidating trends between DASA-loading and two different curing conditions. Finally, the covalent attachment of DASA to PEI and a polysiloxane backbone were demonstrated, in chapter 4.